

AD-A274 079

2

WL-TR-93-5029



**THREE-WAVE NONLINEAR INTERACTIONS IN  
KTiOPO<sub>4</sub> (KTP) AND KTP ISOMORPHS**



**DALE L. FENIMORE  
KENNETH L. SCHEPLER**

**SEPTEMBER 1993**



**FINAL REPORT FOR THE PERIOD OF MAY 1993 TO SEPTEMBER 1993**

**APPROVED FOR PUBLIC RELEASE, DISTRIBUTION IS UNLIMITED.**

Solid State Electronics Directorate  
Wright Laboratory  
Air Force Materiel Command  
Wright-Patterson Air Force Base OH 45433-7405

**93-30826**



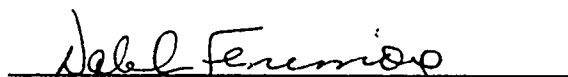
119775

## NOTICE

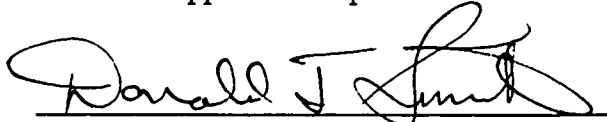
WHEN GOVERNMENT DRAWINGS, SPECIFICATIONS, OR OTHER DATA ARE USED FOR ANY PURPOSE OTHER THAN IN CONNECTION WITH A DEFINITELY GOVERNMENT-RELATED PROCUREMENT, THE UNITED STATES GOVERNMENT INCURS NO RESPONSIBILITY OR ANY OBLIGATION WHATSOEVER. THE FACT THAT THE GOVERNMENT MAY HAVE FORMULATED OR IN ANYWAY SUPPLIED THE SAID DRAWINGS, SPECIFICATIONS, OR OTHER DATA, IS NOT TO BE REGARDED BY IMPLICATION, OR OTHERWISE IN ANY MANNER CONSTRUED, AS LICENSING THE HOLDER, OR ANY OTHER PERSON OR CORPORATION; OR AS CONVEYING ANY RIGHTS OR PERMISSION TO MANUFACTURE, USE, OR SELL ANY PATENTED INVENTION THAT MAY IN ANY WAY BE RELATED THERETO.

This report is releasable to the National Technical Information Service (NTIS). At NTIS, it will be available to the general public, including foreign nations.

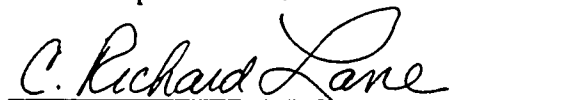
This technical report has been reviewed and is approved for publication.



DALE L. FENIMORE, Captain, USAF  
Electro-Optics Projects Officer  
Electro-Optics Sources Branch



DONALD J. SMITH, Chief  
Electro-Optics Sources Branch  
Electro-Optics Division



C. RICHARD LANE, Actg Chief  
Electro-Optics Division  
Solid State Electronics Directorate

If your address has changed, if you wish to be removed from our mailing list, or if the addressee is no longer employed by your organization, please notify, WL/ELO Building 22B, 2700 D Street, Ste #2, Wright-Patterson AFB OH 45433-7405 to help us maintain a current mailing list.

Copies of this report should not be returned unless return is required by security considerations, contractual obligations, or notice on a specific document.

REPORT DOCUMENTATION PAGE			Form Approved OMB No. 0704-0188	
Public reporting burden for this collection of information is estimated to average 1 hour per response, including the time for reviewing instructions, searching existing data sources, gathering and maintaining the data needed, and completing and reviewing the collection of information. Send comments regarding this burden estimate or any other aspect of this collection of information, including suggestions for reducing this burden, to Washington Headquarters Services, Directorate for Information Operations and Reports, 1215 Jefferson Davis Highway, Suite 1204, Arlington, VA 22202-4302, and to the Office of Management and Budget, Paperwork Reduction Project (0704-0188), Washington, DC 20503.				
1. AGENCY USE ONLY (Leave blank)		2. REPORT DATE 14 September 1993		3. REPORT TYPE AND DATES COVERED Final, May 93 - Sep 93
4. TITLE AND SUBTITLE Three-Wave Nonlinear Interactions in $\text{KTiOPO}_4$ (KTP) and KTP Isomorphs			5. FUNDING NUMBERS  PR - 2001 TA - 05 WC - 01 PE - 62204F	
6. AUTHOR(S) Dale L. Fenimore, Captain, WL/ELOS WPAFB OH; Dr Kenneth L. Schepler, WL/ELOS WPAFB OH				
7. PERFORMING ORGANIZATION NAME(S) AND ADDRESS(ES) Electro-Optics Sources Branch Solid State Electronics Directorate Wright Laboratory Air Force Materiel Command Wright-Patterson Air Force Base OH 45433-7405			8. PERFORMING ORGANIZATION REPORT NUMBER  WL-TR-93-5029	
9. SPONSORING/MONITORING AGENCY NAME(S) AND ADDRESS(ES) Solid State Electronics Directorate Wright Laboratory Air Force Materiel Command Wright-Patterson Air Force Base OH 45433-7126			10. SPONSORING/MONITORING AGENCY REPORT NUMBER  WL-TR-93-5029	
11. SUPPLEMENTARY NOTES				
12a. DISTRIBUTION / AVAILABILITY STATEMENT Approved for public release, distribution is unlimited.			12b. DISTRIBUTION CODE	
13. ABSTRACT (Maximum 200 words) <p>This document reports an investigation of three-wave interactions in positive (nonlinear) biaxial crystals—specifically, the crystal <math>\text{KTiOPO}_4</math> (KTP) and its crystallographic isomorphs: <math>\text{RbTiOPO}_4</math> (RTP), <math>\text{KTiOAsO}_4</math> (KTA), <math>\text{RbTiOAsO}_4</math> (RTA), and <math>\text{CsTiOAsO}_4</math> (CTA). The results are characterized in terms of phase matching angles, effective nonlinear coefficients, and walkoff angles for the optical beams.</p> <p>In phase matching angles, RTP and CTA showed larger variations in <math>\theta</math> (i.e., were more birefringent) than the other isomorphs (which were more uniaxial-like). Where KTP did not have the largest <math>d_{\text{eff}}</math>, the difference from the isomorph which did was typically no more than 0.7 pm/V. Although overall walkoff was less than <math>3^\circ</math> for all isomorphs; the arsenates had around half the walkoff of the phosphates. Strictly from a performance characteristics basis, for uses at wavelengths less than <math>2.75 \mu\text{m}</math> there is little reason to select one of the other isomorphs over KTP. RTP is acceptable for OPO usage to <math>3.17 \mu\text{m}</math>, though an arsenate, CTA, is a better choice (higher <math>d_{\text{eff}}</math>, less walkoff, and negligible absorption). Above <math>3.2 \mu\text{m}</math>, the arsenates, with their smaller walkoff angles and minimal absorption losses, are considerably better choices than the phosphates.</p>				
14. SUBJECT TERMS  nonlinear optics, nonlinear frequency conversion, lasers, infrared			15. NUMBER OF PAGES 125	
			16. PRICE CODE	
17. SECURITY CLASSIFICATION OF REPORT Unclassified	18. SECURITY CLASSIFICATION OF THIS PAGE Unclassified	19. SECURITY CLASSIFICATION OF ABSTRACT Unclassified	20. LIMITATION OF ABSTRACT UL	

## TABLE of CONTENTS

---

1. INTRODUCTION .....	1
2. ANGULAR PHASE MATCHING .....	2
a. Phase Matching Theory .....	2
b. Description of the Computer-Based Equations. ....	6
3. EFFECTIVE NONLINEAR COEFFICIENT, $d_{eff}$ .....	10
a. Effective Nonlinear Coefficient Theory .....	10
b. Description of the Computer-Based Equations .....	14
4. WALKOFF ANGLE .....	17
a. Theory for the Walkoff Angle Calculations .....	17
b. Use of the Computer-Based Equations. ....	18
5. LINEAR AND NONLINEAR PROPERTIES OF KTP ISOMORPHS .....	19
a. List of Properties Used in Calculations .....	19
b. Nonlinear ( $d_{ijk}$ ) Coefficients .....	20
i. Basic Tensor Background .....	20
ii. Tensor Matrix for KTP Isomorphs .....	21
c. Caveats .....	21
i. $d$ -Coefficients .....	22
ii. Miller's Rule .....	22
iii. Sellmeier Coefficients .....	23
6. ISOMORPH COMPARISONS .....	24
a. Introduction. ....	24
b. Phase Matching Characteristics .....	24
i. Second Harmonic Generation .....	24
(1) Type I .....	24
(2) Type II .....	25
(3) Type III .....	25
ii. Optical Parametric Oscillator .....	26
(1) Type I .....	26
(2) Type II .....	27
(3) Type III .....	28
c. Effective Nonlinear Coefficients ( $d_{eff}$ ) .....	29
i. Second Harmonic Generation (SHG) Wavelengths .....	29
ii. Optical Parametric Oscillator (OPO) Wavelengths .....	29
d. Walkoff .....	30
i. Partial Phase Match Regions .....	31
ii. Walkoff Variations .....	31
iii. Walkoff Similarities .....	31

7. CONCLUSIONS/OBSERVATIONS. ....	32
a. Crystal Characteristics. ....	32
b. Conclusions ....	34

REFERENCES ....	38
-----------------	----

## LIST OF FIGURES

Figure 1. Phase Matching Types and Associated Polarizations .....	3
Figure 2. Spherical Projection Showing the Slow ( $e_1$ ) and Fast ( $e_2$ ) Eigenmodes of a Wavefront in a Biaxial Crystal .....	3
Figure 3. Dielectric Ellipsoid for a Biaxial Crystal with Wavefront .....	4
Figure 4. First Octant of a Proposed Positive Nonlinear Reporting Frame. ....	6
Figure 5. Relationship Between $\vec{E}$ , $\vec{k}$ , $\vec{S}$ , and $\vec{D}$ .....	17
Figure 6. An $mm2$ Crystal Class Tensor Arrangement. ....	21
Figure 7. SHG Phase Matching, Type I, 1.064/1.064/0.532 $\mu\text{m}$ . ....	25
Figure 8. SHG Phase Matching, Type I, 1.35/1.35/0.675 $\mu\text{m}$ . ....	25
Figure 9. SHG Phase Matching, Type II/III, 1.064/1.064/0.532 $\mu\text{m}$ . ....	26
Figure 10. SHG Phase Matching, Type II/III, 1.35/1.35/0.675 $\mu\text{m}$ . ....	26
Figure 11. OPO Phase Matching, Type I, 4.043/1.444/1.064 $\mu\text{m}$ . ....	27
Figure 12. OPO Phase Matching, Type I, 3.17/1.60/1.064 $\mu\text{m}$ . ....	27
Figure 13. OPO Phase Matching, Type II, 4.043/1.444/1.064 $\mu\text{m}$ . ....	27
Figure 14. OPO Phase Matching, Type II, 3.17/1.60/1.064 $\mu\text{m}$ . ....	27
Figure 15. OPO Phase Matching, Type III, 3.17/1.60/1.064 $\mu\text{m}$ . ....	28
Figure 16. Phosphate Isomorph Transmission Spectra .....	33
Figure 17. Arsenate Isomorph Transmission Spectra .....	34

## LIST OF TABLES

Table 1. Potentially Phase-Matchable Combinations of $e_1$ and $e_2$ Eigenmodes, Where $\lambda_1 \geq \lambda_2 > \lambda_3$ .....	5
Table 2. Sellmeier Coefficients of KTP Isomorphs .....	19
Table 3. Nonlinear Optical Properties of KTP Isomorphs .....	20
Table 4. Effective Nonlinearity for Type II SHG in the Principal Planes .....	21
Table 5. Miller's Rule Applied to 1.064 $\mu\text{m}$ KTP $d$ Values ..	23
Table 6. Type I SHG Variations in $\theta$ .....	24
Table 7. Type II SHG Variation in $\theta$ .....	25
Table 8. Type I OPO Variation in $\theta$ .....	26
Table 9. Type II OPO Variation in $\theta$ .....	27
Table 10. Type III OPO Variation in $\theta$ .....	28
Table 11. Isomorph Maximum $d_{eff}$ for SHG and OPO .....	30
Table 12. Isomorph Selection Synopsis .....	37

## LIST OF APPENDICES

APPENDIX A	Phase Match Calculations Worksheet .....	40
APPENDIX B	Effective Non-Linear Coefficient ( $d_{eff}$ ) and Walkoff Calculations Worksheet .....	47
APPENDIX C	KTP Isomorph Phase Match Ranges .....	53
APPENDIX D	KTP Isomorph Nonlinear Characteristics .....	60
APPENDIX E	KTP Isomorph Nonlinear Coefficient ( $d_{eff}$ ) .....	67
APPENDIX F	KTP Isomorph WalkOff Angle, $\rho$ .....	93

Accession For	
NTIS	<input checked="" type="checkbox"/>
CRA&I	<input checked="" type="checkbox"/>
DTIC	<input checked="" type="checkbox"/>
TAB	<input checked="" type="checkbox"/>
Unannounced	<input type="checkbox"/>
Justification .....	
By .....	
Distribution ;	
Availability Codes	
Dist	Avail and/or Special
A-1	

DTIC QUALITY INSPECTED 3

## ACKNOWLEDGEMENTS

---

We would like to thank Brian K. Bailey<sup>1</sup>, Department of Physics at Carnegie Mellon University, Pittsburgh PA, for his assistance in performing computer runs which compiled data used to create the charts and tables in this document. We also acknowledge and thank the useful commentary and discussions (especially with respect to Miller's Rule) with Dr Sylvester Wong<sup>2</sup>.

---

<sup>1</sup> Work performed while on assignment to Wright Laboratory, Solid State Electronics Directorate, Wright-Patterson AFB OH

<sup>2</sup> Visiting scientist from the Defence Research Establishment Valcartier, Quebec Canada

## 1. INTRODUCTION

---

The discovery of optical second harmonic generation (SHG) in 1961, coupled with more recent advances in laser technology and nonlinear materials, has led to increasingly rapid progress in the application of nonlinear materials to nonlinear frequency conversion [1, 2, 3, 4].

This document reports the results in the investigation of three-wave interactions in positive biaxial (nonlinear) crystals. The results are characterized in terms of:

- Phase matching angles,
- Effective nonlinear coefficients, and
- Walkoff angles for the optical beams.

Specifically, this report concentrates on  $\text{KTiOPO}_4$  (KTP) and its crystallographic isomorphs:  $\text{RbTiOPO}_4$  (RTP),  $\text{KTiOAsO}_4$  (KTA),  $\text{RbTiOAsO}_4$  (RTA), and  $\text{CsTiOAsO}_4$  (CTA). The isomorphs KTA, RTA, CTA, and RTP are relatively new and show promise as nonlinear crystals. Potassium Titanyl Phosphate (KTP) is a widely used nonlinear optical material which, since there is a large library of information for this particular crystal, was used to validate the computer model calculations developed for this study.

Prior to this study, most calculations assumed that the electric field  $\vec{E}$  was perpendicular to the wave vector  $\vec{k}$  and, therefore, replaced  $\vec{E}$  by the electric displacement  $\vec{D}$ . Also, when the walkoff angle was calculated, the fact that optical waves polarized in different directions have different walkoff angles was ignored. The consequence was that the approximate treatment was prone to the introduction of errors or inaccuracies in the final results.

This report will show the results of a translation of an exact mathematical theory developed by Yao and Sheng [3] into a practical computer-based, mathematical model. The model is of a generalized nature which uses accurate, rather than approximate, calculations.



## 2. ANGULAR PHASE MATCHING

### a. Phase Matching Theory.

Nonlinear optical interactions in bulk materials (e.g., harmonic generations, optical frequency mixings, and optical parametric interactions) usually require the technique of phase matching in acentric crystals to achieve high conversion efficiency. In the three-coupled-wave interaction, the conditions of energy and momentum conservation must be obeyed are written as follows:

$$\omega_3 = \omega_2 + \omega_1 \quad (1)$$

$$\vec{k}_3 = \vec{k}_2 + \vec{k}_1 + \Delta\vec{k} \quad (2)$$

where  $\omega$  and  $\vec{k}$  represent angular frequencies and wave vectors, respectively, associated with the three electromagnetic waves. Phase matching is achieved when  $\Delta\vec{k} = 0$ . Eqn (2) can be expressed by the following equation using refractive indices  $n$  for the respective frequencies:

$$\omega_3 n_3 \hat{i}_3 = \omega_2 n_2 \hat{i}_2 + \omega_1 n_1 \hat{i}_1 \quad (3)$$

where  $\hat{i}$  is the unit vector parallel to  $\vec{k}$ . The collinear phase matching condition requires that all three waves propagate in parallel, i.e.,  $\hat{i}_1 = \hat{i}_2 = \hat{i}_3$ , which reduces eqn (3) to the form:

$$\omega_3 n_3 = \omega_2 n_2 + \omega_1 n_1 \quad (4)$$

Eqn (4), written in terms of wavelength becomes:

$$\frac{n_3}{\lambda_3} = \frac{n_2}{\lambda_2} + \frac{n_1}{\lambda_1} \quad (5)$$

Phase matching is customarily realized by using the birefringent and dispersive properties of anisotropic crystals. Three types of phase matching are possible, in principle, in birefringent crystals with both uniaxial and biaxial characteristics. They are Type I, where  $\omega_1$  and  $\omega_2$  are of the same polarization, and Types II and III, where  $\omega_1$  and  $\omega_2$  are of orthogonal polarizations (see Figure 1). Types II and III phase matching differ in the selection of  $\omega_1$ . In Type III phase matching,  $\omega_1$  is smaller than  $\omega_2$ . As such,  $\omega_2$  will have larger eigenpolarization index differences than those seen by  $\omega_1$ . In general, this makes Type III phase matching more difficult to achieve. According to the Biot-Fresnel theorem [5], an optical wave propagating in a biaxial crystal with a wave vector  $\vec{k}(\theta, \phi)$  can be decomposed into two components with mutually perpendicular polarization directions denoted by  $e_1$  (slow ray) and  $e_2$  (fast ray), respectively. Beams polarized in these and only these directions will propagate in the  $\vec{k}(\theta, \phi)$  direction without change in polarization through the anisotropic crystal. But, as implied above, the two orthogonal polarizations do not, in general, have the same refractive index,  $n$ .

In uniaxial and biaxial crystals there exists a direction (one in the case of a uniaxial crystal and two for a biaxial crystal) in which the polarizations do have equal refractive indices. This direction is called the optic axis (see Figure 2). A uniaxial crystal is essentially a special case of a biaxial crystal so the discussion will continue for the biaxial case.

In biaxial crystals, the allowed polarization directions for a given direction of propagation are as follows. The spherical projection in Figure 2 is used to represent the directions inside the crystal. Let the direction of  $\vec{k}$  be that of light propagation, and OA and OB the two optical axes in the XZ plane. Spherical triangle AKB is obtained by drawing the great circle AK and BK on the sphere. Then the polarization direction of the optical wave whose velocity is lower than the other is that of the bisector of angle AKB, i.e., the direction of  $e_1$ . The faster ray is perpendicular to  $e_1$ , i.e., the direction of  $e_2$ . Hence the relation  $n^{e_1} > n^{e_2}$  is satisfied for both positive and negative biaxial crystals, where superscripts  $e_1$  and  $e_2$  indicate the polarization directions of the propagating waves. Note that these polarization directions lie on the surface of the sphere. These properties are usually called Biot-Fresnel's theorem. [5, 6].

The refractive-index for an optical wave of wavelength  $\lambda$  in a biaxial crystal satisfies:

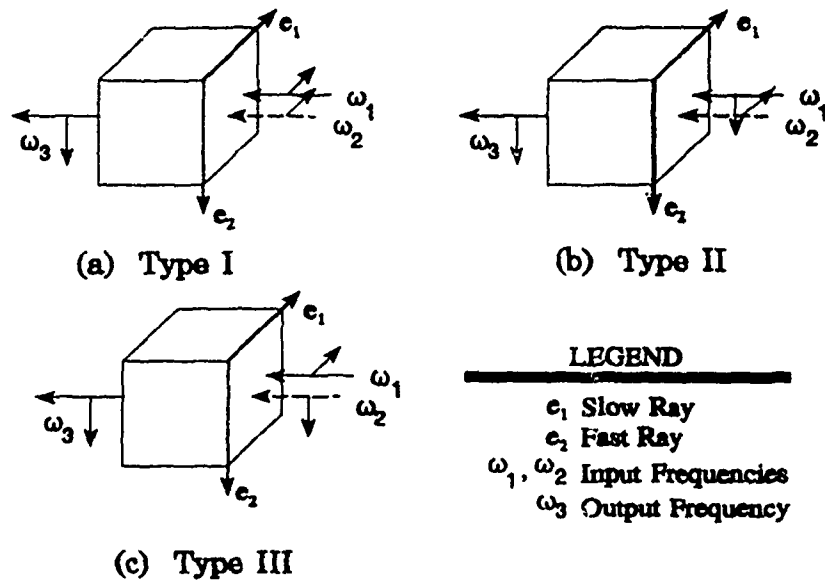


Figure 1. Phase Matching Types and Associated Polarizations

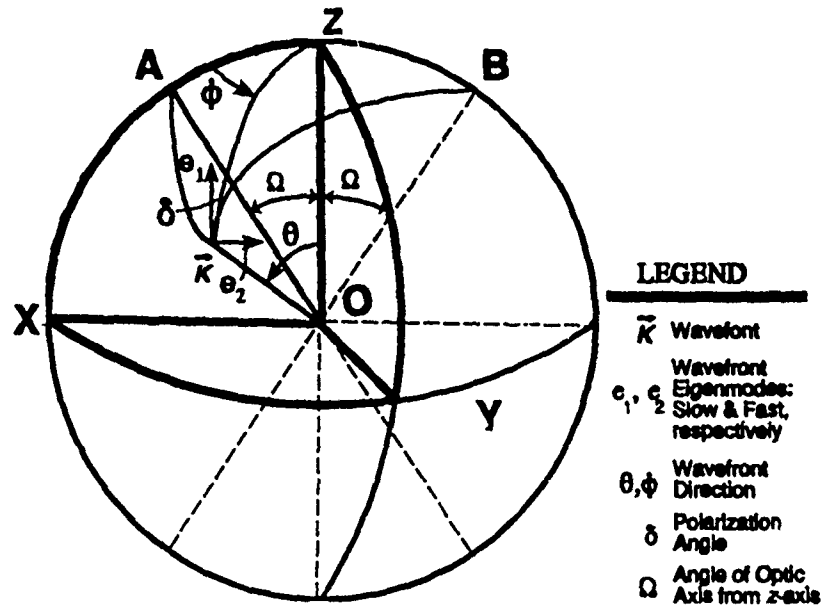


Figure 2. Spherical Projection Showing the Slow ( $e_1$ ) and Fast ( $e_2$ ) Eigenmodes of a Wavefront in a Biaxial Crystal

$$\frac{\sin^2\theta \cos^2\phi}{n^{-2} - n_x^{-2}} + \frac{\sin^2\theta \sin^2\phi}{n^{-2} - n_y^{-2}} + \frac{\cos^2\theta}{n^{-2} - n_z^{-2}} = 0 \quad (6)$$

where  $\theta$  (the angle from the z-axis) and  $\phi$  (the angle from the x-axis in the xy plane) together define the internal direction of the incident wave normal;  $n_x$ ,  $n_y$ , and  $n_z$  (the principal indices of refraction) are found using Sellmeier equations (which are obtained as a result of best fits to index versus  $\lambda$  measurements). Note: Figure 3 identifies the indicatrix ellipsoid for biaxial crystals in which the crystal indices have been defined as  $n_z > n_y > n_x$ . Rearranging eqn (6) into a form more easily handled and making the following substitutions (to increase readability):

$$x = n_{\omega}^{-2}, \quad a = n_{x,\omega}^{-2}, \quad b = n_{y,\omega}^{-2}, \quad c = n_{z,\omega}^{-2} \quad (7)$$

$$k_x = \sin^2\theta \cos^2\phi, \quad k_y = \sin^2\theta \sin^2\phi, \quad k_z = \cos^2\theta$$

we obtain:

$$x^2 + [-k_x^2(b+c) - k_y^2(a+c) - k_z^2(a+b)]x + (k_x^2bc + k_y^2ac + k_z^2ab) = 0 \quad (8)$$

The basic form of eqn (8) is  $x^2 + Bx + C = 0$ . Using the substitutions:

$$B = -k_x^2(b+c) - k_y^2(a+c) - k_z^2(a+b) \quad (9)$$

$$C = k_x^2bc + k_y^2ac + k_z^2ab$$

and reducing results in the following form:

$$n_{\omega} = \frac{\sqrt{2}}{\sqrt{-B \pm \sqrt{(B)^2 - 4C}}} \quad (10)$$

In eqn (9), the terms  $a$ ,  $b$ , and  $c$  are obtained from Sellmeier equations with the appropriate Sellmeier coefficients for a given wavelength (represented by " $\omega$ "), temperature (we used room temperature) and crystal. Eqn (10) is solved for each of the three wavelengths used in an optical parametric oscillator (OPO), optical parametric amplifier (OPA) or second harmonic generation (SHG) condition. The two real solutions are the index of refraction for the slow and fast rays. For the slow ray the index of refraction is represented by:

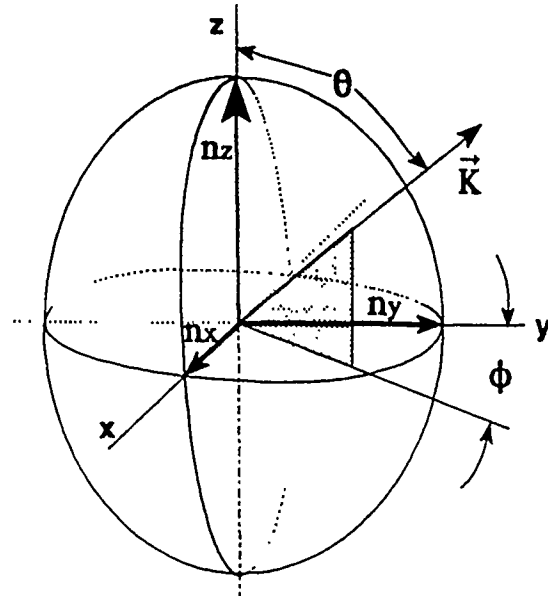


Figure 3. Dielectric Ellipsoid for a Biaxial Crystal with Wavefront

$$n_s = \frac{\sqrt{2}}{\sqrt{-B - \sqrt{(B)^2 - 4C}}} \quad (11)$$

and the fast ray's index of refraction is represented by:

$$n_f = \frac{\sqrt{2}}{\sqrt{-B + \sqrt{(B)^2 - 4C}}} \quad (12)$$

Of the six available wavelength dependent refractive index values for three-wave interactions, only three are suitable for determining phase match conditions. Table 1 indicates the appropriate slow and fast ray equation combinations which satisfy the necessary conservation of momentum condition. Note that Table 1 has a "+" or a "-" after the phase match type. This indicates a positive or negative nonlinear crystal for the associated phase matching type; this study only deals with positive nonlinear crystals. However, using Table 1 assignments for the eigenmodes of positive and negative crystals, the MathCad® phase matching worksheet (see Appendix A) easily handles negative nonlinear crystals without modification.

**Table 1.** Potentially Phase-Matchable Combinations of  $e_1$  and  $e_2$  Eigenmodes, Where  $\lambda_1 \geq \lambda_2 > \lambda_3$

Polz Type	SHG,SFM		DFM <sub>32</sub> , OPA <sub>32</sub>		DFM <sub>31</sub> , OPA <sub>31</sub>		OPO	
	In	Out	In	Out	In	Out	In	Out
	$\lambda_1, \lambda_2 \rightarrow \lambda_3$		$\lambda_3, \lambda_2 \rightarrow \lambda_1$		$\lambda_3, \lambda_1 \rightarrow \lambda_2$		$\lambda_3 \rightarrow \lambda_1, \lambda_2$	
I <sup>+</sup>	$e_1, e_1 \rightarrow e_2$		$e_2, e_1 \rightarrow e_1$		$e_2, e_1 \rightarrow e_1$		$e_2 \rightarrow e_1, e_1$	
I <sup>-</sup>	$e_2, e_2 \rightarrow e_1$		$e_1, e_2 \rightarrow e_2$		$e_1, e_2 \rightarrow e_2$		$e_1 \rightarrow e_2, e_2$	
II <sup>+</sup>	$e_2, e_1 \rightarrow e_2$		$e_2, e_1 \rightarrow e_2$		$e_2, e_2 \rightarrow e_1$		$e_2 \rightarrow e_2, e_1$	
II <sup>-</sup>	$e_1, e_2 \rightarrow e_1$		$e_1, e_2 \rightarrow e_1$		$e_1, e_1 \rightarrow e_2$		$e_1 \rightarrow e_1, e_2$	
III <sup>+</sup>	$e_1, e_2 \rightarrow e_2$		$e_2, e_2 \rightarrow e_1$		$e_2, e_1 \rightarrow e_2$		$e_2 \rightarrow e_1, e_2$	
III <sup>-</sup>	$e_2, e_1 \rightarrow e_1$		$e_1, e_1 \rightarrow e_2$		$e_1, e_2 \rightarrow e_1$		$e_1 \rightarrow e_2, e_1$	

**NOTES:**

- (1) For Birefringent Positive and Negative Crystals in the Appropriate Nonlinear Reporting Frame [4]
- (2) Eigenmodes  $e_1$  and  $e_2$  ("e" and "o" in the uniaxial limit) are the slow, fast eigenmodes for positive crystals and the fast, slow eigenmodes for negative crystals. Hence, fast and slow assignments for respective waves  $i = 1, 2, 3$  are identical for positive and negative crystals, and  $\lambda_3$  is always the fast eigenmode.

Solving the appropriate combinations of eqns (11) and (12) (identified in Table 1) provides two solutions in the form of an index of refraction value at a given  $\theta, \phi$  angle pair. For instance, for Type II OPO phase matching to exist (based upon the II\* line of Table 1), the following equation must be satisfied:

$$\frac{n_f(\lambda_3)}{\lambda_3} = \frac{n_f(\lambda_2)}{\lambda_2} + \frac{n_s(\lambda_1)}{\lambda_1} \quad (13)$$

One method useful in identifying the index of refraction equation combinations which provide a phase matching solution is the graphical method. The solutions to the wavelength dependent indices (see eqn (10)) are plotted over a range of  $\theta$  at a specific  $\phi$ . The initially chosen values of  $\phi$  are typically the start and end points of the  $xy$  plane (i.e.,  $\phi = 0^\circ$  or  $90^\circ$ ). The plot of the resulting solution set identifies any existing phase match condition—represented by the meeting/crossing point of the two plots (i.e., if a phase match condition exists then only one point in the solution “set” exists for which a combination of the applied wavelength’s fast and slow eigenmodes index of refraction is equal to the index of refraction for the generated wavelength (defined by eqn (13)). This method is explained further in the discussion below.

#### b. Description of the Computer-Based Equations.

See Appendix A for the worksheet listing. MathCad® 4.0, a Microsoft® Windows® application from MathSoft Inc., was used to develop the computer-based equations. We used MathCad® because it required a minimum of programming, was very flexible, and the worksheets developed were very easy to debug. MathCad® has proved a very powerful tool for our purposes.

The MathCad® 4.0 worksheet restricts the equations to the first quadrant when searching for a values of  $\theta$ . The resulting solutions are then plotted (i.e., the phase matched combination of the  $n_1/\lambda_1$  and  $n_2/\lambda_2$  terms is set equal to the associated  $n_3/\lambda_3$  curve). The resulting phase match angle pairs ( $\theta, \phi$ ) may then be used in the calculation of the effective nonlinear coefficients ( $d_{eff}$ ) for the desired range(s) and the associated walkoff angle(s).

##### Sellmeier Coefficients.

The worksheet reads the Sellmeier coefficients from a disk-based ASCII file. This file is composed of three rows of four columns. Each row represents the coefficients for the  $x$ ,  $y$ , and  $z$  axis, respectively. Each column represents the A, B, C, and D Sellmeier coefficients for the following form of the Sellmeier equation:

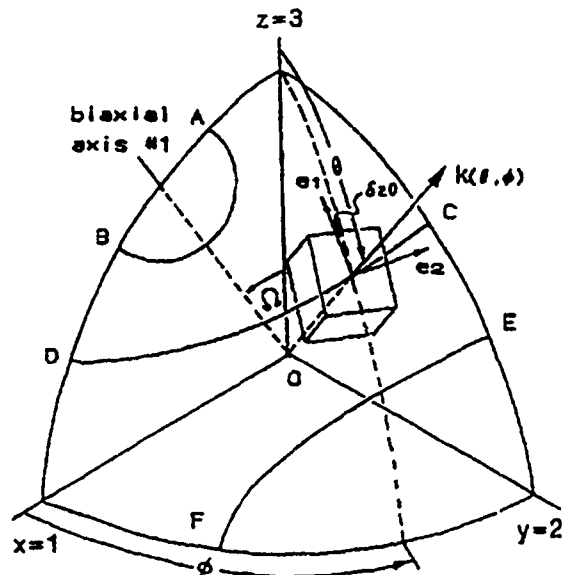


Figure 4. First Octant of a Proposed Positive Nonlinear Reporting Frame.

$$n_{axis}(\lambda) = \left( A + \frac{B}{1 - (C/\lambda)^2} - D \cdot \lambda^2 \right) \quad (14)$$

where *axis* represents the *x*, *y*, or *z* axis (the index of refraction for the axes  $n_x$ ,  $n_y$ , or  $n_z$ ) at the wavelength specified by " $\lambda$ ". MathCad reads the file of Sellmeier coefficients (see eqn A-1) into the variable *S* (defined as *S* := READPRN(*filename*), where *filename* is the name of the file containing the Sellmeier coefficients for the crystal being evaluated). NOTE: MathCad reads all data files from the same subdirectory to which the worksheet has been stored (or retrieved from), unless *filename* is an "associated" file (see MathCad documentation).

#### The Identification of the Three-Wavelengths.

The worksheet expects the user to identify two of the three wavelengths from which MathCad calculates the third. The user should ensure that the two wavelengths entered result in MathCad calculating a positive valued wavelength. See eqns A-3a through A-3c. Next, an assignment of the three wavelengths as  $\lambda_1$ ,  $\lambda_2$ , and  $\lambda_3$  is expected (see eqns A-3d through A-3f) so that  $\lambda_1 \geq \lambda_2 > \lambda_3$  (the results of the assignments are displayed immediately below each assignment).

#### Phase Matching Type Category.

Although the mathematics are essentially the same when calculating phase matching for SHG, OPA, or OPO cases, the worksheet (eqn A-4) provides the option (for those who so desire) to select from the following four categories: SHG/SFM, OPA-32/DFM-32, OPA-31/DFM-31, or OPO. The category selection is used by eqns A-11a through A-22f to identify the correct wavelength dependent index of refraction equations to use in the phase match solve block (see eqns A-13, A-14, and A-15) for Type I, II, and III phase matching. Note however, that only when it is time to calculate the nonlinear coefficient,  $d_{eff}$ , (see appendix B) must a category type actually be defined. See chapter 3 which deals with the calculation of  $d_{eff}$ .

#### Indices of Refraction.

The Sellmeier coefficient matrix, the variable *S* (see eqn A-1), is used by the Sellmeier equations (see eqns A-5a through A-5c) to calculate the indices of refraction for the crystal axes ( $n_x(\lambda)$ ,  $n_y(\lambda)$ , and  $n_z(\lambda)$ ) according to the wavelengths defined in eqns A-3d through A-3f. These values are stored in a matrix identified by the variable *n* (see eqn A-5d). This variable, *n*, is saved to disk in eqn A-5e: WRITEPRN(*filename*), where *filename* is the name of the file to which the matrix of axes indices of refraction is stored.

Modifications. If the Sellmeier equations provided are not appropriate (i.e., the point group is different, the Sellmeier equation form has been changed, etc), eqns eqns A-5a through A-5c must be modified accordingly. This is a simple edit and should be the only modification required.

#### Refractive-Index Equation.

The solution to eqn (6) is developed with eqns A-6a through A-8f. The solutions of the refractive-index equations are given by eqns A-9a through A-9f and represent the indices for the fast and slow rays for each of the three wavelengths. The wavelength dependent versions of these equations are given in eqn A-10a through A-10f. They are then arranged by eqn A-11a through A-12o into formats given in Table 1 for the various SHG, OPO, and OPA combinations.

### Phase Match Equations.

The first step in finding the appropriate phase matching equations is in defining the wavelength dependent refractive-index equations. These are arranged so that two ray solutions sets are set equal to a third solution set while watching the fast and slow ray conditions set by Table 1. Eqns A-11a through A-12o define the wavelength dependent indices while equations A-13 through A-15 define the appropriate equations to use in the phase match solve blocks as defined by the category (SHG, OPA, OPO, etc.) selected.

The phase match solutions are actually found by the solve blocks. Each solve block (a set of equations defining a solution) is composed of three parts: (1) the appropriate phase match equation (see eqns A-13a, A-14a, and A-15a), (2) the region in which to search for a phase match (this worksheet restricts that search to the first quadrant; see eqns A-13b, A-14b, and A-15b), and (3) the equation solution request command (i.e., FIND; see eqns A-13c, A-14c, and A-15c).

### Phase Match Angle/Type Determination.

Eqns A-16 through A-22f and Figures A-1a through A-2c are used to obtain and display the solutions to the phase matching equations.

To begin, we first determine if a solution set exists at the y-axis in the xy plane (i.e.,  $\phi = 90^\circ$ ). This location is chosen because, since  $n_x > n_y > n_z$ , if phase matching does not occur in the yz plane, it will not occur anywhere. Eqn A-17a sets the value of  $\phi$  to  $90^\circ$ , eqn A-17b sets the range of  $\theta$  (the angular range from the z-axis toward the y-axis) over which to search for a phase match angle, and eqn A-17c converts this angular range to radians (MathCad does trigonometric calculations in radians). Eqns A-18a through A-18f assign the wavelength dependent refractive-index equations defined in eqns A-11a through A-11f to variables for use in Figures A-1a through A-1c to graphically display the results. Type I phase matching equations use variables A and B (see eqns A-18a and A-18d, respectively), Type II phase matching uses variables C and D (see eqns A-18b and A-18d, respectively), and Type III phase matching uses variables E and F (see eqns A-18c and A-18f, respectively). When one line in any of the figures meets or crosses the other line, a phase match exists at that point for the associated phase match type.

The value of the variables A through F are shown above each figure. These displayed values are especially useful for when the two index of refraction curves appear close in value, but an actual phase match cannot be visually determined. There should be at least six digits displayed to the right of the decimal point to ensure correct identification of a phase match condition. A phase match condition exists when the lower number (indicated by variable B, D, and/or F) is equal to or larger than the upper number (indicated by variable A, C, and/or E).

Eqn A-19a through A-22f and Figures A-2a through A-2c are used to determine where phase matching each phase match type. These are the same equations and figures as described above, except for the following:

- Eqns A-19a through A-19c identify a discrete value of  $\phi$  at which to begin a phase match search (i.e., eqn A-19a identifies a  $\phi$  value for Type I, eqn A-19b identifies a  $\phi$  value for Type II, and eqn A-19c identifies a value of  $\phi$  for Type III). Eqn A-21 assigns the range of  $\theta$ , defined by eqns A-20a through A-20c, to the variable  $\theta$ .
- The values for eqns A-19a, A-19b, and A-19c are manually varied to locate the start of phase match region for each phase match type (for those phase match types for which a phase match region exists at  $\phi=90^\circ$  but not at  $\phi=0^\circ$ ).

The start of the phase match region found in eqns A-19a through A-19c is used by eqns A-23a, A-24a, and A-25a to define the phase matching ranges for Types I, II, and III, respectively. If a particular phase match type does not exist, the value of  $\theta$  for all values of  $\phi$  ( $0^\circ$  to  $90^\circ$ ) are automatically zeroed by eqns A-24b, A-24c, A-25b, and A-25c (Types II and III only, since, if Type I does not exist there is, by definition no phase matching at the selected wavelengths). *NOTE: MathCad may require manually zeroing a phase match region (i.e., eqn A-24c and/or A-25c) if it could not find a phase match for that phase match type.*

#### Saving the Phase Match Results.

Once phase match values within a region have been defined, they should be stored to disk for (1) easy access later and/or (2) for use by the worksheet which calculates the  $d_{eff}$  and walkoff angles. This is performed by eqns A-28a through A-29b. To aid in defining the data file, eqn A-27 identifies the phase match region for which the values will be defined. This should be set to a range of 0 to 90 to allow values of  $\phi$  over the entire  $xy$  plane. Eqn A-26 provides conversion of radians to degrees used by eqns A-28c, A-28e, A-28f, A-28h, and A-28i (the worksheet stores angle data to file in degree format, not radians). Eqns A-28a through A-28i define a value for each range index value (i.e., the integer value of  $\phi$ ). These values are then arranged into a data file by eqn A-29a. The data file should be 91 rows (0-90, as defined by eqn A-27) of 7 columns (in the following format:  $\lambda_1$ ,  $\lambda_2$ ,  $\lambda_3$ ,  $\phi$ ,  $\theta(I)$ ,  $\theta(II)$ , and  $\theta(III)$ , where the first 3 values are the 3 wavelengths used, the next value is the integer value of  $\phi$ , and the final 3 values are the  $\theta$  values for Type I, II, and III phase matching for the associated value of  $\phi$ ). The variable "data", eqn A-29a, is now a matrix of values which is written to disk by eqn A-29b. This equation is written as `WRITEPRN(filename) := data`, where *filename* is the file to which the values of the variable "data" will be written. Note that the first three columns of data each have identical numbers. This redundancy is required to allow writing the data as a single matrix with information which unambiguously identifies the data as belonging to a particular wavelength set.

#### Final Comments.

- (1) The value of  $\phi$  used by this study was necessarily restricted to integer values. This is fine for phase match regions which extend across the entire  $xy$  plane but insufficient for when  $0^\circ < \phi < 90^\circ$ . Therefore, the scratch pad region provided is useful for determining the value of  $\phi$  for where  $\theta$  approaches  $90^\circ$ . Specifically, the value of  $\phi$  is varied until the effective value of  $\theta$  is  $90^\circ$ . Note that the equation must be appropriate to the phase match type (I, II, or III) for which a value of  $\phi$  is desired for a  $\theta=90^\circ$ .
- (2) MathCad provides a method of converting between degrees and radians automatically by the *deg* function. However, since the *same* function is used to convert between the two, unless carefully used, the resulting conversion may not be as expected. Therefore, the worksheets define variables which perform the necessary conversion where confusion would most likely occur when using the MathCad conversion function.
- (3) Phase match calculations for positive or negative biaxial/uniaxial crystals are identical with the supplied worksheet. No modifications are necessary. Not until calculating the value of  $d_{eff}$  must the crystal type be identified. See paragraph 3.b.ii for additional information.



### 3. EFFECTIVE NONLINEAR COEFFICIENT, $d_{eff}$

#### a. Effective Nonlinear Coefficient Theory.

In a nonlinear medium, two electric fields with frequencies  $\omega_1$  and  $\omega_2$  give rise to induced polarizations at frequencies  $\omega_1 + \omega_2$  and  $\omega_1 - \omega_2$ . The energy conversion efficiency of a three-wave nonlinear process, such as SHG, is dependent upon the size of this induced polarization. The second-order polarization  $P(\omega_3)$ , induced by the interaction of two applied electric fields  $\vec{E}(\omega_2)$  and  $\vec{E}(\omega_1)$ , can be expressed by eqn (15), where:  $\hat{a}_i$ ,  $\hat{a}_j$ , and  $\hat{a}_k$  are the unit vector

$$\begin{aligned} P(\omega_3) &= \hat{a}_i \vec{d}_{ijk} \hat{a}_j \hat{a}_k |E(\omega_2)| |E(\omega_1)| \\ &= d_{eff} |E(\omega_2)| |E(\omega_1)| \end{aligned} \quad (15)$$

components of  $P(\omega_3)$ ,  $\vec{E}(\omega_2)$ , and  $\vec{E}(\omega_1)$ , respectively;  $\vec{d}_{ijk}$  is the second-order polarization tensor of the nonlinear crystal; and  $i, j$ , and  $k$  each represent the  $x, y$ , and  $z$  axes. The effective nonlinear coefficient is a function of the angular orientation, the crystal symmetry, and the values of the individual  $d_{ijk}$  components. The effective nonlinear coefficient is, thus, given by:

$$d_{eff} = \hat{a}_i \vec{d}_{ijk} \hat{a}_j \hat{a}_k \quad (16)$$

In a three-wave interaction process,  $d_{ijk}$  is equivalent to  $d_{ikj}$ , so that it can be expressed by a  $3 \times 6$  matrix (as  $d_{ij}$ ). For a more complete discussion on the second order polarization tensor see paragraph 5.b.

To calculate the effective nonlinear coefficient we need to calculate the values for the  $\hat{a}_i$ ,  $\hat{a}_j$ , and  $\hat{a}_k$  components. The value of  $d_{eff}$  is dependent upon the direction of the  $\vec{k}$  and since we know that  $\vec{D} \perp \vec{k}$  we will use the electric displacement vectors,  $\vec{D}_t(\omega_m)$  to calculate  $\hat{a}_i$ ,  $\hat{a}_j$ , and  $\hat{a}_k$ . The electric displacement vectors,  $\vec{D}_t(\omega_m)$ , where  $t = 1$  (slow rays) or  $t = 2$  (fast rays) for these two components, and their projections on the coordinate axis are represented by:

$$\vec{D}_i(\omega_m) = \hat{b}_i^m D_t(\omega_m) \quad (17)$$

where  $i = x, y$ , and  $z$ , and  $m = \lambda_1, \lambda_2$  and  $\lambda_3$  [3]. The slow ray ( $e_1$ ) unit vector is given by:

$$\begin{aligned} \hat{b}_{i,t=1}^m &= \begin{pmatrix} -\cos\theta \cos\phi \cos\delta_i^m + \sin\phi \sin\delta_i^m \\ -\cos\theta \sin\phi \cos\delta_i^m - \cos\phi \sin\delta_i^m \\ +\sin\theta \cos\delta_i^m \end{pmatrix} \\ &= \begin{pmatrix} b_{x,t=1}^m \\ b_{y,t=1}^m \\ b_{z,t=1}^m \end{pmatrix} \end{aligned} \quad (18)$$

and the fast ray,  $e_2$ , unit vector given by:

$$\begin{aligned}\hat{b}_{i,t=2}^m &= \begin{pmatrix} -\cos\theta \cos\phi \sin\delta_i^m - \sin\phi \cos\delta_i^m \\ -\cos\theta \sin\phi \sin\delta_i^m + \cos\phi \cos\delta_i^m \\ +\sin\theta \sin\delta_i^m \end{pmatrix} \\ &= \begin{pmatrix} b_{x,t=2}^m \\ b_{y,t=2}^m \\ b_{z,t=2}^m \end{pmatrix}\end{aligned}\quad (19)$$

where  $\delta_i^m$ , the polarization angle (formed between the two eigenmodes,  $e_1$  and  $e_2$ , and the  $zk$  plane) is expressed as a function of  $\theta$ ,  $\phi$ , and  $\Omega_i^m$  (see eqn (20) as well as Figure 2 and Figure 4). See references [4] and [6] for further details.

$$\delta_i^m = \arctan\left(\frac{\sin 2\phi \cos\theta}{\cot^2 \Omega_i^m \sin^2\theta + \sin^2\phi - \cos^2\theta \cos^2\phi}\right) * 0.5 \quad (20)$$

The angle  $\Omega_i^m$ , given by eqn (21) below, is the angle formed between one of the two biaxial optic axes and the  $z$ -axis (the optic axis is located  $\pm\Omega$  from the  $z$ -axis) in the  $xz$  plane [4]. The unit

$$\Omega_i^m = \pm \arcsin\left[\frac{n_z(\omega_m)}{n_y(\omega_m)} \cdot \left[\frac{n_y^2(\omega_m) - n_x^2(\omega_m)}{n_z^2(\omega_m) - n_x^2(\omega_m)}\right]^{1/2}\right] \quad (21)$$

vectors  $\hat{b}_i^m$  (eqns (18) and (19), respectively) denote polarizations of electric displacement  $\vec{D}$  for biaxial eigenmodes  $e_1$  and  $e_2$  (see Figure 2 and Figure 4) which are "e" and "o", respectively, in the uniaxial limits. In a principal-axis system,  $\vec{E}$  and  $\vec{D}$  are related as shown by eqn (22) below.

$$\begin{pmatrix} E_x \\ E_y \\ E_z \end{pmatrix} = \begin{pmatrix} 1/n_x^2 & 0 & 0 \\ 0 & 1/n_y^2 & 0 \\ 0 & 0 & 1/n_z^2 \end{pmatrix} \begin{pmatrix} D_x \\ D_y \\ D_z \end{pmatrix} \quad (22)$$

Thus, in general, the unit vectors for the electric fields' two polarization components are given by:

$$\begin{aligned}\vec{E}_i(\omega_m) &= \left[ \frac{(b_{x,t})^2}{n_1^4(\omega_m)} + \frac{(b_{y,t})^2}{n_2^4(\omega_m)} + \frac{(b_{z,t})^2}{n_2^4(\omega_m)} \right]^{1/2} \vec{D}_i(\omega_m) \\ &= P_i(\omega_m) \vec{D}_i(\omega_m)\end{aligned}\quad (23)$$

Denoting the unit vectors of  $\vec{E}_i(\omega_m)$  as  $\hat{a}_i(\omega_m) = \hat{a}_i^m$  we obtain eqn (24) — the unit vectors for the electric field polarization component:

$$\begin{aligned}\hat{a}_i(\omega_m) \equiv \hat{a}_i^m &= \frac{1}{E_i(\omega_m)} \begin{pmatrix} E_{x,t}(\omega_m) \\ E_{y,t}(\omega_m) \\ E_{z,t}(\omega_m) \end{pmatrix} \\ &= \frac{1}{P_i(\omega_m)} \begin{pmatrix} n_x^{-2}(\omega_m) b_{x,t} \\ n_y^{-2}(\omega_m) b_{y,t} \\ n_z^{-2}(\omega_m) b_{z,t} \end{pmatrix} = \begin{pmatrix} a_{x,t}^m \\ a_{y,t}^m \\ a_{z,t}^m \end{pmatrix}\end{aligned}\quad (24)$$

Multiplying these unit vectors together results in column vectors which define the pseudo-vectors to be used on the right side of eqn (16) below). Note:  $m$ ,  $n$ , and  $o$  represent the three wavelengths ( $\lambda_1$ ,  $\lambda_2$ , and  $\lambda_3$ ) involved [3, 4].

Equation (25) defines the electric field polarization column vector for Type I SHG phase matching (rays of the same polarization and frequency):

$$\{\hat{a}_{i=1}(\omega_m)\} \{\hat{a}_{i=1}(\omega_m)\} \equiv a_{i=1}^m a_{i=1}^m = \begin{pmatrix} (a_{x,t=1}^m)^2 \\ (a_{y,t=1}^m)^2 \\ (a_{z,t=1}^m)^2 \\ 2a_{y,t=1}^m a_{z,t=1}^m \\ 2a_{x,t=1}^m a_{z,t=1}^m \\ 2a_{x,t=1}^m a_{y,t=1}^m \end{pmatrix}\quad (25)$$

Equation (26) defines the electric field polarization column vector for Type I OPO phase matching (rays of the same polarization/different frequency):

$$\{\hat{a}_{t=1}(\omega_n)\} \{\hat{a}_{t=1}(\omega_o)\} \equiv a_{t=1}^n a_{t=1}^o = \begin{pmatrix} a_{x,t=1}^n a_{x,t=1}^o \\ a_{y,t=1}^n a_{y,t=1}^o \\ a_{z,t=1}^n a_{z,t=1}^o \\ a_{y,t=1}^n a_{z,t=1}^o + a_{z,t=1}^n a_{y,t=1}^o \\ a_{x,t=1}^n a_{z,t=1}^o + a_{z,t=1}^n a_{x,t=1}^o \\ a_{x,t=1}^n a_{y,t=1}^o + a_{y,t=1}^n a_{x,t=1}^o \end{pmatrix} \quad (26)$$

Equation (27) defines the electric field polarization column vector for Type II/III SHG phase matching (rays of different polarization/same frequency):

$$\{\hat{a}_{t=1}(\omega_m)\} \{\hat{a}_{t=2}(\omega_m)\} \equiv a_{t=1}^m a_{t=2}^m = \begin{pmatrix} a_{x,t=1}^m a_{x,t=2}^m \\ a_{y,t=1}^m a_{y,t=2}^m \\ a_{z,t=1}^m a_{z,t=2}^m \\ a_{y,t=1}^m a_{z,t=2}^m + a_{z,t=1}^m a_{y,t=2}^m \\ a_{x,t=1}^m a_{z,t=2}^m + a_{z,t=1}^m a_{x,t=2}^m \\ a_{x,t=1}^m a_{y,t=2}^m + a_{y,t=1}^m a_{x,t=2}^m \end{pmatrix} \quad (27)$$

Equation (28) defines the electric field polarization column vector for Type II/III OPO phase matching (different polarization and frequency):

$$\{\hat{a}_{t=1}(\omega_n)\} \{\hat{a}_{t=2}(\omega_o)\} \equiv a_{t=1}^n a_{t=2}^o = \begin{pmatrix} a_{x,t=1}^n a_{x,t=2}^o \\ a_{y,t=1}^n a_{y,t=2}^o \\ a_{z,t=1}^n a_{z,t=2}^o \\ a_{y,t=1}^n a_{z,t=2}^o + a_{z,t=1}^n a_{y,t=2}^o \\ a_{x,t=1}^n a_{z,t=2}^o + a_{z,t=1}^n a_{x,t=2}^o \\ a_{x,t=1}^n a_{y,t=2}^o + a_{y,t=1}^n a_{x,t=2}^o \end{pmatrix} \quad (28)$$

From these results we are able to obtain the general expressions for the effective nonlinear coefficients  $d_{eff}(I)$  and  $d_{eff}(II)$  for Types I and II phase matching, respectively, using the definition for  $d_{eff}$  from eqn (16) [3, 6]. Type III phase matching uses the  $d_{eff}(II)$  equation. Since the difference between Type II and III phase matching is that the polarizations for the two smaller frequencies are exchanged, we can inspect eqn (27) and note that  $\{\hat{a}_{t=1}(\omega_m)\} \{\hat{a}_{t=2}(\omega_m)\}$  is exactly

the same as  $\{\hat{a}_{i=2}(\omega_m)\} \{\hat{a}_{i=1}(\omega_m)\}$  or eqn (28) where we note that  $\{\hat{a}_{i=1}(\omega_n)\} \{\hat{a}_{i=2}(\omega_n)\}$  is exactly the same as  $\{\hat{a}_{i=2}(\omega_n)\} \{\hat{a}_{i=1}(\omega_n)\}$ . Therefore, a separate equation to calculate  $d_{eff}$  for Type III is unnecessary. Note, however, though the form is the same, the phase matching angles for Types II and III phase matching are NOT the same and there will be a different  $d_{eff}$  for each (e.g., see Figure E-8 and Figure E-9).

$$d_{eff}(I_{SHG}) = a_{i,t=2}^m d_{ijk} a_{j,t=1}^m a_{k,t=1}^m \quad (29)$$

$$d_{eff}(I_{OPO}) = a_{i,t=2}^m d_{ijk} a_{j,t=1}^n a_{k,t=1}^o \quad (30)$$

$$d_{eff}(II_{SHG}) = a_{i,t=2}^m d_{ijk} a_{j,t=1}^m a_{k,t=2}^m \quad (31)$$

$$d_{eff}(II_{OPO}) = a_{i,t=2}^m d_{ijk} a_{j,t=1}^n a_{k,t=2}^o \quad (32)$$

The subscripts i, j, and k each represent the x, y, and z axes. It should be noted that these equations are applicable in situations where  $\vec{E}$  is not necessarily perpendicular to  $\vec{k}$ .

b. **Description of the Computer-Based Equations.** See Appendix B for the worksheet listing.

i. Data Retrieval/Initialization.

This worksheet begins by reading the data to evaluate from three ASCII files. These files are the data file of phase match information (eqn B-1a), the 2<sup>nd</sup> order polarization tensor (i.e., the  $d_{ij}$  matrix; eqn B-1b), and the indices of refraction for the wavelengths identified by the first three columns of the data file (eqn B-1c). Note: the data file and the indices of refraction file must have been created for the same wavelength values. Next, the identification of the origin for matrices is identified as "0" (i.e., row 1, column 1 is identified as 0,0 while row 3, column 6, is identified as 2,5) by eqn B-2.

ii. Positive/Negative Nonlinear Crystal Identification.

It is extremely important to identify whether or not the crystal being evaluated is positive or negative. Improper identification of the type of crystal may result in  $d_{eff}$  values which exactly opposite that expected at a given location (i.e., a maximum  $d_{eff}$  rather than an expected minimum). Identifying the positive or negative crystal type is performed by eqn B-3.

iii. Angle.

Eqn B-4 identifies the angle  $\phi$  for which a phase match  $\theta$  counterpart is desired. The angle pair  $(\theta, \phi)$ , when found, is used to calculate the associated  $d_{eff}$  and walkoff at that point.

iv. Wavelengths.

The three wavelengths values are parsed from the retrieved data file and assigned to variable  $\lambda_1$ ,  $\lambda_2$ , and  $\lambda_3$  by eqns B-5a through B-5d. Note that each row of the data file matrix begins with the first three columns being the wavelengths at which the data was collected.

v. Phase Match Angles.

The phase match angles for Type I, II and III phase matching are also parsed from the data file by eqns B-6a through B-6c, respectively. For proper analysis to proceed, the worksheet must know which phase match type to use for subsequent calculations. For this purpose, the value of eqn B-7a is manually set to "1," "2," or "3." Eqn B-7b then takes that number and identifies the associated phase match type matrix (I, II, or III). This identification is used by eqns B-7c and B-7e to assign values for  $\theta$  and  $\phi$ , respectively. These assigned values are redefined specifically as  $\theta$  and  $\phi$  by eqns B-7d and B-7f, respectively. These are the assignments used by the equations which follow. Eqn B-8 selects the desired category type (SHG/SFM, OPA/DFM or OPO) for which calculations are desired. Note that if the first two wavelengths are equal the worksheet automatically selects category 1 (i.e., SHG) regardless of the category manually selected.

vi. Miscellaneous.

Eqns B-9 through B-16 are discussed in the theory (see chapters 2 and 3) above. In short, however, the following is calculated:

- (1) Eqn B-9 calculates the value of  $\Omega$  (the angle from the z-axis to the optic axis).
- (2) Eqn B-10a is used by eqn B-10c which calculates the value of  $\delta$  (the polarization angle formed by the direction of the slow ray,  $e_1$ , with respect to the surface of the plane formed by the wavefront vector,  $\vec{k}$ , and the z-axis). We've arbitrarily restricted the value of  $|\delta_i|$  to  $\leq 90^\circ$ . The sign of  $\delta$  is the same as that given by the numerator in eqn B-10a. Therefore, when the value of the numerator in eqn B-10a is less than zero, a value of  $\pi$  is added to the value of  $\text{atan}(\tan(2\delta))$  before halving it to get the correct  $\delta_i$ . This is done by eqn B-10b.
- (3) Eqns B-11a through B-11l are setup for Eqns B-11m and B-11n which calculate the electric displacement unit vectors for the slow rays and the fast rays, respectively.
- (4) Eqn B-12 calculates the electric field polarization components.
- (5) Eqns B-13a and B-13b calculate the unit vectors for the polarization components of the electric fields for the slow rays and fast rays, respectively.
- (6) Eqns B-14a through B-14c identify the proper columns of eqns B-13a and B-13b to use when calculating the values of  $a_i$  (polarization unit vector for the "generated" wavelength),  $a_j$ , and  $a_k$  (polarization unit vectors for the "applied" wavelengths).
- (7) Eqns B-15a and B-15d identify the polarization unit vectors  $a_i$ ,  $a_j$ , and  $a_k$ .
- (8) Eqns B-16a and B-16b identify the fast and slow column vectors,  $a_{jk}$  (a.k.a., pseudo-vectors). Eqn B-16c selects the appropriate column vector, based upon the phase match type selected, to multiply with the second order polarization tensor,  $d_{ij}$ .

vii. Calculating the Effective Nonlinear Coefficient,  $d_{eff}$ .

- (1) The calculation for SHG/SFM and OPO  $d_{eff}$  results in exactly the value. Also, the calculation for  $d_{eff}$  for OPA-32 results in the same value as for OPA-31. However, if the same

wavelengths used for SHG/SFM or OPO are used to calculate  $d_{eff}$  for an OPA case, the  $d_{eff}$  will be different. Therefore, it is important to ensure that the proper category is selected.

(2) Eqn B-17 calculates phase match type (i.e., I, II, or III)  $d_{eff}$ .

viii. Saving the Resulting Calculations. The data associated with the  $d_{eff}$  and walkoff angle calculations are compiled into a single row matrix. This matrix is composed of the three wavelengths used, the phase match angles ( $\theta, \phi$ ), the  $d_{eff}$  value, and the walkoff angles (for the discussion on walkoff angles see chapter 4) for the phase match type for which this data was calculated.

Eqn B-19a provides a variable for converting from radians to degrees. Eqns B-19b through B-19d selects the correct fast or slow walkoff angle for wavelengths  $\lambda_1$ ,  $\lambda_2$ , and  $\lambda_3$ . The matrix is assigned to the variable "data" (eqn B-20a) which can then be used to append to an existing matrix file (as an additional row of data). This equation (eqn B-20b), `APPENDPRN(filename) := data`, defines *filename* as the file to which to append the data, and *data* is the variable containing the single row matrix of data described above.

#### 4. WALKOFF ANGLE

##### a. Theory for the Walkoff Angle Calculations.

The walkoff angle of a light wave in a nonlinear crystal is the angle between the wave vector  $\vec{k}$  and the Poynting vector  $\vec{S}$ . It is, therefore, also the angle between the electric field  $\vec{E}$  and the electric displacement vector  $\vec{D}$  [3]. See Figure 5 below. To illustrate, consider the following which says that the magnitude of the electric field is the same as the magnitude of the electric displacement vector times the electric field polarization.

$$|E| = P |D| \quad (33)$$

where:

$$P = \left( \sum_i \frac{b_i^2}{n_i^4} \right)^{1/2} \quad (34)$$

where  $i = x, y, \text{ and } z$ ;  $b_i$  is a unit vector component of the electric displacement vector for the slow and fast rays (see eqns (18) and (19)); and  $n_i$  is index of refraction for each crystal axis for a given material. Since the following relationship is true by definition of the dot product,

$$\cos \rho = \frac{\vec{E} \cdot \vec{D}}{|\vec{E}| |\vec{D}|} \quad (35)$$

and the fact that  $\vec{E} \perp \vec{S}$  and  $\vec{D} \perp \vec{k}$ , finding the angle between the wave vector and the Poynting vector is the same as finding the angle between the electric field and the electric displacement vector. Now, let  $E_i = |E| a_i$ . And, using eqns (17) and (23), we can say:

$$\vec{E} \cdot \vec{D} = \sum_i (|E| a_i) (|D| b_i) \quad (36)$$

which leads to:

$$\begin{aligned} \vec{E} \cdot \vec{D} &= |E| |D| \sum_i \frac{1}{P} \frac{b_i}{n_i^2} b_i \\ &= \frac{|E| |D|}{P} \sum_i \frac{b_i^2}{n_i^2} \end{aligned} \quad (37)$$

and therefore we get:

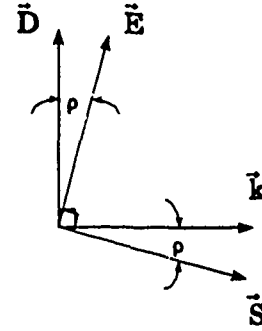


Figure 5. Relationship Between  $\vec{E}$ ,  $\vec{k}$ ,  $\vec{S}$ , and  $\vec{D}$



$$\frac{\vec{E} \cdot \vec{D}}{|\vec{E}| |\vec{D}|} = \left( \sum_i \frac{b_i^2}{n_i^2} \right) / \left( \sum_i \frac{b_i^2}{n_i^2} \right)^{1/2} \quad (38)$$

Now, using eqn (35), we reduce eqn (38) to a trigonometric equation:

$$\cos \rho = \left( \sum_i \frac{b_i^2}{n_i^2} \right) / \left( \sum_i \frac{b_i^2}{n_i^2} \right)^{1/2} \quad (39)$$

which reduces to:

$$\rho = \arccos \left[ \left( \sum_i \frac{b_i^2}{n_i^2} \right) / \left( \sum_i \frac{b_i^2}{n_i^2} \right)^{1/2} \right] \quad (40)$$

which is the form used in eqn (41) (the form used in the MathCad worksheet) below. Consequently, the walkoff angles of the light waves polarizing in  $e_i$ , (where  $i = 1$  or  $i = 2$ ) in a nonlinear crystal can generally be expressed as [3]:

$$\rho_i^m = \arccos \left[ \frac{\left( \frac{b_{x,i}^m}{n_x(\omega_m)^2} \right)^2 + \left( \frac{b_{y,i}^m}{n_y(\omega_m)^2} \right)^2 + \left( \frac{b_{z,i}^m}{n_z(\omega_m)^2} \right)^2}{\left[ \left( \frac{b_{x,i}^m}{n_x(\omega_m)^2} \right)^2 + \left( \frac{b_{y,i}^m}{n_y(\omega_m)^2} \right)^2 + \left( \frac{b_{z,i}^m}{n_z(\omega_m)^2} \right)^2 \right]^{1/2}} \right] \quad (41)$$

#### b. Use of the Computer-Based Equations.

See Appendix B for the listing. Eqn B-23 calculates the walkoff angles for the slow and fast rays. The calculation is straight forward and requires no explanation beyond that described in the theory above. There are no user modifications, additions, or changes required. However, as in the case of the calculation of  $d_{eff}$ , the proper data files must be retrieved and the phase match type (I, II, or III) must be identified. See paragraph 3.b for more information on data retrieval and initialization within MathCad.

## 5. LINEAR AND NONLINEAR PROPERTIES OF KTP ISOMORPHS.

### a. List of Properties Used in Calculations.

Table 2 and Table 3 summarize the Sellmeier coefficients and nonlinear coefficients of the KTP isomorphs, respectively. All calculations in the phase matching and  $d_{eff}$ /walk-off MathCad worksheets use the information supplied by these tables. Phase matching curves derived for these isomorphs are qualitative for wavelengths longer than 1.15  $\mu\text{m}$  because of less experimental testing.

**Table 2. Sellmeier Coefficients of KTP Isomorphs**

Axis	KTP	RTP	KTA	RTA	CTA
$A_x$	2.11460	2.15559	2.11055	2.22681	2.34498
$B_x$	0.89188	0.93307	1.03177	0.99616	1.04863
$C_x$	0.20861	0.20994	0.21088	0.21423	0.22044
$D_x$	0.01320	0.1452	0.01064	0.01369	0.01483
$A_y$	2.15180	2.38494	2.38888	1.97756	2.74440
$B_y$	0.87862	0.73603	0.77900	1.25726	0.70733
$C_y$	0.21801	0.23891	0.23784	0.20448	0.26033
$D_y$	0.01327	0.01583	0.01501	0.00865	0.01526
$A_z$	2.31360	2.27723	2.34723	2.28779	2.53666
$B_z$	1.00012	1.11030	1.10111	1.20629	1.10600
$C_z$	0.23831	0.23454	0.24016	0.23484	0.24988
$D_z$	0.01679	0.01995	0.01739	0.01583	0.01711
<p><i>Sellmeier coefficients of best fit to index data, with</i>  <math>n_i^2 = A_i + (B_i / [1 - (C_i / \lambda)^2]) - D_i^2</math>, where <math>i = x, y</math>, and <math>z</math>, respectively  (corresponding to the crystallographic axes <math>a, b</math> and <math>c</math>.) [7]</p>					

**Table 3. Nonlinear Optical Properties of KTP Isomorphs**

$d_{ij}$	KTP	RTP <sup>†</sup>	KTA	RTA <sup>†</sup>	CTA <sup>†</sup>
$d_{33}$	16.9	17.1	16.2	15.8	18.1
$d_{32}$	4.4	4.1	4.2	3.8	3.4
$d_{31}$	2.5	3.3	2.8	2.3	2.1
$d_{24}$	3.6	3.6	1.7 x $d_{15}$ of KTP @ 1.3 $\mu$ m	3.6	3.6
$d_{15}$	1.9	1.9	1.2 x $d_{15}$ of KTP @ 1.3 $\mu$ m	1.9	1.9
<p>SHG <math>d_{ij}</math> coefficients at 1.064 <math>\mu</math>m (in pm/V; experimental uncertainties: <math>\pm 10\%</math> for <math>d_{33}</math>, <math>d_{24}</math>, and <math>d_{15}</math>; <math>\pm 20\%</math> for <math>d_{32}</math> and <math>d_{31}</math> [7])</p> <p><sup>†</sup> <math>d_{15}</math> and <math>d_{24}</math> were not measured by Cheng, Cheng, and Bierlein (see reference [7]) — so the KTP value was used here. However, they did state that within experimental errors, there is no detectable variation of the <math>d</math> coefficients among the isomorphs</p>					

**b. Nonlinear ( $d_{ijk}$ ) Coefficients.**

**i. Basic Tensor Background.**

Eqn (15), shown again as eqn (42), represents the nonlinear (2nd order) polarization. Since no physical significance can be attached to an exchange of  $E_{\omega_1}$  and  $E_{\omega_2}$  it follows that  $d_{ijk} = d_{ikj}$ .

$$P(\omega_3) = d_{eff} |\vec{E}(\omega_1)| |\vec{E}(\omega_2)| \quad (42)$$

This means we can replace the subscripts  $kj$  by a single symbol (e.g.,  $kj$  may be represented by only  $j$  term without any loss of information or accuracy) according to the contraction:

$$\begin{aligned} xx = 1 \quad yy = 2 \quad zz = 3 \\ yz = zy = 4 \quad xy = zx = 5 \quad xy = yx = 6 \end{aligned}$$

The resulting  $d_{ij}$  tensor forms a  $3 \times 6$  matrix (down from a multidimensional  $3 \times 3 \times 3$  array that operates on the  $E^2$  column tensor to yield  $P$  according to eqn (43). The contracted  $d_{ij}$  tensor obeys the same symmetry restrictions as the  $d_{ijk}$  tensor, and in crystals of a given point-group symmetry it has the same form. [9]

$$\begin{pmatrix} P_x \\ P_y \\ P_z \end{pmatrix} = \begin{pmatrix} d_{11} & d_{12} & d_{13} & d_{14} & d_{15} & d_{16} \\ d_{21} & d_{22} & d_{23} & d_{24} & d_{25} & d_{26} \\ d_{31} & d_{32} & d_{33} & d_{34} & d_{35} & d_{36} \end{pmatrix} \begin{pmatrix} E_x^2 \\ E_y^2 \\ E_z^2 \\ 2E_xE_y \\ 2E_xE_z \\ 2E_yE_z \end{pmatrix} \quad (43)$$

## ii. Tensor Matrix for KTP Isomorphs.

The KTP family of crystals belongs to a noncentrosymmetrical class called *orthorhombic*. In that class, the nonlinear optical tensor is of class *mm2*. It has the form shown in Figure 6. The symbol "•" indicates a zero modulus and "●" indicates a nonzero modulus. Notice that according to the given form, KTP has five nonzero  $d$  coefficients:  $d_{33}$ ,  $d_{32}$ ,  $d_{31}$ ,  $d_{24}$ , and  $d_{15}$ . The coefficient  $d_{33}$  is approximately 9 times greater in magnitude than the diagonal coefficients ( $d_{15}$  and  $d_{24}$ ) whose values are within a factor of two of each other. The effective nonlinearity for Type II (or Type III) in the principal planes is given by Table 4 below (note: for this to be true,  $\vec{E}$  must be parallel to  $\vec{D}$ ).

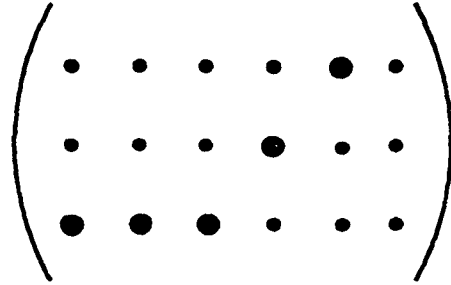


Figure 6. An *mm2* Crystal Class Tensor Arrangement.

Table 4. Effective Nonlinearity for Type II SHG in the Principal Planes

PLANE	$d_{eff}$
x-z	$d_{24} \sin\theta$
y-z	$d_{15} \sin\theta$
x-y	$d_{15} \sin^2\phi + d_{24} \cos^2\phi$

Thus, the larger  $d_{33}$  coefficient has only a very minor influence on the magnitude of  $d_{eff}$ . Also, since  $d_{24}$  is greater than  $d_{15}$ , Type II/III phase matching is generally more efficient in the xz plane than in the yz plane [7].

## c. Caveats.

No study is complete without identifying baselines used to obtain or calculate data. A number of assumptions were made in this study because of the newness of the crystals being studied and because of the controversy surrounding certain values of those crystals.

i. *d*-Coefficients.

The isomorph *d*-values used are the most recent available at this writing (see Reference [7]). Only the values for KTP and KTA are well-known, although still apparently not fully agreed upon. These values, supported by [10], result in a  $d_{eff}$  which is roughly half of earlier reported values. The  $d_{15}$  and  $d_{24}$  values for RTP, RTA, and CTA were not known (or published) at the time of this writing so the associated values for KTP were substituted. For this reason, the results calculated for those crystals may slightly differ from their true values. However, according to [7], within experimental error there is no detectable variation of the *d* coefficients among the isomorphs. Further study is required.

ii. Miller's Rule.

Miller showed that although nonlinear coefficients may vary considerably among nonlinear crystals, a parameter ( $\Delta_{ijk}$ ) relating the nonlinear and linear optical susceptibilities is constant to within an order of magnitude. This constant is defined by eqn (44) [11, 12]:

$$\Delta_{ijk} = \frac{d_{ijk}}{\epsilon_0 [n_i^2(\omega_3) - 1] [n_j^2(\omega_2) - 1] [n_k^2(\omega_1) - 1]} \quad (44)$$

The values of  $n_i$ ,  $n_j$ , and  $n_k$  represent the indices of refraction along the principal axes. Experimental values for  $d_{ijk}$  used in this study were at the "base" 3-wave interaction of 1.064  $\mu\text{m}$  SHG [7]. Adjustments to the *d*-values for use at other wavelengths are made by application of Miller's Rule. The following background information should help considerably in properly applying Miller's Rule.

As stated in paragraph 5.b above, the  $d_{ij}$  tensor is a contracted form of a multidimensional set of 3x3x3 matrices ( $d_{ijk}$ ). The resulting form (identified in Figure 6) is displayed in eqn (45) below with the tensor matrix identification. This form identifies the correct indices of refraction to use

$$d_{ij} = \begin{pmatrix} xxx & xyy & xzz & xyz & xxz & xxy \\ yxx & yyy & yyz & yyz & yxz & yxy \\ zxx & zyy & zzz & zyz & zxz & zxy \end{pmatrix} \quad (45)$$

when applying Miller's Rule. Therefore, the five nonzero *d*-values for KTP and its isomorphs are more correctly identified as:  $d_{15} = d_{xxz}$ ,  $d_{24} = d_{yyz}$ ,  $d_{31} = d_{zzx}$ ,  $d_{32} = d_{zyy}$ , and  $d_{33} = d_{zzz}$ . In applying this information, note that the first value indicates that the refractive index value of the identified axis at  $\omega_3$  (the calculated wavelength, i.e.,  $\omega_3 = \omega_2 + \omega_1$ ), the second value is for the refractive index value of the identified axis at  $\omega_2$ , and the same thing applies for  $\omega_1$ . Also, note that the indices of refraction at a specific wavelength are applied according to  $\omega_3 \leq \omega_2 < \omega_1$ . Each letter in the tensor matrix values identifies the axis of the appropriate index of refraction. NOTE: because  $d_{ijk} = d_{ikj}$ , the last two indices of refraction may be exchanged without changing the value

of  $d_{ij}$  (e.g.,  $d_{15} = d_{xx}$  or  $d_{15} = d_{xx}$ ). For example, in applying Miller's Rule to calculate  $\Delta_{15}$  for  $d_{15}$ , eqn (44) would appear as follows:

$$\Delta_{15} = \frac{d_{15}}{\epsilon_0 \cdot (n_x^2(\omega_3) - 1) \cdot (n_x^2(\omega_2) - 1) \cdot (n_z^2(\omega_1) - 1)} \quad (46)$$

To obtain the corrected  $d_{ij}$   $d$ -value at the new wavelengths, eqn (44) is rearranged as:

$$d_{ijk} = \Delta_{ijk} \epsilon_0 [n_i^2(\omega_3) - 1] [n_j^2(\omega_2) - 1] [n_k^2(\omega_1) - 1] \quad (47)$$

Taking Miller's Rule into account for SHG in KTP of 1.064  $\mu\text{m}$  fundamental input (the three-wave interaction for which the  $d$ -values of KTP are given) and making adjustments to  $d$ -values at the SHG and OPO wavelengths used in this study, we obtained the data presented in Table 5 below.

Miller's Rule corrections to (1.064/1.064/0.532  $\mu\text{m}$ )  $d$ -values for the other interactions considered represent changes of 22% or less. However, since a considerable amount controversy exists as to exactly what are the true values of  $d$  and experimental measurements are only good to 10-20%, the importance of Miller's Rule is considerably minimized. Therefore, Miller's Rule corrections were not used in this study.

**Table 5. Miller's Rule Applied to 1.064  $\mu\text{m}$  KTP  $d$  Values**

KTP	Wavelengths (μm)				d-value Uncertainty Range (pm/V)	Experimental Uncertainty [7]
	1.064/1.064/ 0.532	1.35/1.35/ 0.675	4.043/1.444/ 1.064	3.17/1.60/ 1.064		
	d (pm/V)					
d <sub>33</sub>	16.9	15.72	13.25	13.87	15.2-18.7	±10%
d <sub>32</sub>	4.4	4.11	3.51	3.66	4.0-4.8	±10%
d <sub>31</sub>	2.5	2.34	2.00	2.08	2.3-2.8	±10%
d <sub>24</sub>	3.6	3.39	2.88	3.01	2.9-4.3	±20%
d <sub>15</sub>	1.9	1.79	1.53	1.60	1.5-2.3	±20%

### iii. Sellmeier Coefficients.

There is a difference in the Sellmeier coefficients depending upon whether KTP was flux or hydrothermally grown. This fact could have a small impact upon the phase matching results. The same situation might also apply to the KTP isomorphs.

## 6. ISOMORPH COMPARISONS

### a. Introduction.

The interacting frequencies (wavelengths) considered for this study were of interest for on-going in-house experiments. Second harmonic (SHG) calculations used 1.064 and 1.35  $\mu\text{m}$  as the fundamental wavelengths since these are commonly available Nd-laser wavelengths. Optical parametric oscillator (OPO) calculations considered 1.064  $\mu\text{m}$  as the pump wavelength, 1.444 and 1.60  $\mu\text{m}$  as the signal wavelengths, and 4.043 and 3.17  $\mu\text{m}$  as the idler wavelengths, respectively. These wavelengths were chosen because of current investigations using OPO and DFM to generate mid-infrared wavelength laser sources.

### b. Phase Matching Characteristics.

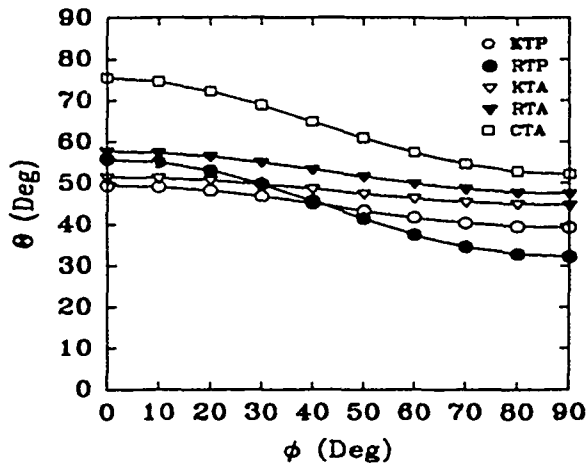
The range over which phase matching is possible for the four three-wave interactions is shown in tabular form in Appendix C. Plots of phase matching are shown in Figure 7 through Figure 15. Calculations were made at  $1^\circ$  intervals of  $\phi$ ; the symbols are shown every  $10^\circ$  for labeling. All plots show a decrease in  $\theta$  with an increasing  $\phi$ . The overall change in  $\theta$  over the available phase match range is given by the value  $\Gamma$ . Clearly a value of  $\Gamma = 0$  indicates a uniaxial case. Thus, this value is an indicator of how close to uniaxial each biaxial crystal is over a given phase match region. Table 6 through Table 10 summarize the angular phase matching ranges.

#### i. Second Harmonic Generation.

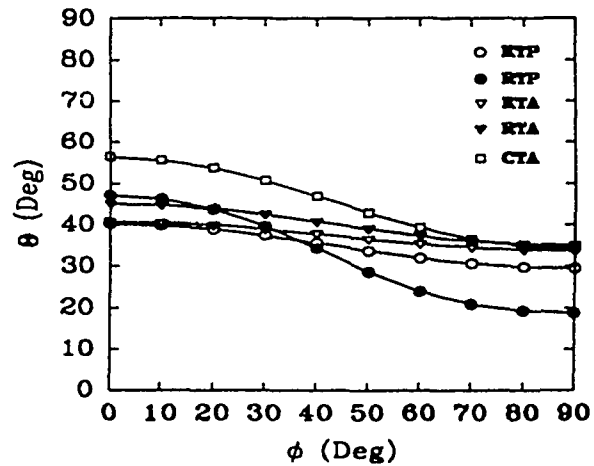
(1) Type I. Figure 7 and Figure 8 show Type I SHG phase matching for the KTP isomorphs. Type I phase matching is possible with all isomorphs throughout the  $\phi$ -angle range. RTP and CTA have much greater  $\Gamma$ 's than the other isomorphs by approximately factors of 3 and 2.5, respectively.

Table 6. Type I SHG Variations in  $\theta$

Crystal (Type I SHG)	1.064/1.064/0.532		1.35/1.35/0.675	
	Range of $\theta$	$\Gamma$	Range of $\theta$	$\Gamma$
KTP	49.41° - 39.20°	0.11	40.25° - 29.57°	0.12
RTP	55.83° - 32.17°	0.30	47.12° - 18.82°	0.31
KTA	51.47° - 44.69°	0.08	40.76° - 33.79°	0.08
RTA	57.66° - 47.48°	0.11	45.08° - 35.06°	0.11
CTA	75.50° - 52.22°	0.25	56.37° - 34.26°	0.25



**Figure 7.** SHG Phase Matching, Type I, 1.064/1.064/0.532  $\mu\text{m}$ .



**Figure 8.** SHG Phase Matching, Type I, 1.35/1.35/0.675  $\mu\text{m}$ .

(2) Type II. Figure 9 and Figure 10 show Type II SHG phase matching curves. None of the three arsenate isomorphs exhibited Type II phase matching for SHG using 1.064  $\mu\text{m}$  at any orientation. Even the phosphates had a limited range of  $\phi$  angles at 1.064  $\mu\text{m}$ . At 1.35  $\mu\text{m}$ , SHG Type II phase matching was more easily achieved with all five isomorphs phase matchable and only CTA having a restricted  $\phi$  range.

**Table 7.** Type II SHG Variation in  $\theta$

Crystal (Type II SHG)	1.064/1.064/0.532		1.35/1.35/0.675	
	Range of $\theta$	$\Gamma$	Range of $\theta$	$\Gamma$
KTP	90.00° - 68.67°	0.33	49.11° - 39.42°	0.11
RTP	90.00° - 64.62°	0.53	65.95° - 43.91°	0.24
KTA	-----	---	67.67° - 54.67°	0.08
RTA	-----	---	70.40° - 59.73°	0.12
CTA	-----	---	90.00° - 72.04°	0.49

(3) Type III. For SHG phase matching purposes, this type is exactly the same as Type II since the two input photons have the same wavelength. As soon as the degeneracy is lifted though, they become different and this will become significant for the OPO calculations discussed below.



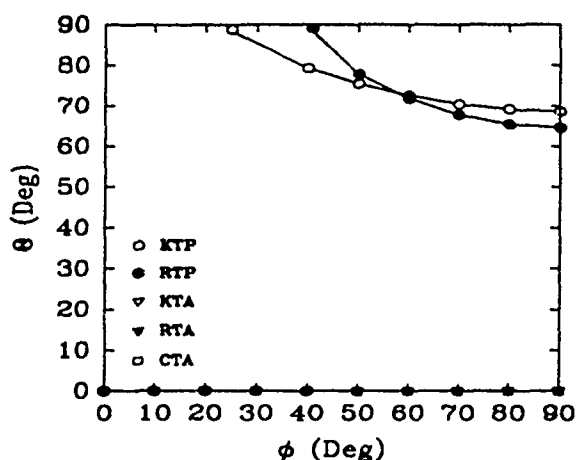


Figure 9. SHG Phase Matching, Type II/III, 1.064/1.064/0.532  $\mu\text{m}$ .

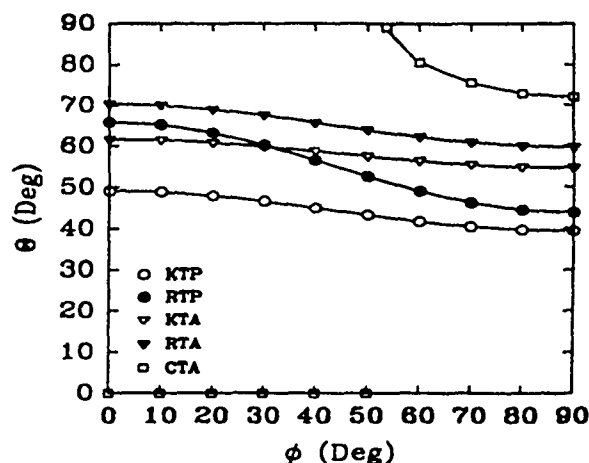


Figure 10. SHG Phase Matching, Type II/III, 1.35/1.35/0.675  $\mu\text{m}$ .

## ii. Optical Parametric Oscillator.

(1) Type I. Figure 11 shows Type I phase matching for an OPO pumped at 1.064  $\mu\text{m}$  with 1.444  $\mu\text{m}$  signal and 4.043  $\mu\text{m}$  idler wavelengths. Figure 12 shows the phase matching results for the 1.60  $\mu\text{m}$  signal and 3.17  $\mu\text{m}$  case. Like the SHG results, Type I phase matching is possible for all isomorphs at all  $\phi$  angles.

Table 8. Type I OPO Variation in  $\theta$

Crystal (Type I OPO)	4.043/1.444/1.064 $\mu\text{m}$		3.17/1.60/1.064 $\mu\text{m}$	
	Range of $\theta$	$\Gamma$	Range of $\theta$	$\Gamma$
KTP	39.24° - 29.06°	0.11	37.62° - 27.03°	0.12
RTP	47.61° - 19.74°	0.32	45.85° - 15.77°	0.33
KTA	37.30° - 32.98°	0.05	35.95° - 30.92°	0.06
RTA	41.94° - 27.80°	0.16	40.35° - 26.65°	0.15
CTA	53.80° - 29.52°	0.28	51.89° - 26.41°	0.24

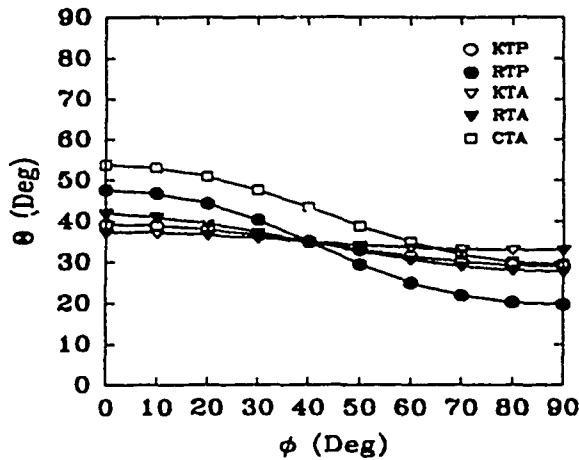


Figure 11. OPO Phase Matching, Type I, 4.043/1.444/1.064  $\mu\text{m}$ .

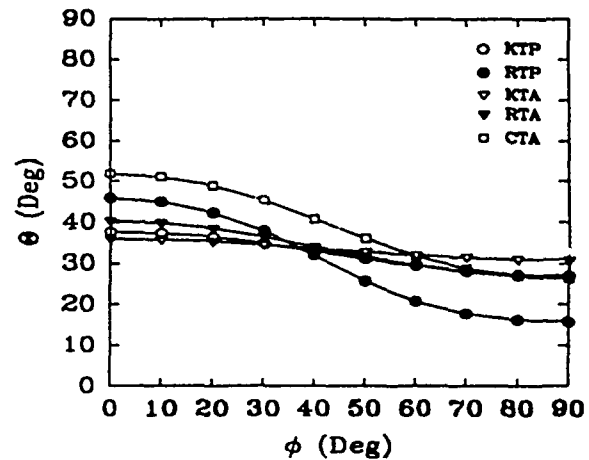


Figure 12. OPO Phase Matching, Type I, 3.17/1.60/1.064  $\mu\text{m}$ .

(2) Type II. Type II OPO phase matching curves are shown in Figure 13 and Figure 14. Like Type I, Type II phase matching is achievable over all  $\phi$  values in all isomorphs. The basic difference is that the Type II  $\theta$  phase matching angles vs.  $\phi$  are a few degrees higher than the corresponding  $\theta$ 's for Type I.

Table 9. Type II OPO Variation in  $\theta$

Crystal (Type II OPO)	4.043/1.444/1.064 $\mu\text{m}$		3.17/1.60/1.064 $\mu\text{m}$	
	Range of $\theta$	$\Gamma$	Range of $\theta$	$\Gamma$
KTP	44.33° - 35.47°	0.10	44.85° - 35.96°	0.10
RTP	52.79° - 28.08°	0.27	53.16° - 28.67°	0.27
KTA	43.72° - 34.82°	0.12	46.01° - 36.30°	0.11
RTA	42.48° - 39.65°	0.03	44.43° - 40.17°	0.05
CTA	61.59° - 40.06°	0.24	62.60° - 41.18°	0.24

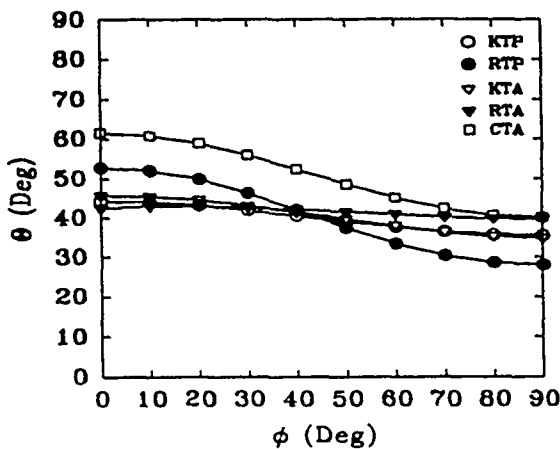


Figure 13. OPO Phase Matching, Type II, 4.043/1.444/1.064  $\mu\text{m}$ .

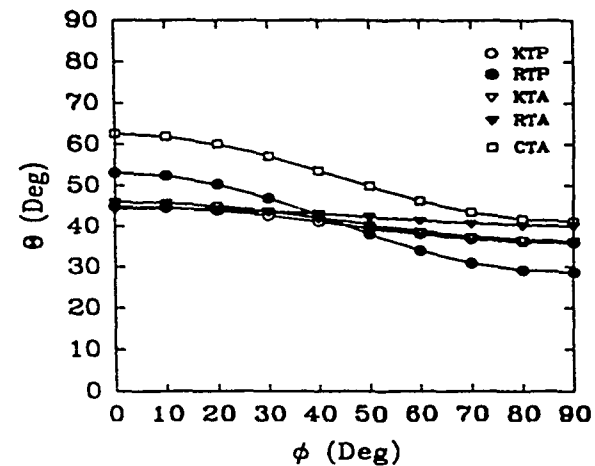


Figure 14. OPO Phase Matching, Type II, 3.17/1.60/1.064  $\mu\text{m}$ .

(3) Type III. No Type III phase matching could be achieved by any isomorph at 4.034/1.444/1.064  $\mu\text{m}$ . Because dispersion decreases with increasing wavelength,

$$n_{\text{fast}}(\lambda_{\text{signal}}) - n_{\text{slow}}(\lambda_{\text{signal}}) > n_{\text{fast}}(\lambda_{\text{idler}}) - n_{\text{slow}}(\lambda_{\text{idler}}) \quad (48)$$

Adding:

$$n_{\text{slow}}(\lambda_{\text{signal}}) + n_{\text{slow}}(\lambda_{\text{idler}}) \quad (49)$$

yields:

$$n_{\text{fast}}(\lambda_{\text{signal}}) + n_{\text{slow}}(\lambda_{\text{idler}}) > n_{\text{fast}}(\lambda_{\text{idler}}) + n_{\text{slow}}(\lambda_{\text{signal}}) \quad (50)$$

Here, the left side is the index sum used for Type II and the right side is the index sum for Type III. Usually, lack of phase matching means that the sum is insufficient to match the pump index. Thus, Type II phase matching is "easier" since it always has a larger sum and, for the above case, (4.034/1.444/1.064  $\mu\text{m}$ ) Type II works while Type III does not.

For the 3.17/1.60/1.064  $\mu\text{m}$  case, Type III phase matching was possible for all isomorphs except for CTA. Since CTA has the largest  $\theta$  value at a given  $\phi$  for all types of phase matching, it logically would be the first to fail to phase match for Type III where higher  $\theta$  values are needed. Only KTP could be phase matched for all  $\phi$  values.

Table 10. Type III OPO Variation in  $\theta$

Crystal (Type III OPO)	3.17/1.60/1.064 $\mu\text{m}$	
	Range of $\theta$	$\Gamma$
KTP	77.36° - 65.90°	0.13
RTP	90.00° - 66.88°	0.52
KTA	90.00° - 71.37°	0.25
RTA	90.00° - 81.52°	0.27
CTA	---	---

### iii. Comments.

The largest variations in  $\theta$  were present for the crystals RTP and CTA while KTA, KTP, and RTA showed much smaller  $\theta$  variations. Thus, KTA, KTP, and RTA are very uniaxial-like in nature (i.e.,  $n_x \approx n_y$ ) and the RTP and CTA crystals are more biaxial in nature (i.e.,  $n_x \ll n_y$ ).

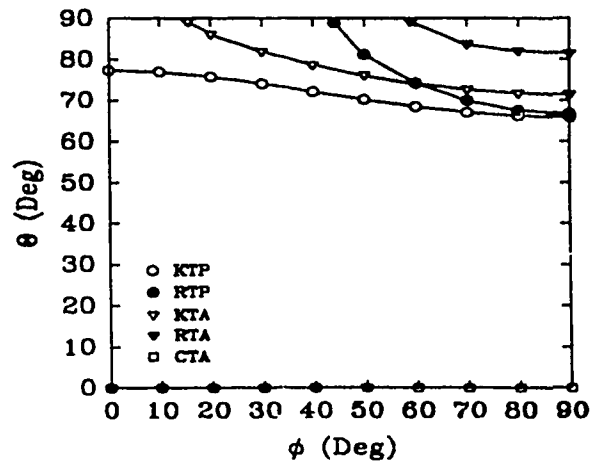


Figure 15. OPO Phase Matching, Type III, 3.17/1.60/1.064  $\mu\text{m}$ .

### c. Effective Nonlinear Coefficients ( $d_{eff}$ ).

Appendix E shows  $d_{eff}$  calculations for all SHG and OPO interaction types considered. Each plot shows  $d_{eff}$  as a magnitude above the  $\theta\phi$  phase matching plane. All plots in Appendix E use the same vertical scale for ease of comparison. The maximum  $d_{eff}$  for each isomorph at the SHG and OPO wavelengths according to phase matching type is shown in Table 11. Recommendations for any particular crystal in this section are related only to the largest value of  $d_{eff}$  found.

#### i. Second Harmonic Generation (SHG) Wavelengths.

(1) Type I Phase Match Region. The plots of  $d_{eff}$  for 1.064/1.064/0.532  $\mu\text{m}$  SHG are shown in Figure E-1 (KTP), Figure E-10 (RTP), Figure E-19 (KTA), Figure E-27 (RTA), and Figure E-36 (CTA). The  $d_{eff}$  plots for 1.35/1.35/0.675  $\mu\text{m}$  SHG are shown in Figure E-3 (KTP), Figure E-12 (RTP), Figure E-20 (KTA), Figure E-28 (RTA), and Figure E-36 (CTA). In all cases the  $d_{eff}$  goes to zero at the  $\phi = 0^\circ$  and  $90^\circ$  extrema. The maximum  $d_{eff}$  is typically near, but not exactly,  $\phi = 45^\circ$  due to the varying contributions of  $d_{15}$  and  $d_{24}$ . For all isomorphs the  $d_{eff}$  values were small (see Table 11); RTA and KTP had the largest values, but even they were only on the order of 0.5 pm/V.

(2) Type II Phase Match Region. Plots of  $d_{eff}$  for 1.064/1.064/0.532  $\mu\text{m}$  are presented in Figure E-2 (KTP) and Figure E-11 (RTP). Only KTP and RTP are shown because none of the arsenates are capable of Type II phase matching. For 1.35/1.35/0.675  $\mu\text{m}$  SHG,  $d_{eff}$  plots are shown in Figure E-4 (KTP), Figure E-13 (RTP), Figure E-21 (KTA), Figure E-29 (RTA), and Figure E-37 (CTA). The maximum  $d_{eff}$  was found where  $\phi$  was at a minimum value and  $\theta$  was at a maximum value. The minimum  $d_{eff}$  occurred at  $\phi = 90^\circ$  (which is also where the minimum value of  $\theta$  existed). Differences in  $d_{eff}$  among the isomorphs was minimal for both SHG cases.

(3) Final Comment. When phase matching was possible, RTA had the largest  $d_{eff}$  for SHG in both Type I and Type II cases. The exception was Type II 1.064  $\mu\text{m}$  SHG where KTP was the winner because RTA did not phase match. Type II phase matching  $d_{eff}$  values are always larger than those found for Type I phase matching; about six times larger. However, the change ranged from nearly 24 times (RTP 1.064  $\mu\text{m}$  SHG) to about 6.8 times (RTA 1.35  $\mu\text{m}$  SHG).

#### ii. Optical Parametric Oscillator (OPO) Wavelengths

(1) Type I Phase Match Region. Plots of  $d_{eff}$  for 4.043/1.444/1.064  $\mu\text{m}$  are shown in Figure E-5 (KTP), Figure E-14 (RTP), Figure E-22 (KTA), Figure E-30 (RTA), and Figure E-38 (CTA). Plots of  $d_{eff}$  for 3.17/1.60/1.064  $\mu\text{m}$  are shown in Figure E-7 (KTP), Figure E-16 (RTP), Figure E-24 (KTA), Figure E-32 (RTA), and Figure E-40 (CTA). In all cases the  $d_{eff}$  goes to zero at the  $\phi = 0^\circ$  and  $90^\circ$  extrema. The maximum  $d_{eff}$  is generally near, but not exactly at,  $\phi = 45^\circ$  due to the varying contributions of  $d_{15}$  and  $d_{24}$ . The isomorph RTA for 4.043/1.444/1.064  $\mu\text{m}$  and 3.17/1.60/1.064  $\mu\text{m}$  has values of  $\theta$  which are significantly larger than the other isomorphs maximum  $d_{eff}$ . Between the other isomorphs the difference in  $d_{eff}$  values is minimal. Except for RTA  $d_{eff}$  values (where  $d_{eff}$  values were over 1.46 pm/V at 4.043  $\mu\text{m}$  and 0.95 pm/V at 3.17  $\mu\text{m}$ ) the isomorph's  $d_{eff}$  values were fairly small (see Table 11), only on the order of about 0.4 pm/V.

(2) Type II Phase Match Region. The plots for  $d_{eff}$  at 4.043/1.444/1.064  $\mu\text{m}$  are displayed in Figure E-6 (for KTP), Figure E-15 (RTP), Figure E-23 (KTA), Figure E-31 (RTA), and Figure E-39 (CTA). For 3.17/1.60/1.064  $\mu\text{m}$ , the  $d_{eff}$  plots are shown in Figure E-8 (KTP),

Figure E-17 (RTP), Figure E-25 (KTA), Figure E-33 (RTA), and Figure E-41 (CTA). Maximum  $d_{eff}$  was where  $\theta$  was maximum and  $\phi$  was minimum; minimum  $d_{eff}$  was where  $\theta$  was minimum and  $\phi$  was maximum. The difference in  $d_{eff}$  between the various isomorphs was not significant.

(3) Type III Phase Match Region. There are no plots of  $d_{eff}$  at 4.043/1.444/1.064  $\mu\text{m}$  since none of the isomorphs phase matched at this wavelength and phase match type. For plots of  $d_{eff}$  at 3.17/1.60/1.064  $\mu\text{m}$  refer to Figure E-9 (KTP), Figure E-18 (RTP), Figure E-26 (KTA), and Figure E-34 (RTA). CTA does not Type III phase match at this wavelength combination. Maximum and minimum  $d_{eff}$  values occurred as at Type II phase matching. The largest  $d_{eff}$  values were found in KTP and KTA and the difference in their values was very minimal. The difference between the other two isomorphs (RTP and RTA)  $d_{eff}$  values was minor.

(4) Final Comments. The crystal RTA has the largest  $d_{eff}$  in the Type I phase matching regions. The crystal CTA has the largest  $d_{eff}$  in the Type II phase matching regions. At Type III phase matching (which only occurred at 3.17  $\mu\text{m}$  OPO) the crystal KTP has the largest  $d_{eff}$ . Type II and Type III phase matching  $d_{eff}$  values are always larger than those found for Type I phase matching; about six times larger. However, the difference ranged from 23 times (CTA 4.043  $\mu\text{m}$  OPO) to as little as 1.6 times (RTA 4.043  $\mu\text{m}$  OPO).

Table 11. Isomorph Maximum  $d_{eff}$  for SHG and OPO

Maximum $d_{eff}$ (pm/V)									
CRYSTAL	SHG				OPO				
	TYPE I	TYPE II	TYPE I	TYPE II	TYPE I	TYPE II	TYPE I	TYPE II	TYPE III
KTP	0.420	<b>3.268</b>	0.366	2.603	0.437	2.387	0.398	2.412	<b>3.496</b>
RTP	0.126	2.815	0.322	3.225	0.342	2.751	0.431	2.768	2.696
KTA	0.231	—	0.163	2.781	0.407	2.210	0.174	2.320	3.148
RTA	<b>0.468</b>	—	<b>0.494</b>	<b>3.357</b>	<b>1.462</b>	2.320	<b>0.951</b>	2.413	2.341
CTA	0.216	—	0.226	2.471	0.134	<b>3.110</b>	0.176	<b>3.145</b>	—
	1.064/1.064/0.532 $\mu\text{m}$		1.35/1.35/0.675 $\mu\text{m}$		4.043/1.444/1.064 $\mu\text{m}$		3.17/1.60/1.064 $\mu\text{m}$		

• Shaded regions indicate the largest value in each column

#### d. Walkoff.

Appendix F, Isomorph Walkoff Angles, shows walkoff angle as a function of angle  $\phi$  for the three-wave interactions. Since, in a biaxial crystal, both eigenpolarizations can have walkoff, we show true values of walkoff for all three wavelengths. Of course, for efficient wavelength conversion, it is most desirable to have all wavelengths with walkoffs as similar as possible.

Walkoff angles in the KTP isomorphs never exceed  $3^\circ$ . This corresponds to only 1 mm of walkoff in a 2-cm long crystal so, in all cases, walkoff is small in the KTP isomorphs. However, with judicious selection of phase matching type and crystal orientation, walkoff can often be made to approach zero.

### i. Partial Phase Match Regions.

Interestingly, for isomorphs in which phase matching did not exist over the entire  $xy$  plane (i.e.,  $\phi = 0^\circ$  to  $90^\circ$ ) and where the value of  $\theta$  approached  $90^\circ$ , the walkoff angles of the three wavelengths converged to near zero values. Type II 1.064  $\mu\text{m}$  SHG in KTP (Figure F-2), for example, shows this convergence effect. However, 1.35  $\mu\text{m}$  doubling in KTP is phase matchable for all  $\phi$  angles and the result is that relative walkoff of the beams never gets less than  $\sim 2^\circ$  (see Figure F-4). RTP (see Figure F-11) and CTA (see Figure F-34) were the only other isomorphs which had walkoff convergence at 1.064  $\mu\text{m}$  SHG. No isomorph showed this effect at 1.35  $\mu\text{m}$ .

For OPO interactions, walkoff convergence occurs only for RTP (see Figure F-18), KTA (see Figure F-26), and RTA (see Figure F-34) for the 3.17/1.60/1.064  $\mu\text{m}$  triplet. There are no cases of convergence for the 1.444  $\mu\text{m}$  signal wavelength case; neither OPO case displays convergence for Type II phase matching.

### ii. Walkoff Variations.

Among the isomorphs, walkoff for the Type I phase match region for RTP (except for 1.064/1.064/0.532  $\mu\text{m}$  SHG which is unremarkable with respect to the other isomorphs) shows the widest walkoff variation by far across the phase match region (see Figure F-12, Figure F-14, and Figure F-16).

### iii. Walkoff Similarities.

(1) Types I and II phase matching at 4.043/1.444/1.064  $\mu\text{m}$  OPO for KTA and RTA is interesting from the perspective that the plots of the  $\lambda_1$  walkoff angles appear similar except that the maximum walkoff angles are located at opposite ends of the  $xy$  plane with respect to each other. The plots show a rather rapid increase in difference in walkoff (i.e., from no difference:  $0^\circ$ ) between  $\lambda_1$  and  $\lambda_3$  at one end of the  $xy$  plane followed by a consistent and steady decrease in the difference in the walkoff angle between the two wavelengths until  $0^\circ$  of walkoff is again reached at the other end of the  $xy$  plane. For instance, in Type II phase matching (see Figure F-23 for KTA and Figure F-31 for RTA), the maximum amount of walkoff between  $\lambda_1$  and  $\lambda_3$  for KTA is located in the first half of the  $xy$  plane ( $\phi \approx 0^\circ$  to  $35^\circ$ ) whereas in RTA it is located in the latter half ( $\phi \approx 65^\circ$  to  $90^\circ$ ). In the other isomorphs the difference in walkoff angle between  $\lambda_1$  and one of the other wavelengths ( $\lambda_2$  or  $\lambda_3$ ) is minimal throughout the  $xy$  plane. The walkoff angle differences noted are pronounced compared to the other isomorphs.

(2) For Type I phase matching for KTA and RTA at 3.17/1.60/1.064  $\mu\text{m}$  OPO, a similar walkoff phenomenon occurs as at 4.043/1.444/1.064  $\mu\text{m}$  OPO. See Figures F-24 and F-32. In this case, the walkoff for KTA between  $\lambda_1$  and  $\lambda_2$  is maximum at  $\phi=0^\circ$  and approaches a minimum at  $\phi=90^\circ$ . In RTA, the reverse occurs (minimum at  $\phi=0^\circ$  and maximum at  $\phi=90^\circ$ ); the walkoff variation in KTA is somewhat less pronounced than in RTA.

## 7. CONCLUSIONS/OBSERVATIONS.

---

The choice of crystal for any particular application depends upon a number of things (application, availability, cost, wavelength at which it will be used, temperature considerations, absorption, transmission range, etc). However, this study has a purely theoretical focus and maximized performance is considered based upon phase matching,  $d_{eff}$ , walkoff, and transmission. Table 12 synthesizes the results by making recommendations for the crystal to use at what phase matching type and at what three-wavelength interaction.

### a. Crystal Characteristics.

Clearly no one single crystal does it all and does it well. However, the following comments are valid for making recommendations.

#### i. SHG.

(1) Nonlinear Coefficient. Type II SHG has  $d_{eff}$  values which are six times higher than those of Type I. The crystal RTA has the highest  $d_{eff}$  value for SHG except at Type II 1.064  $\mu\text{m}$  SHG (where KTP has the highest value). KTP has the next highest Type I  $d_{eff}$  while RTP has the next largest Type II  $d_{eff}$ .

(2) Phase Matching. The crystals RTP and CTA are highly biaxial (i.e., the value of  $\theta$  changes considerably throughout the  $xy$  plane) in nature compared to the other isomorphs. KTA is the most uniaxial-like (i.e., changes in  $\theta$  are minimal throughout the  $xy$  plane) of the isomorphs at all SHG wavelengths.

#### ii. OPO.

(1) Nonlinear Coefficient. At Type I phase matching, the crystal KTA has the highest  $d_{eff}$  values; the next highest levels are with the crystals RTA (4.043/1.444/1.064  $\mu\text{m}$ ) and RTP (3.17/1.60/1.064  $\mu\text{m}$ ). For Type II phase matching the highest  $d_{eff}$  values are with the crystal CTA; the crystal RTP has the next highest values. For Type III phase matching, KTP has the highest value of  $d_{eff}$ ; the crystal KTA has the next highest value. Types II and III phase matching  $d_{eff}$  values are 2 to 4 times higher than those of Type I.

(2) Phase Matching. KTA is the most uniaxial-like (i.e.,  $n_x \approx n_y$ ) of the isomorphs at all Type I OPO wavelengths. RTA is the most uniaxial-like for Type II OPO wavelengths. KTP was the most uniaxial-like of the isomorphs at Type III phase matching; however, not to the same degree as either KTA and RTA.

#### iii. General Considerations.

(1) The larger  $|n_x - n_y|$  differences in CTA and RTP resulted in larger variations of  $\theta$  over the phase match range of  $\phi$  for each phase matching wavelength and type. Variation among the other isomorphs was minimal. However, variation in  $\theta$  for KTA was, overall, the least of all the isomorphs. In other words, KTA was the most uniaxial-like isomorph.

(2) Maximum  $d_{eff}$  does not occur exactly where walkoff between the 3-wave interactions is minimized at any wavelength or phase match type. Maximizing  $d_{eff}$  while

minimizing walkoff (i.e., maximizing signal out of the crystal) necessarily represents a tradeoff between the two ( $d_{eff}$  and walkoff angles). However, in those crystals where a limited range of  $\phi$  phase matching values exists, maximum  $d_{eff}$  is very close to where the difference in walkoff between the three waves is nonexistent or extremely minimal. Thus, this represents a case where tradeoffs between walkoff and maximum  $d_{eff}$  are not necessary. However, this works only for specific wavelengths and phase matching types. In this study this situation exists only at Type II 1.064/1.064/0.532  $\mu\text{m}$  SHG (KTP and RTP), Type II 1.35/1.35/0.675  $\mu\text{m}$  SHG (CTA), and Type III 4.043/1.444/1.064  $\mu\text{m}$  OPO (RTP, KTA, and RTA).

(3) Maximum  $d_{eff}$  for Type I phase matching is basically in the central area of the phase match region. For Type II and III phase matching the maximum  $d_{eff}$  is at the smallest angle  $\phi$  (and largest value of  $\theta$ ) at which phase matching occurs.

#### iv. Crystal Transparency.

Choice of a crystal is not usually independent of the wavelength at which it will be used. Therefore, it is important to know the light transmission through the crystal at the chosen wavelength(s). Figure 16 and Figure 17 [13, 14] provide an indication of the amount of light transmission at a given wavelength for each of the KTP isomorphs. The crystals used were uncoated samples. But, because their thicknesses are unknown, correlating the percent of transmission values indicated in each of the figures is not possible. Therefore, the percent of transmission between figures (and curves) should be taken as a relative data item only. With appropriate antireflection (AR) coatings, the percent of light transmission of each of the isomorphs can be made nearly perfect for well grown crystal samples, at least in the "flat" portion of the transmission region. It is important to note where the transparency of the crystal begins to fall. This is where the amount of absorption becomes a factor for consideration since losses due to absorption are not compensated for by AR coatings.

The extended transparency in the infrared of the arsenate crystals (KTA, RTA, and CTA) is clearly an advantage over the phosphate crystals (KTP and RTP) for midinfrared purposes [13]. Note: the isomorph transmission curves in Figure 16 and Figure 17 are digitized representations of the original transmission curves which were found in hardcopy figures. These digitized curves were then replotted here. The transmission curves for CTA, KTA, and KTP were obtained from Reference [13] and the curves for RTP and RTA were obtained from Reference [14].

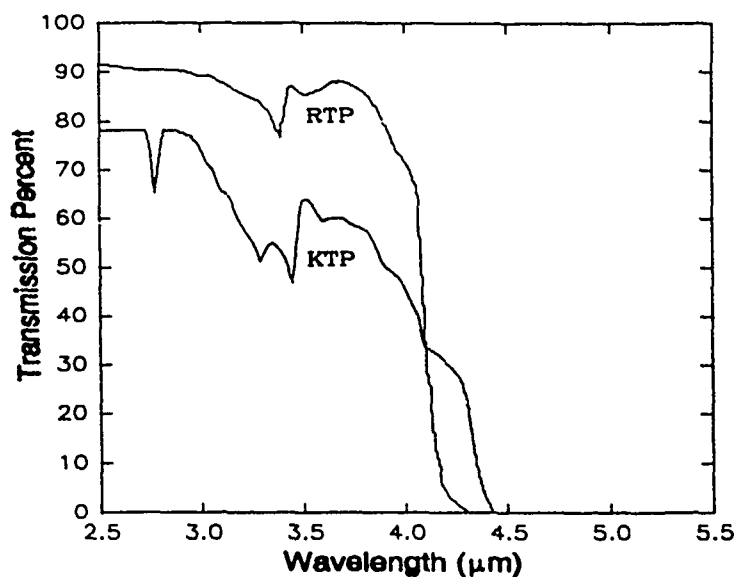


Figure 16. Phosphate Isomorph Transmission Spectra



(1) SHG. Since each of the isomorphs has relatively flat transmission curves at the SHG wavelengths, this region of the isomorph transmission curves is not displayed in either of the two figures above. Transparency at SHG wavelengths in this study is not a useful discriminator as to which crystal to select or reject.

(2) OPO. For the following discussion see Figure 16 and Figure 17 for references to isomorph light transmission curves. The wavelengths of 1.444 and 1.60  $\mu\text{m}$  are used with 1.064  $\mu\text{m}$  to generate the mid-infrared (mid-IR) wavelengths of 4.043 and 3.17  $\mu\text{m}$ , respectively.

The wavelength of 3.17  $\mu\text{m}$  is in the relatively flat transmission curve region for all of the isomorphs (except for KTP) which indicates that the arsenates and RTP are good candidates for use at this mid-IR wavelength. Beyond this wavelength, however, only the arsenates are good mid-IR candidates. At 3.17  $\mu\text{m}$ , the KTP crystal indicates about 18% loss and for RTP, the loss is about 4%. For the arsenates, both CTA and KTA experience about an 8% loss while the loss for RTA appears minimal at best.

At 4.043  $\mu\text{m}$ , the two phosphates (KTP and RTP) are in steep decline with respect to their ability to transmit light (see Figure 16). So, this essentially represents the maximum mid-IR wavelength at which they can (or should) be used (if the amount of absorption can be tolerated). On the other hand, each of the arsenates still has a nearly flat transmission curve at this point. Phosphate losses at 4.043  $\mu\text{m}$  are over 30% for KTP and around 17% for RTP—fairly serious losses. For the arsenates, losses are around 8% for CTA and KTA and minimal for RTA.

The transmission curve for KTP shows that it is most applicable to wavelengths less than 2.75  $\mu\text{m}$  (the flat region of its transmission curve) and perhaps a small region around 2.83 to 2.9  $\mu\text{m}$ . The crystal RTP appears applicable to those wavelengths from about 3.2  $\mu\text{m}$  and less and perhaps a small region around 3.4 to 3.8  $\mu\text{m}$ . The arsenates, on the other hand appear better suited for wavelengths beyond where the phosphates are capable. Both CTA and KTA appear well suited to wavelengths to around 3.65  $\mu\text{m}$  and RTA to around 4.6  $\mu\text{m}$ . A 5% loss from the isomorph's "flat" transmission curve region was used as an arbitrary demarcation point beyond which absorption losses become a concern.

## b. Conclusions.

Table 12 below synthesizes the information available on the isomorphs for use at a given wavelength, phase match type and transmission loss. Since there is little utility in using any of

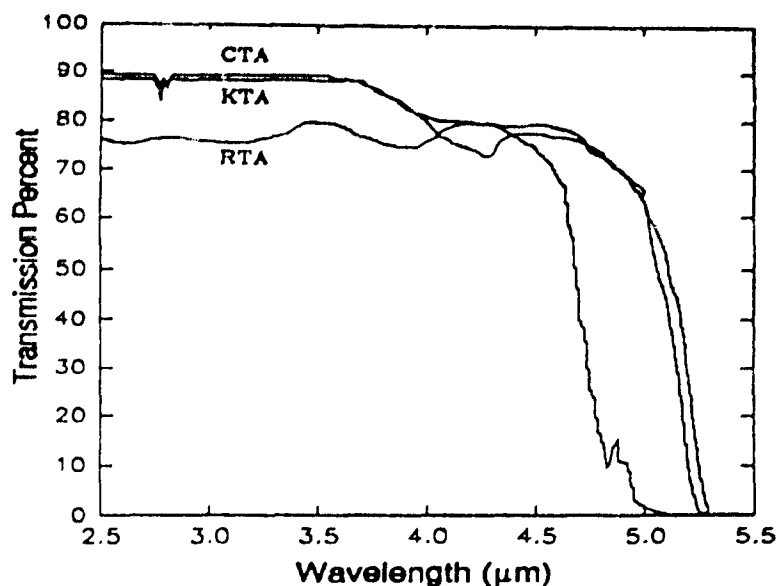


Figure 17. Arsenate Isomorph Transmission Spectra

the crystals in Type I phase matching only the isomorphs with the maximum  $d_{eff}$  are provided in the table. As can be seen, the isomorphs all appear to perform in a manner similar to KTP.

i. SHG. All wavelength selections for the SHG cases were in the spectral regions where losses due to absorption were not an issue.

(1) 1.064/1.064/0.532  $\mu\text{m}$ , Type II. Only KTP and RTP phase matched here. Both perform about the same. However, the  $d_{eff}$  for KTP is better and the walkoff is about three times less than that of RTP. Therefore, KTP is the best option.

(2) 1.35/1.35/0.675  $\mu\text{m}$ , Type II. All isomorphs phase matched and all performed well in this region. However, RTA was slightly better in terms of  $d_{eff}$  value and walkoff (which is just over half that of the other isomorphs except for CTA). Although CTA had by far the smallest walkoff (about four times less than RTA), it also had the smallest value for  $d_{eff}$ .

ii. OPO. In this type of operation, isomorph transmissivity becomes a major consideration in the preferred choice of crystal.

(1) 4.043/1.444/1.064  $\mu\text{m}$ , Type II. Both CTA and RTA perform very well in this region. The  $d_{eff}$  for CTA is slightly higher than for RTA, its walkoff is about  $\frac{1}{2}^\circ$  less than for RTA, but CTA appears to have higher absorption than RTA. The transmission characteristics for RTA show it to have a relatively flat transmission curve out to about 4.25  $\mu\text{m}$  while for CTA, the flat portion of the transmission curve extends to only about 3.7  $\mu\text{m}$ . The better transparency for RTA at 4.043  $\mu\text{m}$  may compensate for its slightly lower  $d_{eff}$  with respect to CTA. Therefore, RTA is the preferred crystal in this group with CTA a very close second.

Although the phosphates (KTP and RTP) have slightly smaller values of  $d_{eff}$ , the walkoff for each was around one-third larger than that of CTA (and about 25% larger than for RTA). Both phosphates suffer substantial transmission losses which makes them poor OPO candidates for generating 4.043  $\mu\text{m}$ . The crystal KTA has the smallest value of  $d_{eff}$ , a slightly higher walkoff than RTA, and about the same amount of transmission loss as CTA. In short, KTA is a better choice than the phosphates but is not quite as good a choice as either CTA or RTA.

(2) 3.17/1.60/1.064  $\mu\text{m}$ , Type II. The isomorph CTA is clearly the crystal of choice in this region. It has by far the smallest walkoff of any other isomorph and transmission losses are negligible. The phosphates have decent  $d_{eff}$  values but each has large values of walkoff (nearly  $3^\circ$ ). KTP has significant transmission loss which makes it poor a OPO candidate for 3.17  $\mu\text{m}$ . RTP, on the other hand, has a small amount of transmission loss. It might make a decent candidate for OPO use here. RTA has a slightly less  $d_{eff}$  value, about  $0.6^\circ$  more walkoff than CTA and negligible transmission loss; KTA has the smallest  $d_{eff}$ , about  $0.9^\circ$  more walkoff than CTA and about the same transmission loss. In short, the arsenates are the better choices for 3.17  $\mu\text{m}$ , Type II OPO work than the phosphates.

(3) 3.17/1.60/1.064  $\mu\text{m}$ , Type III. The arsenate RTA, while it does have the smallest  $d_{eff}$  value, has very minimal walkoff and negligible transmission loss. KTP has much too much transmission loss to be a viable candidate, even though it does have the largest value of  $d_{eff}$ . The isomorph KTA has small walkoff but its transmission loss cannot be ignored. RTP has a larger  $d_{eff}$  than RTA, four times the walkoff (though it is still fairly small). However, it has a small amount of transmission loss that RTA doesn't have. Therefore, RTA is the isomorph to use here.

### iii. General.

The arsenates characteristically have a smaller walkoff than the phosphates, typically somewhere around  $0.8^\circ$  to  $1.5^\circ$ . However, this represents about 0.5 mm in a 2-cm-long crystal. With careful consideration and design (with respect to crystal size and/or pump beam size, for instance) walkoff effects can be minimized. Where KTP does not have the largest  $d_{eff}$ , the difference from the isomorph which does is typically no more than about 0.7 pm/V.

The bottom line is that, strictly from a performance characteristics basis, as long as the wavelengths are less than about 2.75  $\mu\text{m}$  there appears to be no real reason to switch from KTP to another isomorph. At the OPO wavelengths, however, RTP and RTA are good choices primarily because their losses are less than that of CTA (RTP has about half of the loss experienced by CTA while RTA has negligible loss). Beyond 3.17  $\mu\text{m}$  only the arsenates are good choices because of the significant transmission losses experienced by the phosphates.

Developing the necessary expertise to grow one or more of these crystals for use over the choice of KTP is not justified given the indicated performance characteristics, the cost, and the necessary time provided the wavelengths being considered are less than 2.75  $\mu\text{m}$ . Beyond this is a region in which KTP experiences severe losses and cannot adequately compete.

Further study is necessary to more fully characterize the isomorphs RTP, KTA, RTA, and CTA for applications at wavelengths beyond 2.75  $\mu\text{m}$ . Other differences in the isomorphs, such as the power handling ability (where bulk and/or surface damage occurs), may exist but are not identified in (and are outside the scope of) this study. These differences could prove important.

Table 12. Isomorph Selection Synopsis

Wavelengths (μm) (λ <sub>1</sub> /λ <sub>2</sub> /λ <sub>3</sub> )	Use	Type	Crystal	d <sub>eff</sub>   pm/V	Walkoff (milliradians)			Approx. Transmit Loss (%)
					ρ <sub>1</sub>	ρ <sub>2</sub>	ρ <sub>3</sub>	
1.064/1.064/0.532	S H G	I	RTA	0.468	32.57	32.57	6.976'	N/A
		II	KTP	3.268	3.5'	0	4.9	
RTP			2.815	11.55	0'	13.09		
1.35/1.35/0.675		I	RTA	0.494	32.74	32.74	6.578'	
		II	RTA	3.357	0	27.09	0'	
			RTP	3.225	0	40.82	0'	
			KTA	2.781	0	39.43	0'	
			KTP	2.603	0	49.02	0'	
			CTA	2.471	7.8	0'	7.6	
4.043/1.444/1.064		I	RTA	1.462	22.6	36.84	3.18'	
	II		CTA	3.110	0	30.82	0'	
			RTP	2.751	0'	51.38	0	
			KTP	2.387	0	50.14	0'	
			RTA <sup>♦</sup>	2.320	0	40.95	0'	
	KTA	2.210	0	45.68	0'			
	III	---	---	---	---	---	N/A	
3.17/1.60/1.064	O P O	I	RTA	0.951	26.62	32.91	5.07'	—
		II	CTA	3.145	0	29.85	0'	—
			RTP	2.768	0'	50.74	0	4
			KTP	2.412	0	48.56	0'	18
			RTA	2.341	0	40.91	0'	—
			KTA	2.220	0	45.10	0'	—
		III	KTP	3.496	20.16	0	0'	18
			KTA	3.148	0'	4.48	4.40	—
			RTP	2.696	0'	11.33	11.60	4
			RTA	2.341	0	0'	3.21	—

Notes:

1. Isomorph selections are provided according to decreasing value of  $d_{\text{eff}}$ .
2. Because the importance of Type I phase matching isn't significant compared to Types II and III, only the isomorphs with the largest  $d_{\text{eff}}$  value are listed.
3. Isomorphs in Types II and III which are predicted to be the best performer are highlighted.

Indicators:

- ' Wavelength for which the walkoff values of the other two wavelengths are measured.
- Transmission loss is minimal.
- ♦ Preferred selection in category

## REFERENCES

---

1. P. A. Franken, A. E. Hill, C. W. Peters, and G. Weinreich, "Generation of Optical Harmonics," *Phys. Rev. Lett.*, vol. 7, pp 118-119, 1961.
2. C. Chen, "Recent Advances in Nonlinear Optical and Electro-optical Materials," *Ann. Rev. Mater. Sci.*, vol. 16, pp. 203-243, 1986.
3. Jianquan Yao and Weidong Sheng, "Accurate Calculation of the Optimum Phase-matching Parameters in Three-wave Interactions with Biaxial Nonlinear-optical Crystals," *Journal of Optical Society of America B*, 891 (June 1992).
4. David A. Roberts, "Simplified Characterization of Unusual and Biaxial Nonlinear Optical Crystals: A Plea for Standardization of Nomenclature and Conventions," *IEEE Journal of Quantum Electronics*, 2057, (Vol 28, No. 10, October 1992).
5. M. Born and E. Wolf, *Principles of Optics* (Oxford U. Press, New York, 1970).
6. Hiromasa Ito, Hatsuhiko Naito, Humio Inaba; "Generalized Study on Angular Dependence of Induced Second-order Nonlinear Optical Polarizations and Phase Matching in Biaxial Crystals," *Journal of Applied Physics*, 3992-3995 (Vol 46, No. 9, September 1975).
7. L. T. Cheng, L. K. Cheng, and J. D. Bierlein, "Linear and Nonlinear Optical Properties of the Arsenate Isomorphs of KTP", SPIE OptoElectronics and Lasers Conference, 1993, Los Angeles CA.
8. J. Q. Yao and Theodore S. Fahlen, "Calculations of Optimum Phase Match Parameters for the Biaxial Crystal  $\text{KTiOPO}_4$ ," *Journal of Applied Physics*, 55 (1) (January 1984).
9. Amnon Yariv, "Quantum Electronics," 2nd Edition, (Wiley, New York, 1975), pg 409.
10. Robert C. Eckhard, Hisashi Masuda, Yuan Xuan Fan, and Robert L. Byer, "Absolute and Relative Nonlinear Optical Coefficients of KDP,  $\text{KD}^*\text{P}$ ,  $\text{BaB}_2\text{O}_4$ ,  $\text{LiIO}_3$ ,  $\text{MgO:LiNbO}_3$ , and KTP Measured by Phase-Matched Second-Harmonic Generation," *IEEE Journal of Quantum Electronics*, (Vol 26, No 5, May 1990).
11. Zumsteg, Bierlein, and Gier, *Journal of Applied Physics*, 4984 (Vol 47, No 11, November 1976).
12. Robert C. Miller, "Optical Second Harmonic Generation in Piezoelectric Crystals," *Applied Physics Letters*, 17, (Vol 5, No. 1, 1 July 1964).
13. WL/ML, Personal communication.
14. L. K. Cheng, J. D. Bierlein, and A. A. Ballman, *Journal of Crystal Growth*, 697-703, (Vol 110, 1991).

## APPENDIX A Phase Match Calculations Worksheet

# CALCULATE PHASE MATCHING ANGLES for Positive or Negative Nonlinear Biaxial/Uniaxial Crystals

Worksheet Developed by Capt Dale L Fenimore  
WL/ELOS, Wright-Patterson AFB OH

Sellmeier Values

S:=READPRN(sellmeier RTA)

CRYSTAL: \_\_\_\_\_

Point Group: \_\_\_\_\_

(A-1)

$$S = \begin{pmatrix} 2.22681 & 0.99616 & 0.21423 & 0.01369 \\ 1.97756 & 1.25726 & 0.20448 & 0.00865 \\ 2.28779 & 1.20629 & 0.23484 & 0.01583 \end{pmatrix}$$

ORIGIN := 0

TOL := 0.000001

$$\xi := \frac{\pi}{180}$$

<==== Degrees to Radians Conversion

(A-2a, b)

WAVELENGTHS SELECTED

User Provided #1 ==>

$$\lambda_{\alpha} \approx 1.064$$

<==== Enter user provided values (#1 and #2) such that  $\lambda_{\alpha} \leq \lambda_{\beta}$

(A-3a)

User Provided #2 ==>

$$\lambda_{\beta} \approx 1.60$$

(A-3b)

$\lambda_{calc}$  is positive valued

when  $\lambda_{\alpha} < \lambda_{\beta}$  ==>

$$\lambda_{calc} := \left( \lambda_{\alpha}^{-1} - \lambda_{\beta}^{-1} \right)^{-1}$$

$$\lambda_{calc} = 3.1761194$$

(A-3c)

Assign Wavelengths to satisfy:  $\lambda_1 \geq \lambda_2 > \lambda_3$ .

$$\lambda_1 := \lambda_{calc}$$

$$\lambda_2 := \lambda_{\beta}$$

$$\lambda_3 := \lambda_{\alpha}$$

(A-3d, e, f)

$$\lambda_1 = 3.1761$$

$$\lambda_2 = 1.6000$$

$$\lambda_3 = 1.0640$$

SET the Phase Match Category with which you desire to work according to the following CATEGORIES

(NOTE: SELECTING A PHASE MATCHING IS NOT REQUIRED!):

1 - SHG/SFM

2 - DFM-32/OPA-32

3 - DFM-31/OPA-31

4 - OPO

CAT := 1

(A-4)

Sellmeier Equations:

$$n_x(\lambda) := \left[ s_{0,0} + \frac{s_{0,1}}{1 - \left( \frac{s_{0,2}}{\lambda} \right)^2} - s_{0,3} \lambda^2 \right]^{0.5}$$

$$n_y(\lambda) := \left[ s_{1,0} + \frac{s_{1,1}}{1 - \left( \frac{s_{1,2}}{\lambda} \right)^2} - s_{1,3} \lambda^2 \right]^{0.5}$$

(A-5a, b, c)

$$n_z(\lambda) := \left[ s_{2,0} + \frac{s_{2,1}}{1 - \left( \frac{s_{2,2}}{\lambda} \right)^2} - s_{2,3} \lambda^2 \right]^{0.5}$$

Indices of Refraction

$$n = \begin{pmatrix} n_x(\lambda_1) & n_x(\lambda_2) & n_x(\lambda_3) \\ n_y(\lambda_1) & n_y(\lambda_2) & n_y(\lambda_3) \\ n_z(\lambda_1) & n_z(\lambda_2) & n_z(\lambda_3) \end{pmatrix}$$

$$n = \begin{pmatrix} 1.7577 & 1.7906 & 1.8027 \\ 1.7756 & 1.7982 & 1.8092 \\ 1.8278 & 1.8655 & 1.8809 \end{pmatrix}$$

(A-5d)

WRITEPRN(indicesd nla) = n

# **SETUP Indices of Refraction for Phase Match Equation Use**

$$a_1 := (n_{0,0})^{-2} \quad a_2 := (n_{0,1})^{-2} \quad a_3 := (n_{0,2})^{-2} \quad (\text{A-6a, b, c})$$

$$b_1 := (n_{1,0})^{-2} \quad b_2 := (n_{1,1})^{-2} \quad b_3 := (n_{1,2})^{-2} \quad (\text{A-6d, e, f})$$

$$c_1 := (n_{2,0})^{-2} \quad c_2 := (n_{2,1})^{-2} \quad c_3 := (n_{2,2})^{-2} \quad (\text{A-6g, h, i})$$

The following equations were developed using the 1987 article printed in Applied Physics, 1987, written by Fahlen and Yao.

## **SETUP for Phase Matching Calculations**

$$kx(\theta, \phi) := \sin(\theta) \cdot \cos(\phi) \quad ky(\theta, \phi) := \sin(\theta) \cdot \sin(\phi) \quad kz(\theta, \phi) := \cos(\theta) \quad (\text{A-7a, b, c})$$

## **Setup Each Wavelength for Phase Matching Calculations**

$$B_1(\theta, \phi) := -kx(\theta, \phi)^2 \cdot (b_1 + c_1) - ky(\theta, \phi)^2 \cdot (a_1 + c_1) - kz(\theta, \phi)^2 \cdot (a_1 + b_1) \quad (\text{A-8a})$$

$$C_1(\theta, \phi) := kx(\theta, \phi)^2 \cdot b_1 \cdot c_1 + ky(\theta, \phi)^2 \cdot a_1 \cdot c_1 + kz(\theta, \phi)^2 \cdot a_1 \cdot b_1 \quad (\text{A-8b})$$

$$B_2(\theta, \phi) := -kx(\theta, \phi)^2 \cdot (b_2 + c_2) - ky(\theta, \phi)^2 \cdot (a_2 + c_2) - kz(\theta, \phi)^2 \cdot (a_2 + b_2) \quad (\text{A-8c})$$

$$C_2(\theta, \phi) := kx(\theta, \phi)^2 \cdot b_2 \cdot c_2 + ky(\theta, \phi)^2 \cdot a_2 \cdot c_2 + kz(\theta, \phi)^2 \cdot a_2 \cdot b_2 \quad (\text{A-8d})$$

$$B_3(\theta, \phi) := -kx(\theta, \phi)^2 \cdot (b_3 + c_3) - ky(\theta, \phi)^2 \cdot (a_3 + c_3) - kz(\theta, \phi)^2 \cdot (a_3 + b_3) \quad (\text{A-8e})$$

$$C_3(\theta, \phi) := kx(\theta, \phi)^2 \cdot b_3 \cdot c_3 + ky(\theta, \phi)^2 \cdot a_3 \cdot c_3 + kz(\theta, \phi)^2 \cdot a_3 \cdot b_3 \quad (\text{A-8f})$$

## **Indices of Refraction for Phase Matching Angles ( $\lambda$ 's 1, 2, & 3)**

Column 1: Slow Ray, Column 2: Fast Ray

$$n_{1s}(\theta, \phi) := \frac{\sqrt{2}}{\sqrt{-B_1(\theta, \phi) - \sqrt{B_1(\theta, \phi)^2 - 4C_1(\theta, \phi)}}} \quad n_{1f}(\theta, \phi) := \frac{\sqrt{2}}{\sqrt{-B_1(\theta, \phi) + \sqrt{B_1(\theta, \phi)^2 - 4C_1(\theta, \phi)}}} \quad (\text{A-9a, b})$$

$$n_{2s}(\theta, \phi) := \frac{\sqrt{2}}{\sqrt{-B_2(\theta, \phi) - \sqrt{B_2(\theta, \phi)^2 - 4C_2(\theta, \phi)}}} \quad n_{2f}(\theta, \phi) := \frac{\sqrt{2}}{\sqrt{-B_2(\theta, \phi) + \sqrt{B_2(\theta, \phi)^2 - 4C_2(\theta, \phi)}}} \quad (\text{A-9c, d})$$

$$n_{3s}(\theta, \phi) := \frac{\sqrt{2}}{\sqrt{-B_3(\theta, \phi) - \sqrt{B_3(\theta, \phi)^2 - 4C_3(\theta, \phi)}}} \quad n_{3f}(\theta, \phi) := \frac{\sqrt{2}}{\sqrt{-B_3(\theta, \phi) + \sqrt{B_3(\theta, \phi)^2 - 4C_3(\theta, \phi)}}} \quad (\text{A-9e, f})$$

## **Wavelength Dependent Indices Assignments**

$$n_{\lambda 1s}(\theta, \phi) := \frac{n_{1s}(\theta, \phi)}{\lambda_1} \quad n_{\lambda 2s}(\theta, \phi) := \frac{n_{2s}(\theta, \phi)}{\lambda_2} \quad n_{\lambda 3s}(\theta, \phi) := \frac{n_{3s}(\theta, \phi)}{\lambda_3} \quad (\text{A-10a, b, c})$$

$$n_{\lambda 1f}(\theta, \phi) := \frac{n_{1f}(\theta, \phi)}{\lambda_1} \quad n_{\lambda 2f}(\theta, \phi) := \frac{n_{2f}(\theta, \phi)}{\lambda_2} \quad n_{\lambda 3f}(\theta, \phi) := \frac{n_{3f}(\theta, \phi)}{\lambda_3} \quad (\text{A-10d, e, f})$$



**Assignments for the Appropriate Equations to Use in SOLVING for the Phase Match Conditions for the CATEGORY Desired**

$$\Lambda_{TI}(\theta, \phi) = \text{if}(\text{CAT}=1, n_{\lambda 3f}(\theta, \phi), \text{if}(\text{CAT}=2, n_{\lambda 1s}(\theta, \phi), \text{if}(\text{CAT}=3, n_{\lambda 2s}, n_{\lambda 3f}(\theta, \phi)))) \quad (\text{A-11a})$$

$$\Lambda_{TII}(\theta, \phi) = \text{if}(\text{CAT}=1, n_{\lambda 3f}(\theta, \phi), \text{if}(\text{CAT}=2, n_{\lambda 1f}(\theta, \phi), \text{if}(\text{CAT}=3, n_{\lambda 2s}(\theta, \phi), n_{\lambda 3f}(\theta, \phi)))) \quad (\text{A-11b})$$

$$\Lambda_{TIII}(\theta, \phi) = \text{if}(\text{CAT}=1, n_{\lambda 3f}(\theta, \phi), \text{if}(\text{CAT}=2, n_{\lambda 1s}(\theta, \phi), \text{if}(\text{CAT}=3, n_{\lambda 2f}(\theta, \phi), n_{\lambda 3f}(\theta, \phi)))) \quad (\text{A-11c})$$

$$\begin{aligned} \text{SHG1}(\theta, \phi) &= n_{\lambda 1s}(\theta, \phi) + n_{\lambda 2s}(\theta, \phi) & \text{SHG2}(\theta, \phi) &= n_{\lambda 1f}(\theta, \phi) + n_{\lambda 2s}(\theta, \phi) & \text{SHG3}(\theta, \phi) &= n_{\lambda 1s}(\theta, \phi) + n_{\lambda 2f}(\theta, \phi) \\ \text{OPO1}(\theta, \phi) &= \text{SHG1}(\theta, \phi) & \text{OPO2}(\theta, \phi) &= \text{SHG2}(\theta, \phi) & \text{OPO3}(\theta, \phi) &= \text{SHG3}(\theta, \phi) \end{aligned} \quad (\text{A-12a,b,c})$$

$$\begin{aligned} \text{DFM32\_1}(\theta, \phi) &= n_{\lambda 3f}(\theta, \phi) - n_{\lambda 2s}(\theta, \phi) & \text{DFM32\_2}(\theta, \phi) &= n_{\lambda 3f}(\theta, \phi) - n_{\lambda 2s}(\theta, \phi) & \text{DFM32\_3}(\theta, \phi) &= n_{\lambda 3f}(\theta, \phi) - n_{\lambda 2f}(\theta, \phi) \\ & & & & & (\text{A-12d,e,f}) \end{aligned}$$

$$\begin{aligned} \text{DFM31\_1}(\theta, \phi) &= n_{\lambda 3f}(\theta, \phi) - n_{\lambda 1s}(\theta, \phi) & \text{DFM31\_2}(\theta, \phi) &= n_{\lambda 3f}(\theta, \phi) - n_{\lambda 1f}(\theta, \phi) & \text{DFM31\_3}(\theta, \phi) &= n_{\lambda 3f}(\theta, \phi) - n_{\lambda 1s}(\theta, \phi) \\ & & & & & (\text{A-12g,h,i}) \end{aligned}$$

$$\Lambda_{f}(\theta, \phi) = \text{if}(\text{CAT}=1, \text{SHG1}(\theta, \phi), \text{if}(\text{CAT}=2, \text{DFM32\_1}(\theta, \phi), \text{if}(\text{CAT}=3, \text{DFM31\_1}(\theta, \phi), \text{OPO1}(\theta, \phi)))) \quad (\text{A-12m})$$

$$\Lambda_{II}(\theta, \phi) = \text{if}(\text{CAT}=1, \text{SHG2}(\theta, \phi), \text{if}(\text{CAT}=2, \text{DFM32\_2}(\theta, \phi), \text{if}(\text{CAT}=3, \text{DFM31\_2}(\theta, \phi), \text{OPO2}(\theta, \phi)))) \quad (\text{A-12n})$$

$$\Lambda_{III}(\theta, \phi) = \text{if}(\text{CAT}=1, \text{SHG3}(\theta, \phi), \text{if}(\text{CAT}=2, \text{DFM32\_3}(\theta, \phi), \text{if}(\text{CAT}=3, \text{DFM31\_3}(\theta, \phi), \text{OPO3}(\theta, \phi)))) \quad (\text{A-12o})$$

**SETUP SOLVE BLOCKS FOR TYPE I, II, AND III (as appropriate) PHASE MATCHING**

CAT = 1.0000

CRYSTAL:

**Solve Block for Type I Phase Matching**

Given (A-13)

$$\Lambda_f(\theta, \phi) = \Lambda_{TI}(\theta, \phi) \quad \text{Wavelength Dependent Solution} \quad (\text{A-13a})$$

$$\theta \leq \frac{\pi}{2} \quad \theta \geq 0 \quad \phi \leq \frac{\pi}{2} \quad \phi \geq 0 \quad \text{Constrain to Quadrant 1} \quad (\text{A-13b})$$

$$I_{\text{match}}(\theta, \phi) = \text{FIND}(\theta) \quad \text{Determine Solution} \quad (\text{A-13c})$$

**Solve Block for Type II Phase Matching**

Given (A-14)

$$\Lambda_{II}(\theta, \phi) = \Lambda_{TII}(\theta, \phi) \quad \text{Wavelength Dependent Solution} \quad (\text{A-14a})$$

$$\theta \leq \frac{\pi}{2} \quad \theta \geq 0 \quad \phi \leq \frac{\pi}{2} \quad \phi \geq 0 \quad \text{Constrain to Quadrant 1} \quad (\text{A-14b})$$

$$II_{\text{match}}(\theta, \phi) = \text{FIND}(\theta) \quad \text{Determine Solution} \quad (\text{A-14c})$$

**Solve Block for Type III Phase Matching**

Given (A-15)

$$\Lambda_{III}(\theta, \phi) = \Lambda_{TIII}(\theta, \phi) \quad \text{Wavelength Dependent Solution} \quad (\text{A-15a})$$

$$\theta \leq \frac{\pi}{2} \quad \theta \geq 0 \quad \phi \leq \frac{\pi}{2} \quad \phi \geq 0 \quad \text{Constrain to Quadrant 1} \quad (\text{A-15b})$$

$$III_{\text{match}}(\theta, \phi) = \text{FIND}(\theta) \quad \text{Determine Solution} \quad (\text{A-15c})$$

This page graphs the region for Phase Match Determination (Types I, II, & III)

Crystal: \_\_\_\_\_

PRNPRECISION = 8

CAT = 1

(A-16)

$$\phi = 90 - \frac{\pi}{180} \quad i = 0..90 \quad \theta_i = i \cdot \frac{\pi}{180}$$

(A-17a, b, c)

$$A_i = \Lambda_{TI}(\theta_i, \phi) \quad A_{90} = 1.6942$$

$$C_i = \Lambda_{TII}(\theta_i, \phi) \quad C_{90} = 1.6942$$

$$E_i = \Lambda_{TIII}(\theta_i, \phi) \quad E_{90} = 1.6942$$

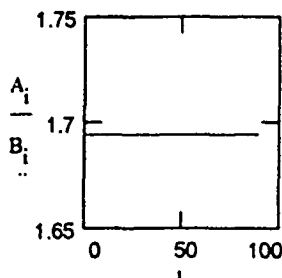
(A-18a, b, c)

$$B_i = \Lambda_I(\theta_i, \phi) \quad B_{90} = 1.7414$$

$$D_i = \Lambda_{II}(\theta_i, \phi) \quad D_{90} = 1.7193$$

$$F_i = \Lambda_{III}(\theta_i, \phi) \quad F_{90} = 1.6946$$

(A-18d, e, f)



Phase Matching: Index of Refraction of Generated vs Applied Wavelengths

Figure A-1a  
Type I

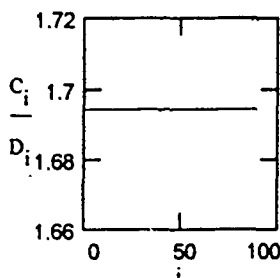


Figure A-1b  
Type II

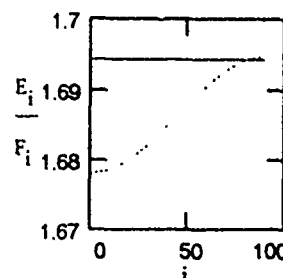


Figure A-1c  
Type III

Vary the value of " $\phi$ \_start" below (where " $\phi$ " = 1, 2, or 3 for the each of the three phase matching types) to locate the beginning of the phase match region shown to end at  $\phi = 90^\circ$  above

$$\lambda_1 = 3.1761$$

$$\lambda_2 = 1.6000$$

$$\lambda_3 = 1.0640$$

$$CAT = 1.0000$$

Type I

$$\phi1\_start = 0$$

$$\phi1 = \phi1\_start \cdot \xi$$

$$i\_start = 0$$

$$\theta_i = i \cdot \xi$$

Type II

$$\phi2\_start = 0$$

$$\phi2 = \phi2\_start \cdot \xi$$

$$i\_end = 90$$

Type III

$$\phi3\_start = 59$$

$$\phi3 = \phi3\_start \cdot \xi$$

$$i = i\_start..i\_end$$

<=== Assign start of phase match region and convert to radians

(A-19a, b, c)

(A-19d, e, f)

<=== Assign test range for figures below

(A-20a, b, c)

<=== Assign range as  $\theta$

(A-21)

$$A_i = \Lambda_{TI}(\theta_i, \phi1) \quad A_{i\_end} = 1.7004$$

$$C_i = \Lambda_{TII}(\theta_i, \phi2) \quad C_{i\_end} = 1.7004$$

$$E_i = \Lambda_{TIII}(\theta_i, \phi3) \quad E_{i\_end} = 1.695852$$

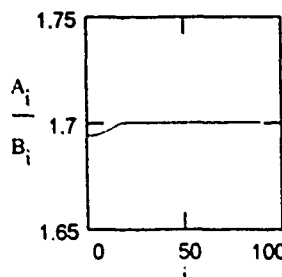
(A-22a, b, c)

$$B_i = \Lambda_I(\theta_i, \phi1) \quad B_{i\_end} = 1.741438$$

$$D_i = \Lambda_{II}(\theta_i, \phi2) \quad D_{i\_end} = 1.7250$$

$$F_i = \Lambda_{III}(\theta_i, \phi3) \quad F_{i\_end} = 1.695859$$

(A-22d, e, f)



Phase Matching: Index of Refraction of Generated vs Applied Wavelengths

Figure A-2a  
Type I

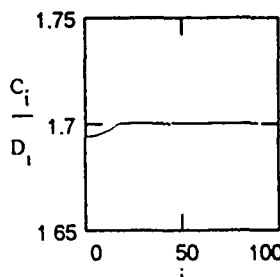


Figure A-2b  
Type II

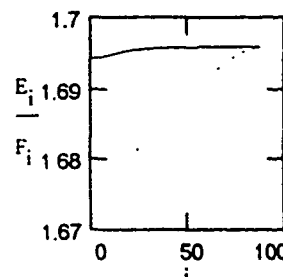


Figure A-2c  
Type III

-----[ INFORMATION ]-----

x =  $\phi 1\_start \dots i\_end$   
 $\theta_x = 1\_match(55 \xi, x \xi)$

y =  $\phi 2\_start \dots i\_end$   
 $\theta 2_y = if(11\_match(55 \xi, y \xi) > 0, 11\_match(55 \xi, y \xi), 0)$   
 $\theta \theta_y = if(\theta 2_y \geq 0, \theta 2_y, 0)$

z =  $\phi 3\_start \dots i\_end$   
 $\theta 3_z = if(111\_match(55 \xi, z \xi) < \frac{\pi}{2}, 111\_match(55 \xi, z \xi), 0)$   
 $\theta \theta \theta_z = if(\theta 3_z \geq 0, \theta 3_z, 0)$

$\theta = \frac{180}{\pi}$  <===== Radians to Degrees Conversion

<u>Start Phase</u>	<u>End Phase</u>	<u>3 Wavelengths</u>	
<u>Match Range</u>	<u>Match Range</u>	<u>Used</u>	
$\phi 1\_start = 0.0000$	$i\_end = 90.0000$	$\lambda_1 = 3.1761$	(A-23a)
$\phi 2\_start = 0.0000$		$\lambda_2 = 1.6000$	(A-23b)
$\phi 3\_start = 59.0000$		$\lambda_3 = 1.0640$	(A-24a)
			(A-24b)
			(A-24c)

(A-25a)  
 (A-25b)  
 (A-25c)

(A-26)

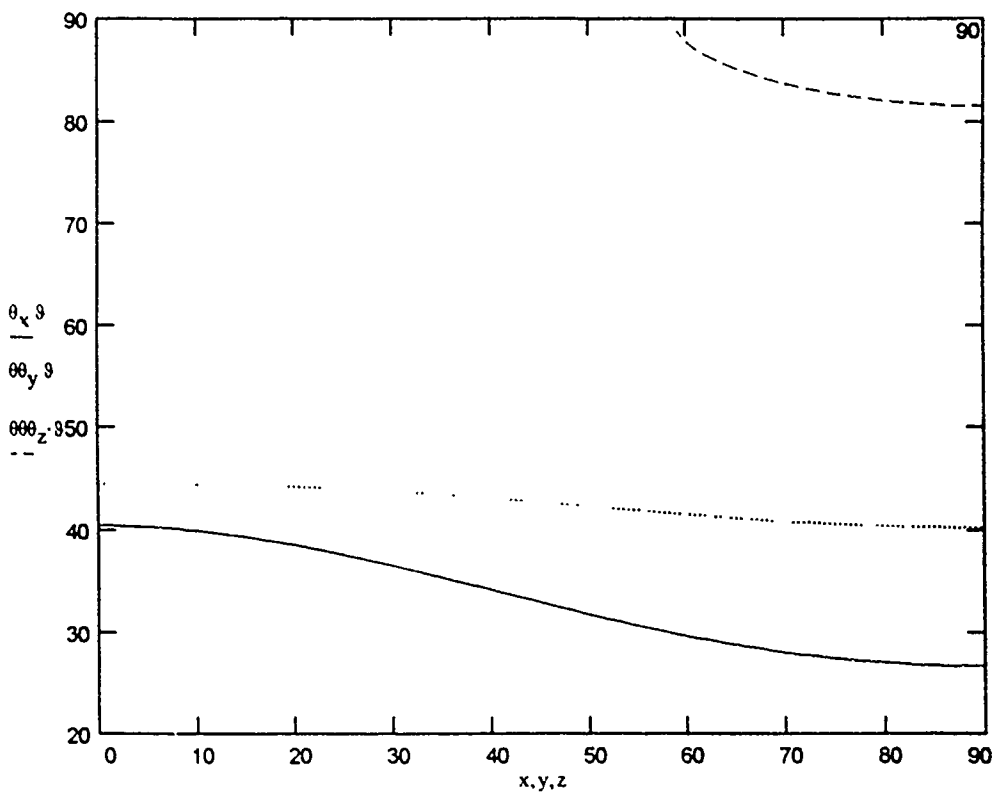


Figure A-3  
 Phase Matching ( $\theta$  vs  $\phi$ )

<u>Start of Phase Match Region</u>	<u>End of Phase Match Region</u>
$\theta \phi 1\_start = 40.3468 \cdot \text{deg}$	$\theta i\_end = 26.6517 \cdot \text{deg}$
$\theta \theta \phi 2\_start = 44.4295 \cdot \text{deg}$	$\theta \theta i\_end = 40.1684 \cdot \text{deg}$
$\theta \theta \theta \phi 3\_start = 88.8583 \cdot \text{deg}$	$\theta \theta \theta i\_end = 81.5161 \cdot \text{deg}$

# Setup for Data File for Phase Match Angles

$$N = 0..90$$

(A-27)

$$w_{1N} = \lambda_1$$

$$\phi_{1N} = N$$

$$\theta_{1N} = 0 \cdot N \cdot 9$$

(A-28a, b, c)

$$w_{2N} = \lambda_2$$

$$\theta_{2N} = 0 \cdot 0 \cdot N \cdot 9$$

$$\theta_{2N} = \text{if}(\theta_{1N} \geq 0, 0 \cdot 0 \cdot N \cdot 9, 0)$$

(A-28d, e, f)

$$w_{3N} = \lambda_3$$

$$\theta_{3N} = 0 \cdot 0 \cdot 0 \cdot N \cdot 9$$

$$\theta_{3N} = \text{if}(\theta_{2N} \geq 0, 0 \cdot 0 \cdot 0 \cdot N \cdot 9, 0)$$

(A-28g, h, i)

"Matrix" of phase match region data values

$$\text{data} = \text{augment}(\text{augment}(\text{augment}(\text{augment}(\text{augment}(\text{w}_1, \text{w}_2), \text{w}_3), \phi), \theta_1), \theta_2), \theta_3)$$

(A-29a)

DATA FILE FORMAT (by Column):  $\lambda_1, \lambda_2, \lambda_3, \phi, \theta(I); \theta(II); \theta(III)$

Saves the Phase Match Angle pairs for Type I, II, & III phase matching

$$\text{WRITEPRN}(\text{PM\_DATA}_{\text{rta}}) = \text{data}$$

(A-29b)

## SCRATCH PAD AREA ..

$$\phi_3_{\text{start}} = 59.0000$$

$$\theta_t = \text{III}_{\text{match}}(55 \cdot \xi, 58.630 \cdot \xi)$$

$$\theta_t = 89.99997094 \cdot \text{deg}$$

$$\theta_t = \text{III}_{\text{match}}(55 \cdot \xi, 58.6299 \cdot \xi)$$

$$\theta_t = 89.99997921 \cdot \text{deg}$$

APPENDIX B Effective Non-Linear Coefficient ( $d_{eff}$ ) and Walkoff Calculations Worksheet

# CALCULATE BIAxIAL/UNIAXIAL CRYSTAL NONLINEAR COEFFICIENT ( $d_{eff}$ ) and WALKOFF ( $\rho$ ) FOR POSITIVE/NEGATIVE CRYSTALS

## OBTAIN DATA FROM DATA FILES

Matrix := READPRN(PM\_DATA RTA)      d<sub>ijk</sub> := READPRN(dijk rta)      n := READPRN(indicesd rta)      (B-1a, b, c)

IDENTIFY ORIGIN FOR WORKSHEET MATRICES

ORIGIN := 0      (B-2)

d<sub>ijk</sub> for the crystal

$$d_{ijk} = \begin{pmatrix} 0.00 & 0.00 & 0.00 & 0.00 & 1.90 & 0.00 \\ 0.00 & 0.00 & 0.00 & 3.60 & 0.00 & 0.00 \\ 2.30 & 3.80 & 15.80 & 0.00 & 0.00 & 0.00 \end{pmatrix}$$

Indices of Refraction ( $\lambda$  by column - left to right,  
axes by row - x, y, and z)

$$n = \begin{pmatrix} 1.757675 & 1.790561 & 1.802654 \\ 1.775611 & 1.798208 & 1.809211 \\ 1.827846 & 1.865507 & 1.880939 \end{pmatrix}$$

Select Positive or Negative Crystal Type with a POSITIVE or NEGATIVE Number.

CT := -1      (B-3)

NOTE: Unless properly selected, the calculated value for  $d_{eff}$  and walkoff angle may not be correct.

PHASE MATCH angles data file LEGEND [Matrix], (by column):  $\lambda_1, \lambda_2$ , &  $\lambda_3$ ;  $\phi$ ;  $\theta(I)$ ;  $\theta(II)$ ;  $\theta(III)$

SELECT AN ANGLE  $\phi$  FOR WHICH AN ANGLE  $\theta$  EXISTS (for Type I, II, or III Selected Below)

i := 0

(B-4)

$$\lambda_i := \left[ \left( \text{Matrix}^{<0>} \right)_i, \left( \text{Matrix}^{<1>} \right)_i, \left( \text{Matrix}^{<2>} \right)_i \right]$$

(B-5a)

$$\lambda_1 := \lambda_{0,0} \quad \lambda_2 := \lambda_{0,1} \quad \lambda_3 := \lambda_{0,2}$$

(B-5b, c, d)

$$\lambda_1 = 3.176 \quad \lambda_2 = 1.6 \quad \lambda_3 = 1.064$$

Selects the Phase Matching Angle Pair from the data file

TYPE I

TYPE II

TYPE III

$$I := \text{augment}(\text{Matrix}^{<4>}, \text{Matrix}^{<3>}) \quad II := \text{augment}(\text{Matrix}^{<5>}, \text{Matrix}^{<3>}) \quad III := \text{augment}(\text{Matrix}^{<6>}, \text{Matrix}^{<3>}) \quad (B-6a, b, c)$$

Identify the Type of Phase Matching Desired (1 = Type I, 2 = Type II, 3 = Type III)

PMID := 1

(B-7a)

Type := if(PMID=1, I, if(PMID=2, II, III))

(B-7b)

$$A_i := \left( \text{Type}^{<0>} \right)_i \cdot \text{deg} \quad \theta := A_i \quad \theta = 40.3468^\circ \text{deg}$$

(B-7c, d)

$$\beta_i := \left( \text{Type}^{<1>} \right)_i \cdot \text{deg} \quad \phi := \beta_i \quad \phi = 0^\circ \text{deg}$$

(B-7e, f)

SELECT Phase Match Category for Desired Nonlinear Coefficient ( $d_{eff}$ )

1 - SHG/SFM ("λ<sub>3</sub>")      2 - DFM-32/OPA-32 ("λ<sub>1</sub>")  
3 - DFM-31/OPA-31 ("λ<sub>2</sub>")      4 - OPO ("λ<sub>1</sub>")

CATEGORY = 4

(B-8)

This region begins the calculation for the effective non-linear coefficient ( $d_{eff}$ ).  
These calculations are NOT limited to the principle-axis.

This is the solution for the OPTIC AXIS,  $\Omega$

$$\Omega = \begin{bmatrix} \arcsin \left[ \frac{n_{2,0}}{n_{1,0}} \cdot \left[ \frac{(n_{1,0})^2 - (n_{0,0})^2}{(n_{2,0})^2 - (n_{0,0})^2} \right]^{.5} \right] + 10^{-18} \\ \arcsin \left[ \frac{n_{2,1}}{n_{1,1}} \cdot \left[ \frac{(n_{1,1})^2 - (n_{0,1})^2}{(n_{2,1})^2 - (n_{0,1})^2} \right]^{.5} \right] + 10^{-18} \\ \arcsin \left[ \frac{n_{2,2}}{n_{1,2}} \cdot \left[ \frac{(n_{1,2})^2 - (n_{0,2})^2}{(n_{2,2})^2 - (n_{0,2})^2} \right]^{.5} \right] + 10^{-18} \end{bmatrix}$$

This angle,  $\Omega$ , is measured from the z-axis to the optic axis.

NOTE. the  $10^{-18}$  value is intended to prevent  $\tan 2\delta$  from experiencing a singularity

$$\Omega = \begin{pmatrix} 31.107 \\ 19.167 \\ 17.333 \end{pmatrix} \text{deg}$$

(B-9)

This is used to calculate the polarization angle, " $\delta$ ". This angle is formed by the direction of the slow ray electric displacement unit vector,  $e_1$ , from the surface of the plane formed by the wavefront vector ( $k$ ) and the z-axis

$$\tan 2\delta = \begin{bmatrix} \frac{\cos(\theta) \cdot \sin(2\phi)}{\cos(\Omega_{0,0})^2 \cdot \sin(\theta)^2 - \cos(\theta)^2 \cdot \cos(\phi)^2 + \sin(\phi)^2} \\ \frac{\cos(\theta) \cdot \sin(2\phi)}{\cos(\Omega_{1,0})^2 \cdot \sin(\theta)^2 - \cos(\theta)^2 \cdot \cos(\phi)^2 + \sin(\phi)^2} \\ \frac{\cos(\theta) \cdot \sin(2\phi)}{\cos(\Omega_{2,0})^2 \cdot \sin(\theta)^2 - \cos(\theta)^2 \cdot \cos(\phi)^2 + \sin(\phi)^2} \end{bmatrix}$$

$$\tan 2\delta = \begin{pmatrix} 0 \\ 0 \\ 0 \end{pmatrix}$$

(B-10a)

$$\delta_{adj} := \text{if}(\cos(\theta) \cdot \sin(2\phi) = 0, 0, \text{if}(\cos(\theta) \cdot \sin(2\phi) > 0, 0, \pi))$$

$$\delta_{adj} = 0$$

$$\cos(\theta) \cdot \sin(2\phi) = 0$$

(B-10b)

$$\delta = \begin{bmatrix} (\arcsin(\tan 2\delta_{0,0}) + \delta_{adj}) \cdot 0.5 \\ (\arcsin(\tan 2\delta_{1,0}) + \delta_{adj}) \cdot 0.5 \\ (\arcsin(\tan 2\delta_{2,0}) + \delta_{adj}) \cdot 0.5 \end{bmatrix}$$

$$\delta = \begin{pmatrix} 0.000 \\ 0.000 \\ 0.000 \end{pmatrix} \text{deg}$$

(B-10c)

The following are the solutions for the SLOW (b1) rays and the FAST (b2) rays. These solutions represent the UNIT VECTORS of the electric displacement vectors. Columns represent  $\lambda_1$ ,  $\lambda_2$ , &  $\lambda_3$ , respectively.

$$a := -\cos(\theta) \cdot \cos(\phi) \cdot \cos(\delta_{0,0}) + \sin(\phi) \cdot \sin(\delta_{0,0})$$

$$b := -\cos(\theta) \cdot \sin(\phi) \cdot \cos(\delta_{0,0}) - \cos(\phi) \cdot \sin(\delta_{0,0})$$

(B-11a,b)

$$c := -\cos(\theta) \cdot \cos(\phi) \cdot \cos(\delta_{1,0}) + \sin(\phi) \cdot \sin(\delta_{1,0})$$

$$d := -\cos(\theta) \cdot \sin(\phi) \cdot \cos(\delta_{1,0}) - \cos(\phi) \cdot \sin(\delta_{1,0})$$

(B-11c,d)

$$e := -\cos(\theta) \cdot \cos(\phi) \cdot \cos(\delta_{2,0}) + \sin(\phi) \cdot \sin(\delta_{2,0})$$

$$f := -\cos(\theta) \cdot \sin(\phi) \cdot \cos(\delta_{2,0}) - \cos(\phi) \cdot \sin(\delta_{2,0})$$

(B-11e,f)

$$aa := -\cos(\theta) \cdot \cos(\phi) \cdot \sin(\delta_{0,0}) - \sin(\phi) \cdot \cos(\delta_{0,0})$$

$$bb := -\cos(\theta) \cdot \sin(\phi) \cdot \sin(\delta_{0,0}) + \cos(\phi) \cdot \cos(\delta_{0,0})$$

(B-11g,h)

$$cc := -\cos(\theta) \cdot \cos(\phi) \cdot \sin(\delta_{1,0}) - \sin(\phi) \cdot \cos(\delta_{1,0})$$

$$dd := -\cos(\theta) \cdot \sin(\phi) \cdot \sin(\delta_{1,0}) + \cos(\phi) \cdot \cos(\delta_{1,0})$$

(B-11i,j)

$$ee := -\cos(\theta) \cdot \cos(\phi) \cdot \sin(\delta_{2,0}) - \sin(\phi) \cdot \cos(\delta_{2,0})$$

$$ff := -\cos(\theta) \cdot \sin(\phi) \cdot \sin(\delta_{2,0}) + \cos(\phi) \cdot \cos(\delta_{2,0})$$

(B-11k,l)

$$b_1 = \begin{pmatrix} a & c & e \\ b & d & f \\ \sin(\theta) \cdot \cos(\delta_{0,0}) & \sin(\theta) \cdot \cos(\delta_{1,0}) & \sin(\theta) \cdot \cos(\delta_{2,0}) \end{pmatrix}$$

$$b_2 = \begin{pmatrix} aa & cc & ee \\ bb & dd & ff \\ \sin(\theta) \cdot \sin(\delta_{0,0}) & \sin(\theta) \cdot \sin(\delta_{1,0}) & \sin(\theta) \cdot \sin(\delta_{2,0}) \end{pmatrix}$$

(B-11m,n)

**This section calculates the electric field's two polarization components,  $\lambda_1$ ,  $\lambda_2$ , and  $\lambda_3$  (top to bottom), respectively.**

Column 1 is for the "SLOW" rays ( $a_1$ ); column 2 calculates the "FAST" rays ( $a_2$ ).

$$Pb := \begin{bmatrix} \left[ \frac{(b_{10,0})^2}{(n_{0,0})^4} + \frac{(b_{11,0})^2}{(n_{1,0})^4} + \frac{(b_{12,0})^2}{(n_{2,0})^4} \right]^{0.5} & \left[ \frac{(b_{20,0})^2}{(n_{0,0})^4} + \frac{(b_{21,0})^2}{(n_{1,0})^4} + \frac{(b_{22,0})^2}{(n_{2,0})^4} \right]^{0.5} \\ \left[ \frac{(b_{10,1})^2}{(n_{0,1})^4} + \frac{(b_{11,1})^2}{(n_{1,1})^4} + \frac{(b_{12,1})^2}{(n_{2,1})^4} \right]^{0.5} & \left[ \frac{(b_{20,1})^2}{(n_{0,1})^4} + \frac{(b_{21,1})^2}{(n_{1,1})^4} + \frac{(b_{22,1})^2}{(n_{2,1})^4} \right]^{0.5} \\ \left[ \frac{(b_{10,2})^2}{(n_{0,2})^4} + \frac{(b_{11,2})^2}{(n_{1,2})^4} + \frac{(b_{12,2})^2}{(n_{2,2})^4} \right]^{0.5} & \left[ \frac{(b_{20,2})^2}{(n_{0,2})^4} + \frac{(b_{21,2})^2}{(n_{1,2})^4} + \frac{(b_{22,2})^2}{(n_{2,2})^4} \right]^{0.5} \end{bmatrix} \quad (B-12)$$

**This section calculates the UNIT VECTORS for the polarization components for the electric fields.** The "SLOW" rays are calculated by "a1," the "FAST" rays by "a2." The rows represent the x, y, and z-axis components, respectively, the columns represent  $\lambda_1$ ,  $\lambda_2$  &  $\lambda_3$  (left to right), respectively.

$$a1 := \begin{bmatrix} \frac{b_{10,0}}{Pb_{0,0} \cdot (n_{0,0})^2} & \frac{b_{10,1}}{Pb_{1,0} \cdot (n_{0,1})^2} & \frac{b_{10,2}}{Pb_{2,0} \cdot (n_{0,2})^2} \\ \frac{b_{11,0}}{Pb_{0,1} \cdot (n_{1,0})^2} & \frac{b_{11,1}}{Pb_{1,1} \cdot (n_{1,1})^2} & \frac{b_{11,2}}{Pb_{2,1} \cdot (n_{1,2})^2} \\ \frac{b_{12,0}}{Pb_{0,2} \cdot (n_{2,0})^2} & \frac{b_{12,1}}{Pb_{1,2} \cdot (n_{2,1})^2} & \frac{b_{12,2}}{Pb_{2,2} \cdot (n_{2,2})^2} \end{bmatrix} \quad a2 := \begin{bmatrix} \frac{b_{20,0}}{Pb_{0,1} \cdot (n_{0,0})^2} & \frac{b_{20,1}}{Pb_{1,1} \cdot (n_{0,1})^2} & \frac{b_{20,2}}{Pb_{2,1} \cdot (n_{0,2})^2} \\ \frac{b_{21,0}}{Pb_{0,1} \cdot (n_{1,0})^2} & \frac{b_{21,1}}{Pb_{1,1} \cdot (n_{1,1})^2} & \frac{b_{21,2}}{Pb_{2,1} \cdot (n_{1,2})^2} \\ \frac{b_{22,0}}{Pb_{0,1} \cdot (n_{2,0})^2} & \frac{b_{22,1}}{Pb_{1,1} \cdot (n_{2,1})^2} & \frac{b_{22,2}}{Pb_{2,1} \cdot (n_{2,2})^2} \end{bmatrix} \quad (B-13a, b)$$

**Categories:** CATEGORY = 4  
1 = SHG/SFM, 2 = OPO-32/DFM-32  
3 = OPO-31/DFM-31, 4 = OPO

**Crystal Type** (Positive or Negative  
Number indicates Type)  
CT = -1

**Phase Match Type**  
PMID = 1

Identify which column to use for the specific phase match category selected

$$C_i := \text{if}(\text{CATEGORY} = 1, 2, \text{if}(\text{CATEGORY} = 2, 0, \text{if}(\text{CATEGORY} = 3, 1, 2)))$$

$$C_i = 2 \quad (a_i) \quad (B-14a)$$

$$C_j := \text{if}(\text{CATEGORY} = 1, 0, \text{if}(\text{CATEGORY} = 2, 1, \text{if}(\text{CATEGORY} = 3, 0, 0)))$$

$$C_j = 0 \quad (a_j) \quad (B-14b)$$

$$C_k := \text{if}(\text{CATEGORY} = 1, 1, \text{if}(\text{CATEGORY} = 2, 2, \text{if}(\text{CATEGORY} = 3, 2, 1)))$$

$$C_k = 1 \quad (a_k) \quad (B-14c)$$

**Setup the  $a_{1i}$ ,  $a_{1j}$ , and  $a_{1k}$  vectors**

Type I, II, and III

$$a_{1i} := \text{if}(CT \geq 0, a_2^{<C_i>}, a_1^{<C_i>}) \quad a_{1k} := \text{if}(CT \geq 0, a_1^{<C_k>}, a_2^{<C_k>}) \quad (B-15a, b)$$

Type I

Type II/III

$$a_{1j} := \text{if}(CT \geq 0, a_1^{<C_j>}, a_2^{<C_j>}) \quad a_{2j} := \text{if}(CT \geq 0, a_2^{<C_j>}, a_1^{<C_j>}) \quad a_j := \text{if}(PMID > 1, a_{2j}, a_{1j}) \quad (B-15c, d, e)$$



### Setup the $a_{jk}$ column-vectors

Type I

$$a_{1jk} := \begin{bmatrix} a_{10,0} \cdot a_{k0,0} \\ a_{11,0} \cdot a_{k1,0} \\ a_{12,0} \cdot a_{k2,0} \\ a_{11,0} \cdot a_{k2,0} + a_{12,0} \cdot a_{k1,0} \\ a_{10,0} \cdot a_{k2,0} + a_{12,0} \cdot a_{k0,0} \\ a_{10,0} \cdot a_{k1,0} + a_{11,0} \cdot a_{k0,0} \end{bmatrix}$$

Type II/III

$$a_{2jk} := \begin{bmatrix} a_{20,0} \cdot a_{k0,0} \\ a_{21,0} \cdot a_{k1,0} \\ a_{22,0} \cdot a_{k2,0} \\ a_{21,0} \cdot a_{k2,0} + a_{22,0} \cdot a_{k1,0} \\ a_{20,0} \cdot a_{k2,0} + a_{22,0} \cdot a_{k0,0} \\ a_{20,0} \cdot a_{k1,0} + a_{21,0} \cdot a_{k0,0} \end{bmatrix} \quad (B-16a, b)$$

### Select the appropriate $a_{jk}$ column vector

$$a_{jk} := \text{if}(\text{PMID} > 1, a_{2jk}, a_{1jk}) \quad (B-16c)$$

### Effective Nonlinear Coefficient

PMID = 1

$$d_{\text{eff}} := |a_i \cdot (d_{ijk} a_{jk})| \quad d_{\text{eff}} = 2.33754626 \quad (B17)$$

### WALKOFF Angle ( $\rho$ ) Calculations (column1: SLOW rays, column 2: FAST rays)

By row, starting at the top is the calculation for the  $\lambda_1$ ,  $\lambda_2$ , &  $\lambda_3$ , respectively

$$\rho = \text{Re} \begin{bmatrix} \left[ \frac{\left( \frac{b_{10,0}}{n_{0,0}} \right)^2 + \left( \frac{b_{11,0}}{n_{1,0}} \right)^2 + \left( \frac{b_{12,0}}{n_{2,0}} \right)^2}{Pb_{0,0}} \right] \quad \left[ \frac{\left( \frac{b_{20,0}}{n_{0,0}} \right)^2 + \left( \frac{b_{21,0}}{n_{1,0}} \right)^2 + \left( \frac{b_{22,0}}{n_{2,0}} \right)^2}{Pb_{0,1}} \right] \\ \left[ \frac{\left( \frac{b_{10,1}}{n_{0,1}} \right)^2 + \left( \frac{b_{11,1}}{n_{1,1}} \right)^2 + \left( \frac{b_{12,1}}{n_{2,1}} \right)^2}{Pb_{1,0}} \right] \quad \left[ \frac{\left( \frac{b_{20,1}}{n_{0,1}} \right)^2 + \left( \frac{b_{21,1}}{n_{1,1}} \right)^2 + \left( \frac{b_{22,1}}{n_{2,1}} \right)^2}{Pb_{1,1}} \right] \\ \left[ \frac{\left( \frac{b_{10,2}}{n_{0,2}} \right)^2 + \left( \frac{b_{11,2}}{n_{1,2}} \right)^2 + \left( \frac{b_{12,2}}{n_{2,2}} \right)^2}{Pb_{2,0}} \right] \quad \left[ \frac{\left( \frac{b_{20,2}}{n_{0,2}} \right)^2 + \left( \frac{b_{21,2}}{n_{1,2}} \right)^2 + \left( \frac{b_{22,2}}{n_{2,2}} \right)^2}{Pb_{2,1}} \right] \end{bmatrix} \quad (B-18)$$

### Select correct walkoff angles according to phase match category

$$v := \frac{180}{\pi} \quad (B-19a)$$

$$wo_1 := \text{if}(\text{CATEGORY} = 2, \text{if}(\text{PMID} \geq 0, \rho_{0,1}, \rho_{0,0}), \text{if}(\text{PMID} \geq 0, \rho_{0,0}, \rho_{0,1})) \cdot v \quad (B-19b)$$

$$wo_2 := \text{if}(\text{CATEGORY} = 3, \text{if}(\text{PMID} \geq 0, \rho_{1,1}, \rho_{1,0}), \text{if}(\text{PMID} \geq 0, \rho_{1,0}, \rho_{1,1})) \cdot v \quad (B-19c)$$

$$wo_3 := \text{if}(\text{PMID} \geq 0, \rho_{2,1}, \rho_{2,0}) \cdot v \quad (B-19d)$$

PMID = 1    ORIGIN = 0    CATEGORY = 4    CT = -1

### Create the Matrix for Writing a Line of Data to the Data File

$$\text{data} := (\lambda_1 \quad \lambda_2 \quad \lambda_3 \quad \theta v \quad o v \quad d_{\text{eff}} \quad wo_1 \quad wo_2 \quad wo_3) \quad (B-20a)$$

### Writes Data to the Data File Specified

$$\text{APPENDPRN}(\text{pmold} \quad \text{ita}) = \text{data} \quad (B-20b)$$

## CONSOLIDATED INFORMATION

Electric Displacement Unit Vectors, b1 = "slow" ray, b2 = "fast" ray

$$b_1 = \begin{pmatrix} -0.76213977 & -0.76213977 & -0.76213977 \\ 0 & 0 & 0 \\ 0.64741252 & 0.64741252 & 0.64741252 \end{pmatrix}$$

$$b_2 = \begin{pmatrix} 0 & 0 & 0 \\ 1 & 1 & 1 \\ 0 & 0 & 0 \end{pmatrix}$$

Polarization Components for the Electric Fields (cols = "slow" & "fast" respectively)

$$Pb = \begin{pmatrix} 0.31369897 & 0.31717898 \\ 0.30185472 & 0.30925747 \\ 0.29747807 & 0.30550741 \end{pmatrix}$$

Polarization Unit vectors, a1 = "slow" rays, a2 = "fast" rays

$$a_1 = \begin{pmatrix} -0.78640149 & -0.78751432 & -0.78841497 \\ 0 & 0 & 0 \\ 0.61771571 & 0.61629635 & 0.61514375 \end{pmatrix}$$

$$a_2 = \begin{pmatrix} 0 & 0 & 0 \\ 1 & 1 & 1 \\ 0 & 0 & 0 \end{pmatrix}$$

Polarization Unit vectors

ai = "Generated Wavelength", aj and ak are the "Applied" Wavelengths

$$a_i = \begin{pmatrix} -0.78841497 \\ 0 \\ 0.61514375 \end{pmatrix}$$

$$a_j = \begin{pmatrix} 0 \\ 1 \\ 0 \end{pmatrix}$$

$$a_k = \begin{pmatrix} 0 \\ 1 \\ 0 \end{pmatrix}$$

$$a_{jk} = \begin{bmatrix} 0 \\ 1 \\ 0 \\ 0 \\ 0 \\ 0 \end{bmatrix}$$

Column vector from "applied" Wavelengths ==>

dij Tensor

$$d_{ijk} = \begin{pmatrix} 0 & 0 & 0 & 0 & 1.9 & 0 \\ 0 & 0 & 0 & 3.6 & 0 & 0 \\ 2.3 & 3.8 & 15.8 & 0 & 0 & 0 \end{pmatrix}$$

Indices of Refraction (λ by columns)

$$n = \begin{pmatrix} 1.7576751 & 1.7905609 & 1.8026541 \\ 1.7756109 & 1.7982079 & 1.8092106 \\ 1.8278463 & 1.8655065 & 1.8809392 \end{pmatrix}$$

Polarization Vector

$$d_{ajak} := d_{ijk} \cdot a_{jk}$$

$$d_{ajak} = \begin{pmatrix} 0 \\ 0 \\ 3.8 \end{pmatrix}$$

$$a_i \cdot d_{aiak} = 2.33754626$$

Walkoff, column 1 = "slow" rays  
column 2 = "fast" rays, λ by rows)

$$\rho = \begin{pmatrix} 2.19728498 & 0 \\ 2.30062428 & 0 \\ 2.38443356 & 0 \end{pmatrix} \text{deg}$$

Phase Match Type: Crystal Type (+/- number indicates type)

$$PMID = 1 \quad CT = -1$$

$$\Omega = \begin{pmatrix} 0.54291921 \\ 0.33452255 \\ 0.30252184 \end{pmatrix}$$

Effective Nonlinear Coefficient

$$d_{eff} = 2.33754626$$

Worksheet Walkoff values (according to phase match type selected)

$$wo_1 = 2.19728498$$

$$wo_2 = 2.30062428$$

$$wo_3 = 0$$

$$\lambda_1 \quad \lambda_2 \quad \lambda_3$$

Walkoff Angle in degrees, by Type

$$\rho_I := (p_{0,0} \ p_{1,0} \ p_{2,1}) \cdot v \quad \rho_I = (2.19728498 \ 2.30062428 \ 0)$$

$$\rho_{II} := (p_{0,1} \ p_{1,0} \ p_{2,1}) \cdot v \quad \rho_{II} = (0 \ 2.30062428 \ 0)$$

$$\rho_{III} := (p_{0,0} \ p_{0,1} \ p_{2,1}) \cdot v \quad \rho_{III} = (2.19728498 \ 0 \ 0)$$

### NOTES:

1. This worksheet treats uniaxial crystals as a simple case of a biaxial crystal, hence 3-axes vs 2 (i.e., ooe vs oe)
2. For negative crystals, the definition of "slow" and "fast" rays are "reversed" from what they mean for positive crystals
3. The effective nonlinear coefficient,  $c_{\theta h}$  is same for SHG/SFM and OPO categories (i.e., categories 1 and 4). Likewise, the two OPA/DFM cases (categories 2 and 3) have the same  $c_{\theta h}$ .

## APPENDIX C    KTP Isomorph Phase Match Ranges

## List of Tables, Appendix C

---

Table C-1	Phase Match Range, KTP .....	54
Table C-2	Phase Match Range, RTP .....	55
Table C-3	Phase Match Range, KTA .....	56
Table C-4	Phase Match Range, RTA .....	57
Table C-5	Phase Match Range, CTA .....	58

Table C-1 Phase Match Range, KTP

— KTP — Wavelength ( $\mu\text{m}$ )			Phase Match Type	Phase Match Range $\theta, \phi$ (Degrees)			
$\lambda_1$	$\lambda_2$	$\lambda_3$		$\theta$	$\phi$	$\Delta\theta$	$\Delta\phi$
1.064	1.064	0.532	I	49.41, 39.20	0, 90	10.21	90
			II	90.00, 68.67	26.0, 90	21.34	64
1.35	1.35	0.675	I	40.25, 29.57	0, 90	10.68	90
			II	49.11, 39.42	0, 90	9.70	90
4.043	1.444	1.064	I	39.24, 29.06	0, 90	10.18	90
			II	44.33, 35.47	0, 90	8.86	90
			III				
3.176	1.60	1.064	I	37.62, 27.03	0, 90	10.58	90
			II	44.85, 35.96	0, 90	8.89	90
			III	77.36, 65.90,	0, 90	11.46	90

Table C-2 Phase Match Range, RTP

- RTP - Wavelength ( $\mu\text{m}$ )			Phase Match Type	Phase Match Range $\theta, \phi$ (Degrees)			
$\lambda_1$	$\lambda_2$	$\lambda_3$		$\theta$	$\phi$	$\Delta\theta$	$\Delta\phi$
1.064	1.064	0.532	I	55.83, 32.17	0, 90	23.66	90
			II	90, 64.62	41.70, 90	25.38	48.3
1.35	1.35	0.675	I	47.12, 18.82	0, 90	28.31	90
			II	65.95, 43.91	0, 90	22.05	90
4.043	1.444	1.064	I	47.61, 19.74	0, 90	27.88	90
			II	52.79, 28.08	0, 90	24.71	90
			III				
3.176	1.60	1.064	I	45.85, 15.77	0, 90	30.08	90
			II	53.16, 28.67	0, 90	24.49	90
			III	90, 66.68	43.35, 90	23.32	44.65

**Table C-3 Phase Match Range, KTA**

- KTA - Wavelength ( $\mu\text{m}$ )			Phase Match Type	Phase Match Range $\theta, \phi$ (Degrees)			
$\lambda_1$	$\lambda_2$	$\lambda_3$		$\theta$	$\phi$	$\Delta\theta$	$\Delta\phi$
1.064	1.064	0.532	I	51.47, 44.69	0, 90	6.78	90
			II				
1.35	1.35	0.675	I	40.76, 33.79	0, 90	6.97	90
			II	67.67, 54.67	0, 90	7.00	90
4.043	1.444	1.064	I	37.30, 32.98	0, 90	4.32	90
			II	45.72, 34.82	0, 90	10.90	90
			III				
3.176	1.60	1.064	I	35.95, 30.92	0, 90	5.02	90
			II	46.01, 36.30	0, 90	9.71	90
			III	90, 71.37	16.40, 90	18.63	73.6

Table C-4 Phase Match Range, RTA

- RTA - Wavelength ( $\mu\text{m}$ )			Phase Match Type	Phase Match Range $\theta, \phi$ (Degrees)			
$\lambda_1$	$\lambda_2$	$\lambda_3$		$\theta$	$\phi$	$\Delta\theta$	$\Delta\phi$
1.064	1.064	0.532	I	57.66, 47.48	0, 90	10.18	90
			II				
1.35	1.35	0.675	I	45.08, 35.06	0, 90	10.02	90
			II	70.40, 59.73	0, 90	10.67	90
4.043	1.444	1.064	I	41.94, 27.80	0, 90	14.14	90
			II	42.48, 39.65	0, 90	2.82	90
			III				
3.176	1.60	1.064	I	40.35, 26.65	0, 90	13.70	90
			II	44.43, 40.17	0, 90	4.26	90
			III	90, 81.52	58.63, 90	8.48	31.37



Table C-5 Phase Match Range, CTA

— CTA — Wavelength ( $\mu\text{m}$ )			Phase Match Type	Phase Match Range $\theta, \phi$ (Degrees)			
$\lambda_1$	$\lambda_2$	$\lambda_3$		$\theta$	$\phi$	$\Delta\theta$	$\Delta\phi$
1.064	1.064	0.532	I	75.50, 52.22	0, 90	23.29	90
			II				
1.35	1.35	0.675	I	56.37, 34.26	0, 90	22.11	90
			II	90, 72.04	53.40, 90	17.96	36.60
4.043	1.444	1.064	I	53.80, 29.52	0, 90	24.29	90
			II	61.59, 40.06	0, 90	21.45	90
			III				
3.176	1.60	1.064	I	51.89, 26.41	0, 90	25.49	90
			II	62.60, 41.18	0, 90	21.18	90
			III				

## APPENDIX D    KTP Isomorph Nonlinear Characteristics

## List of Tables, Appendix D

---

Table D-1	Nonlinear Characteristics, KTP	61
Table D-2	Nonlinear Characteristics, RTP	62
Table D-3	Nonlinear Characteristics, KTA	63
Table D-4	Nonlinear Characteristics, RTA	64
Table D-5	Nonlinear Characteristics, CTA	65

Table D-1 Nonlinear Characteristics, KTP

KTP									
Wavelength ( $\mu\text{m}$ )			Phase Match Type	k - Vector (degrees)		Walk-Off (milli-radians)			$ d_{\text{eff}} $ pm/V
$\lambda_1$	$\lambda_2$	$\lambda_3$		$\theta$	$\phi$	$\rho_1$	$\rho_2$	$\rho_3$	
1.064	1.064	0.532	I	45.8	36	40.14	40.14	8.33*	0.4805
			II	90.0	26.0	3.5*	0	4.9	3.267
1.35	1.35	0.675	I	37.284	31	37.18	37.18	8.13*	0.4073
			II	49.112	0	0	49.02	0*	2.591
4.043	1.444	1.064	I	34.823	30	32.04	37.84	6.93*	0.390
			II	44.33	0	0	50.14	0*	2.403
			III						
3.176	1.60	1.064	I	34.823	30	33.02	36.04	7.30*	0.386
			II	44.852	0	0	48.56	0*	2.421
			III	77.358	0	20.16	0	0*	3.496

- 1 Starred (\*) walk-off angle indicates the walk-off angle from which the other two are referenced
- 2 All measurements made where  $d_{\text{eff}}$  was at maximum value
- 3 SHG Measurements made for: 1.064/1.064/0.532 and 1.35/1.35/0.675
- 4 OPO Measurements made for: 4.043/1.444/1.064 and 3.176/1.60/1.064

Table D-2 Nonlinear Characteristics, RTP

RTP									
Wavelength ( $\mu\text{m}$ )			Phase Match Type	$\kappa$ - Vector (degrees)		Walk-Off (milli-radians)			$ d_{\text{eff}} $ pmV
$\lambda_1$	$\lambda_2$	$\lambda_3$		$\theta$	$\phi$	$\rho_1$	$\rho_2$	$\rho_3$	
1.064	1.064	0.532	I	52.180	23	36.92	36.92	13.47*	0.1194
			II	90	41.70	11.55	0*	13.09	2.826
1.35	1.35	0.675	I	27.127	53	14.90	14.90	17.57*	0.3350
			II	65.951	0	0	40.82	0*	3.218
4.043	1.444	1.064	I	27.9948	53	13.01*	14.37	3.61	0.3369
			II	52.789	0	0*	51.38	0	2.774
			III						
3.176	1.60	1.064	I	25.701	50	9.58	12.43	17.82*	0.426
			II	53.158	0	0*	50.74	0	2.78
			III	90.0	45.35	0*	11.33	11.60	2.723

- 1 Starred (\*) walk-off angle indicates the walk-off angle from which the other two are referenced
- 2 All measurements made where  $d_{\text{eff}}$  was at maximum value
- 3 SHG Measurements made for 1.064/1.064/0.532 and 1.35/1.35/0.675
- 4 OPO Measurements made for 4.043/1.444/1.064 and 3.176/1.60/1.064

Table D-3 Nonlinear Characteristics, KTA

KTA									
Wavelength ( $\mu\text{m}$ )			Phase Match Type	k - Vector (degrees)		Walk-Off (milli-radians)			$ d_{\text{eff}} $ pm/V
$\lambda_1$	$\lambda_2$	$\lambda_3$		$\theta$	$\phi$	$\rho_1$	$\rho_2$	$\rho_3$	
1.064	1.064	0.532	I	48.63	40	40.58	40.58	5.23*	0.253
			II						
1.35	1.35	0.675	I	38.52	34	38.00	38.00	5.32*	0.1998
			II	61.673	0	0	39.43	0*	2.773
4.043	1.444	1.064	I	33.21	67	10.82	35.53	3.58*	1.289
			II	45.718	0	0	45.68	0*	2.239
			III						
3.176	1.60	1.064	I	32.490	53	0.595	33.54	5.15*	0.729
			II	46.007	0	0	45.10	0*	2.237
			III	90.0	16.40	0*	4.48	4.40	3.460

1 Starred (\*) walk-off angle indicates the walk-off angle from which the other two are referenced

2 All measurements made where  $d_{\text{eff}}$  was at maximum value

3 SHG Measurements made for 1.064/1.064/0.532 and 1.35/1.35/0.675

4 OPO Measurements made for 4.043/1.444/1.064 and 3.176/1.60/1.064

Table D-4 Nonlinear Characteristics, RTA

RTA									
Wavelength ( $\mu\text{m}$ )			Phase Match Type	k - Vector (degrees)		Walk-Off (milli-radians)			$ d_{\text{eff}} $ pm/V
$\lambda_1$	$\lambda_2$	$\lambda_3$		$\theta$	$\phi$	$\rho_1$	$\rho_2$	$\rho_3$	
1.064	1.064	0.532	I	53.1755	41	32.57	32.57	6.976*	0.5300
			II						
1.35	1.35	0.675	I	41.525	36	32.74	32.74	6.578*	0.5058
			II	70.396	0	0	27.09	0*	3.353
4.043	1.444	1.064	I	40.245	15	22.76	36.84	3.18*	1.234
			II	42.476	0	0	40.95	0*	2.329
			III						
3.176	1.60	1.064	I	34.049	40	27.77	28.59	6.51*	0.402
			II	44.429	0	0	40.91	0*	2.418
			III	90.0	58.63	0	0*	3.21	2.347

- 1 Starred (\*) walk-off angle indicates the walk-off angle from which the other two are referenced
2. All measurements made where  $d_{\text{eff}}$  was at maximum value
- 3 SHG Measurements made for 1.064/1.064/0.532 and 1.35/1.35/0.675
- 4 OPO Measurements made for 4.043/1.444/1.064 and 3.176/1.60/1.064

Table D-5 Nonlinear Characteristics, CTA

CTA									
Wavelength ( $\mu\text{m}$ )			Phase Match Type	k - Vector (degrees)		Walk-Off (milli-radians)			$ d_{\text{eff}} $ pm/V
$\lambda_1$	$\lambda_2$	$\lambda_3$		$\theta$	$\phi$	$\rho_1$	$\rho_2$	$\rho_3$	
1.064	1.064	0.532	I	64.12	42	16.66	16.66	9.655*	0.185
			II						
1.35	1.35	0.675	I	32.08	26	24.35	24.35	8.688*	0.1331
			II	90	53.4	7.8	0*	7.6	2.490
4.043	1.444	1.064	I	37.52	53	10.49*	17.42	0.340	0.2608
			II	61.508	0	0	30.82	0*	3.115
			III						
3.176	1.60	1.064	I	34.60	53	10.978*	15.29	0.152	0.2872
			II	62.595	0	0	29.85	0*	3.148
			III						

- 1 Starred (\*) walk-off angle indicates the walk-off angle from which the other two are referenced
- 2 All measurements made where  $d_{\text{eff}}$  was at maximum value
- 3 SHG Measurements made for 1.064/1.064/0.532 and 1.35/1.35/0.675
- 4 OPO Measurements made for 4.043/1.444/1.064 and 3.176/1.60/1.064



## APPENDIX E    KTP Isomorph Nonlinear Coefficient ( $d_{eff}$ )

# List of Figures, Appendix E

Figure E-1	$d_{eff}$ versus Phase Match Region, 1.064/1.064/0.532 $\mu\text{m}$ , Type I, KTP	68
Figure E-2	$d_{eff}$ versus Phase Match Region, 1.064/1.064/0.532 $\mu\text{m}$ , Type II, KTP	68
Figure E-3	$d_{eff}$ versus Phase Match Region, 1.35/1.35/0.675 $\mu\text{m}$ , Type I, KTP	69
Figure E-4	$d_{eff}$ versus Phase Match Region, 1.35/1.35/0.675 $\mu\text{m}$ , Type II, KTP	69
Figure E-5	$d_{eff}$ versus Phase Match Region, 4.043/1.444/1.064 $\mu\text{m}$ , Type I, KTP	70
Figure E-6	$d_{eff}$ versus Phase Match Region, 4.043/1.444/1.064 $\mu\text{m}$ , Type II, KTP	70
Figure E-7	$d_{eff}$ versus Phase Match Region, 3.17/1.60/1.064 $\mu\text{m}$ , Type I, KTP	71
Figure E-8	$d_{eff}$ versus Phase Match Region, 3.17/1.60/1.064 $\mu\text{m}$ , Type II, KTP	71
Figure E-9	$d_{eff}$ versus Phase Match Region, 3.17/1.60/1.064 $\mu\text{m}$ , Type III, KTP	72
Figure E-10	$d_{eff}$ versus Phase Match Region, 1.064/1.064/0.532 $\mu\text{m}$ , Type I, RTP	73
Figure E-11	$d_{eff}$ versus Phase Match Region, 1.064/1.064/0.532 $\mu\text{m}$ , Type II, RTP	73
Figure E-12	$d_{eff}$ versus Phase Match Region, 1.35/1.35/0.675 $\mu\text{m}$ , Type I, RTP	74
Figure E-13	$d_{eff}$ versus Phase Match Region, 1.35/1.35/0.675 $\mu\text{m}$ , Type II, RTP	74
Figure E-14	$d_{eff}$ versus Phase Match Region, 4.043/1.444/1.064 $\mu\text{m}$ , Type I, RTP	75
Figure E-15	$d_{eff}$ versus Phase Match Region, 4.043/1.444/1.064 $\mu\text{m}$ , Type II, RTP	75
Figure E-16	$d_{eff}$ versus Phase Match Region, 3.17/1.60/1.064 $\mu\text{m}$ , Type I, RTP	76
Figure E-17	$d_{eff}$ versus Phase Match Region, 3.17/1.60/1.064 $\mu\text{m}$ , Type II, RTP	76
Figure E-18	$d_{eff}$ versus Phase Match Region, 3.17/1.60/1.064 $\mu\text{m}$ , Type III, RTP	77
Figure E-19	$d_{eff}$ versus Phase Match Region, 1.064/1.064/0.532 $\mu\text{m}$ , Type I, KTA	78
Figure E-20	$d_{eff}$ versus Phase Match Region, 1.35/1.35/0.675 $\mu\text{m}$ , Type I, KTA	79
Figure E-21	$d_{eff}$ versus Phase Match Region, 1.35/1.35/0.675 $\mu\text{m}$ , Type II, KTA	79
Figure E-22	$d_{eff}$ versus Phase Match Region, 4.043/1.444/1.064 $\mu\text{m}$ , Type I, KTA	80
Figure E-23	$d_{eff}$ versus Phase Match Region, 4.043/1.444/1.064 $\mu\text{m}$ , Type II, KTA	80
Figure E-24	$d_{eff}$ versus Phase Match Region, 3.17/1.60/1.064 $\mu\text{m}$ , Type I, KTA	81
Figure E-25	$d_{eff}$ versus Phase Match Region, 3.17/1.60/1.064 $\mu\text{m}$ , Type II, KTA	81
Figure E-26	$d_{eff}$ versus Phase Match Region, 3.17/1.60/1.064 $\mu\text{m}$ , Type III, KTA	82
Figure E-27	$d_{eff}$ versus Phase Match Region, 1.064/1.064/0.532 $\mu\text{m}$ , Type I, RTA	83
Figure E-28	$d_{eff}$ versus Phase Match Region, 1.35/1.35/0.675 $\mu\text{m}$ , Type I, RTA	84
Figure E-29	$d_{eff}$ versus Phase Match Region, 1.35/1.35/0.675 $\mu\text{m}$ , Type II, RTA	84
Figure E-30	$d_{eff}$ versus Phase Match Region, 4.043/1.444/1.064 $\mu\text{m}$ , Type I, RTA	85
Figure E-31	$d_{eff}$ versus Phase Match Region, 4.043/1.444/1.064 $\mu\text{m}$ , Type II, RTA	85
Figure E-32	$d_{eff}$ versus Phase Match Region, 3.17/1.60/1.064 $\mu\text{m}$ , Type I, RTA	86
Figure E-33	$d_{eff}$ versus Phase Match Region, 3.17/1.60/1.064 $\mu\text{m}$ , Type II, RTA	86
Figure E-34	$d_{eff}$ versus Phase Match Region, 3.17/1.60/1.064 $\mu\text{m}$ , Type III, RTA	87
Figure E-35	$d_{eff}$ versus Phase Match Region, 1.064/1.064/0.532 $\mu\text{m}$ , Type I, CTA	88
Figure E-36	$d_{eff}$ versus Phase Match Region, 1.35/1.35/0.675 $\mu\text{m}$ , Type I, CTA	89
Figure E-37	$d_{eff}$ versus Phase Match Region, 1.35/1.35/0.675 $\mu\text{m}$ , Type II, CTA	89
Figure E-38	$d_{eff}$ versus Phase Match Region, 4.043/1.444/1.064 $\mu\text{m}$ , Type I, CTA	90
Figure E-39	$d_{eff}$ versus Phase Match Region, 4.043/1.444/1.064 $\mu\text{m}$ , Type II, CTA	90
Figure E-40	$d_{eff}$ versus Phase Match Region, 3.17/1.60/1.064 $\mu\text{m}$ , Type I, CTA	91
Figure E-41	$d_{eff}$ versus Phase Match Region, 3.17/1.60/1.064 $\mu\text{m}$ , Type II, CTA	91

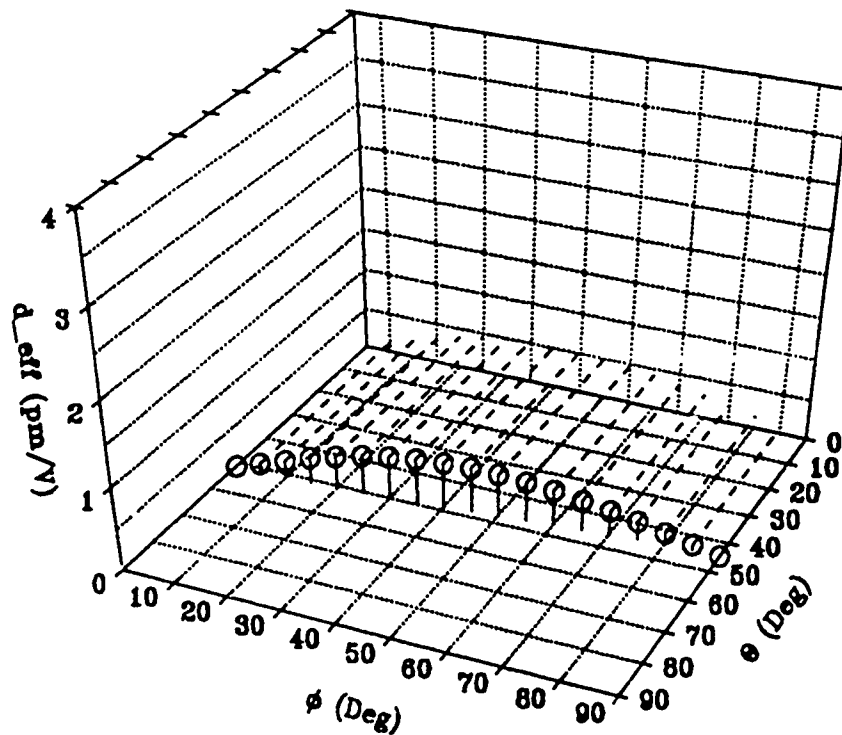


Figure E-1  $d_{eff}$  versus Phase Match Region, 1.064/1.064/0.532  $\mu\text{m}$ , Type I, KTP

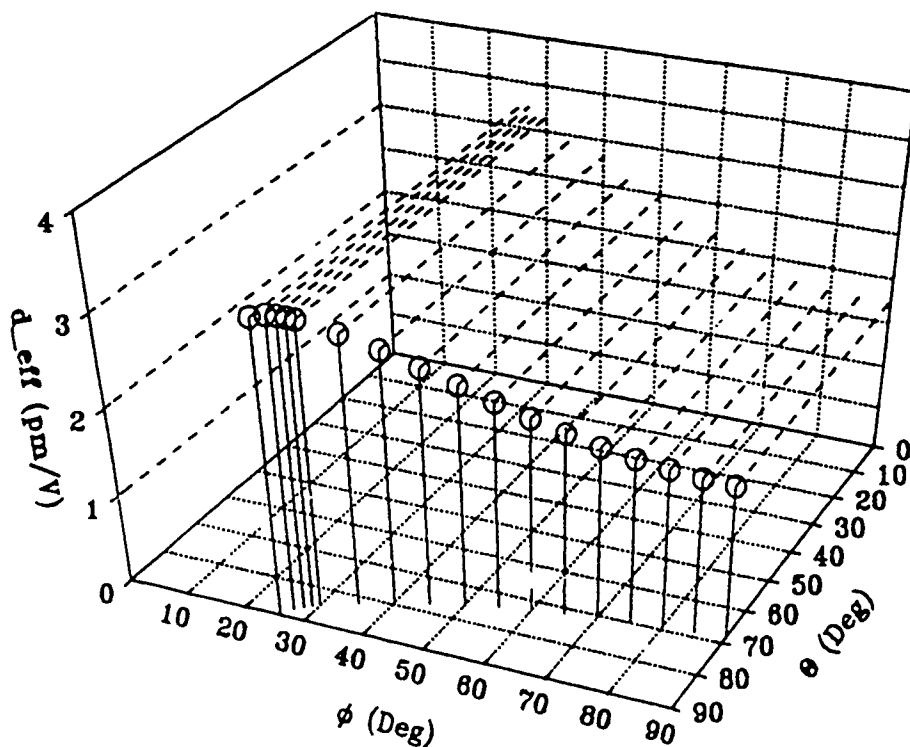


Figure E-2  $d_{eff}$  versus Phase Match Region, 1.064/1.064/0.532  $\mu\text{m}$ , Type II, KTP

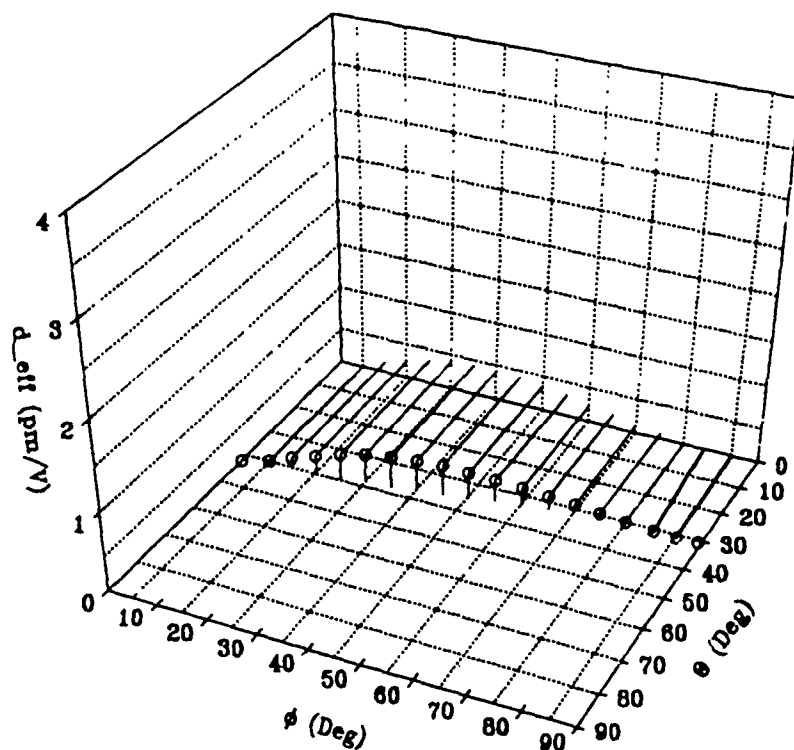


Figure E-3  $d_{eff}$  versus Phase Match Region, 1.35/1.35/0.675  $\mu\text{m}$ , Type I, KTP

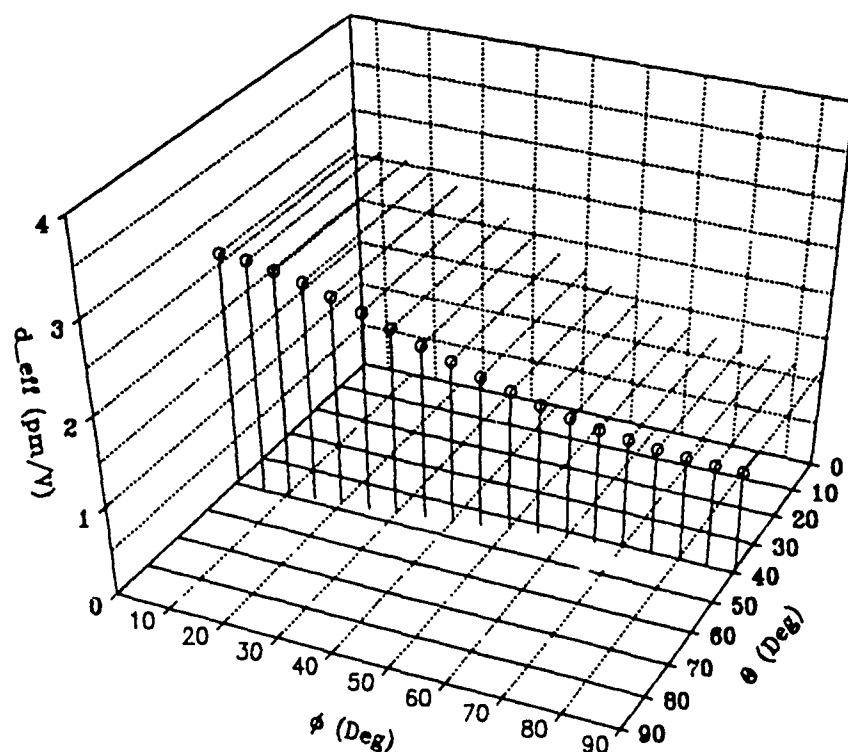


Figure E-4  $d_{eff}$  versus Phase Match Region, 1.35/1.35/0.675  $\mu\text{m}$ , Type II, KTP

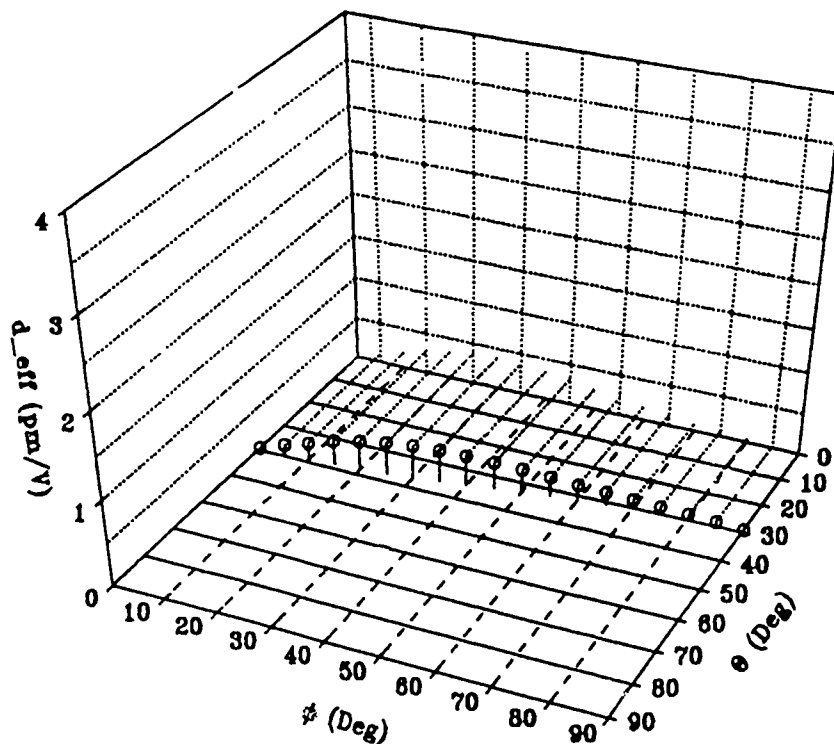


Figure E-5  $d_{eff}$  versus Phase Match Region, 4.043/1.444/1.064  $\mu\text{m}$ , Type I, KTP

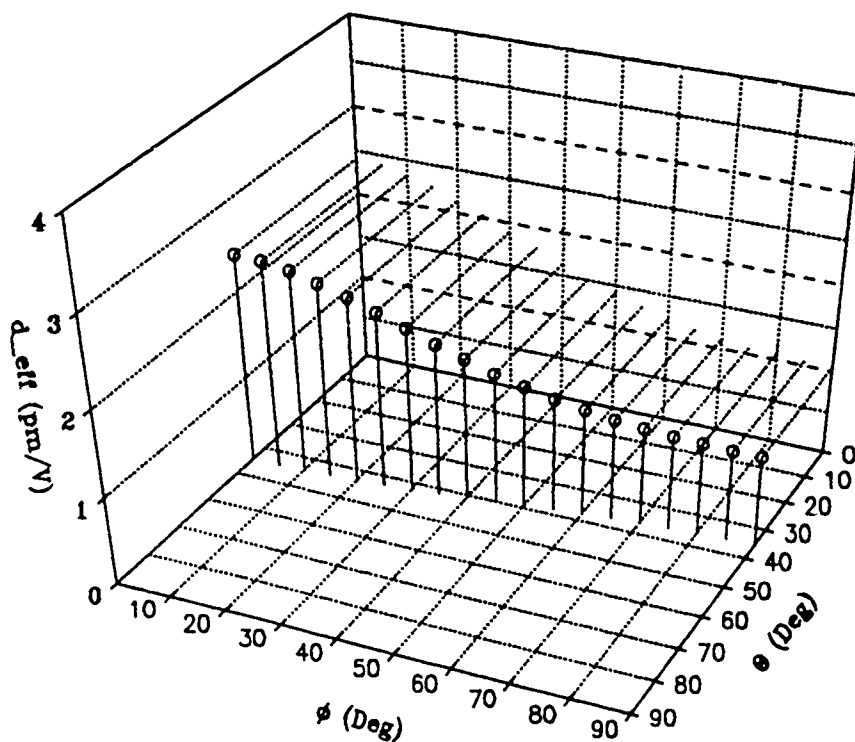


Figure E-6  $d_{eff}$  versus Phase Match Region, 4.043/1.444/1.064  $\mu\text{m}$ , Type II, KTP

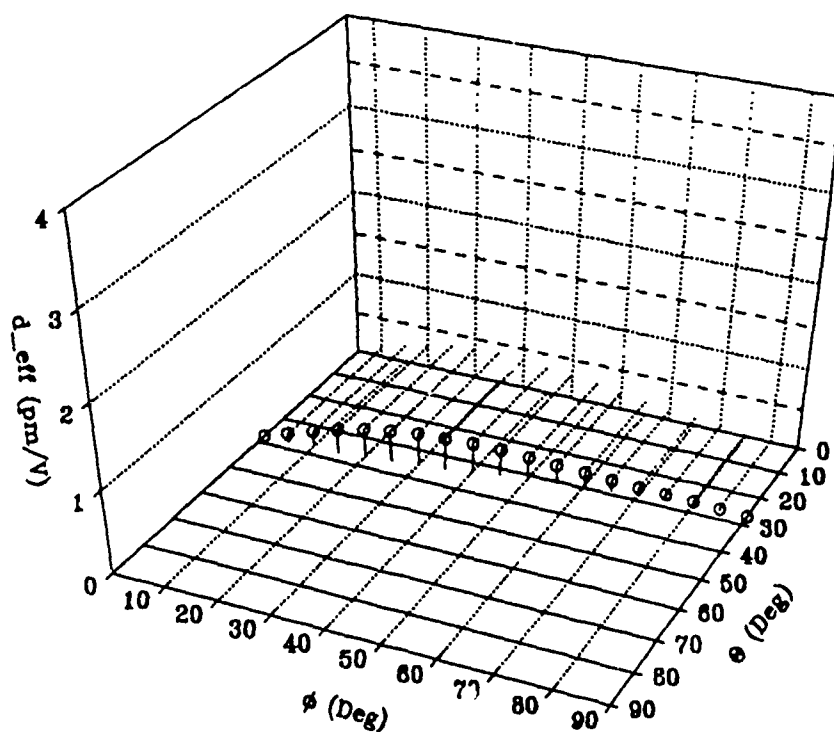


Figure E-7  $d_{eff}$  versus Phase Match Region, 3.17/1.60/1.064  $\mu\text{m}$ , Type I, KTP

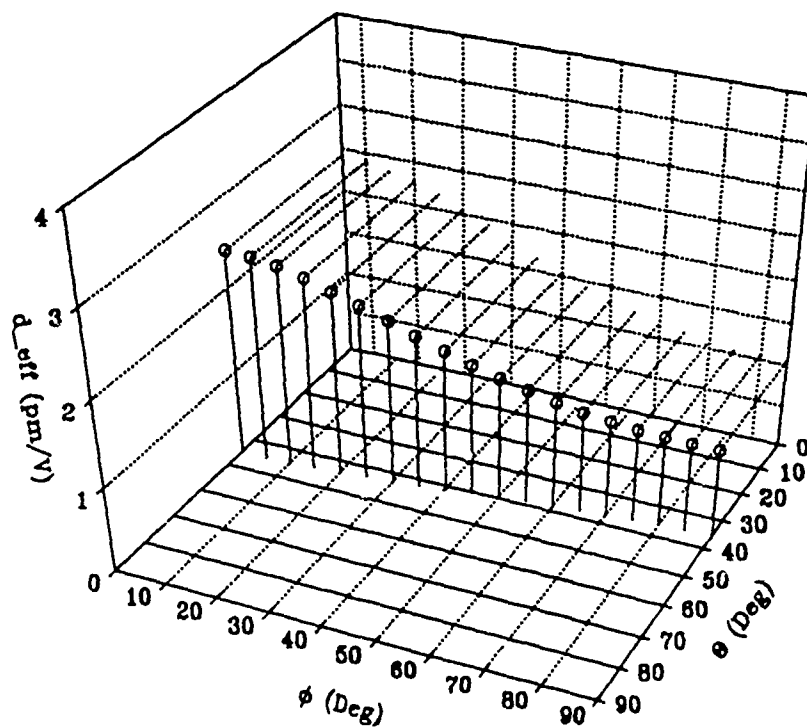


Figure E-8  $d_{eff}$  versus Phase Match Region, 3.17/1.60/1.064  $\mu\text{m}$ , Type II, KTP

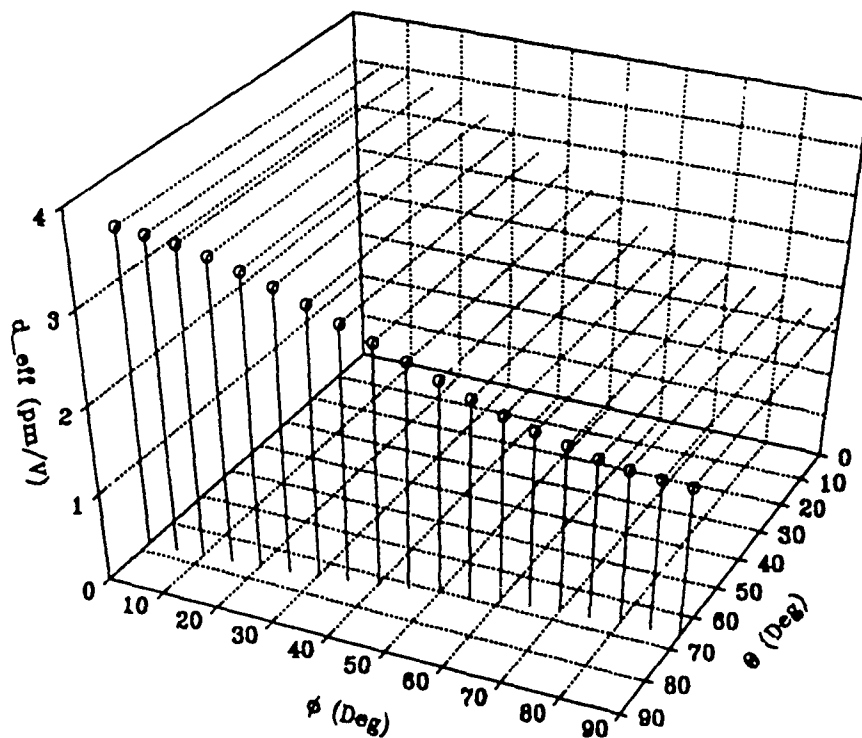


Figure E-9  $d_{eff}$  versus Phase Match Region, 3.17/1.60/1.064  $\mu\text{m}$ . Type III, KTP

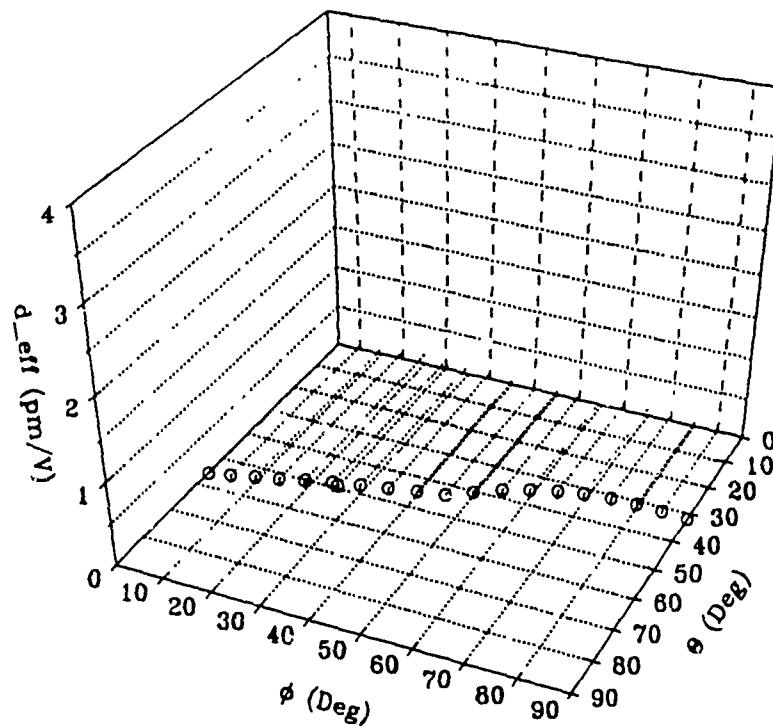


Figure E-10  $d_{eff}$  versus Phase Match Region, 1.064/1.064/0.532  $\mu\text{m}$ , Type I, RTP

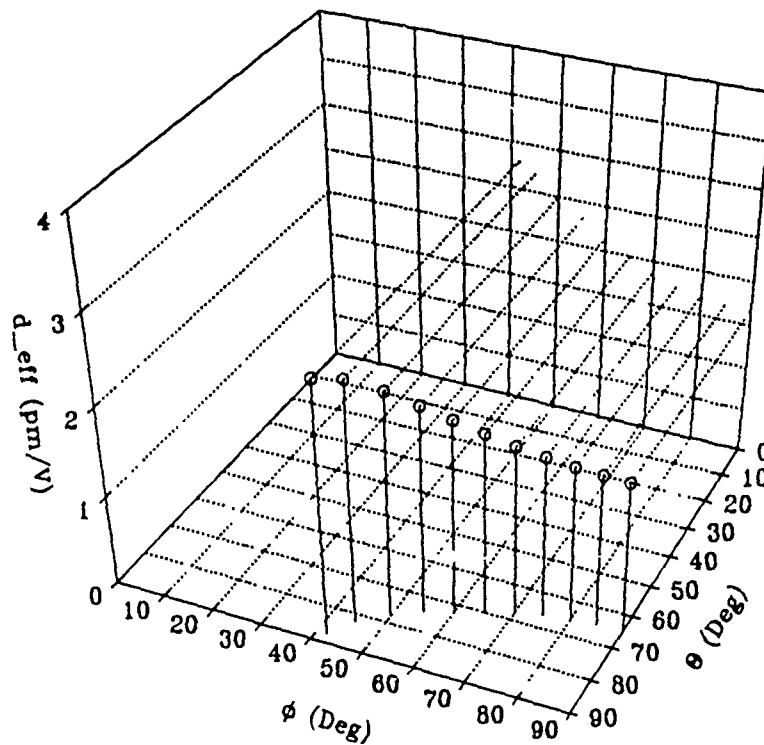


Figure E-11  $d_{eff}$  versus Phase Match Region, 1.064/1.064/0.532  $\mu\text{m}$ , Type II, RTP



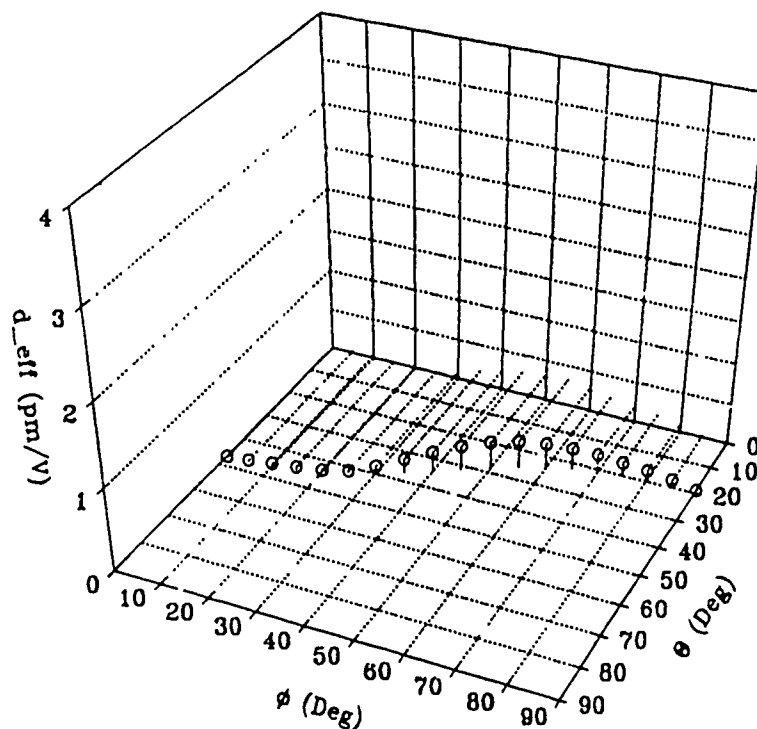


Figure E-12  $d_{eff}$  versus Phase Match Region, 1.35/1.35/0.675  $\mu\text{m}$ , Type I, RTP

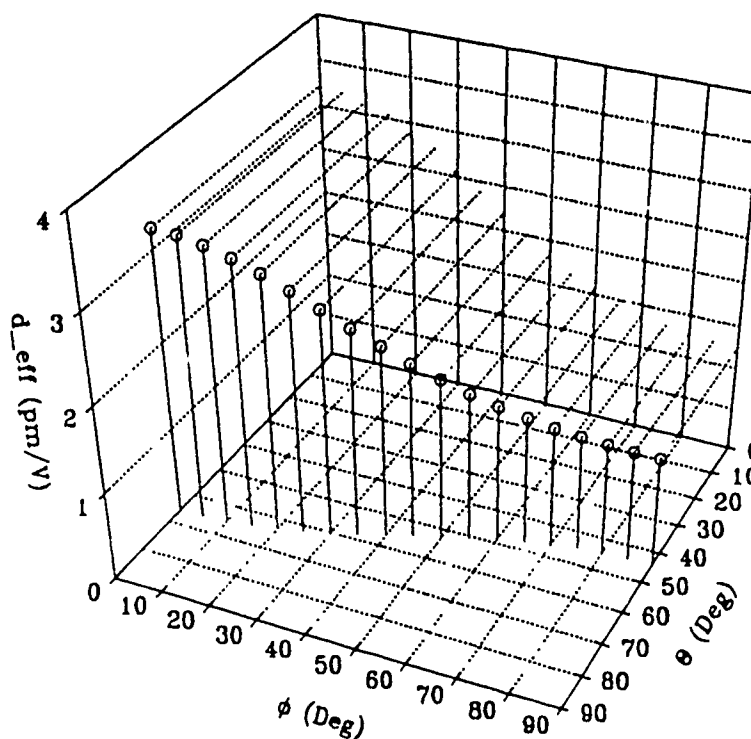


Figure E-13  $d_{eff}$  versus Phase Match Region, 1.35/1.35/0.675  $\mu\text{m}$ , Type II, RTP

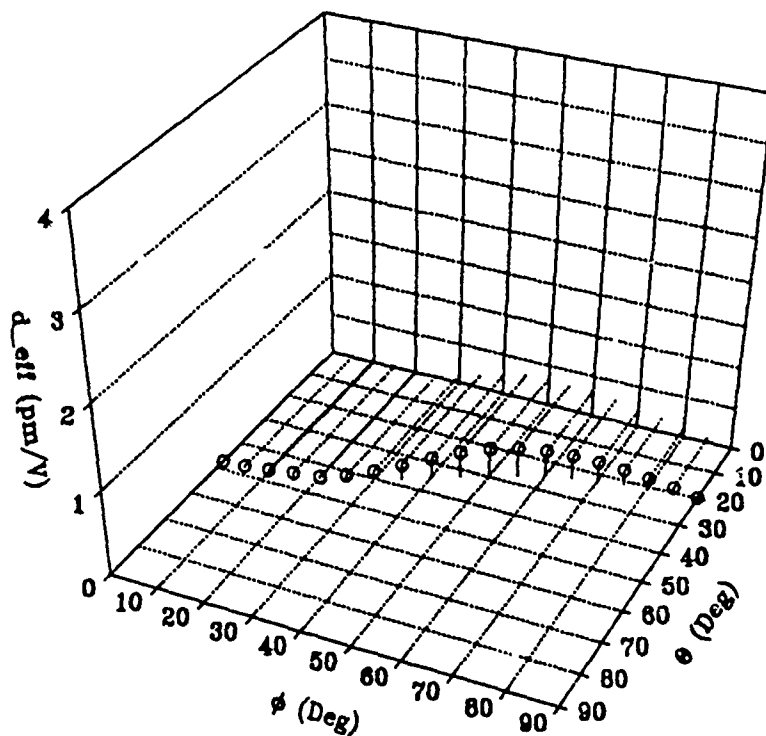


Figure E-14  $d_{eff}$  versus Phase Match Region, 4.043/1.444/1.064  $\mu\text{m}$ , Type I, RTP

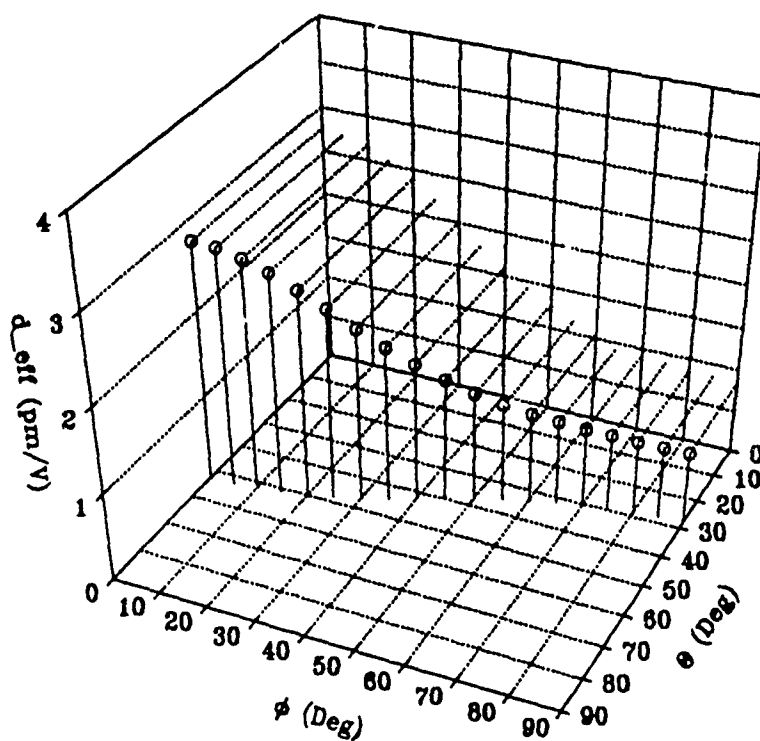


Figure E-15  $d_{eff}$  versus Phase Match Region, 4.043/1.444/1.064  $\mu\text{m}$ , Type II, RTP

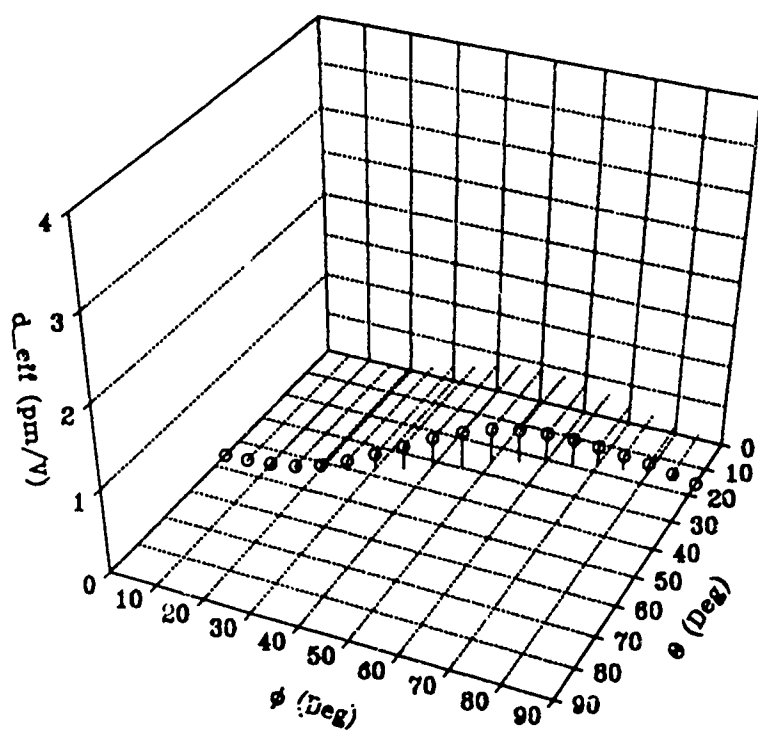


Figure E-16  $d_{eff}$  versus Phase Match Region, 3.17/1.60/1.064  $\mu\text{m}$ , Type I, RTP

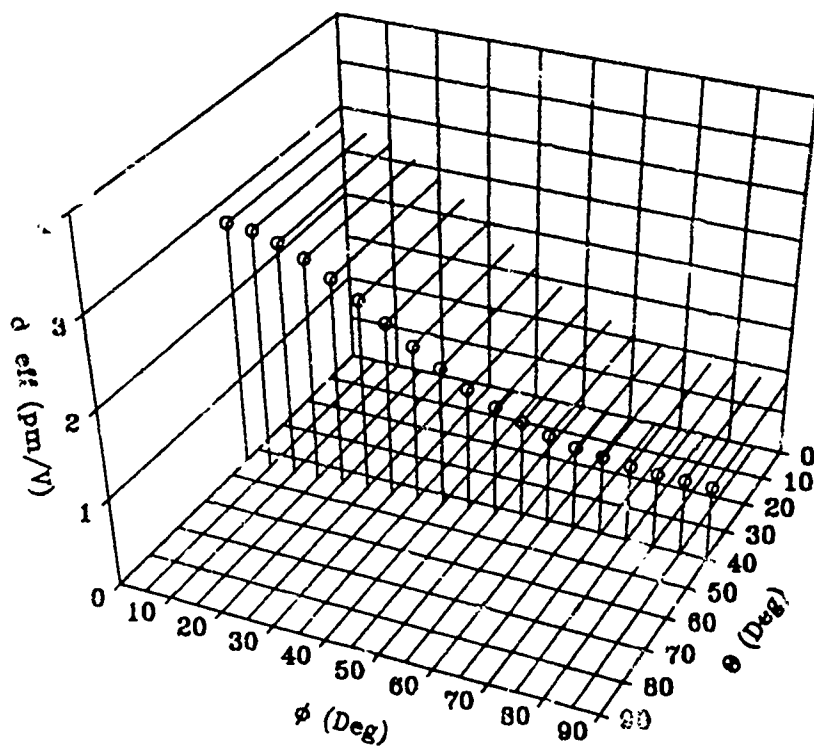


Figure E-17  $d_{eff}$  versus Phase Match Region, 3.17/1.60/1.064  $\mu\text{m}$ , Type II, RTP

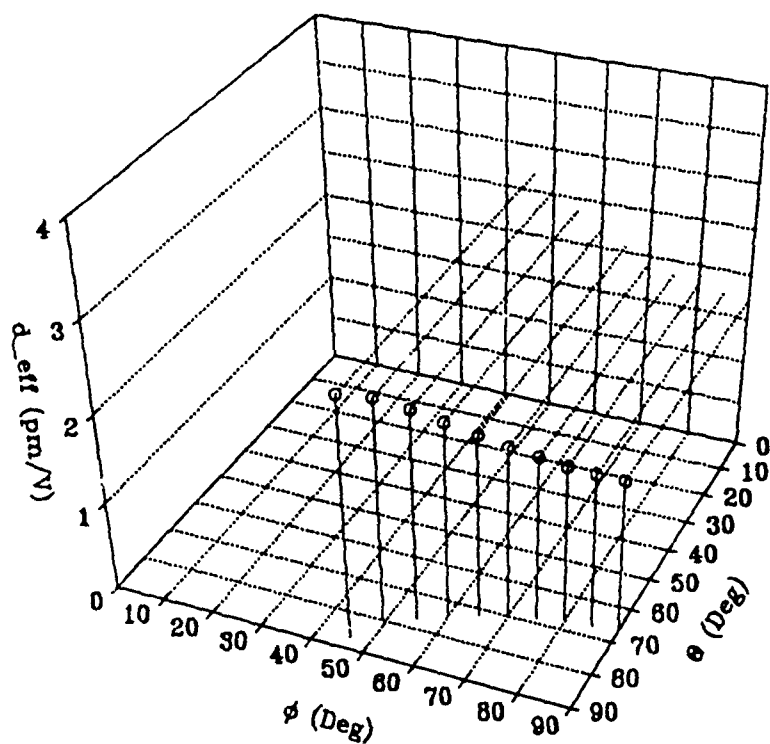


Figure E-18  $d_{eff}$  versus Phase Match Region, 3.17/1.60/1.064  $\mu\text{m}$ . Type III, RTP

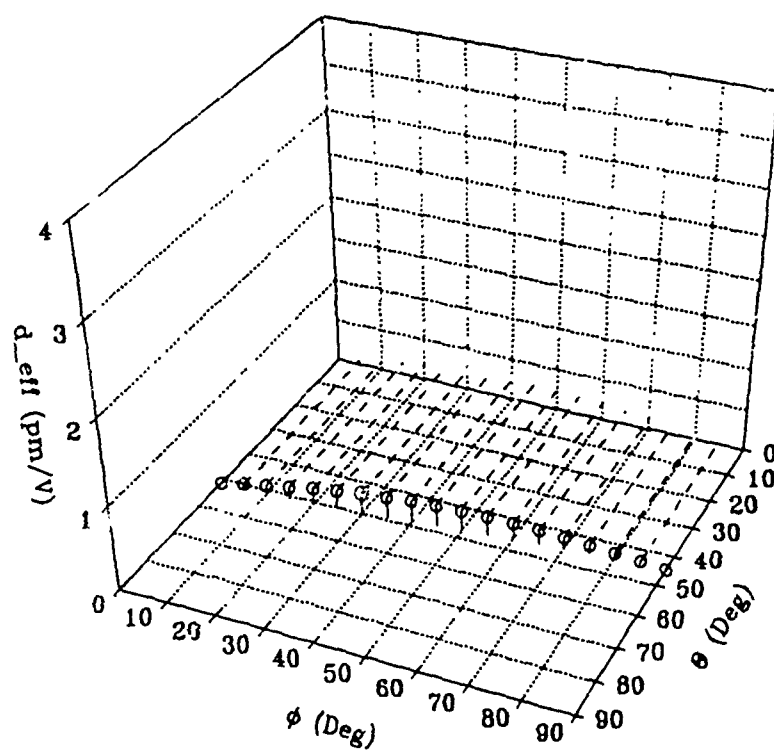


Figure E-19  $d_{eff}$  versus Phase Match Region, 1.064/1.064/0.532  $\mu\text{m}$ , Type I, KTA

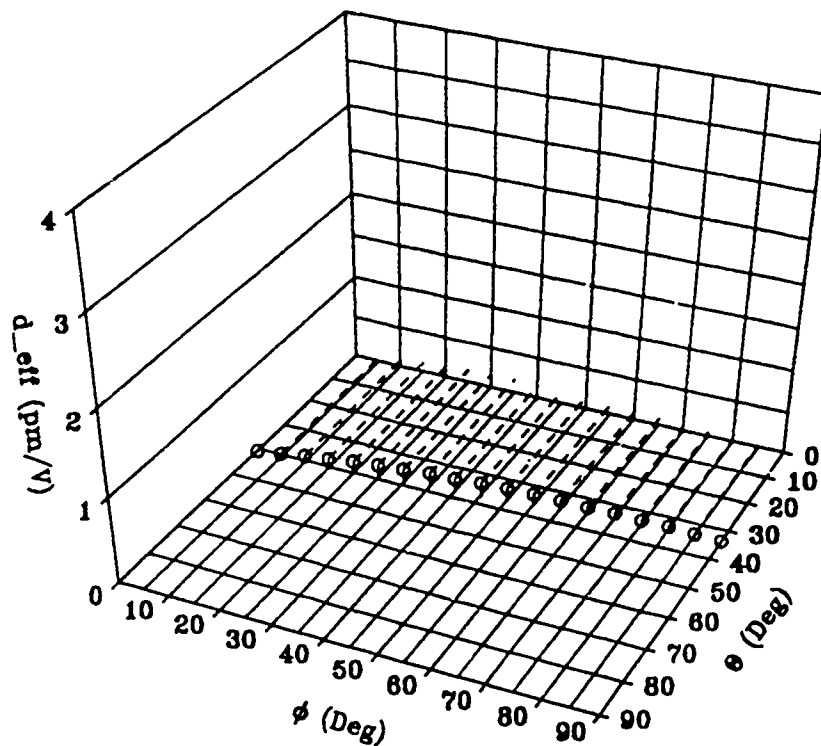


Figure E-20  $d_{eff}$  versus Phase Match Region, 1.35/1.35/0.675  $\mu\text{m}$ , Type I, KTA

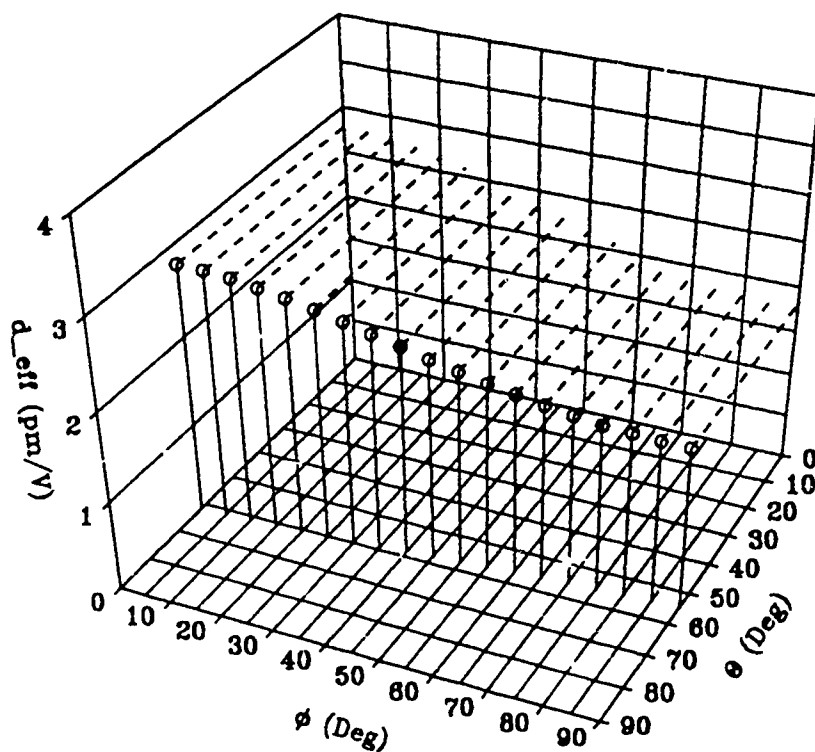


Figure E-21  $d_{eff}$  versus Phase Match Region, 1.35/1.35/0.675  $\mu\text{m}$ , Type II, KTA

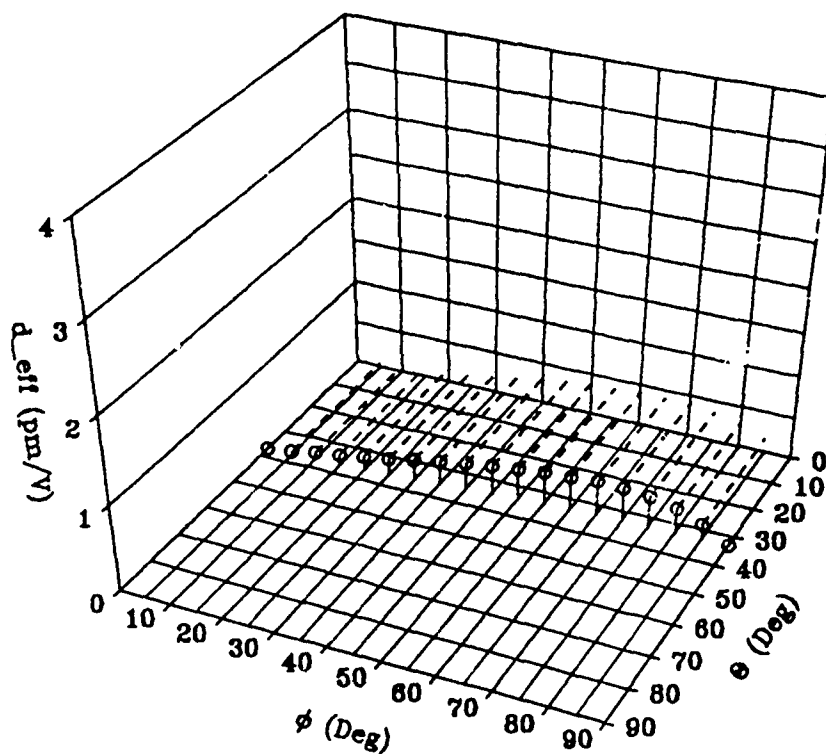


Figure E-22  $d_{eff}$  versus Phase Match Region, 4.043/1.444/1.064  $\mu\text{m}$ , Type I, KTA

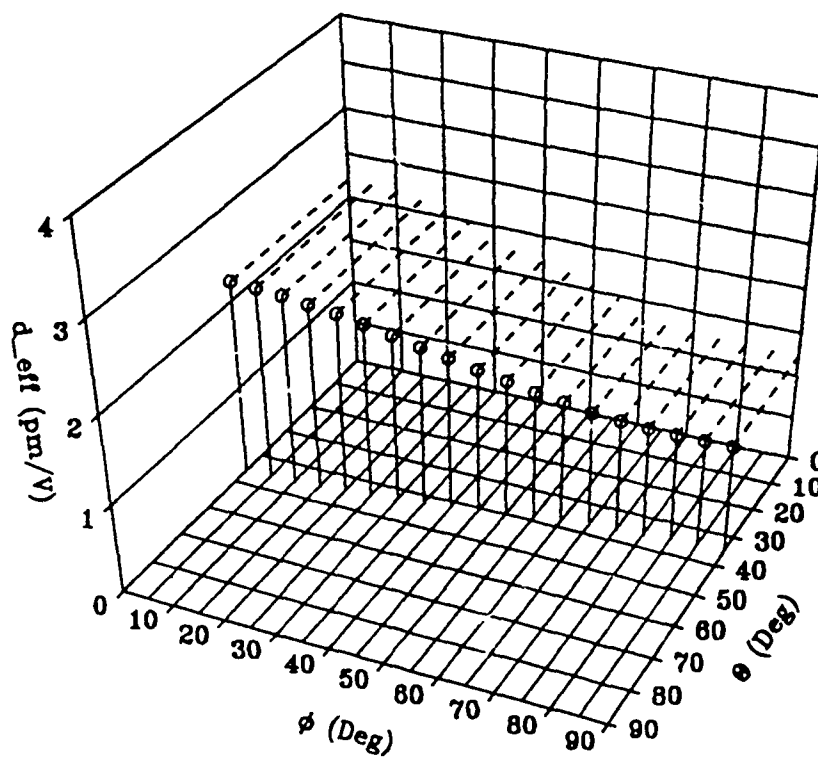


Figure E-23  $d_{eff}$  versus Phase Match Region, 4.043/1.444/1.064  $\mu\text{m}$ , Type II, KTA

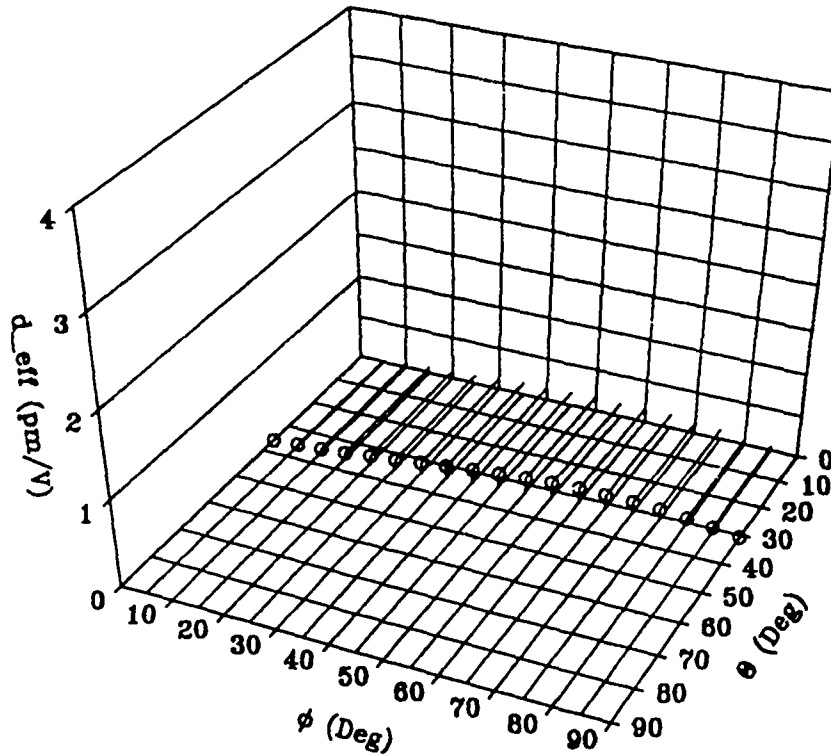


Figure E-24  $d_{eff}$  versus Phase Match Region, 3.17/1.60/1.064  $\mu\text{m}$ , Type I, KTA

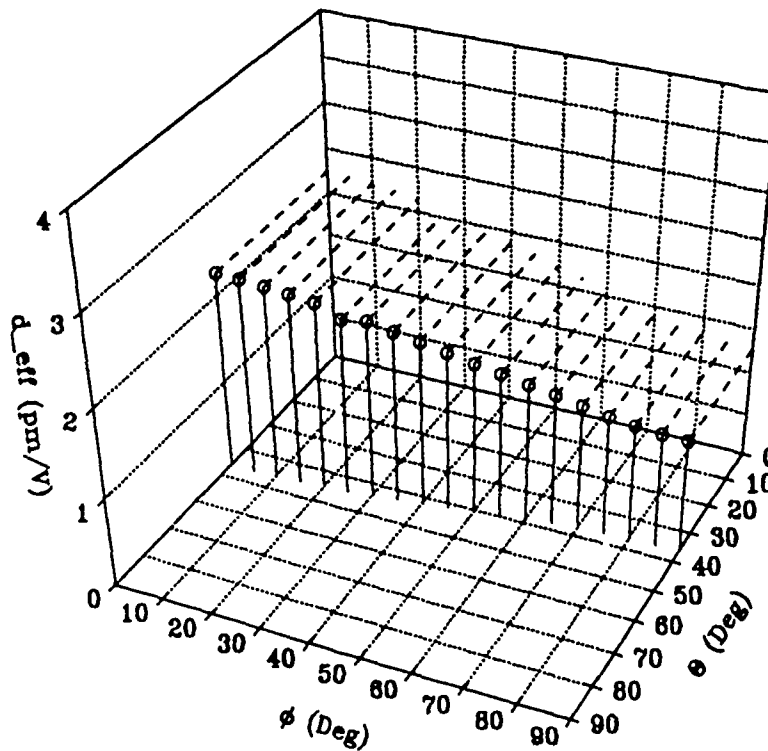


Figure E-25  $d_{eff}$  versus Phase Match Region, 3.17/1.60/1.064  $\mu\text{m}$ , Type II, KTA



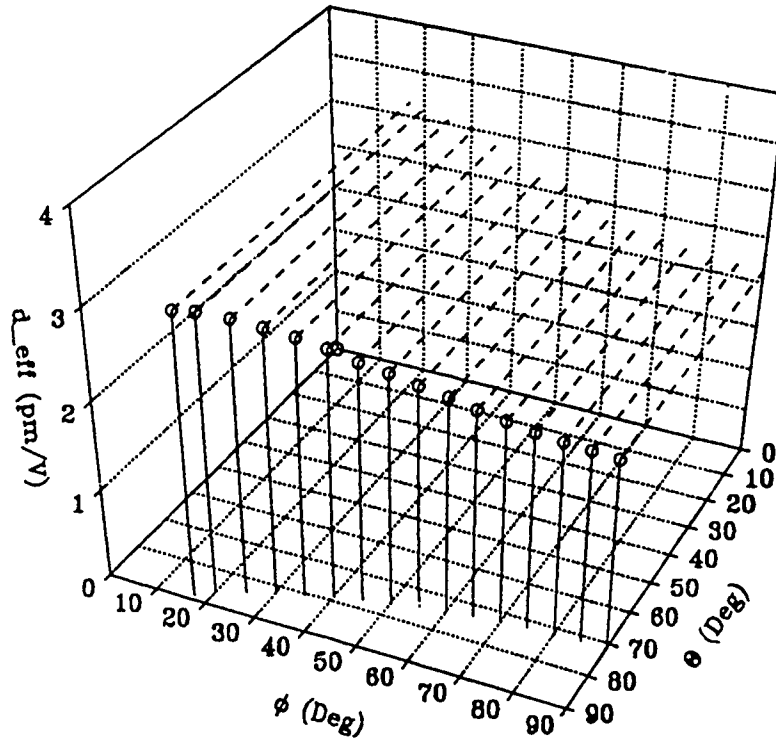


Figure E-26  $d_{eff}$  versus Phase Match Region, 3.17/1.60/1.064  $\mu\text{m}$ , Type III, KTA

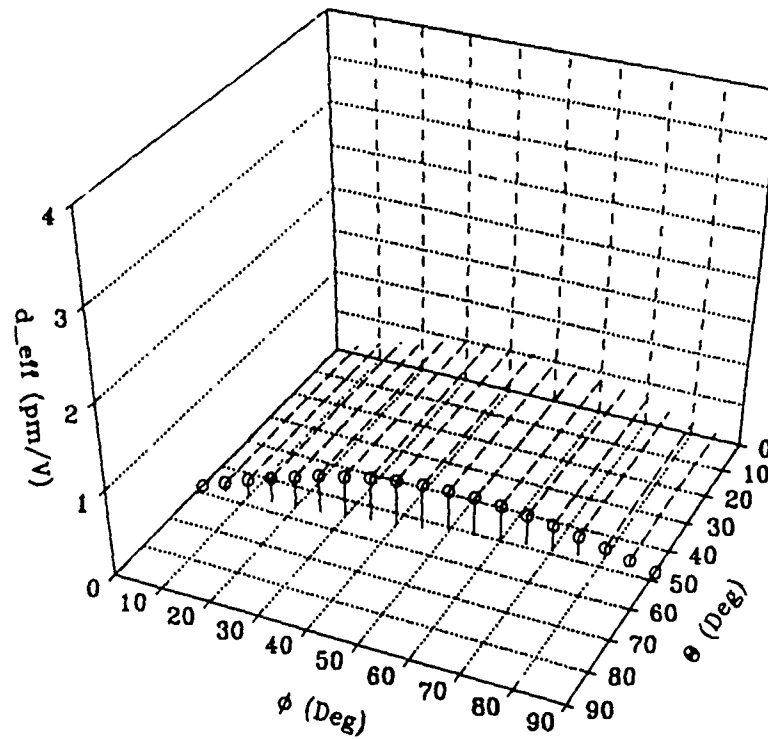


Figure E-27.  $d_{eff}$  versus Phase Match Region, 1.064/1.064/0.532  $\mu\text{m}$ , Type I, RTA

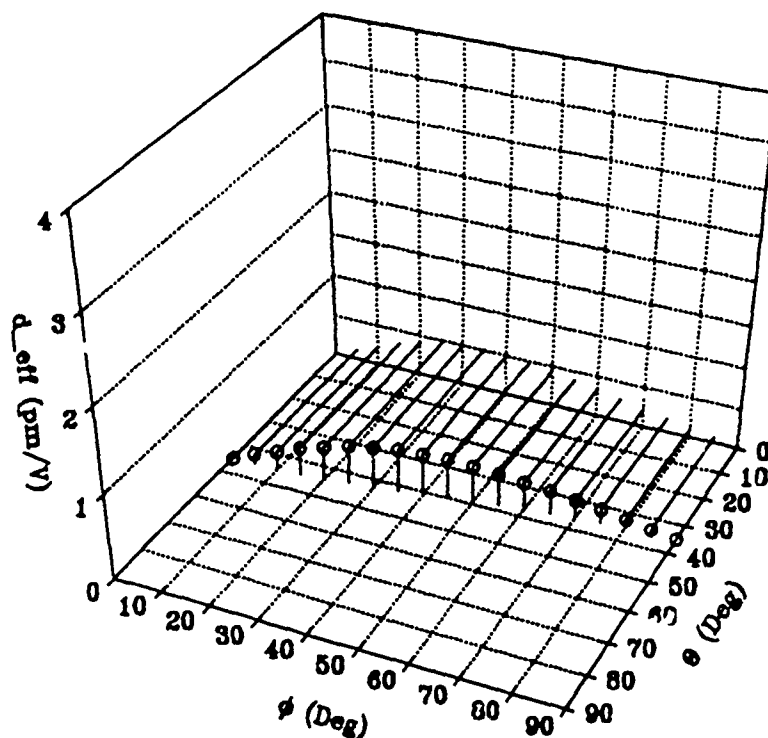


Figure E-28  $d_{eff}$  versus Phase Match Region, 1.35/1.35/0.675  $\mu\text{m}$ , Type I, RTA

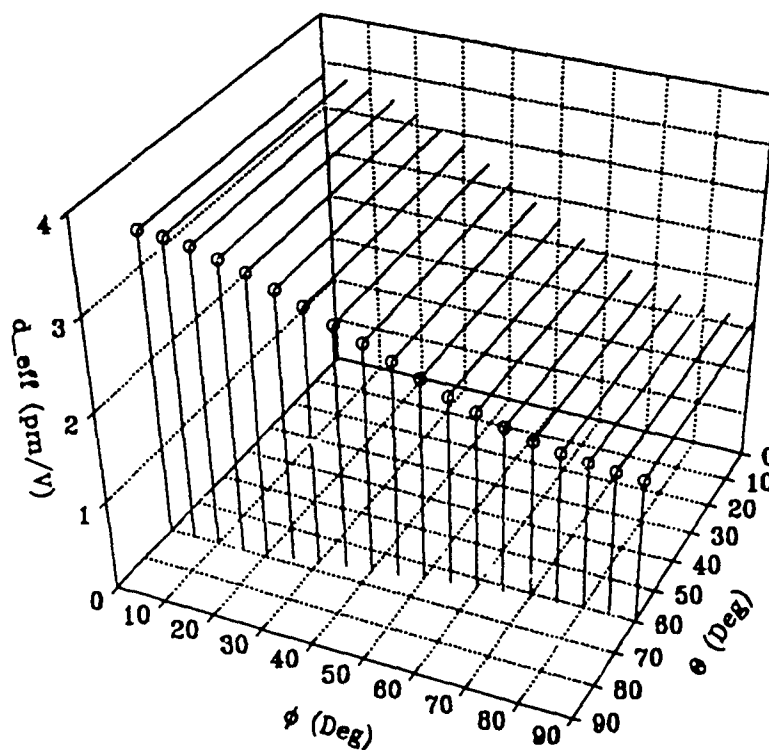


Figure E-29  $d_{eff}$  versus Phase Match Region, 1.35/1.35/0.675  $\mu\text{m}$ , Type II, RTA

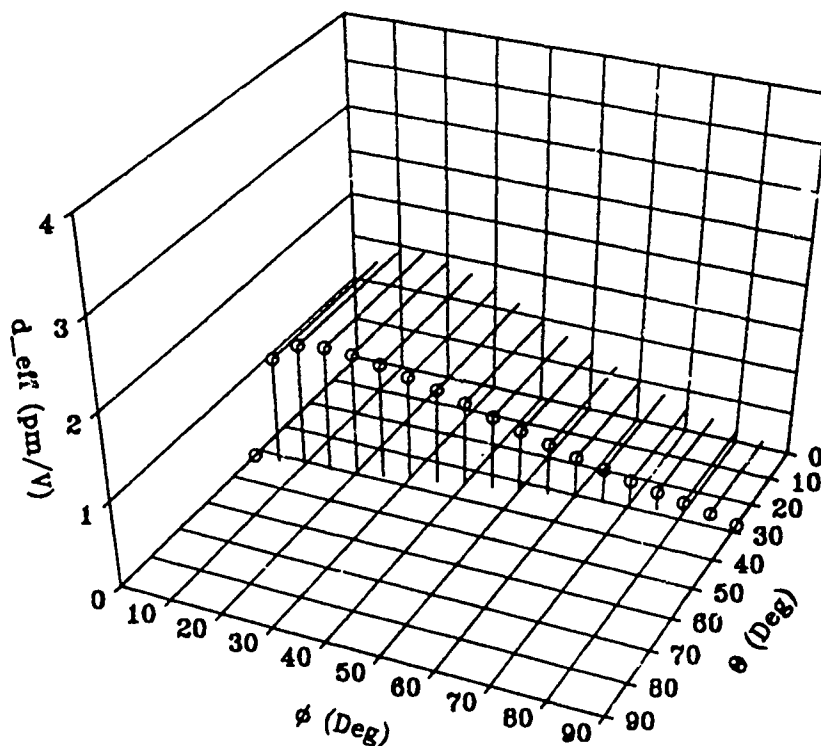


Figure E-30  $d_{eff}$  versus Phase Match Region, 4.043/1.444/1.064  $\mu\text{m}$ , Type I, RTA

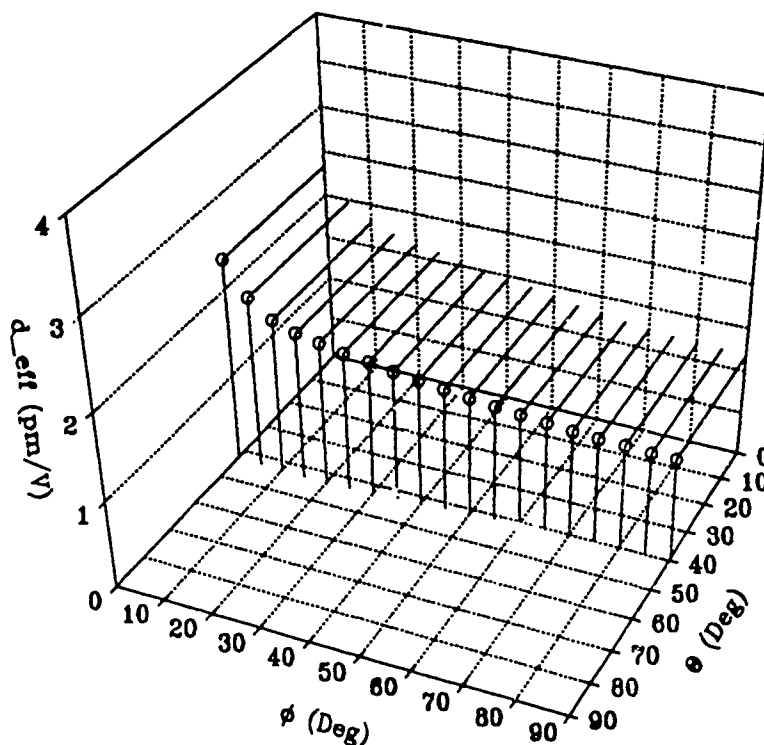


Figure E-31  $d_{eff}$  versus Phase Match Region, 4.043/1.444/1.064  $\mu\text{m}$ , Type II, RTA

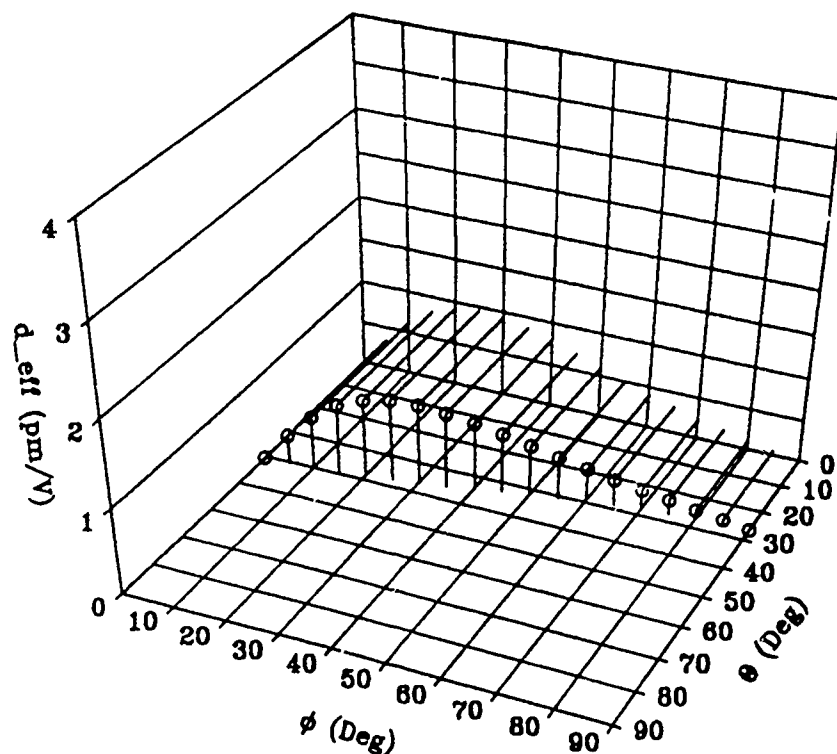


Figure E-32  $d_{eff}$  versus Phase Match Region, 3.17/1.60/1.064  $\mu\text{m}$ , Type I, RTA

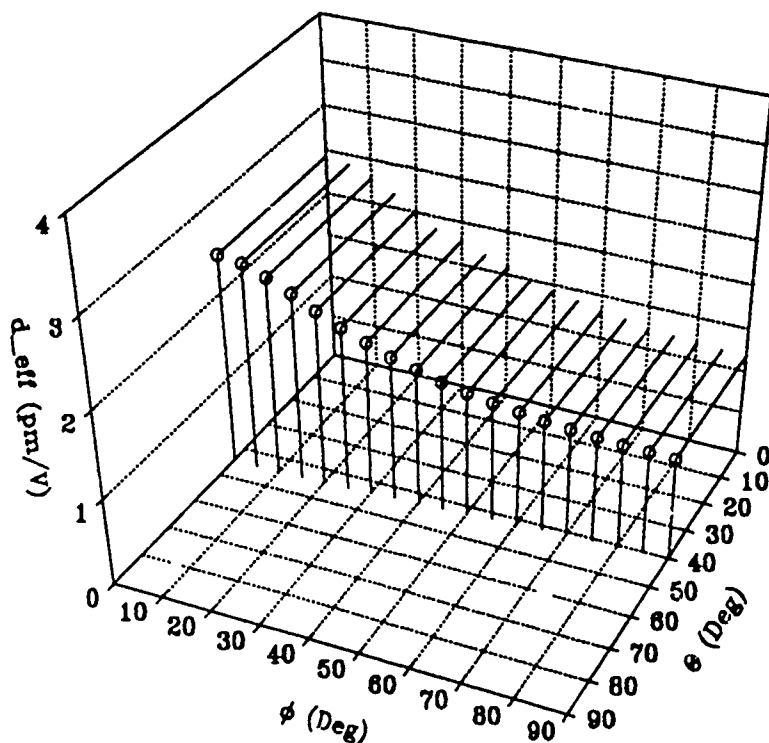


Figure E-33  $d_{eff}$  versus Phase Match Region, 3.17/1.60/1.064  $\mu\text{m}$ , Type II, RTA

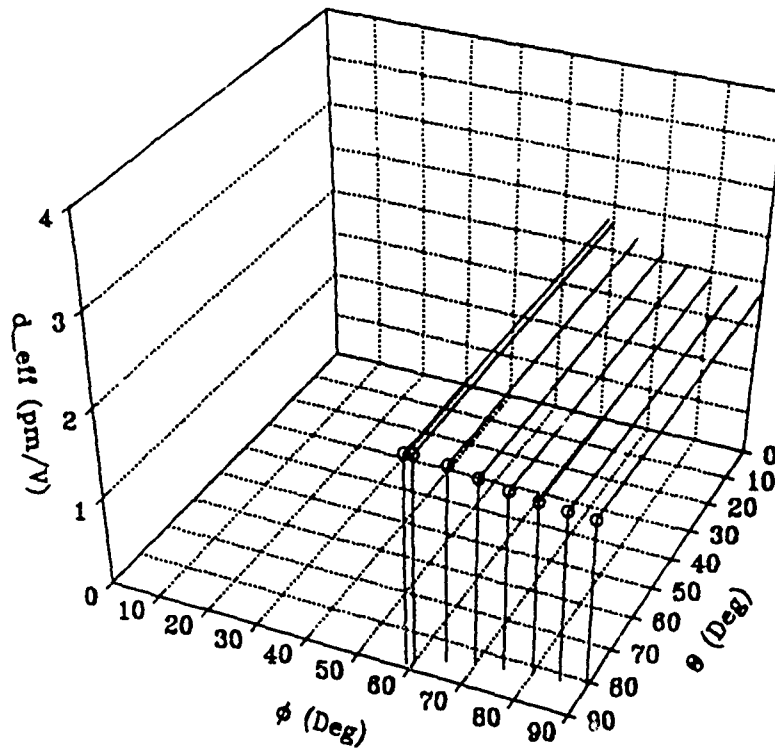


Figure E-34  $d_{eff}$  versus Phase Match Region, 3.17/1.60/1.064  $\mu\text{m}$ , Type III, RTA

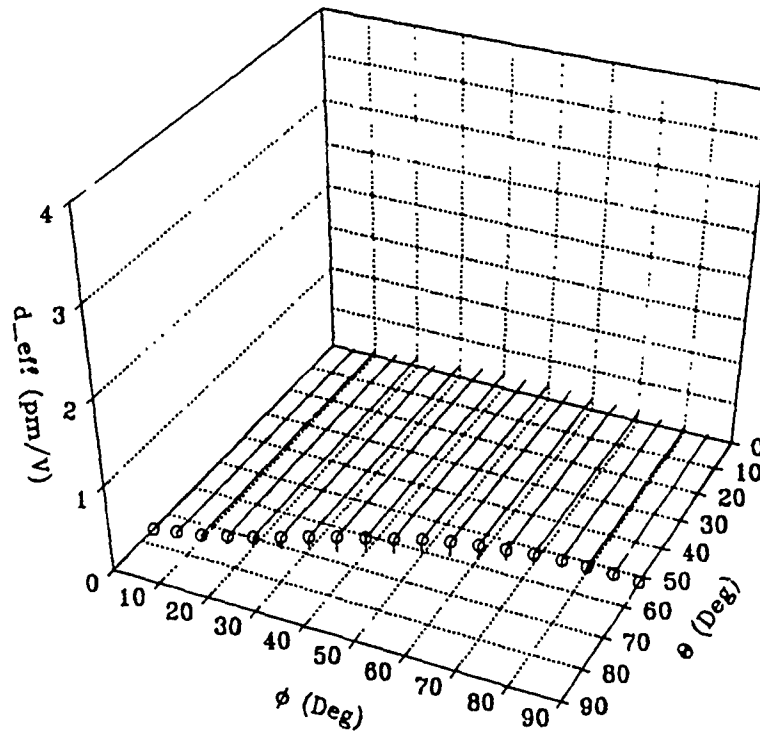


Figure E-35  $d_{eff}$  versus Phase Match Region. 1.064/1.064/0.532  $\mu\text{m}$ , Type I, CTA

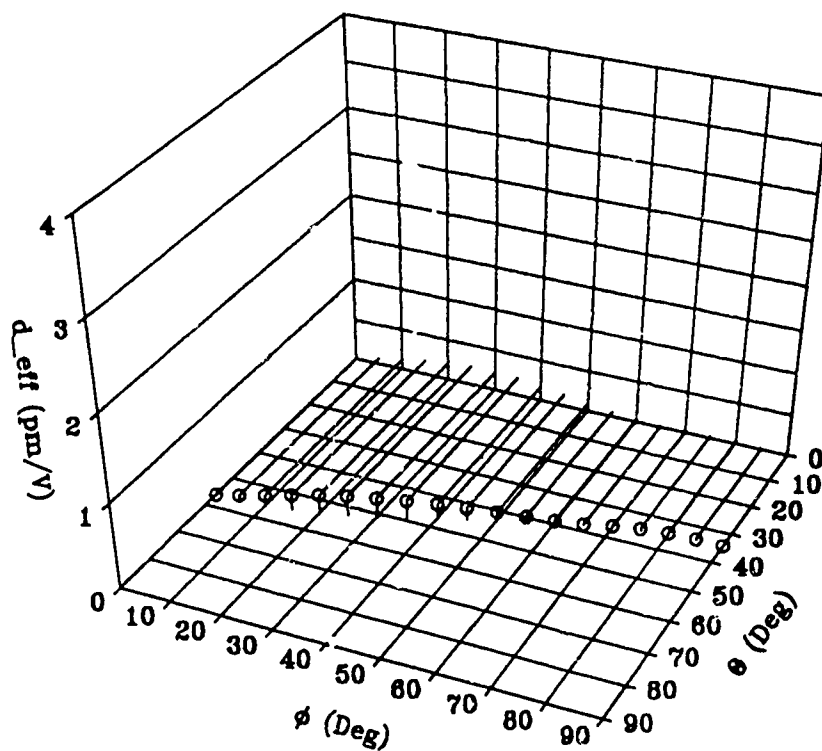


Figure E-36  $d_{eff}$  versus Phase Match Region, 1.35/1.35/0.675  $\mu\text{m}$ , Type I, CTA

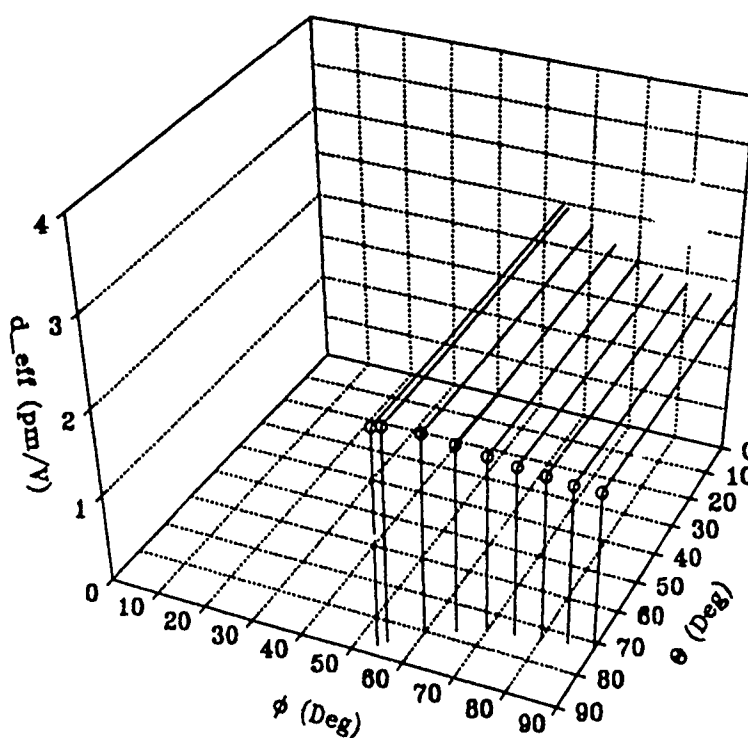


Figure E-37  $d_{eff}$  versus Phase Match Region, 1.35/1.35/0.675  $\mu\text{m}$ , Type II, CTA



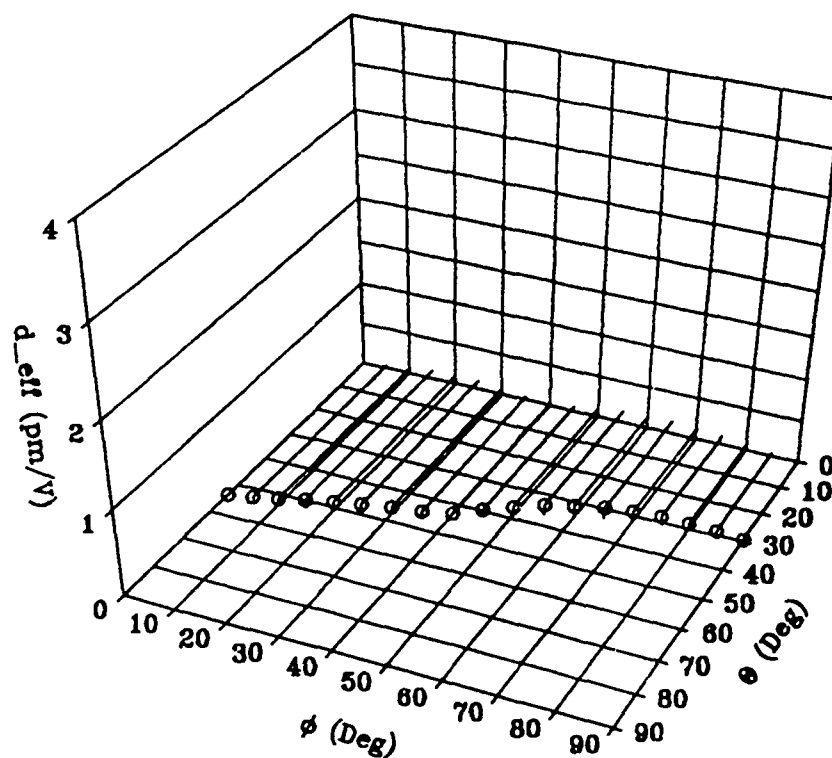


Figure E-38  $d_{eff}$  versus Phase Match Region, 4.043/1.444/1.064  $\mu\text{m}$ , Type I, CTA

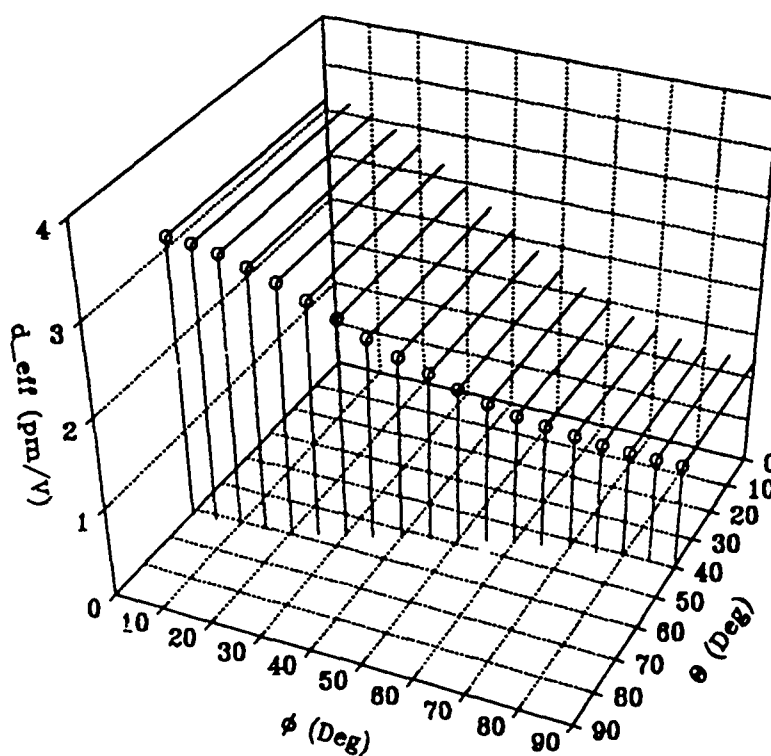


Figure E-39  $d_{eff}$  versus Phase Match Region, 4.043/1.444/1.064  $\mu\text{m}$ , Type II, CTA

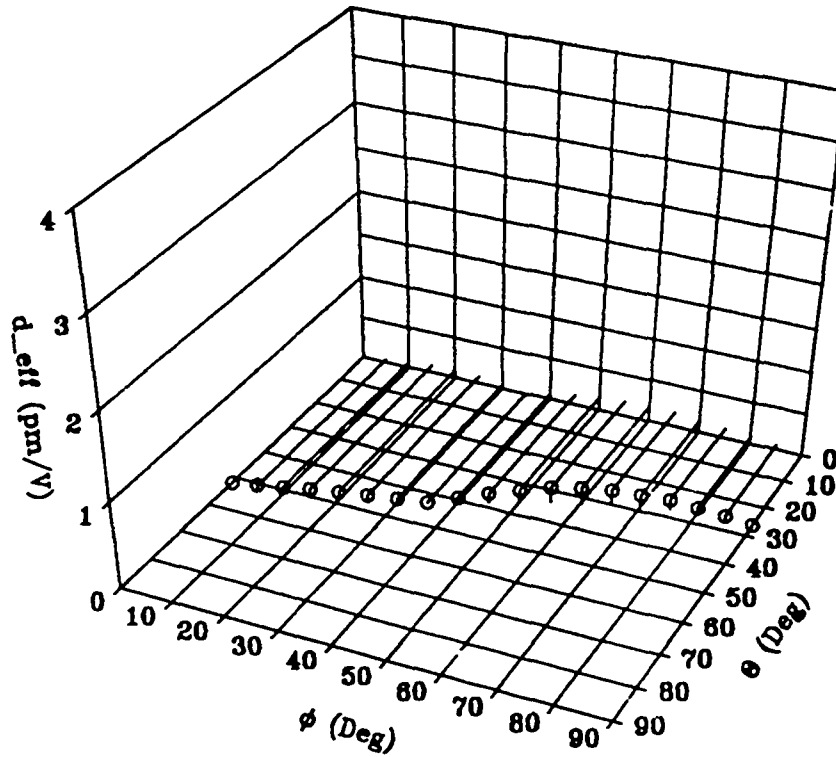


Figure E-40  $d_{eff}$  versus Phase Match Region, 3.17/1.60/1.064  $\mu\text{m}$ , Type I, CTA

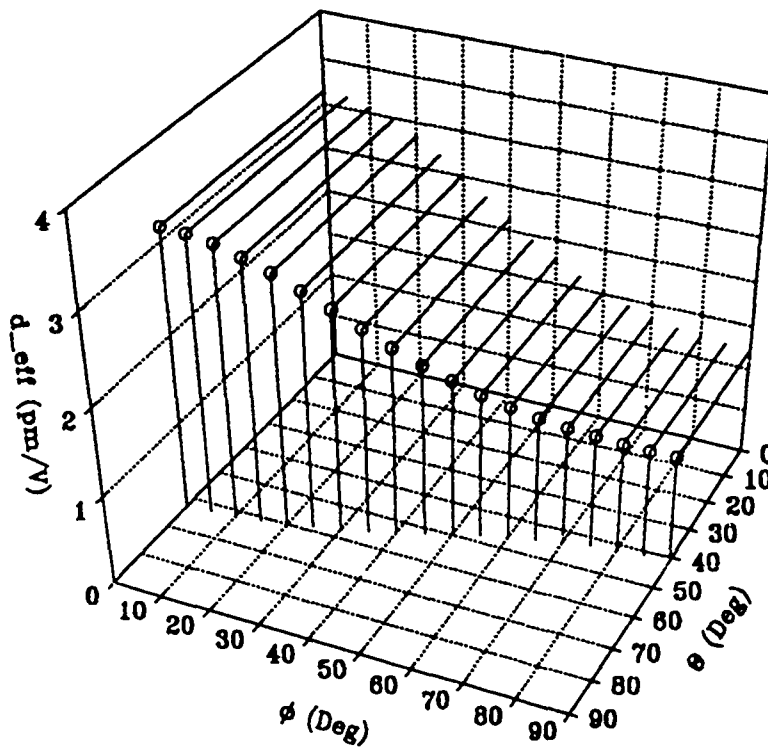


Figure E-41  $d_{eff}$  versus Phase Match Region, 3.17/1.60/1.064  $\mu\text{m}$ , Type II, CTA

## APPENDIX F    KTP Isomorph WalkOff Angle, $\rho$

## List of Figures, Appendix F

Figure F-1	Walkoff, SHG, 1.064/1.064/0.532 $\mu\text{m}$ , Type I, KTP	94
Figure F-2	Walkoff, SHG, 1.064/1.064/0.532 $\mu\text{m}$ , Type II, KTP	94
Figure F-3	Walkoff, SHG, 1.35/1.35/0.675 $\mu\text{m}$ , Type I, KTP	95
Figure F-4	Walkoff, SHG, 1.35/1.35/0.675 $\mu\text{m}$ , Type II, KTP	95
Figure F-5	Walkoff, OPO, 4.043/1.444/1.064 $\mu\text{m}$ , Type I, KTP	96
Figure F-6	Walkoff, OPO, 4.043/1.444/1.064 $\mu\text{m}$ , Type II, KTP	96
Figure F-7	Walkoff, OPO, 3.17/1.60/1.064 $\mu\text{m}$ , Type I, KTP	97
Figure F-8	Walkoff, OPO, 3.17/1.60/1.064 $\mu\text{m}$ , Type II, KTP	97
Figure F-9	Walkoff, OPO, 3.17/1.60/1.064 $\mu\text{m}$ , Type III, KTP	98
Figure F-10	Walkoff, SHG, 1.064/1.064/0.532 $\mu\text{m}$ , Type I, RTP	99
Figure F-11	Walkoff, SHG, 1.064/1.064/0.532 $\mu\text{m}$ , Type II, RTP	99
Figure F-12	Walkoff, SHG, 1.35/1.35/0.675 $\mu\text{m}$ , Type I, RTP	100
Figure F-13	Walkoff, SHG, 1.35/1.35/0.675 $\mu\text{m}$ , Type II, RTP	100
Figure F-14	Walkoff, OPO, 4.043/1.444/1.064 $\mu\text{m}$ , Type I, RTP	101
Figure F-15	Walkoff, OPO, 4.043/1.444/1.064 $\mu\text{m}$ , Type II, RTP	101
Figure F-16	Walkoff, OPO, 3.17/1.60/1.064 $\mu\text{m}$ , Type I, RTP	102
Figure F-17	Walkoff, OPO, 3.17/1.60/1.064 $\mu\text{m}$ , Type II, RTP	102
Figure F-18	Walkoff, OPO, 3.17/1.60/1.064 $\mu\text{m}$ , Type III, RTP	103
Figure F-19	Walkoff, SHG, 1.064/1.064/0.532 $\mu\text{m}$ , Type I, KTA	104
Figure F-20	Walkoff, SHG, 1.35/1.35/0.675 $\mu\text{m}$ , Type I, KTA	105
Figure F-21	Walkoff, SHG, 1.35/1.35/0.675 $\mu\text{m}$ , Type II, KTA	105
Figure F-22	Walkoff, OPO, 4.043/1.444/1.064 $\mu\text{m}$ , Type I, KTA	106
Figure F-23	Walkoff, OPO, 4.043/1.444/1.064 $\mu\text{m}$ , Type II, KTA	106
Figure F-24	Walkoff, OPO, 3.17/1.60/1.064 $\mu\text{m}$ , Type I, KTA	107
Figure F-25	Walkoff, OPO, 3.17/1.60/1.064 $\mu\text{m}$ , Type II, KTA	107
Figure F-26	Walkoff, OPO, 3.17/1.60/1.064 $\mu\text{m}$ , Type III, KTA	108
Figure F-27	Walkoff, SHG, 1.064/1.064/0.532 $\mu\text{m}$ , Type I, RTA	109
Figure F-28	Walkoff, SHG, 1.35/1.35/0.675 $\mu\text{m}$ , Type I, RTA	110
Figure F-29	Walkoff, SHG, 1.35/1.35/0.675 $\mu\text{m}$ , Type II, RTA	110
Figure F-30	Walkoff, OPO, 4.043/1.444/1.064 $\mu\text{m}$ , Type I, RTA	111
Figure F-31	Walkoff, OPO, 4.043/1.444/1.064 $\mu\text{m}$ , Type II, RTA	111
Figure F-32	Walkoff, OPO, 3.17/1.60/1.064 $\mu\text{m}$ , Type I, RTA	112
Figure F-33	Walkoff, OPO, 3.17/1.60/1.064 $\mu\text{m}$ , Type II, RTA	112
Figure F-34	Walkoff, OPO, 3.17/1.60/1.064 $\mu\text{m}$ , Type III, RTA	113
Figure F-35	Walkoff, SHG, 1.064/1.064/0.532 $\mu\text{m}$ , Type I, CTA	114
Figure F-36	Walkoff, SHG, 1.35/1.35/0.675 $\mu\text{m}$ , Type I, CTA	115
Figure F-37	Walkoff, SHG, 1.35/1.35/0.675 $\mu\text{m}$ , Type II, CTA	115
Figure F-38	Walkoff, OPO, 4.043/1.444/1.064 $\mu\text{m}$ , Type I, CTA	116
Figure F-39	Walkoff, OPO, 4.043/1.444/1.064 $\mu\text{m}$ , Type II, CTA	116
Figure F-40	Walkoff, OPO, 3.17/1.60/1.064 $\mu\text{m}$ , Type I, CTA	117
Figure F-41	Walkoff, OPO, 3.17/1.60/1.064 $\mu\text{m}$ , Type II, CTA	117

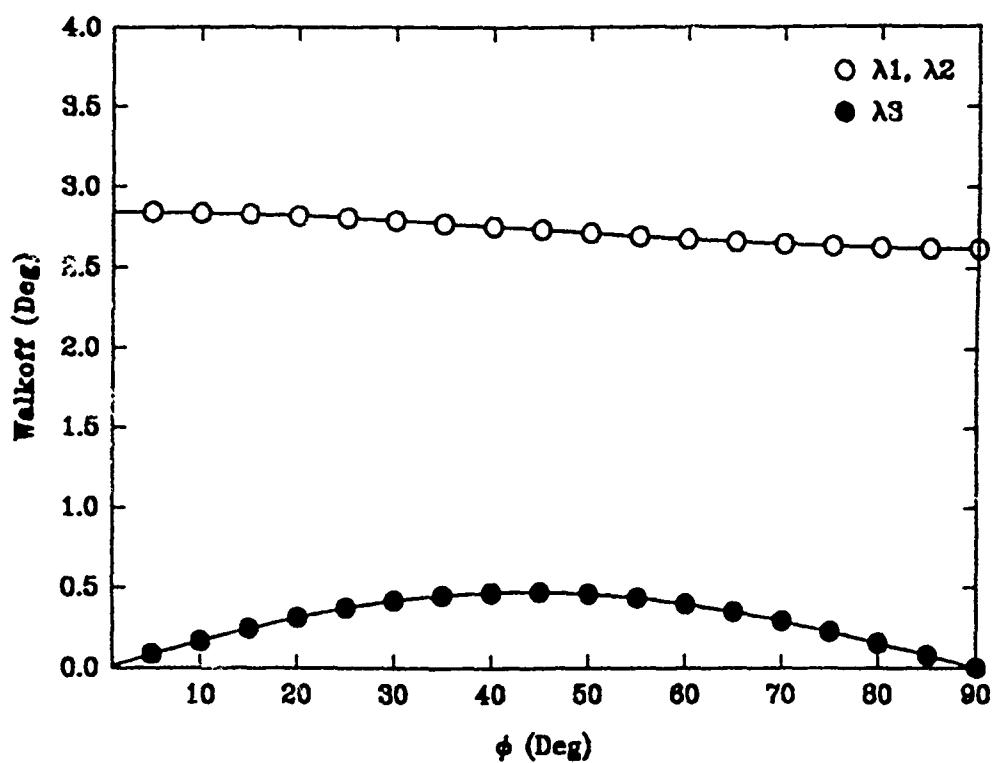


Figure F-1 Walkoff, SHG, 1.064/1.064/0.532  $\mu\text{m}$ , Type I, KTP

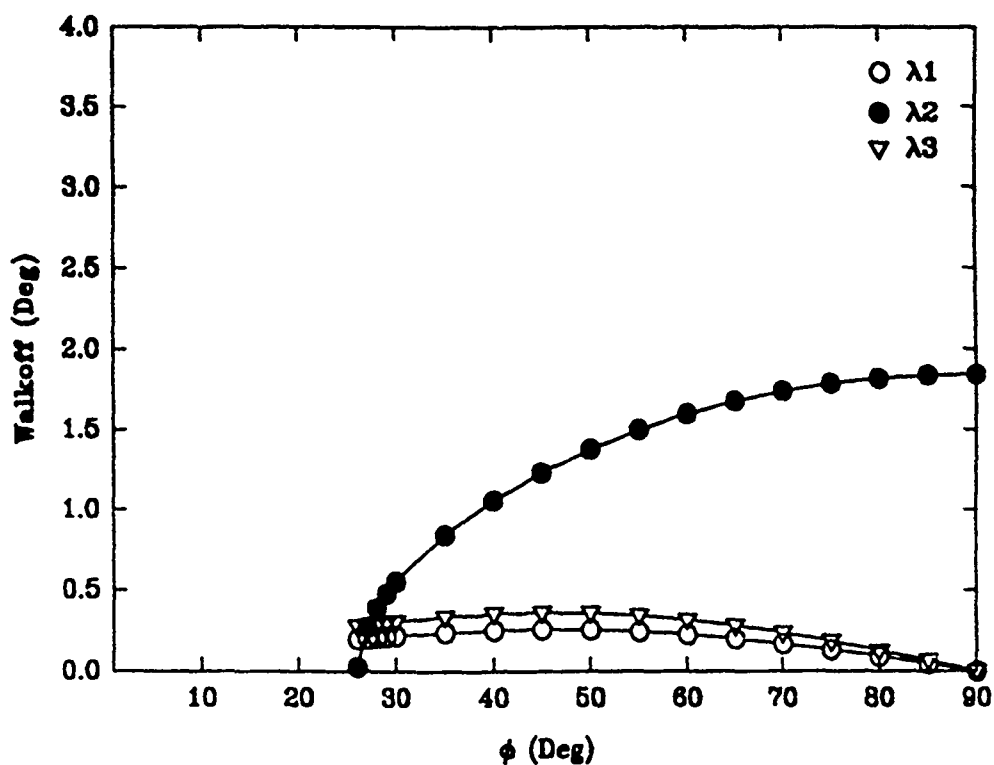


Figure F-2 Walkoff, SHG, 1.064/1.064/0.532  $\mu\text{m}$ , Type II, KTP

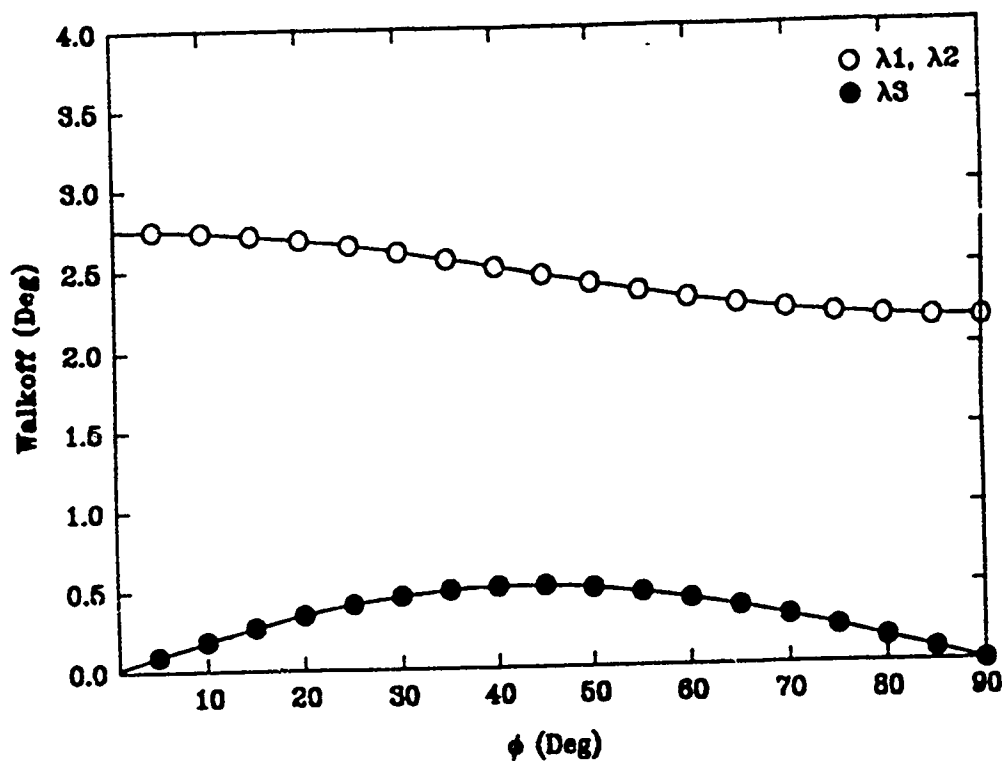


Figure F-3 Walkoff, SHG, 1.35/1.35/0.675  $\mu\text{m}$ , Type I. KTP

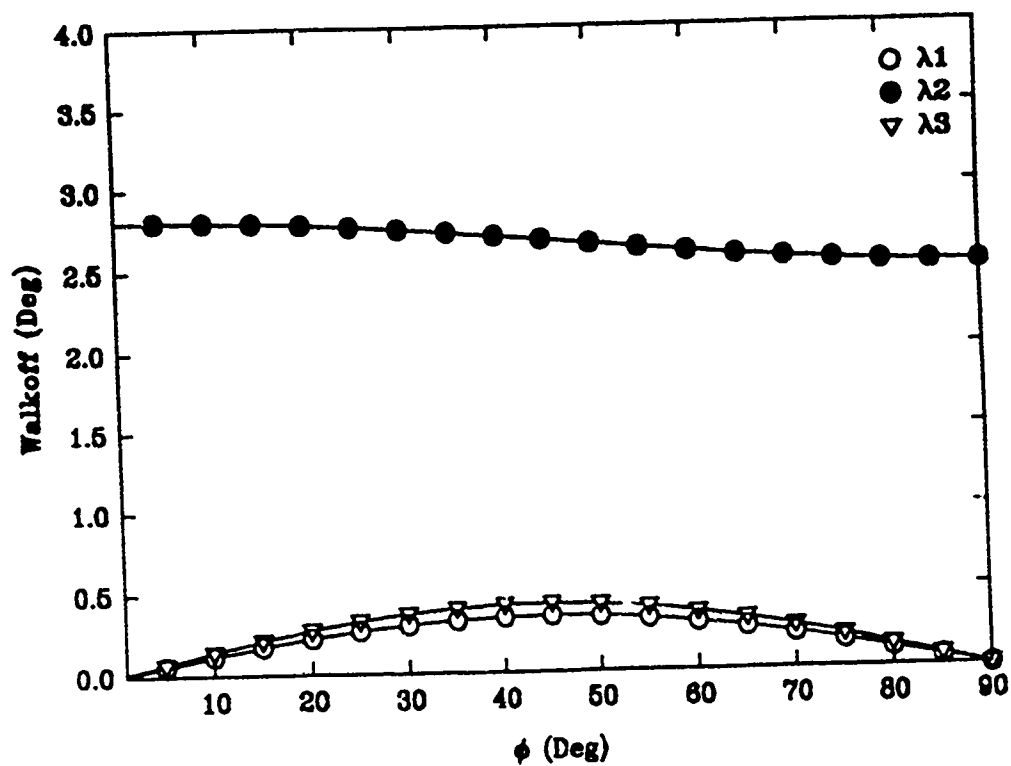


Figure F-4 Walkoff, SHG, 1.35/1.35/0.675  $\mu\text{m}$ , Type II. KTP

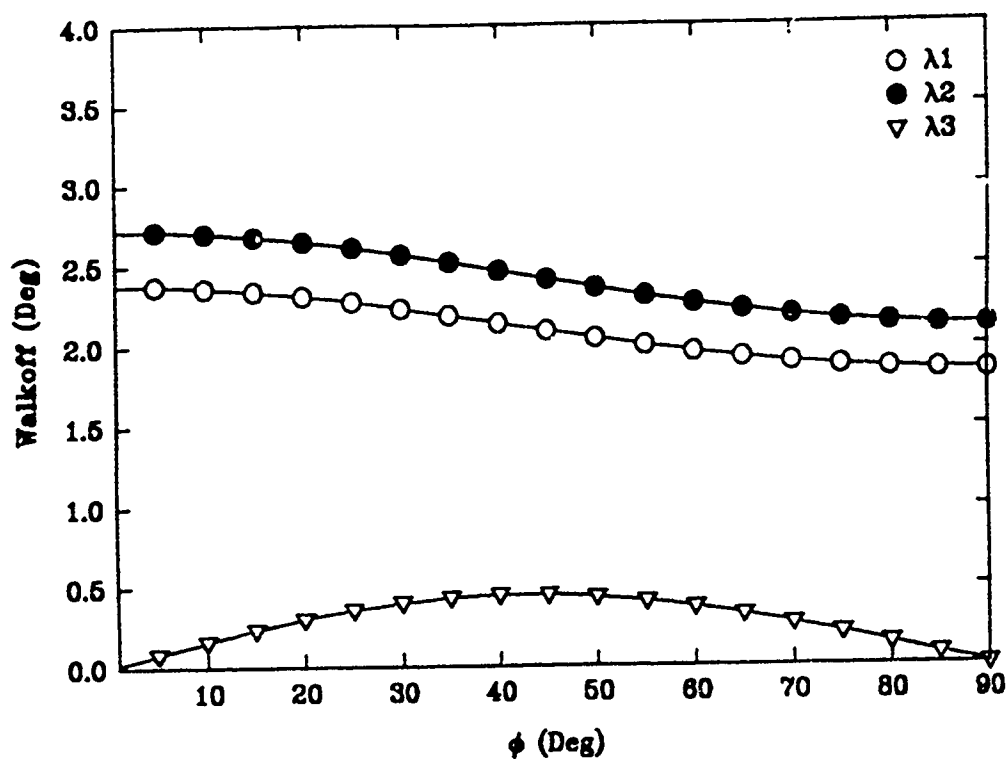


Figure F-5 Walkoff, OPO, 4.043/1.444/1.064  $\mu\text{m}$ , Type I, KTP

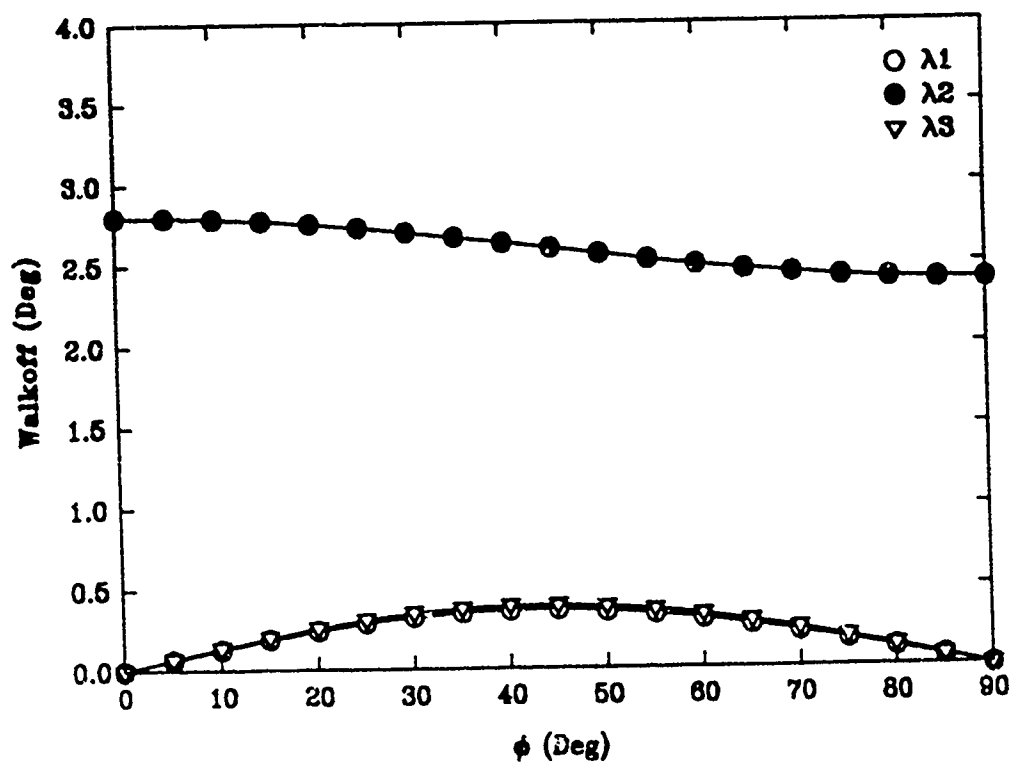


Figure F-6 Walkoff, OPO, 4.043/1.444/1.064  $\mu\text{m}$ , Type II, KTP

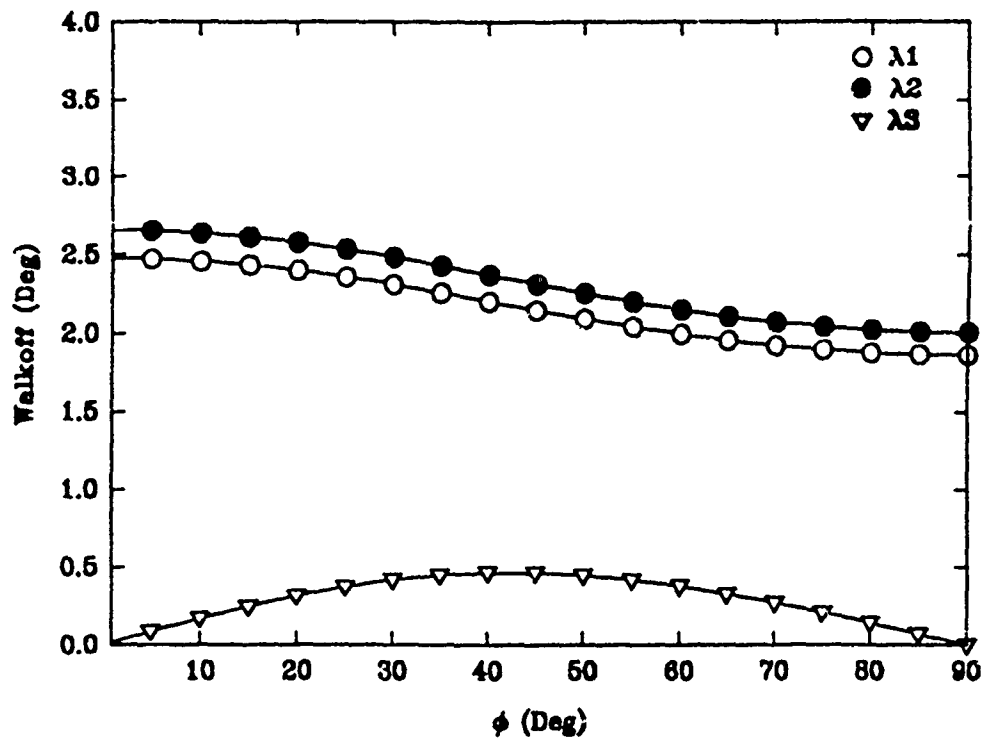


Figure F-7 Walkoff, OPO, 3.17/1.60/1.064  $\mu\text{m}$ , Type I, KTP

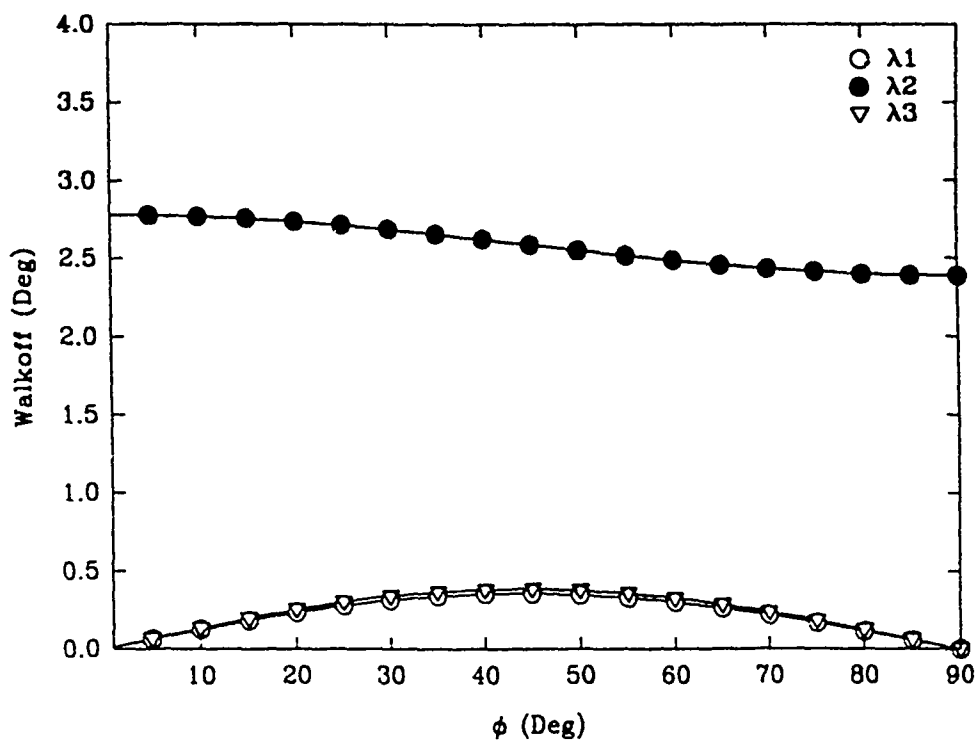


Figure F-8 Walkoff, OPO, 3.17/1.60/1.064  $\mu\text{m}$ , Type II, KTP



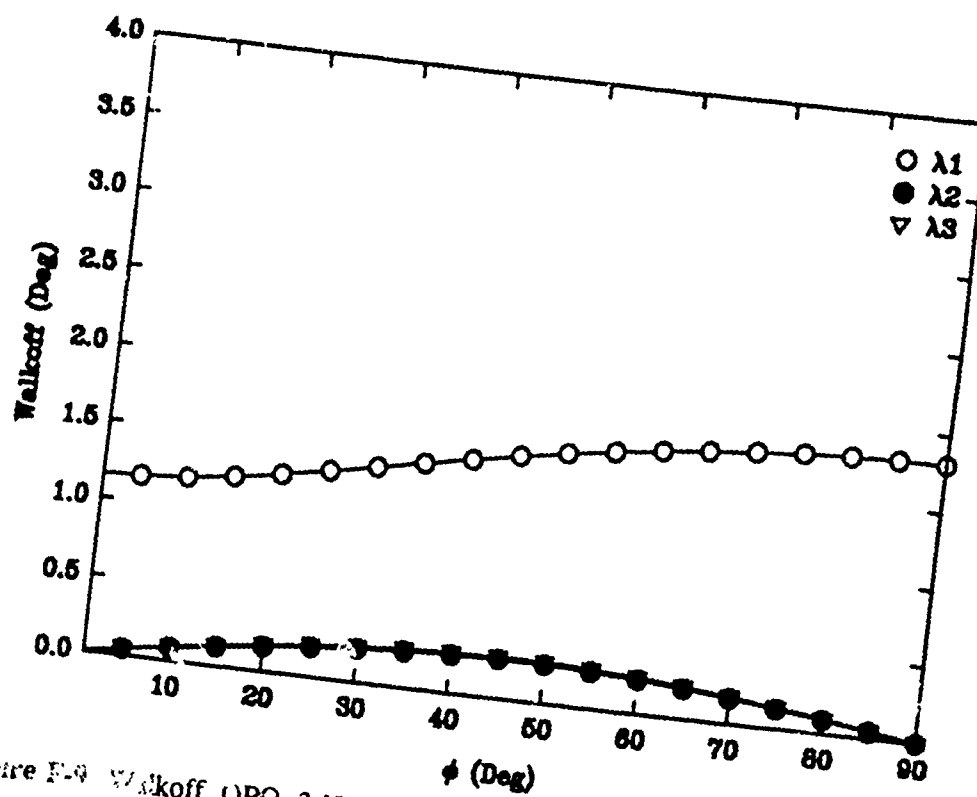


Figure F-9 Walkoff, OPO, 3.17/1.60/1.064  $\mu\text{m}$ , Type III, KTP

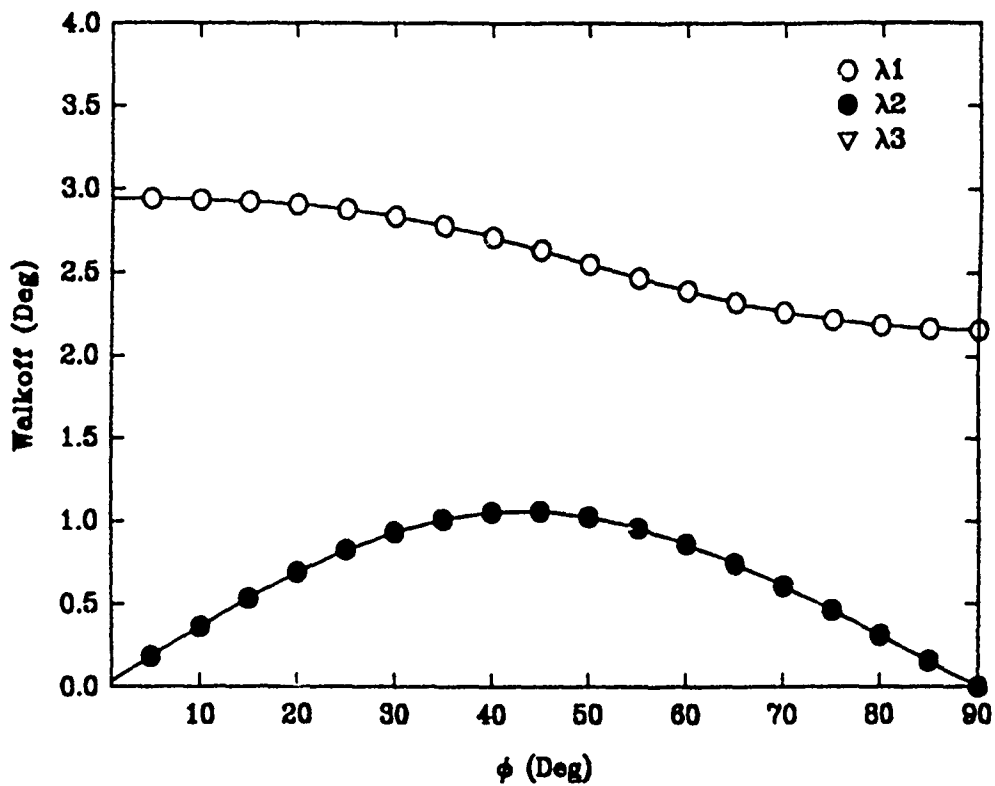


Figure F-10 Walkoff, SHG, 1.064/1.064/0.532  $\mu\text{m}$ , Type I, RTP

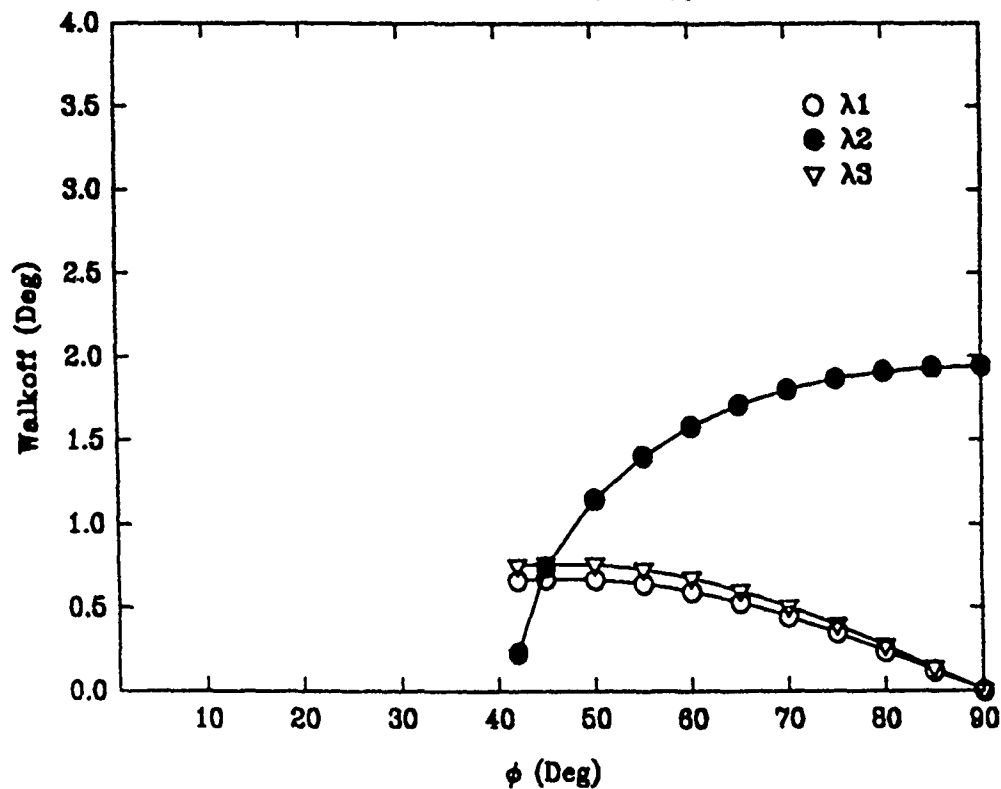


Figure F-11 Walkoff, SHG, 1.064/1.064/0.532  $\mu\text{m}$ , Type II, RTP

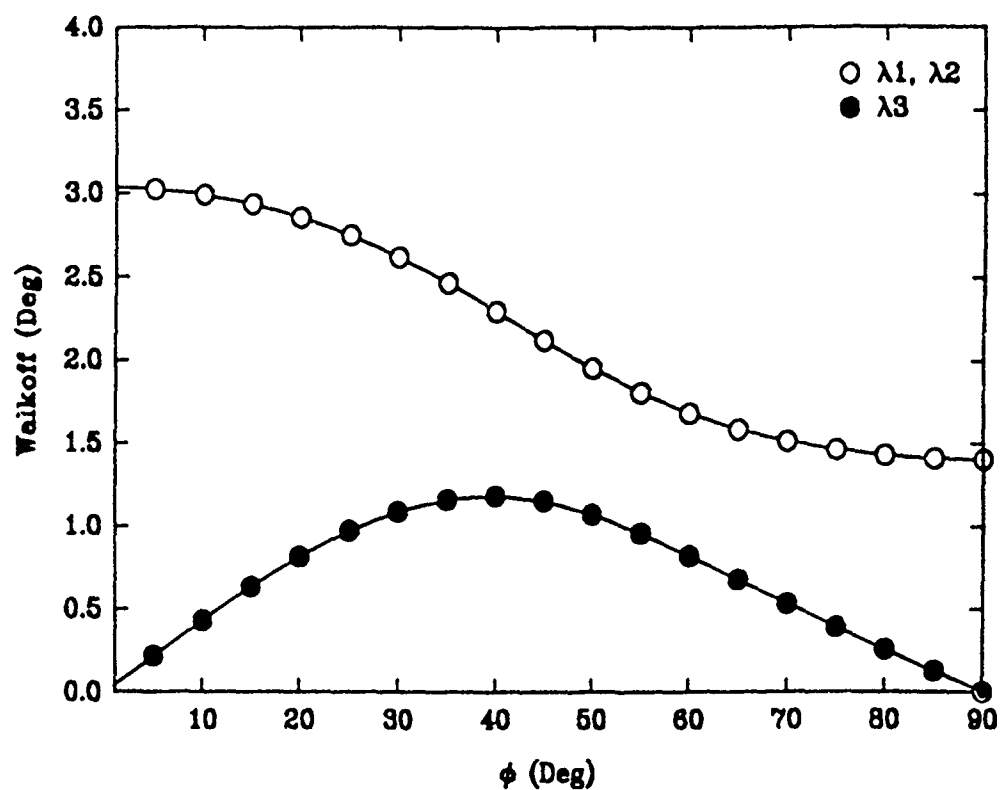


Figure F-12 Walkoff, SHG, 1.35/1.35/0.675  $\mu\text{m}$ , Type I, RTP

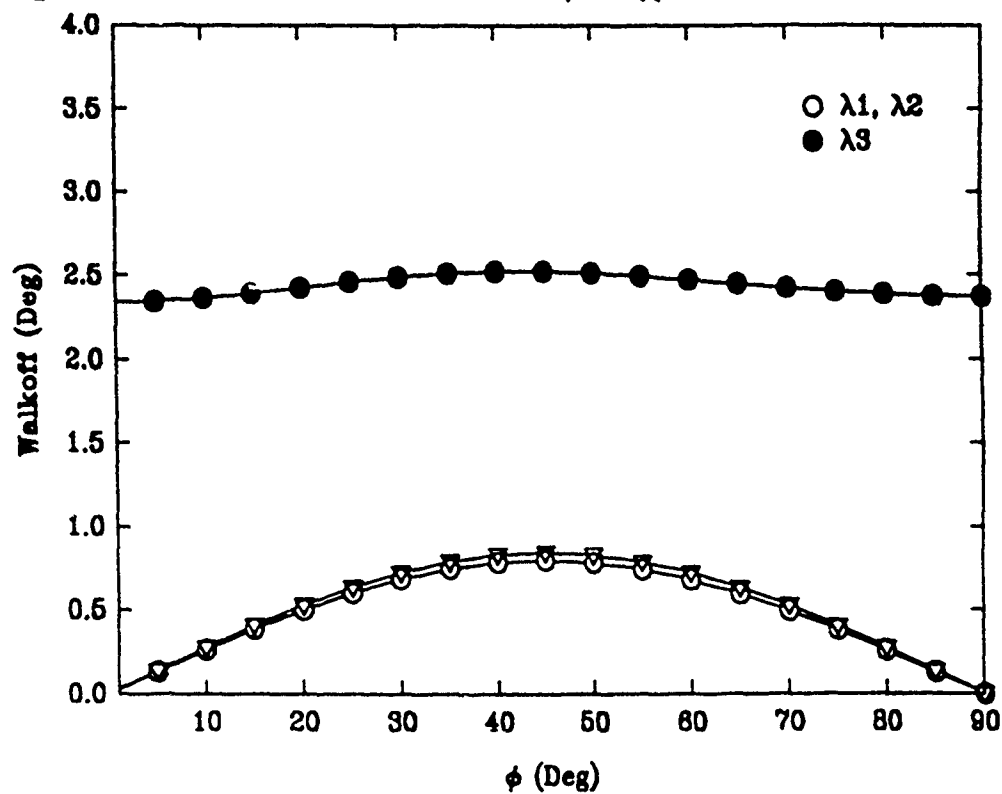


Figure F-13 Walkoff, SHG, 1.35/1.35/0.675  $\mu\text{m}$ , Type II, RTP

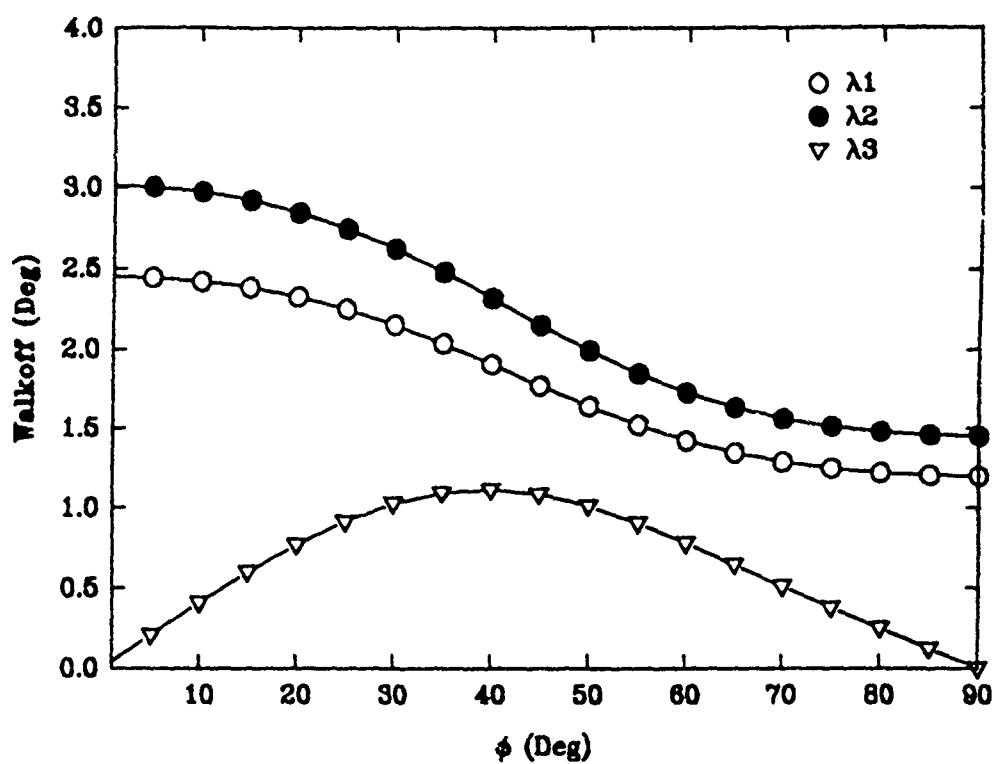


Figure F-14 Walkoff, OPO, 4.043/1.444/1.064  $\mu\text{m}$ , Type I, RTP

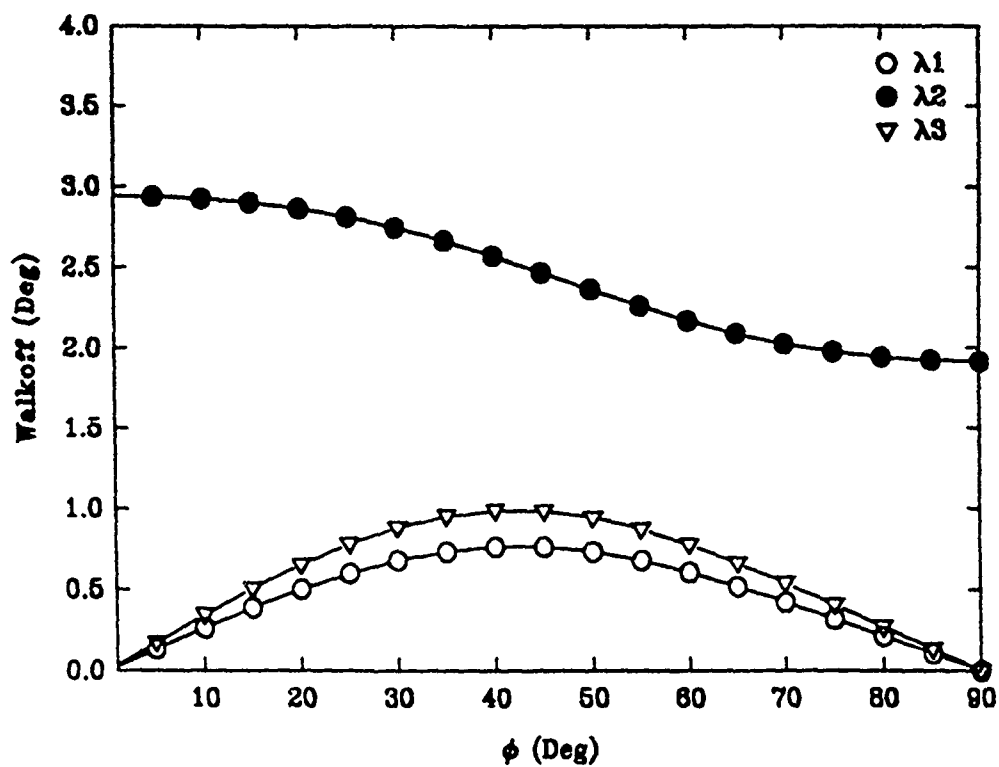


Figure F-15 Walkoff, OPO, 4.043/1.444/1.064  $\mu\text{m}$ , Type II, RTP

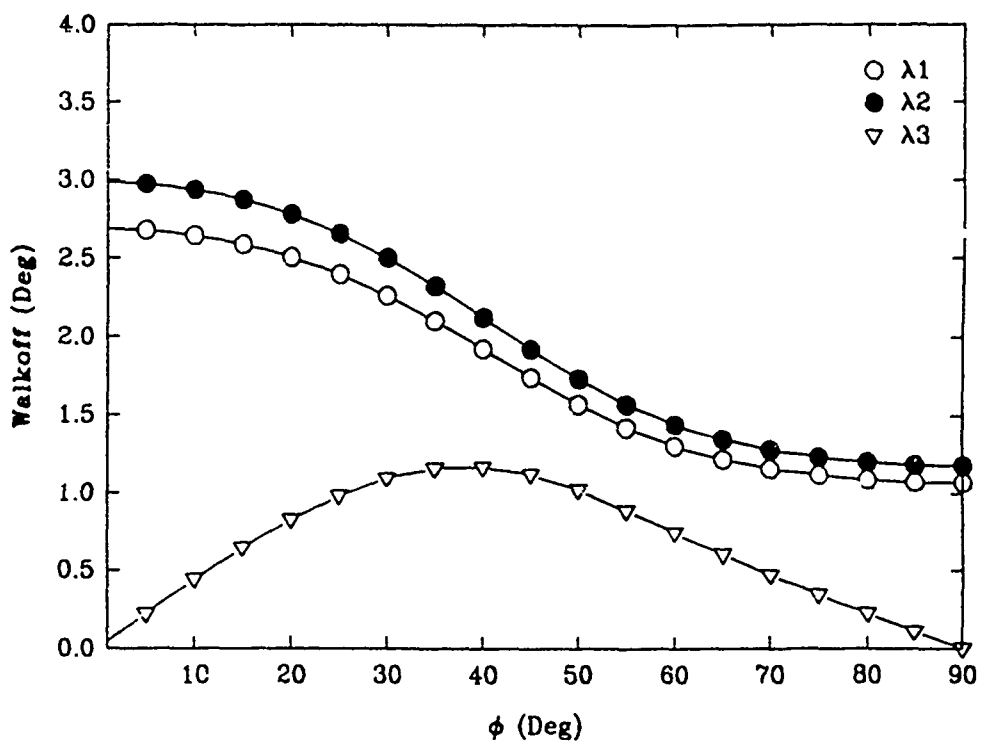


Figure F-16 Walkoff, OPO, 3.17/1.60/1.064  $\mu\text{m}$ , Type I, RTP

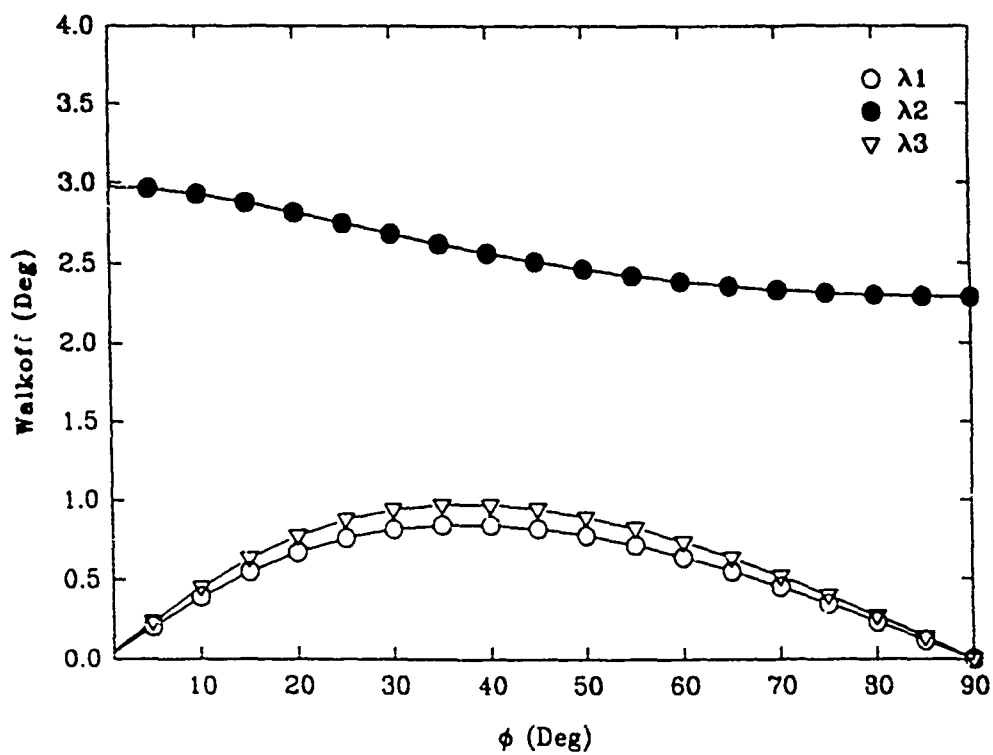


Figure F-17 Walkoff, OPO, 3.17/1.60/1.064  $\mu\text{m}$ , Type II, RTP

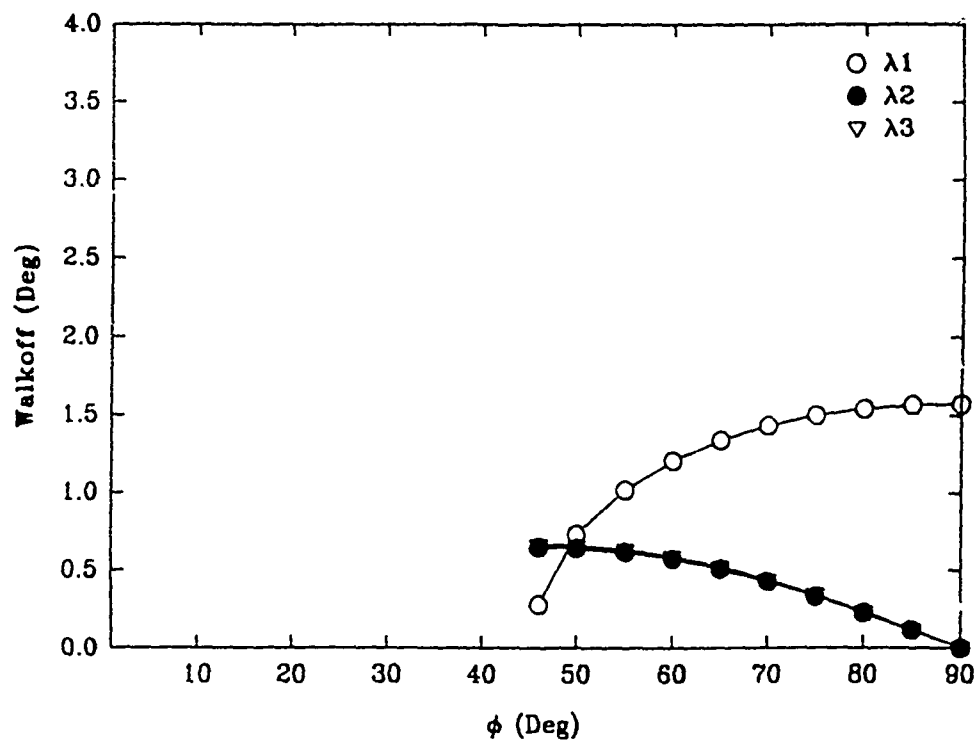


Figure F-18 Walkoff, OPO. 3.17/1.60/1.064  $\mu\text{m}$ , Type III, RTP

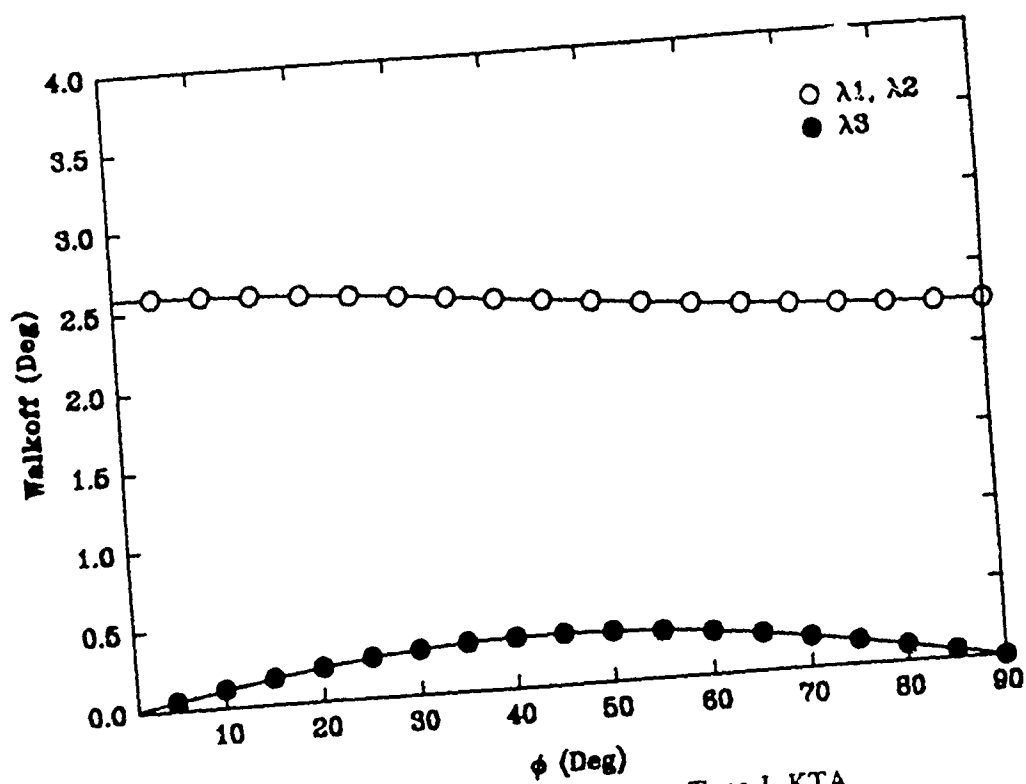


Figure F-19 Walkoff, SHG, 1.064/1.064/0.532  $\mu\text{m}$ , Type 1, KTA

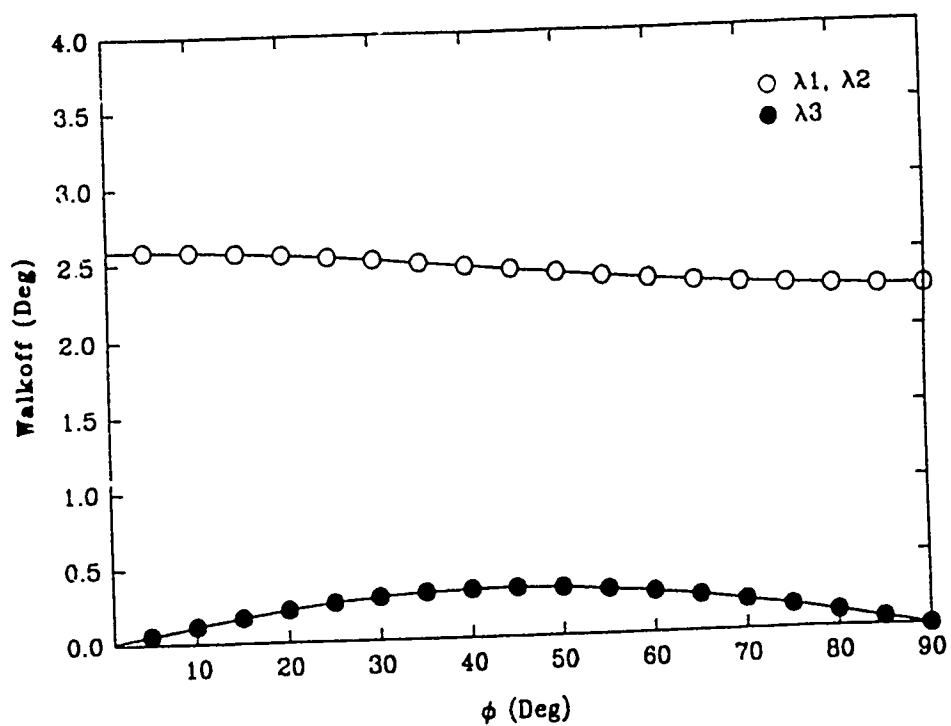


Figure F-20 Walkoff, SHG, 1.35/1.35/0.675  $\mu\text{m}$ , Type I, KTA

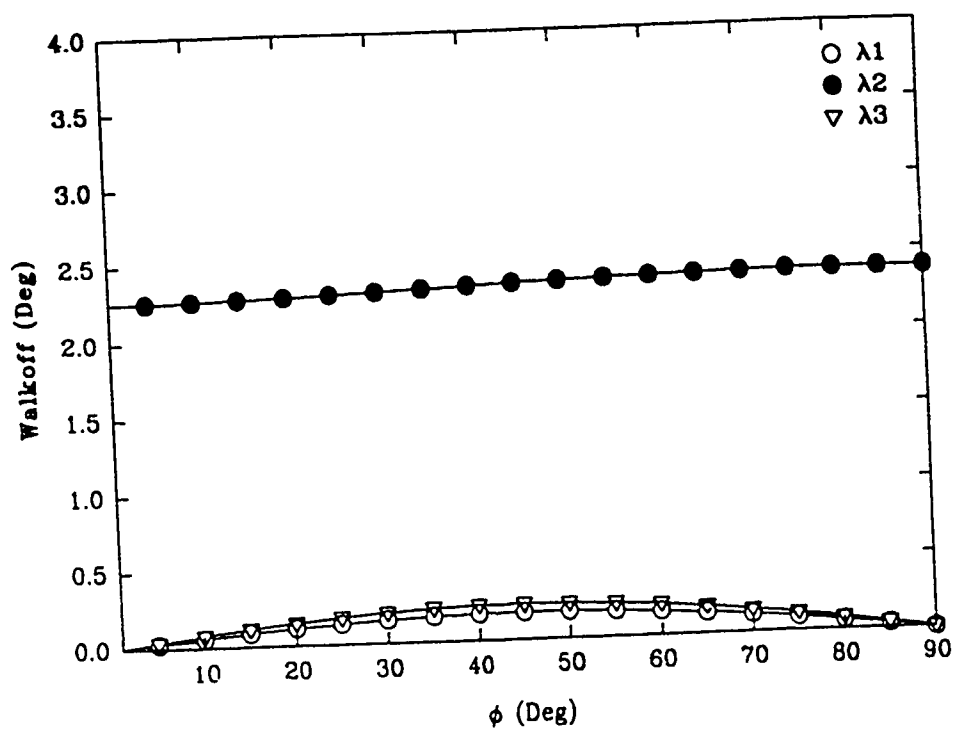


Figure F-21 Walkoff, SHG, 1.35/1.35/0.675  $\mu\text{m}$ , Type II, KTA



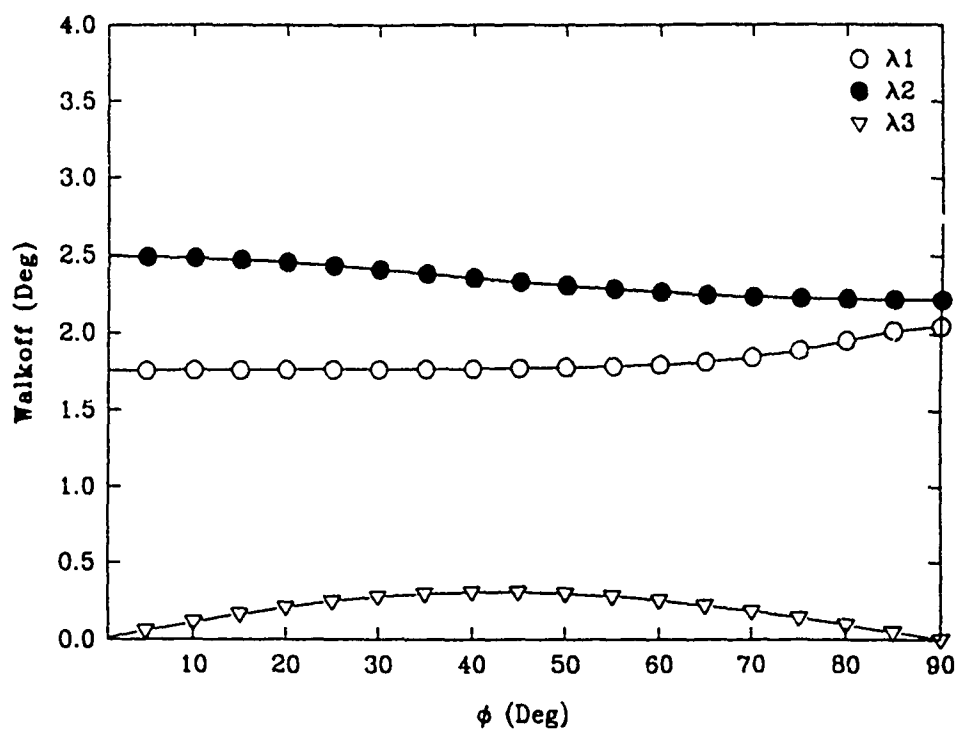


Figure F-22 Walkoff, OPO, 4.043/1.444/1.064  $\mu\text{m}$ , Type I, KTA

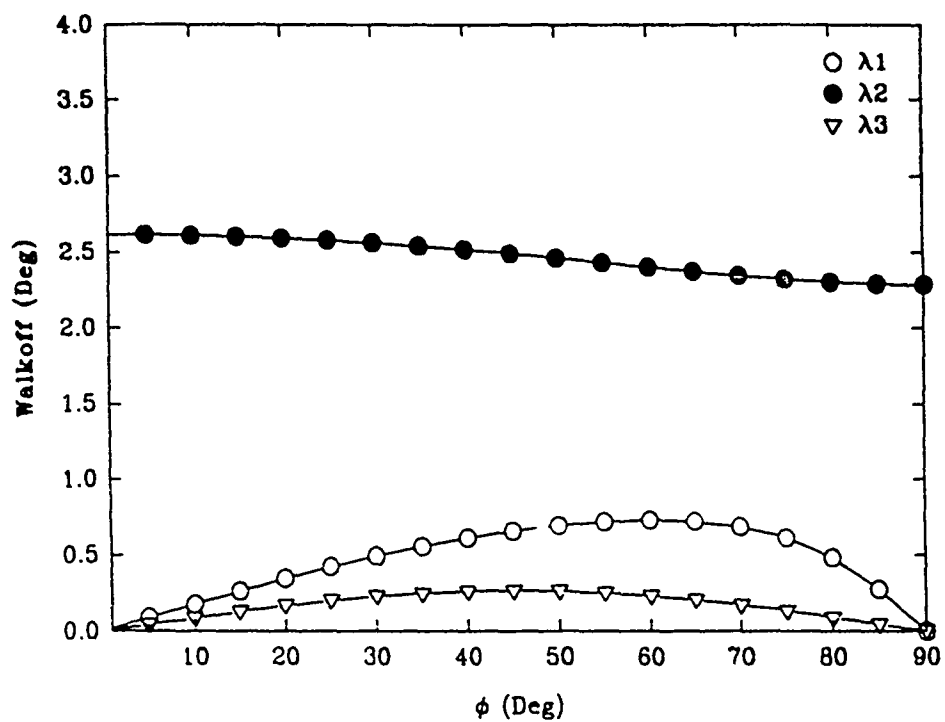


Figure F-23 Walkoff, OPO, 4.043/1.444/1.064  $\mu\text{m}$ , Type II, KTA

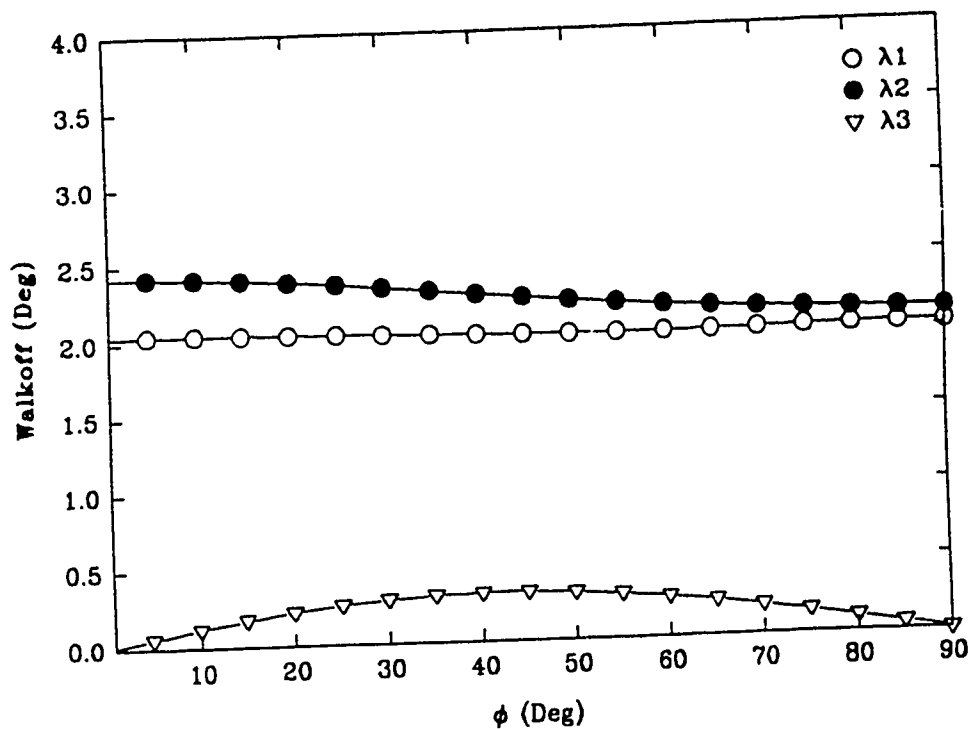


Figure F-24 Walkoff, OPO, 3.17/1.60/1.064  $\mu\text{m}$ , Type I, KTA

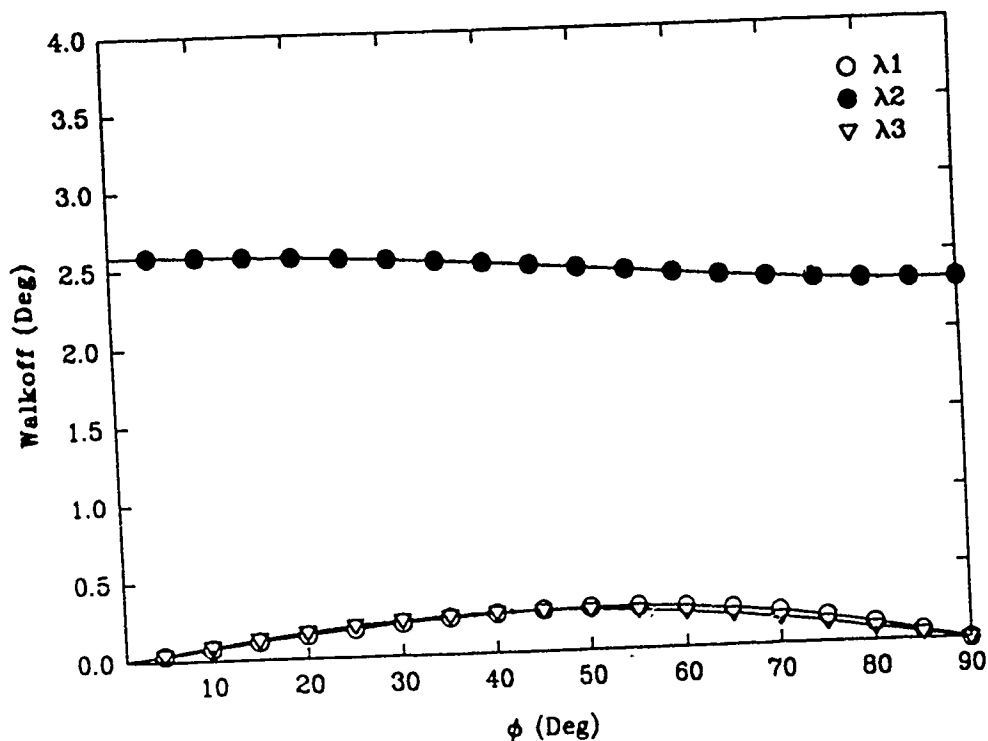


Figure F-25 Walkoff, OPO, 3.17/1.60/1.064  $\mu\text{m}$ , Type II, KTA

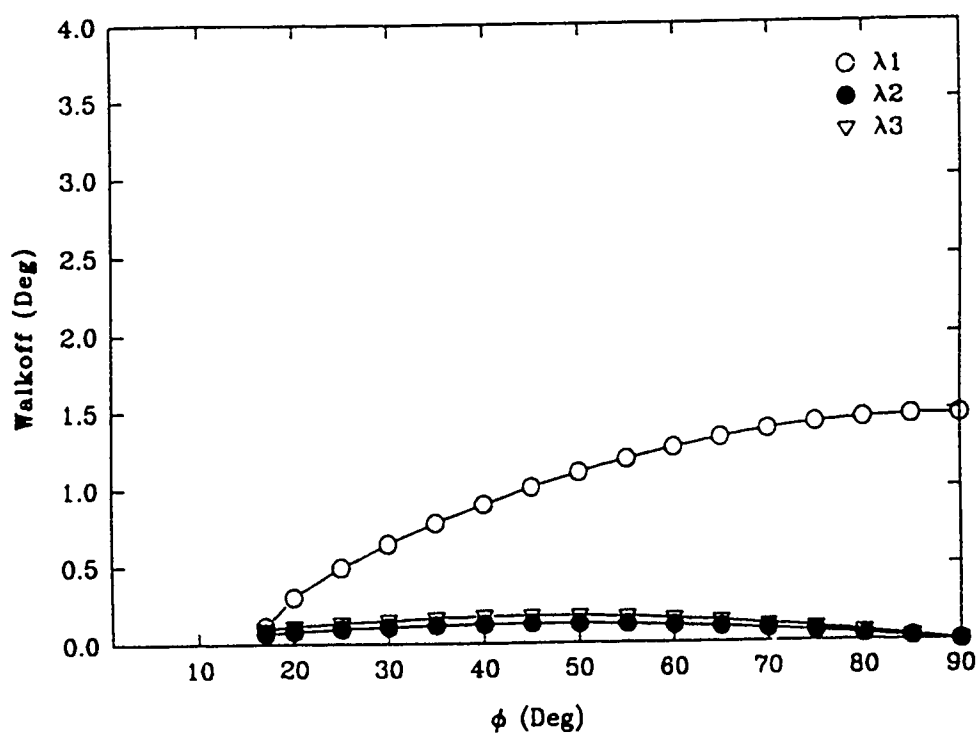


Figure F-26 Walkoff, OPO, 3.17/1.60/1.064  $\mu\text{m}$ , Type III, KTA

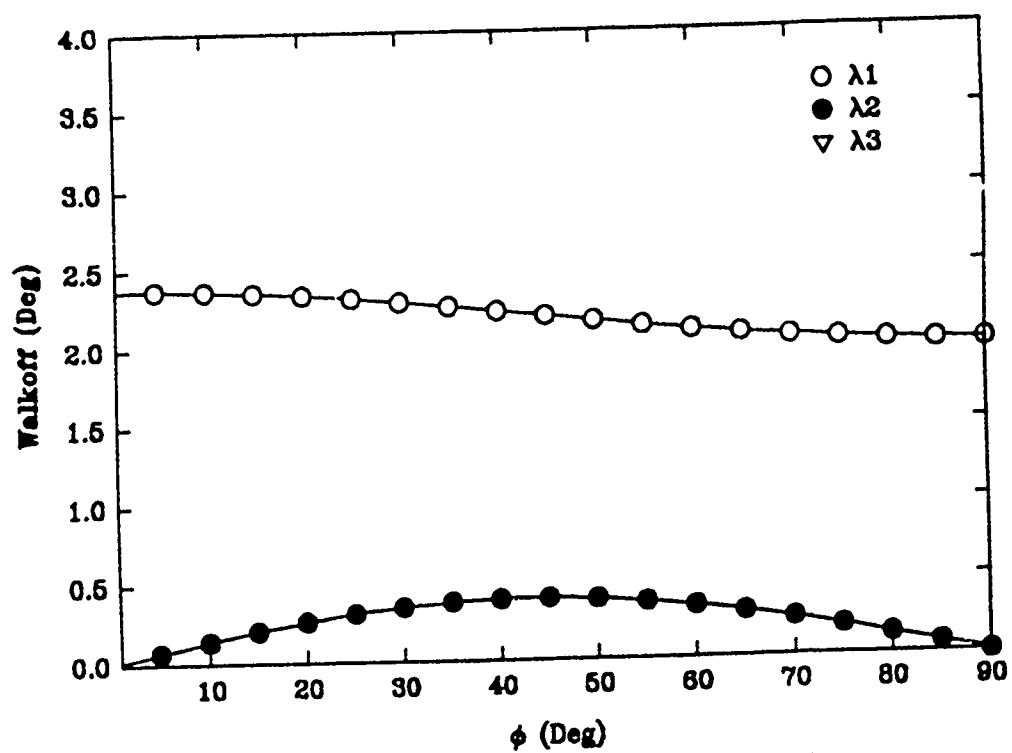


Figure F-27 Walkoff, SHG, 1.064/1.064/0.532  $\mu\text{m}$ , Type I, RTA

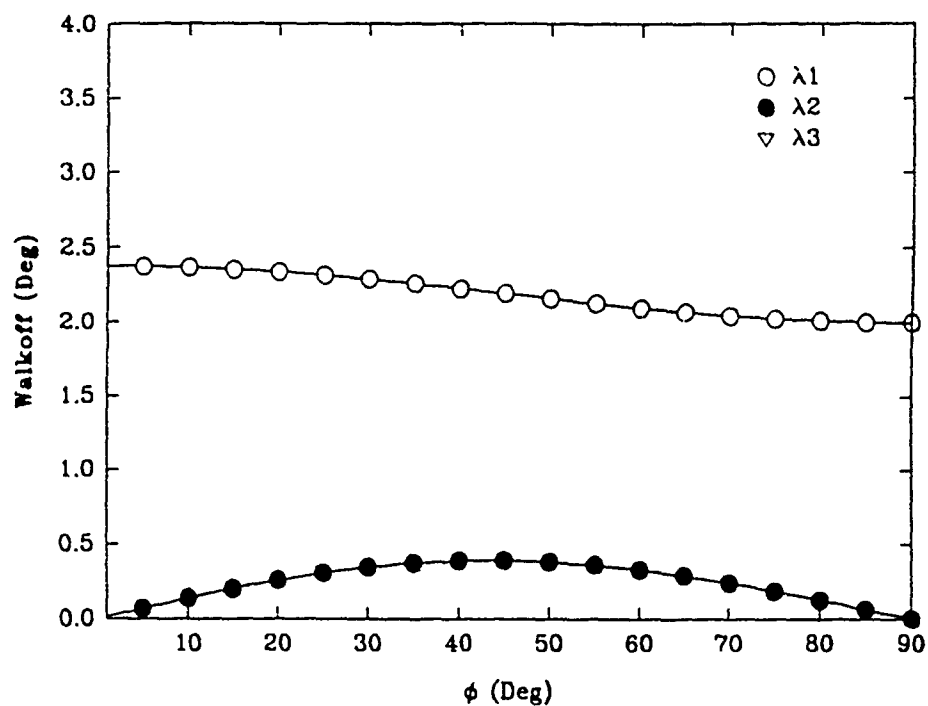


Figure F-28 Walkoff, SHG, 1.35/1.35/0.675  $\mu\text{m}$ , Type I, RTA

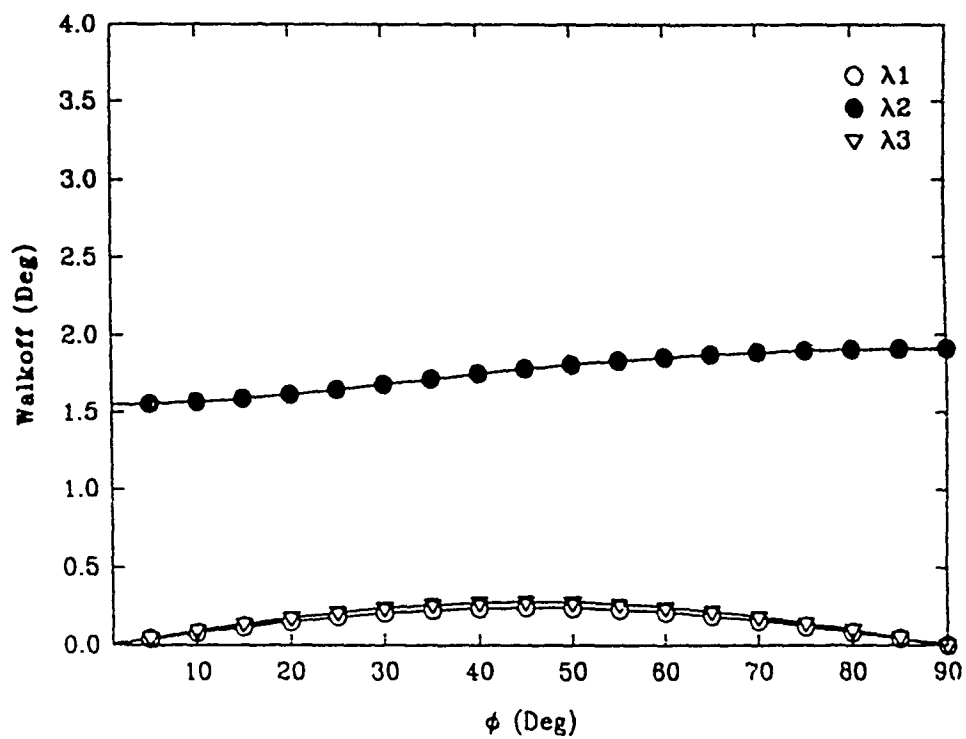


Figure F-29 Walkoff, SHG, 1.35/1.35/0.675  $\mu\text{m}$ , Type II, RTA

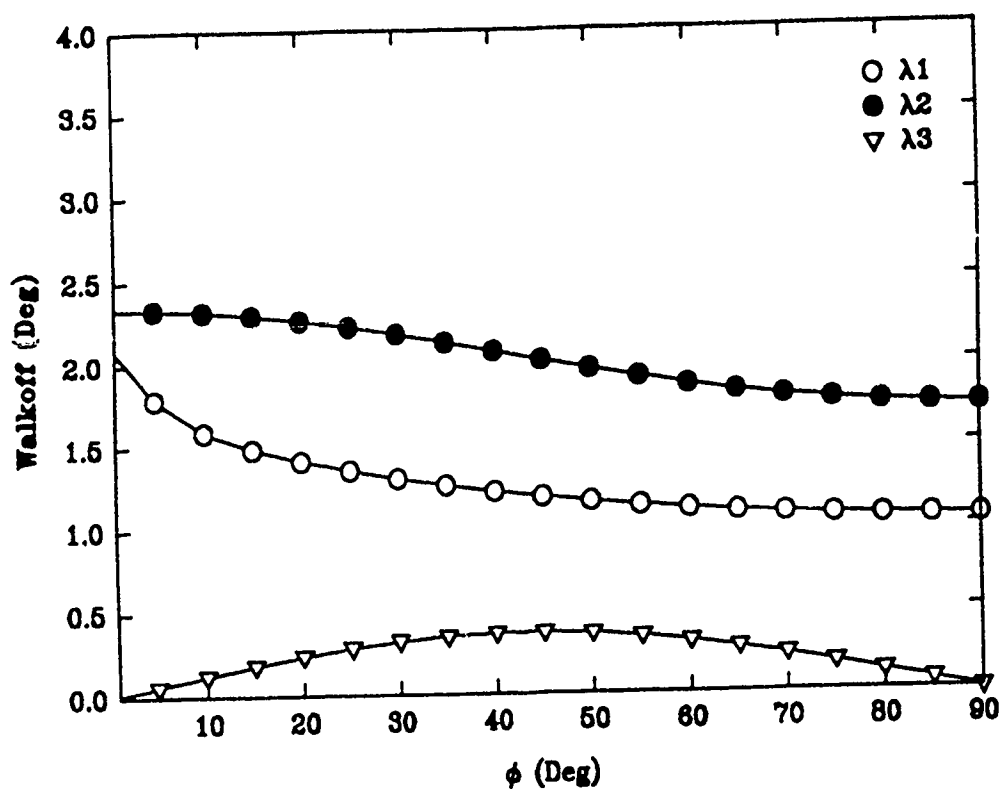


Figure F-30 Walkoff, OPO, 4.043/1.444/1.064  $\mu\text{m}$ , Type I, RTA

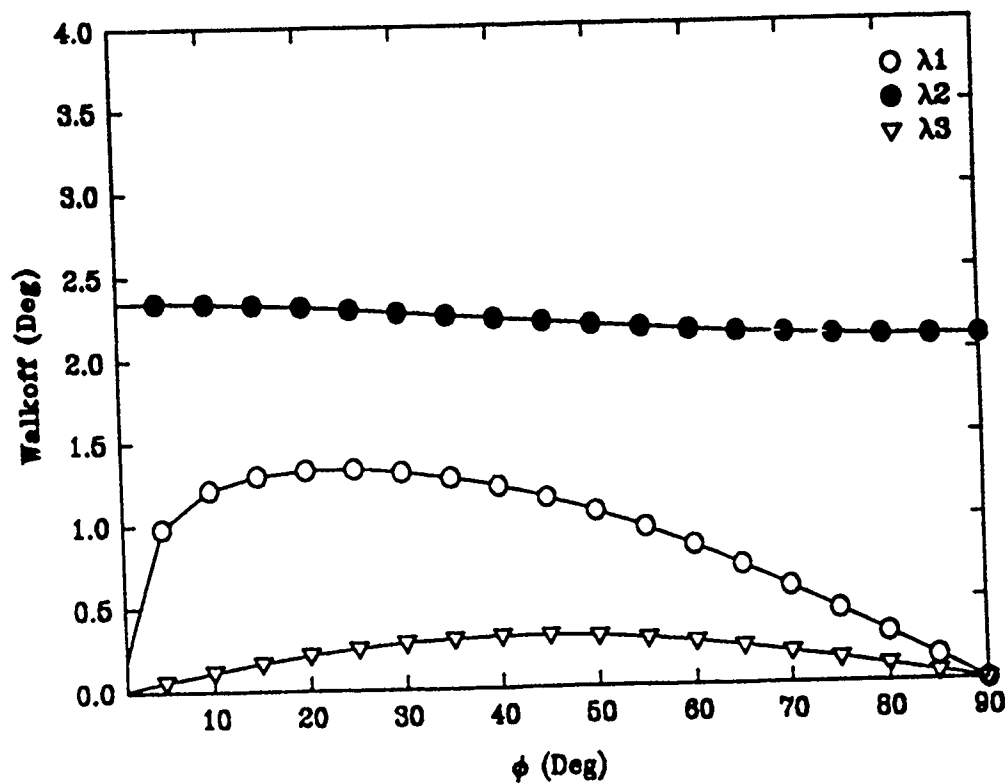


Figure F-31 Walkoff, OPO, 4.043/1.444/1.064  $\mu\text{m}$ , Type II, RTA

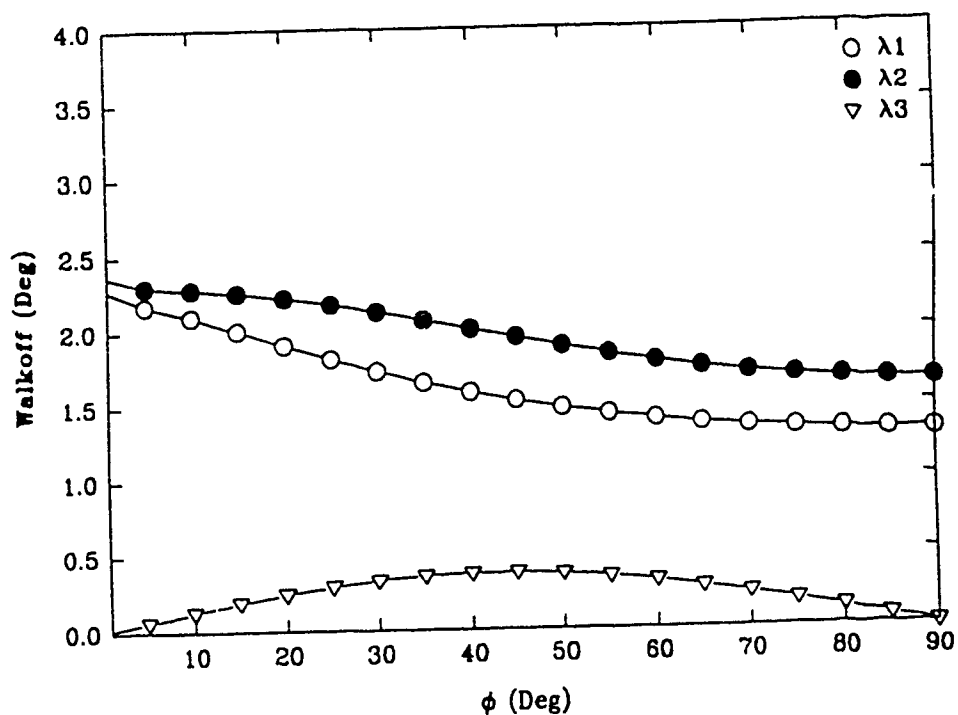


Figure F-32 Walkoff, OPO, 3.17/1.60/1.064  $\mu\text{m}$ , Type I, RTA

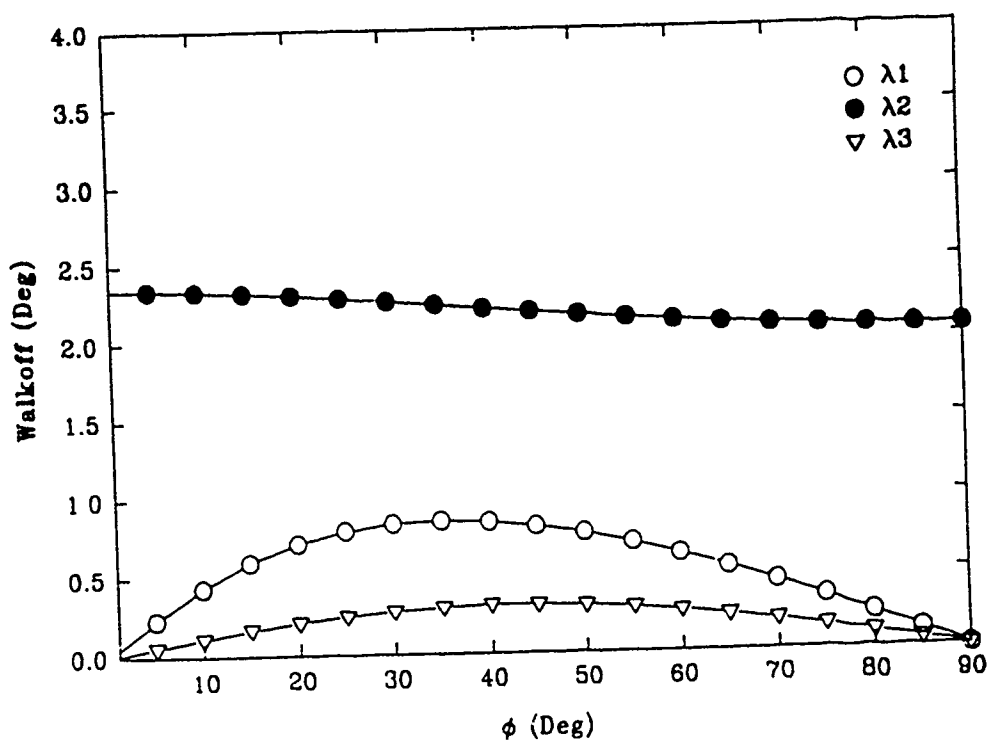


Figure F-33 Walkoff, OPO, 3.17/1.60/1.064  $\mu\text{m}$ , Type II, RTA

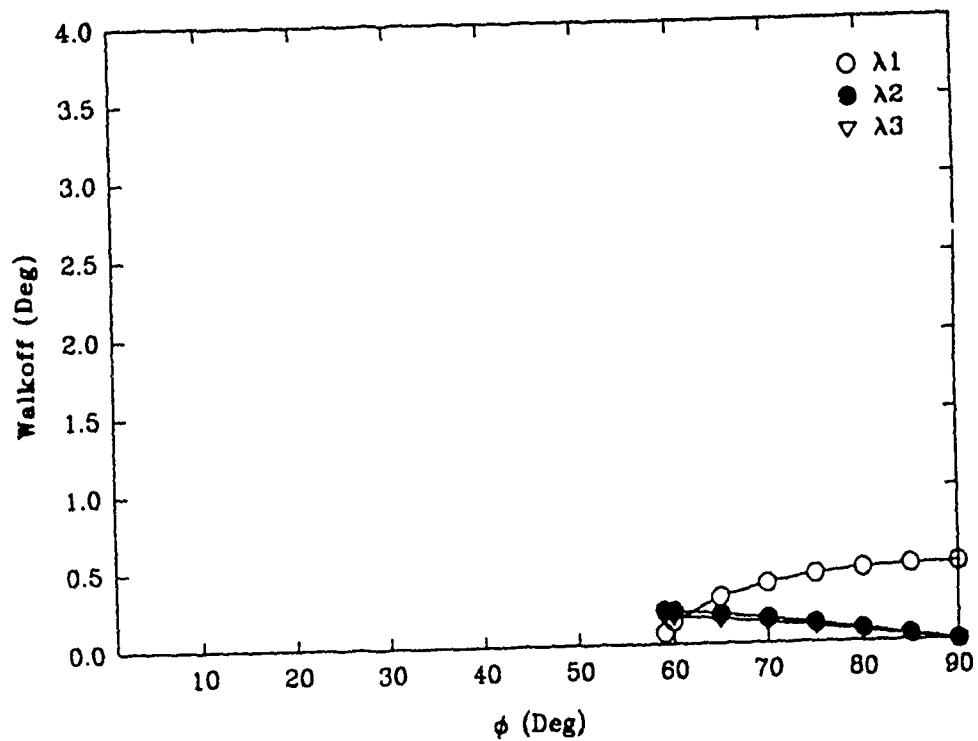


Figure F-34 Walkoff, OPO. 3.17/1.60/1.064  $\mu\text{m}$ . Type III, RTA



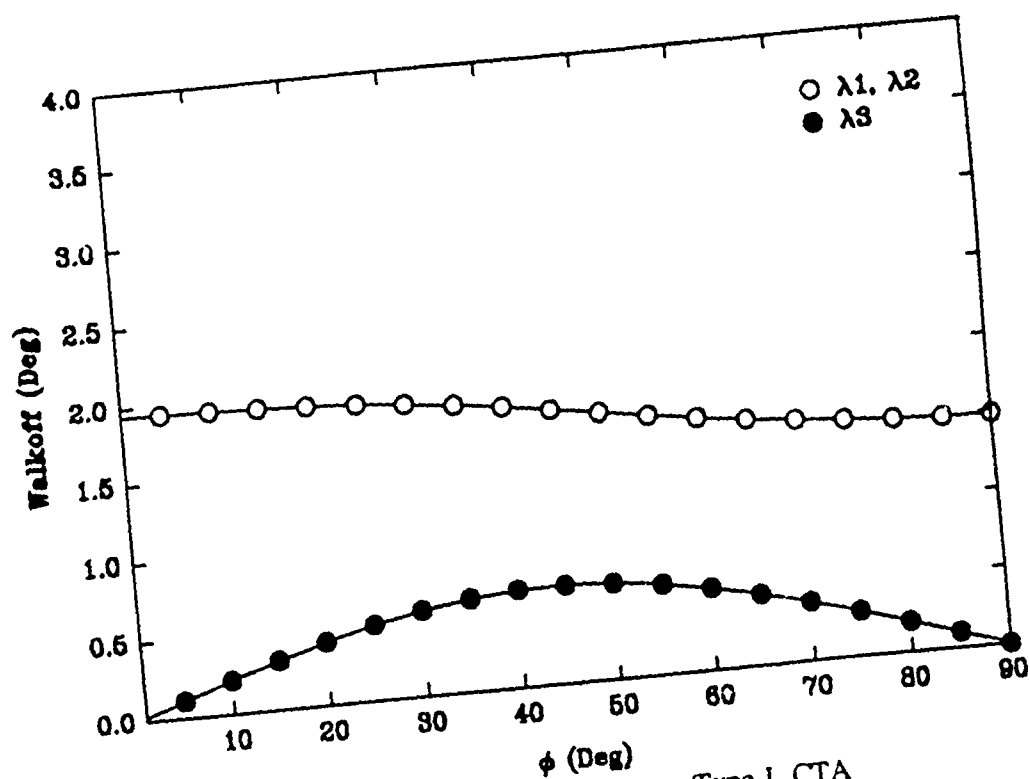


Figure F-35 Walkoff, SHG, 1.064/1.064/0.532  $\mu\text{m}$ . Type I, CTA

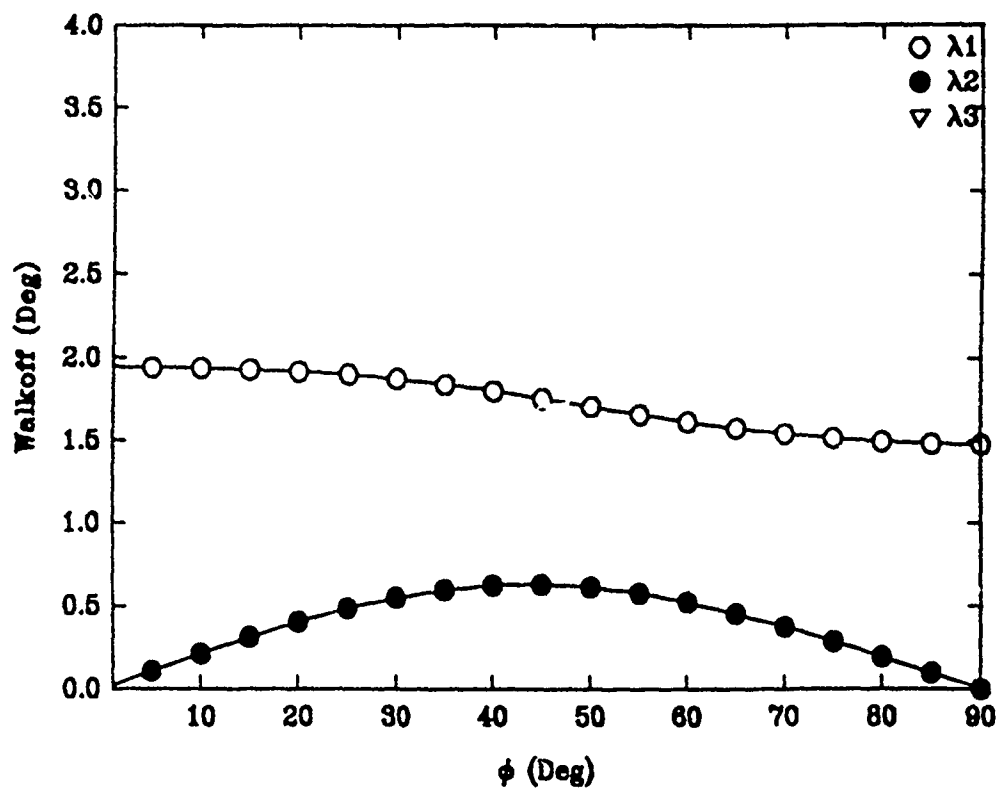


Figure F-36 Walkoff, SHG, 1.35/1.35/0.675  $\mu\text{m}$ , Type I, CTA

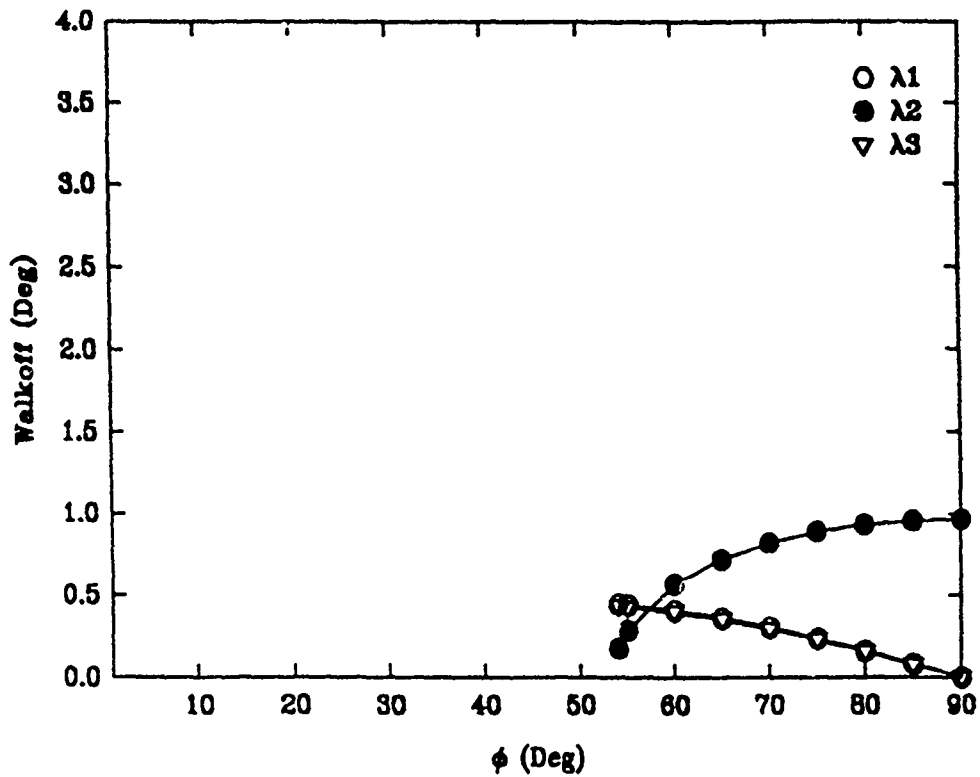


Figure F-37 Walkoff, SHG, 1.35/1.35/0.675  $\mu\text{m}$ , Type II, CTA

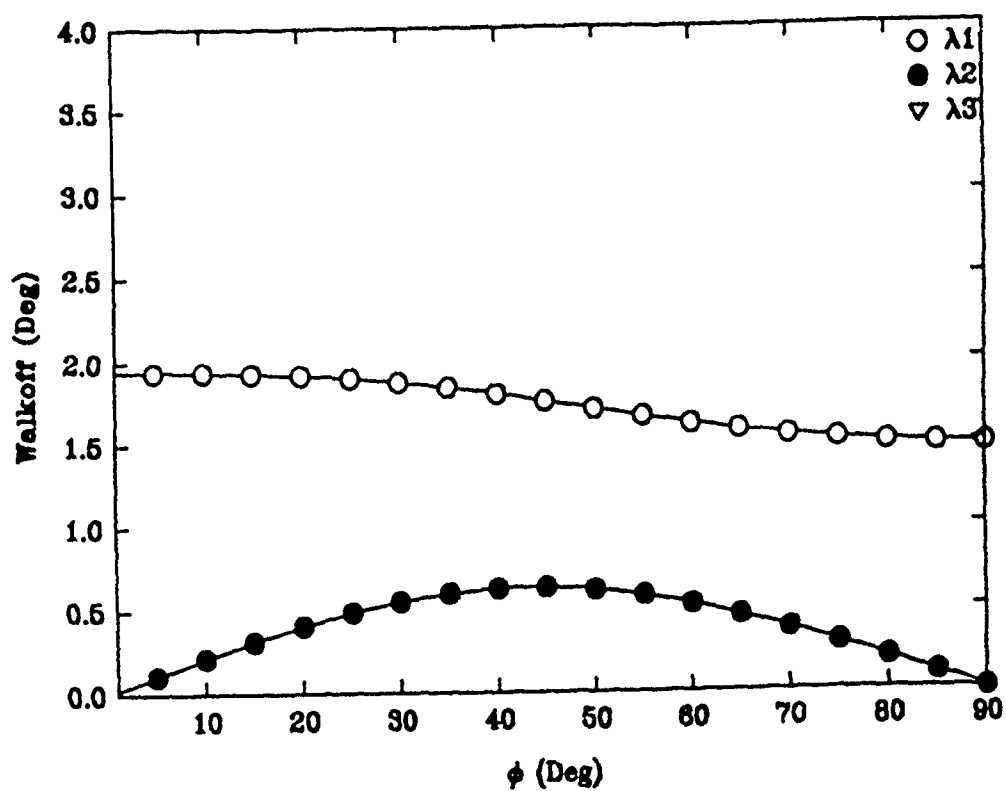


Figure F-36 Walkoff, SHG, 1.35/1.35/0.675  $\mu\text{m}$ , Type I, CTA

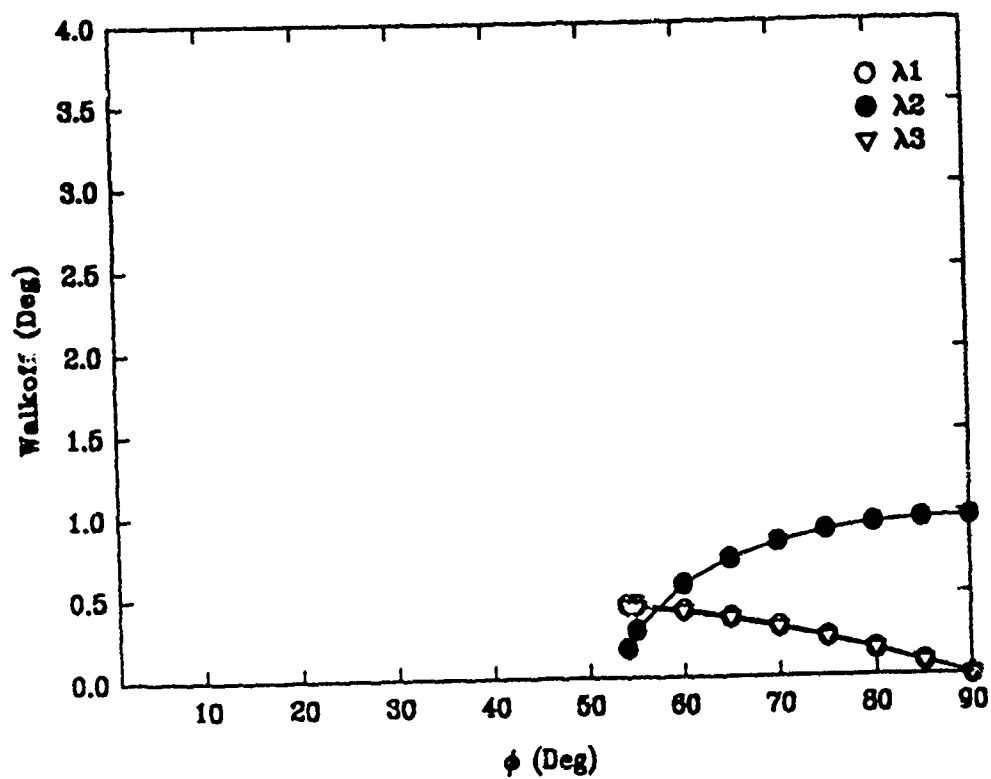


Figure F-37 Walkoff, SHG, 1.35/1.35/0.675  $\mu\text{m}$ , Type II, CTA

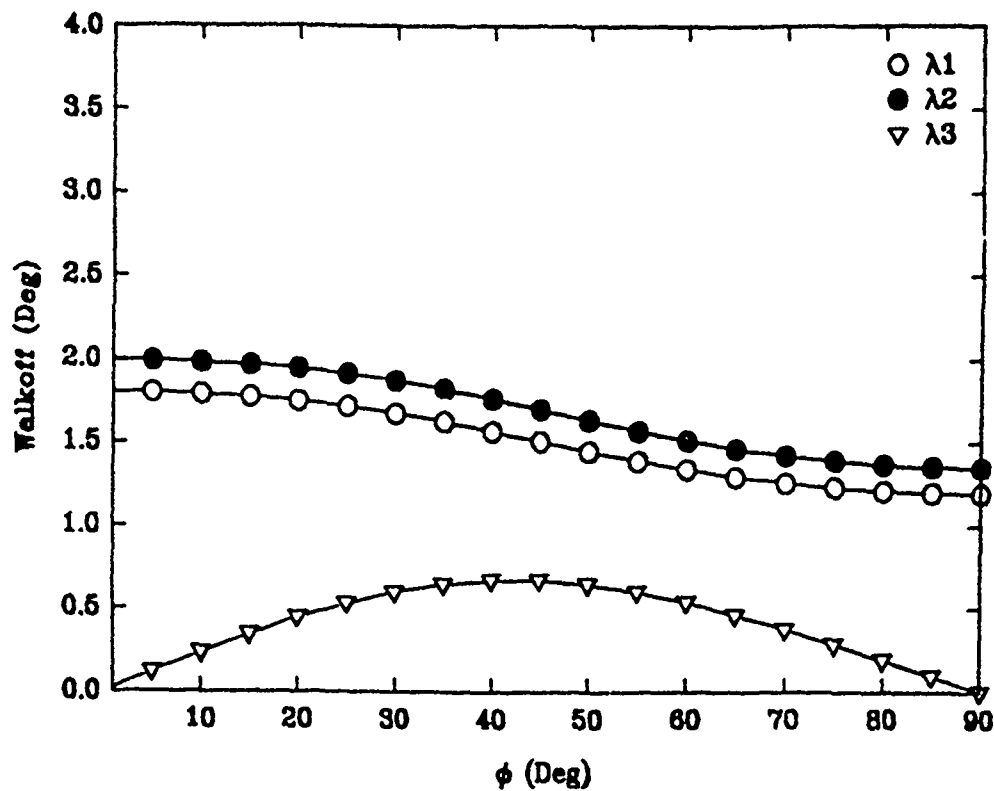


Figure F-38 Walkoff, OPO, 4.043/1.444/1.064  $\mu\text{m}$ , Type I, CTA

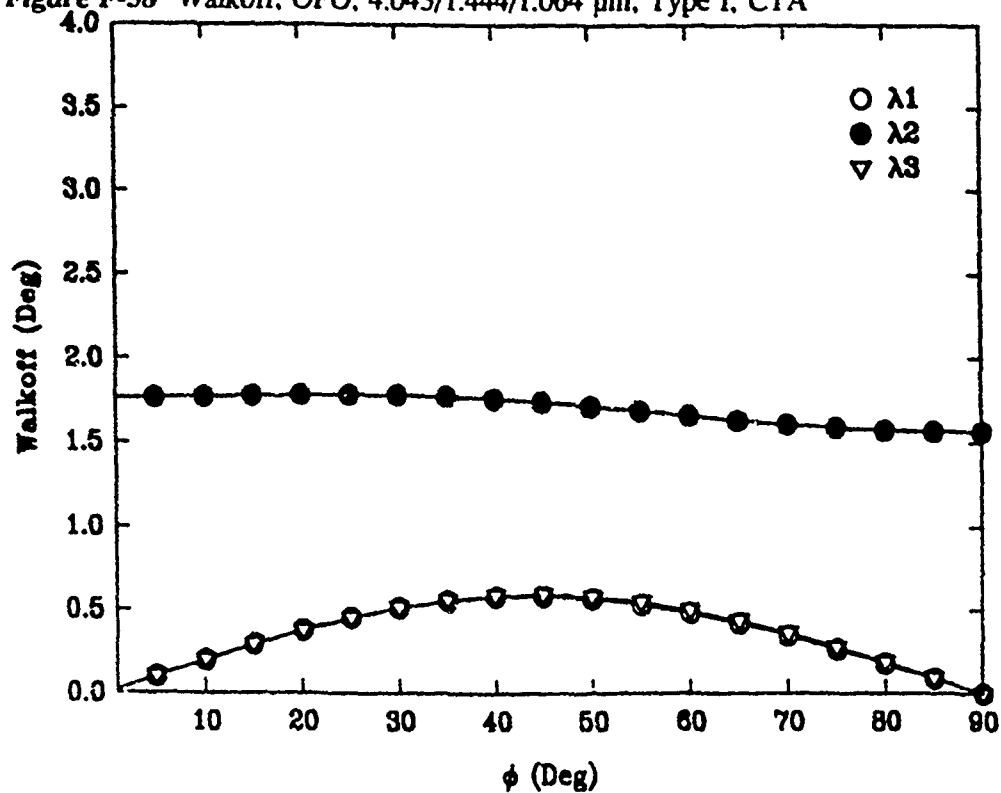


Figure F-39 Walkoff, OPO, 4.043/1.444/1.064  $\mu\text{m}$ , Type II, CTA

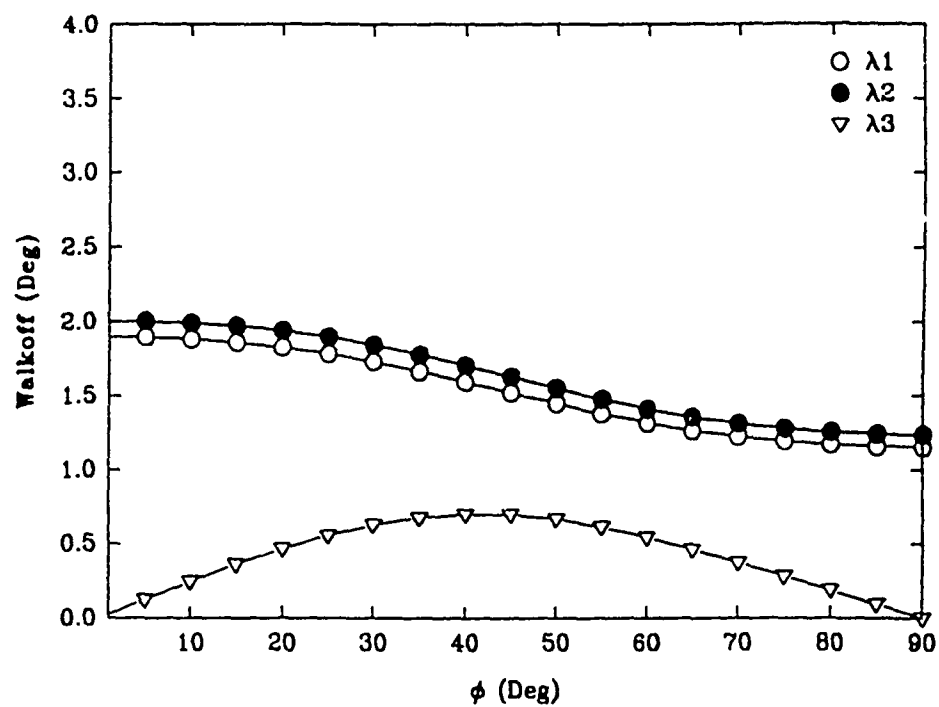


Figure F-40 Walkoff, OPO, 3.17/1.60/1.064  $\mu\text{m}$ , Type I, CTA

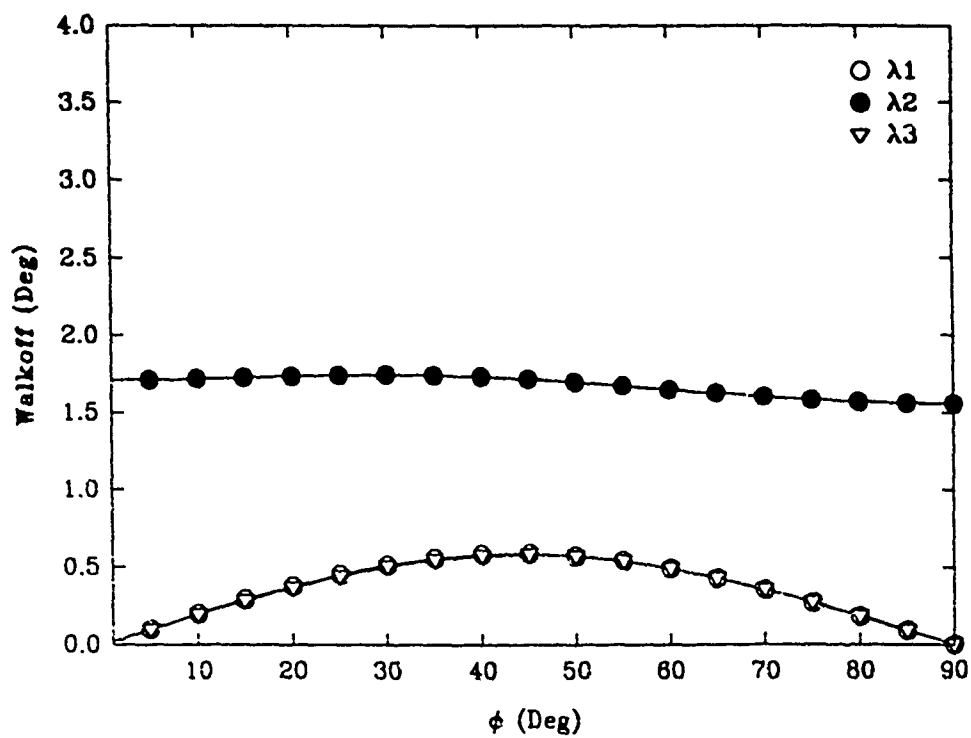


Figure F-41 Walkoff, OPO, 3.17/1.60/1.064  $\mu\text{m}$ , Type II, CTA

**SUPPLEMENTARY**

**INFORMATION**



# DEPARTMENT OF THE AIR FORCE

WRIGHT LABORATORY (AFMC)  
WRIGHT-PATTERSON AIR FORCE BASE, OHIO

21 March 1994

MEMORANDUM FOR DTIC/OCC  
CAMERON STATION BLDG 5  
ALEXANDRIA VA 22304-6145

FROM: WL/ELO Bldg 22B  
2700 D St Ste 2  
Wright-Patterson AFB OH 45433-7405

SUBJECT: Changes/Updates to WL-TR-93-5093, Three-Wave Nonlinear Interactions in  $\text{KTiOPO}_4$  (KTP) and KTO Isomorphs (AD Number A274079)

As with many publications, there are inevitable errors in the final product which need correction—and this report is no exception. Following are changes and corrections:

## Note

The distinction between “ray” and “wave” is somewhat loosely treated in the report. Properly considered, treat  $\vec{k}, \vec{D}$  as a reference to a “wave” and  $\vec{S}, \vec{E}$  as a reference to a “ray.” Specifically,  $\vec{k}$  refers to the wave normal vector (direction of propagation) and  $\vec{S}$  refers to the ray vector (direction of energy flow).

Page 4 Figure 3 incorrectly shows the angle  $\phi$  as being referenced from the y-axis. Modify the figure to indicate reference as being from the x-axis.

Page 6 Figure 4 was obtained from reference [4]. Credit for this figure was inadvertently removed from the Final Report.

Page 10 Last paragraph. Replace the sentence

The value of  $d_{eff}$  is dependent upon the direction of the  $\vec{k}$ ... we will use the electric displacement vectors,  $\vec{D}^i(\omega_m)$  to calculate  $\hat{a}_i$ ,  $\hat{a}_j$ , and  $\hat{a}_k$ .

with

The value of  $d_{eff}$  is dependent upon  $\vec{S}$ . We do, however, know that  $\vec{D} \perp \vec{k}$  and that  $\vec{E} \perp \vec{S}$ . We also know that  $\vec{D}$  and  $\vec{E}$  are related in terms of the polarizability tensor. Therefore, we can use the electric displacement vectors,  $\vec{D}_i(\omega_m)$ , to calculate  $\hat{a}_i$ ,  $\hat{a}_j$ , and  $\hat{a}_k$  of eqn 16.

Page 12 Change the indices of refraction subscripts in eqn 23 from “1, 2 and 2” to “x, y, and z”, respectively.

Page 14 2nd Line. Change “...the same as  $\{\hat{a}_{1,2}(\omega_n)\} \{\hat{a}_{1,2}(\omega_n)\}$ .” to “...the same as  $\{\hat{a}_{1,2}(\omega_o)\} \{\hat{a}_{1,2}(\omega_n)\}$ .”  
Paragraph 3.b.ii, 2nd linc. Change “...which exactly...” to “...which are exactly...”

Page 15 Paragraph 3.b.vii.(1). Change “...exactly the value” to “...exactly the same value”

CRRA-FA AD-A274079

Page 19

Table 2, last cell. The Sellmeier equation should read:

$$n_i^2 = A_i + (B_i / [1 - (C_i/\lambda)^2]) - D_i\lambda^2$$

Page 30

Table 11. Change  $d_{\text{eff}}$  for KTP, 0.675  $\mu\text{m}$ -SHG, Type II from 2.603 to 2.989.

Page 34

Paragraph 7.a.iv.(2). Change the sentence "For the arsenates, both CTA and KTA experience about an 8% loss while the loss for RTA appears minimal at best." to "None of the arsenates experience significant transmission loss at 3.17  $\mu\text{m}$ ."

Page 35

Change paragraph 7.b.ii.(3) to read:

(3) 3.17/1.60/1.064  $\mu\text{m}$ , Type III. While KTP has the largest  $d_{\text{eff}}$ , its absorption loss makes it a poor candidate. The arsenate KTA has the least walkoff, a slightly smaller  $d_{\text{eff}}$  than KTP and negligible transmission loss. The only other isomorph candidate, RTA, has only a slightly smaller  $d_{\text{eff}}$  and slightly larger walkoff than KTA. The preferred isomorph is KTA.

Page 37

Changes to Table 12 are minor and involve small changes to a few  $d_{\text{eff}}$  values, all Type I walkoff angles, and some changes in the reference angle used to calculate the relative walkoff for the other two wavelengths. An updated Table 12 has been provided (note:  $\vec{k}$  added to updated table).

Appendix B,  
pages 47 - 51

Replace with the attached MathCad worksheet. The original worksheet incorrectly treats the isomorph RTA as a negative crystal (it is positive), and incorrectly calculates relative walkoff. Additionally, a few other simplifications were made. Descriptions of the changes are as follows:

Eqns B-3a and B-3b ensure that the crystal type is identified as  $\pm 1$ . Eqns B-6a and B-6b identify the correct angle  $\theta$  column of the data matrix. Eqn B-6c creates the appropriate phase match angle pair matrix for that phase match type. Eqns B-15a, B-15b and B-15c correctly identify the  $a_i$ ,  $a_j$ , and  $a_k$  unit vectors and eqn B-16 creates the column vector,  $a_k$ . Eqns B-19a through B-19c calculate the walkoff angle for the selected phase match type. Eqns B-19d and B-19e setup for eqn B-19g which calculates the relative walkoff angles. The smallest walkoff angle identifies the column which has the correct relative walkoff angles (e.g., if  $\rho_3$  is smaller than the other two angles, then the third column has the correct relative walkoff angle values).

Appendix D,  
pages 61 - 65

Tables D-1 through D-5 are replaced by the attached page of tables.



DALE L. FENIMORE, Captain, USAF  
Electro-Optics Projects Engineer  
Electro-Optics Sources Branch

Attachments:

1. Table 12, Update
2. Appendix B, Update
3. Appendix D, Update



# CALCULATE BIAxIAL/UNIAXIAL CRYSTAL NONLINEAR COEFFICIENT ( $d_{eff}$ ) and WALKOFF ( $\rho$ ) FOR POSITIVE/NEGATIVE CRYSTALS

## OBTAIN DATA FROM DATA FILES

Matrix := READPRN(pm\_data\_rta)      d<sub>ijk</sub> := READPRN(dijk\_rta)      n := READPRN(indicesd\_rta)      (B-1a, b, c)

## IDENTIFY ORIGIN FOR WORKSHEET MATRICES

ORIGIN := 0      (B-2)

d<sub>ijk</sub> for the crystal

$$d_{ijk} = \begin{pmatrix} 0.00 & 0.00 & 0.00 & 0.00 & 1.90 & 0.00 \\ 0.00 & 0.00 & 0.00 & 3.60 & 0.00 & 0.00 \\ 2.30 & 3.80 & 15.80 & 0.00 & 0.00 & 0.00 \end{pmatrix}$$

Indices of Refraction

$$n = \begin{pmatrix} 1.7576751 & 1.7905609 & 1.8026541 \\ 1.7756109 & 1.7982079 & 1.8092106 \\ 1.8278463 & 1.8655065 & 1.8809392 \end{pmatrix}$$

**Select Positive or Negative Crystal Type** with a POSITIVE or NEGATIVE Number.

NOTE: Unless properly selected, the calculated value for  $d_{eff}$  and walkoff angles may not be correct.

CT := 1      CT := if(CT=0, 1, if(|CT| > 1, CT, |CT|<sup>-1</sup>), CT)      CT = 1      (B-3a, b)

PHASE MATCH angles data file LEGEND [Matrix], (by column):  $\lambda_1, \lambda_2$ , &  $\lambda_3$ ;  $\phi$ ;  $\theta(I)$ ;  $\theta(II)$ ;  $\theta(III)$

**SELECT AN ANGLE  $\phi$  FOR WHICH AN ANGLE  $\theta$  EXISTS** (for Type I, II, or III Selected Below)

i := 0      PMID := 2      (B-4)

$\lambda := [(Matrix^{<0>})_i, (Matrix^{<1>})_i, (Matrix^{<2>})_i]$       (B-5a)

$\lambda_1 := \lambda_{0,0}$        $\lambda_2 := \lambda_{0,1}$        $\lambda_3 := \lambda_{0,2}$       (B-5b, c, d)

$\lambda_1 = 3.176$        $\lambda_2 = 1.6000$        $\lambda_3 = 1.0640$

C := (4 5 6)      c := if(PMID=3, C<sub>0,2</sub>, if(PMID=2, C<sub>0,1</sub>, C<sub>0,0</sub>))      (B-6a, b)

T := augment(Matrix<c>, Matrix<3>)      (B-6c)

$A_i := (T^{<0>})_{i,deg}$        $\beta_i := (T^{<1>})_{i,deg}$       (B-7a, b)

$\theta := A_i$        $\phi := \beta_i$       (B-7c, d)

$\theta = 44.4295 \cdot deg$        $\phi = 0.0000 \cdot deg$

## SELECT Phase Match Category for Desired Nonlinear Coefficient ( $d_{eff}$ )

1 - SHG/SFM (" $\lambda_3$ ")      2 - DFM-32/OPA-32 (" $\lambda_1$ ")  
3 - DFM-31/OPA-31 (" $\lambda_2$ ")      4 - OPO (" $\lambda_1$ ")

CATEGORY := 4      (B-8)

This region begins the calculation for the effective non-linear coefficient ( $d_{eff}$ ).  
These calculations are NOT limited to the principle-axis.

This is the solution for the OPTIC AXIS,  $\Omega$

$$\Omega := \begin{bmatrix} \text{asin} \left[ \frac{n_{2,0}}{n_{1,0}} \left[ \frac{(n_{1,0})^2 - (n_{0,0})^2}{(n_{2,0})^2 - (n_{0,0})^2} \right]^{.5} \right] + 10^{-18} \\ \text{asin} \left[ \frac{n_{2,1}}{n_{1,1}} \left[ \frac{(n_{1,1})^2 - (n_{0,1})^2}{(n_{2,1})^2 - (n_{0,1})^2} \right]^{.5} \right] + 10^{-18} \\ \text{asin} \left[ \frac{n_{2,2}}{n_{1,2}} \left[ \frac{(n_{1,2})^2 - (n_{0,2})^2}{(n_{2,2})^2 - (n_{0,2})^2} \right]^{.5} \right] + 10^{-18} \end{bmatrix}$$

This angle,  $\Omega$ , is measured from the z-axis to the optic axis.

NOTE: the  $10^{-18}$  value is intended to prevent  $\tan 2\delta$  from experiencing a singularity.

$$\Omega = \begin{pmatrix} 31.107 \\ 19.167 \\ 17.333 \end{pmatrix} \text{deg}$$

(B-9)

This is used to calculate the polarization angle, " $\delta$ ". This angle is formed by the direction of the slow ray electric displacement unit vector,  $e_1$ , from the surface of the plane formed by the wavefront vector ( $k$ ) and the z-axis

$$\tan 2\delta := \begin{bmatrix} \frac{\cos(\theta) \cdot \sin(2\phi)}{\cot(\Omega_{0,0})^2 \cdot \sin(\theta)^2 - \cos(\theta)^2 \cdot \cos(\phi)^2 + \sin(\phi)^2} \\ \frac{\cos(\theta) \cdot \sin(2\phi)}{\cot(\Omega_{1,0})^2 \cdot \sin(\theta)^2 - \cos(\theta)^2 \cdot \cos(\phi)^2 + \sin(\phi)^2} \\ \frac{\cos(\theta) \cdot \sin(2\phi)}{\cot(\Omega_{2,0})^2 \cdot \sin(\theta)^2 - \cos(\theta)^2 \cdot \cos(\phi)^2 + \sin(\phi)^2} \end{bmatrix}$$

$$\tan 2\delta = \begin{pmatrix} 0.0000 \\ 0.0000 \\ 0.0000 \end{pmatrix}$$

(B-10a)

$$\delta_{adj} := \text{if}(\cos(\theta) \cdot \sin(2\phi) = 0, 0, \text{if}(\cos(\theta) \cdot \sin(2\phi) > 0, 0, \pi))$$

$$\delta_{adj} = 0.0000$$

$$\cos(\theta) \cdot \sin(2\phi) = 0.0000$$

(B-10b)

$$\delta := \begin{bmatrix} (\text{atan}(\tan 2\delta_{0,0}) + \delta_{adj}) \cdot 0.5 \\ (\text{atan}(\tan 2\delta_{1,0}) + \delta_{adj}) \cdot 0.5 \\ (\text{atan}(\tan 2\delta_{2,0}) + \delta_{adj}) \cdot 0.5 \end{bmatrix}$$

$$\delta = \begin{pmatrix} 0.000 \\ 0.000 \\ 0.000 \end{pmatrix} \text{deg}$$

(B-10c)

The following are the solutions for the SLOW (b1) rays and the FAST (b2) rays. These solutions represent the UNIT VECTORS of the electric displacement vector  $D$ . Columns represent  $\lambda_1$ ,  $\lambda_2$ , &  $\lambda_3$ , respectively.

$$a := \cos(\theta) \cdot \cos(\phi) \cdot \cos(\delta_{0,0}) + \sin(\phi) \cdot \sin(\delta_{0,0})$$

$$b := \cos(\theta) \cdot \sin(\phi) \cdot \cos(\delta_{0,0}) - \cos(\phi) \cdot \sin(\delta_{0,0})$$

(B-11a,b)

$$c := \cos(\theta) \cdot \cos(\phi) \cdot \cos(\delta_{1,0}) + \sin(\phi) \cdot \sin(\delta_{1,0})$$

$$d := \cos(\theta) \cdot \sin(\phi) \cdot \cos(\delta_{1,0}) - \cos(\phi) \cdot \sin(\delta_{1,0})$$

(B-11c,d)

$$e := \cos(\theta) \cdot \cos(\phi) \cdot \cos(\delta_{2,0}) + \sin(\phi) \cdot \sin(\delta_{2,0})$$

$$f := \cos(\theta) \cdot \sin(\phi) \cdot \cos(\delta_{2,0}) - \cos(\phi) \cdot \sin(\delta_{2,0})$$

(B-11e,f)

$$aa := \cos(\theta) \cdot \cos(\phi) \cdot \sin(\delta_{0,0}) - \sin(\phi) \cdot \cos(\delta_{0,0})$$

$$bb := \cos(\theta) \cdot \sin(\phi) \cdot \sin(\delta_{0,0}) + \cos(\phi) \cdot \cos(\delta_{0,0})$$

(B-11g,h)

$$cc := \cos(\theta) \cdot \cos(\phi) \cdot \sin(\delta_{1,0}) - \sin(\phi) \cdot \cos(\delta_{1,0})$$

$$dd := \cos(\theta) \cdot \sin(\phi) \cdot \sin(\delta_{1,0}) + \cos(\phi) \cdot \cos(\delta_{1,0})$$

(B-11i,j)

$$ee := \cos(\theta) \cdot \cos(\phi) \cdot \sin(\delta_{2,0}) - \sin(\phi) \cdot \cos(\delta_{2,0})$$

$$ff := \cos(\theta) \cdot \sin(\phi) \cdot \sin(\delta_{2,0}) + \cos(\phi) \cdot \cos(\delta_{2,0})$$

(B-11k,l)

$$b_1 := \begin{pmatrix} a & c & e \\ b & d & f \\ \sin(\theta) \cdot \cos(\delta_{0,0}) & \sin(\theta) \cdot \cos(\delta_{1,0}) & \sin(\theta) \cdot \cos(\delta_{2,0}) \end{pmatrix}$$

$$b_2 := \begin{pmatrix} aa & cc & ee \\ bb & dd & ff \\ \sin(\theta) \cdot \sin(\delta_{0,0}) & \sin(\theta) \cdot \sin(\delta_{1,0}) & \sin(\theta) \cdot \sin(\delta_{2,0}) \end{pmatrix}$$

(B-11m,n)

This section calculates the electric field's two polarization components,  $\lambda_1, \lambda_2$ , and  $\lambda_3$  (top to bottom), respectively.

Column 1 is for the SLOW rays ( $e_1$ ); column 2 calculates the FAST rays ( $e_2$ ).

$$Pb := \begin{bmatrix} \left[ \frac{(b_{10,0})^2}{(n_{0,0})^4} + \frac{(b_{11,0})^2}{(n_{1,0})^4} + \frac{(b_{12,0})^2}{(n_{2,0})^4} \right]^{0.5} & \left[ \frac{(b_{20,0})^2}{(n_{0,0})^4} + \frac{(b_{21,0})^2}{(n_{1,0})^4} + \frac{(b_{22,0})^2}{(n_{2,0})^4} \right]^{0.5} \\ \left[ \frac{(b_{10,1})^2}{(n_{0,1})^4} + \frac{(b_{11,1})^2}{(n_{1,1})^4} + \frac{(b_{12,1})^2}{(n_{2,1})^4} \right]^{0.5} & \left[ \frac{(b_{20,1})^2}{(n_{0,1})^4} + \frac{(b_{21,1})^2}{(n_{1,1})^4} + \frac{(b_{22,1})^2}{(n_{2,1})^4} \right]^{0.5} \\ \left[ \frac{(b_{10,2})^2}{(n_{0,2})^4} + \frac{(b_{11,2})^2}{(n_{1,2})^4} + \frac{(b_{12,2})^2}{(n_{2,2})^4} \right]^{0.5} & \left[ \frac{(b_{20,2})^2}{(n_{0,2})^4} + \frac{(b_{21,2})^2}{(n_{1,2})^4} + \frac{(b_{22,2})^2}{(n_{2,2})^4} \right]^{0.5} \end{bmatrix} \quad (B-12)$$

This section calculates the UNIT VECTORS for the polarization components for the electric fields. The SLOW rays are calculated by "a1," the FAST rays by "a2." The rows represent the x, y, and z-axis components, respectively, the columns represent  $\lambda_1, \lambda_2$  &  $\lambda_3$  (left to right), respectively.

$$a1 := \begin{bmatrix} \frac{b_{10,0}}{Pb_{0,0}(n_{0,0})^2} & \frac{b_{10,1}}{Pb_{1,0}(n_{0,1})^2} & \frac{b_{10,2}}{Pb_{2,0}(n_{0,2})^2} \\ \frac{b_{11,0}}{Pb_{0,1}(n_{1,0})^2} & \frac{b_{11,1}}{Pb_{1,1}(n_{1,1})^2} & \frac{b_{11,2}}{Pb_{2,1}(n_{1,2})^2} \\ \frac{b_{12,0}}{Pb_{0,2}(n_{2,0})^2} & \frac{b_{12,1}}{Pb_{1,2}(n_{2,1})^2} & \frac{b_{12,2}}{Pb_{2,2}(n_{2,2})^2} \end{bmatrix} \quad a2 := \begin{bmatrix} \frac{b_{20,0}}{Pb_{0,1}(n_{0,0})^2} & \frac{b_{20,1}}{Pb_{1,1}(n_{0,1})^2} & \frac{b_{20,2}}{Pb_{2,1}(n_{0,2})^2} \\ \frac{b_{21,0}}{Pb_{0,1}(n_{1,0})^2} & \frac{b_{21,1}}{Pb_{1,1}(n_{1,1})^2} & \frac{b_{21,2}}{Pb_{2,1}(n_{1,2})^2} \\ \frac{b_{22,0}}{Pb_{0,1}(n_{2,0})^2} & \frac{b_{22,1}}{Pb_{1,1}(n_{2,1})^2} & \frac{b_{22,2}}{Pb_{2,1}(n_{2,2})^2} \end{bmatrix} \quad (B-13a, b)$$

Categories: CATEGORY = 4

1 = SHG/SFM, 2 = OPO-32/DFM-32

3 = OPO-31/DFM-31, 4 = OPO

Crystal Type (Positive or Negative  
Number indicates Type)

CT = 1

Phase Match Type

PMID = 2

Identify which column to use for the specific phase match category selected

$$C_i := \text{if}(\text{CATEGORY}=1, 2, \text{if}(\text{CATEGORY}=2, 0, \text{if}(\text{CATEGORY}=3, 1, 2))) \quad C_i = 2 \quad (a_i) \quad (B-14a)$$

$$C_j := \text{if}(\text{CATEGORY}=1, 0, \text{if}(\text{CATEGORY}=2, 1, \text{if}(\text{CATEGORY}=3, 0, 0))) \quad C_j = 0 \quad (a_j) \quad (B-14b)$$

$$C_k := \text{if}(\text{CATEGORY}=1, 1, \text{if}(\text{CATEGORY}=2, 2, \text{if}(\text{CATEGORY}=3, 2, 1))) \quad C_k = 1 \quad (a_k) \quad (B-14c)$$

Setup the  $a_i, a_j$ , and  $a_k$  vectors

Type I, II, and III

$$a_i := \text{if}(CT \geq 0, a2^{<C_i>}, a1^{<C_i>}) \quad (B-15a)$$

$$a_j := \text{if}(CT \geq 0, \text{if}(PMID=2, a2^{<C_j>}, a1^{<C_j>}), \text{if}(PMID=2, a1^{<C_j>}, a2^{<C_j>})) \quad (B-15b)$$

$$a_k := \text{if}(CT \geq 0, \text{if}(PMID=3, a2^{<C_k>}, a1^{<C_k>}), \text{if}(PMID=3, a1^{<C_k>}, a2^{<C_k>})) \quad (B-15c)$$

### Setup the $a_{jk}$ column-vector

$$a_{jk} := \begin{bmatrix} a_{j0,0} a_{k0,0} \\ a_{j1,0} a_{k1,0} \\ a_{j2,0} a_{k2,0} \\ a_{j1,0} a_{k2,0} + a_{j2,0} a_{k1,0} \\ a_{j0,0} a_{k2,0} + a_{j2,0} a_{k0,0} \\ a_{j0,0} a_{k1,0} + a_{j1,0} a_{k0,0} \end{bmatrix} \quad (B-16)$$

### Effective Nonlinear Coefficient

$$d_{eff} := |a_i (d_{ijk} a_{jk})| \quad (B-17)$$

### WALKOFF Angle ( $\rho$ ) Calculations (column1: SLOW rays, column 2: FAST rays)

By row, starting at the top is the calculation for the  $\lambda_1$ ,  $\lambda_2$ , &  $\lambda_3$ , respectively

$$\rho := \begin{bmatrix} \text{acos} \left[ \frac{\left( \frac{b_{10,0}}{n_{0,0}} \right)^2 + \left( \frac{b_{11,0}}{n_{1,0}} \right)^2 + \left( \frac{b_{12,0}}{n_{2,0}} \right)^2}{Pb_{0,0}} \right] & \text{acos} \left[ \frac{\left( \frac{b_{20,0}}{n_{0,0}} \right)^2 + \left( \frac{b_{21,0}}{n_{1,0}} \right)^2 + \left( \frac{b_{22,0}}{n_{2,0}} \right)^2}{Pb_{0,1}} \right] \\ \text{acos} \left[ \frac{\left( \frac{b_{10,1}}{n_{0,1}} \right)^2 + \left( \frac{b_{11,1}}{n_{1,1}} \right)^2 + \left( \frac{b_{12,1}}{n_{2,1}} \right)^2}{Pb_{1,0}} \right] & \text{acos} \left[ \frac{\left( \frac{b_{20,1}}{n_{0,1}} \right)^2 + \left( \frac{b_{21,1}}{n_{1,1}} \right)^2 + \left( \frac{b_{22,1}}{n_{2,1}} \right)^2}{Pb_{1,1}} \right] \\ \text{acos} \left[ \frac{\left( \frac{b_{10,2}}{n_{0,2}} \right)^2 + \left( \frac{b_{11,2}}{n_{1,2}} \right)^2 + \left( \frac{b_{12,2}}{n_{2,2}} \right)^2}{Pb_{2,0}} \right] & \text{acos} \left[ \frac{\left( \frac{b_{20,2}}{n_{0,2}} \right)^2 + \left( \frac{b_{21,2}}{n_{1,2}} \right)^2 + \left( \frac{b_{22,2}}{n_{2,2}} \right)^2}{Pb_{2,1}} \right] \end{bmatrix} \quad (B-18)$$

### Select correct walkoff and relative walkoff angles according to phase match category

$$v := 180 \pi^{-1} \quad (B-19a)$$

$$\rho_1 := \text{Re} \left( \text{if} (CT \geq 0, \text{if} (PMID = 2, \rho_{0,1}, \rho_{0,0}), \text{if} (PMID = 2, \rho_{0,0}, \rho_{0,1})) \cdot v \right) \quad (B-19b)$$

$$\rho_2 := \text{Re} \left( \text{if} (CT \geq 0, \text{if} (PMID = 3, \rho_{1,1}, \rho_{1,0}), \text{if} (PMID = 3, \rho_{1,0}, \rho_{1,1})) \cdot v \right) \quad (B-19c)$$

$$\rho_3 := \text{Re} \left( \text{if} (CT \geq 0, \rho_{2,1}, \rho_{2,0}) \cdot v \right) \quad (B-19d)$$

$$T := \begin{pmatrix} 1 & 2 & 2 \\ 2 & 1 & 2 \\ 2 & 2 & 1 \end{pmatrix} \quad t := \text{if} (PMID = 3, T^{<2>}, \text{if} (PMID = 2, T^{<1>}, T^{<0>})) \quad (B-19e, f)$$

$$\tau p := \begin{bmatrix} \rho_1 & \left( \left| \begin{pmatrix} t_0 & t_0 \\ \rho_1 & -\rho_2 \end{pmatrix} \right| \right)^{(t_0)^{-1}} & \left( \left| \begin{pmatrix} t_1 & t_1 \\ \rho_1 & -\rho_3 \end{pmatrix} \right| \right)^{(t_1)^{-1}} \\ \left( \left| \begin{pmatrix} t_0 & t_0 \\ \rho_2 & -\rho_1 \end{pmatrix} \right| \right)^{(t_0)^{-1}} & \rho_2 & \left( \left| \begin{pmatrix} t_2 & t_2 \\ \rho_2 & -\rho_3 \end{pmatrix} \right| \right)^{(t_2)^{-1}} \\ \left( \left| \begin{pmatrix} t_1 & t_1 \\ \rho_3 & -\rho_1 \end{pmatrix} \right| \right)^{(t_1)^{-1}} & \left( \left| \begin{pmatrix} t_2 & t_2 \\ \rho_3 & -\rho_2 \end{pmatrix} \right| \right)^{(t_2)^{-1}} & \rho_3 \end{bmatrix} \frac{\pi}{0.18} \quad (B-19g)$$

### Create the Matrix for Writing a Line of Data to the Data File

$$data := (\lambda_1 \lambda_2 \lambda_3 \theta v \phi v d_{eff} \rho_1 \rho_2 \rho_3) \quad (B-20a)$$

### Writes Data to the Data File Specified

$$\text{APPENDPRN}(dw\_info \ rta) := data \quad (B-20b)$$

Table D-1. Nonlinear Characteristics, KTP

$\lambda_1/\lambda_2/\lambda_3$	Type	$\vec{k}$ ( $\theta, \phi$ )	$\rho_1/\rho_2/\rho_3$	$d_{eff}$
1.064/1.064/0.532	I	45.64, 36.93	47.63/47.63/*8.49	0.423
	II	90.00, 25.99	3.47/*0.0/4.87	3.268
1.35/1.35/0.675	I	37.24, 31.27	44.53/44.53/*8.16	0.366
	II	58.70, 0.00	*0.0/44.68/0.0	2.989
4.043/1.444/1.064	I	36.31, 31.61	38.07/43.92/*7.12	0.438
	II	44.33, 0.00	*0.0/48.86/0.0	2.387
3.176/1.60/1.064	I	34.81, 30.10	39.62/42.70/*7.32	0.398
	II	44.85, 0.00	*0.0/48.55/0.0	2.412
	III	77.36, 0.00	20.13/*0.0/0.0	3.496

Table D-2. Nonlinear Characteristics, RTP

$\lambda_1/\lambda_2/\lambda_3$	$\vec{k}$ ( $\theta, \phi$ )	$\rho_1/\rho_2/\rho_3$	$d_{eff}$
1.064/1.064/0.532	52.08, 23.32	48.48/48.48/*13.62	0.128
	90.00, 41.70	11.55/*0.0/13.09	2.827
1.35/1.35/0.675	26.89, 53.47	27.15/27.15/*17.37	0.324
	65.95, 0.00	0.0/40.83/*0.0	3.225
4.043/1.444/1.064	27.81, 52.38	21.35/28.33/*16.87	0.355
	52.79, 0.00	*0.0/51.38/0.0	2.751
3.176/1.60/1.064	25.94, 49.60	20.98/24.62/*17.99	0.416
	53.16, 0.00	*0.0/50.74/0.0	2.768
	90.00, 45.35	*0.0/11.33/11.60	2.720

Table D-3. Nonlinear Characteristics, KTA

1.064/1.064/0.532	I	48.64, 39.89	45.52/45.52/*5.26	0.231
1.35/1.35/0.675	I	38.62, 34.09	43.13/43.13/*5.31	0.164
	II	61.67, 0.00	*0.0/39.43/0.0	2.781
4.043/1.444/1.064	I	33.31, 64.32	31.41/39.05/*3.96	0.406
	II	45.72, 0.00	0.0/45.68/*0.0	2.207
3.176/1.60/1.064	I	32.41, 53.98	34.73/38.27/*5.08	0.174
	II	46.01, 0.00	*0.0/45.10/0.0	2.220
	III	90.00, 16.40	*0.0/1.19/1.66	3.154

Table D-4. Nonlinear Characteristics, RTA

1.064/1.064/0.532	53.11, 41.37	38.92/38.99/*6.98	0.469
1.35/1.35/0.675	41.57, 36.72	38.72/38.72/*6.60	0.496
	70.40, 0.00	*0.0/27.10/0.0	3.357
4.043/1.444/1.064	40.48, 13.55	26.22/40.05/*2.89	1.465
	42.48, 0.00	0.0/40.95/*0.0	2.320
3.176/1.60/1.064	37.36, 25.56	31.09/37.54/*5.15	0.952
	44.43, 0.00	0.0/40.92/*0.0	2.413
	90.00, 58.63	*0.0/3.78/3.22	2.355

Table D-5. Nonlinear Characteristics, CTA

1.064/1.064/0.532	I	64.20, 41.82	24.45/24.58/*9.65	0.217
1.35/1.35/0.675	I	51.56, 27.57	31.63/31.63/*9.06	0.226
	II	90.00, 53.40	7.80/*0.0/7.60	2.492
4.043/1.444/1.064	I	34.16, 61.88	21.27/24.47/*8.88	0.135
	II	61.51, 0.00	0.0/30.83/*0.0	3.110
3.176/1.60/1.064	I	31.97, 59.41	20.98/22.79/*9.66	0.177
	II	62.60, 0.00	*0.0/29.85/0.0	3.145

## Notes:

- Wavelengths ( $\lambda_1, \lambda_2, \lambda_3$ ) given in  $\mu\text{m}$
- k-Vector given in degrees
- Walkoff ( $\rho$ ) given in milliradians. Starred angle is the reference angle from which the other two angles are measured
- $d_{eff}$  given in terms of pm/V

These tables replace those found on pages 61 - 65 of the final report.

**SUPPLEMENTARY**

**INFORMATION**



# DEPARTMENT OF THE AIR FORCE

WRIGHT LABORATORY (AFMC)  
WRIGHT-PATTERSON AIR FORCE BASE, OHIO

# ERRATA

21 March 1994

MEMORANDUM FOR WL/DOA BLD 22

WL/DTIC

FROM: WL/ELO Bldg 22B

2700 D St Ste 2

Wright-Patterson AFB OH 45433-7405

SUBJECT: Changes/Updates to WL-TR-93-<sup>5029</sup>~~5093~~, Three-Wave Nonlinear Interactions in  $\text{KTiOPO}_4$  (KTP) and KTO Isomorphs

As with many publications, there are inevitable errors in the final product which need correction—and this report is no exception. Following are changes and corrections:

## Note

The distinction between “ray” and “wave” is somewhat loosely treated in the report. Properly considered, treat  $\vec{k}, \vec{D}$  as a reference to a “wave” and  $\vec{S}, \vec{E}$  as a reference to a “ray.” Specifically,  $\vec{k}$  refers to the wave normal vector (direction of propagation) and  $\vec{S}$  refers to the ray vector (direction of energy flow).

Page 4

Figure 3 incorrectly shows the angle  $\phi$  as being referenced from the y-axis. Modify the figure to indicate reference as being from the x-axis.

Page 6

Figure 4 was obtained from reference [4]. Credit for this figure was inadvertently removed from the Final Report.

Page 10

Last paragraph. Replace the sentence

The value of  $d_{eff}$  is dependent upon the direction of the  $\vec{k}$ ... we will use the electric displacement vectors,  $\vec{D}(\omega_m)$  to calculate  $\hat{a}_i, \hat{a}_j$ , and  $\hat{a}_k$ .

with

The value of  $d_{eff}$  is dependent upon  $\vec{S}$ . We do, however, know that  $\vec{D} \perp \vec{k}$  and that  $\vec{E} \perp \vec{S}$ . We also know that  $\vec{D}$  and  $\vec{E}$  are related in terms of the polarizability tensor. Therefore, we can use the electric displacement vectors,  $\vec{D}(\omega_m)$ , to calculate  $\hat{a}_i, \hat{a}_j$ , and  $\hat{a}_k$  of eqn 16.

Page 12

Change the indices of refraction subscripts in eqn 23 from “1, 2 and 2” to “x, y, and z”, respectively.

Page 14

2nd Line. Change “...the same as  $\{\hat{a}_{i,2}(\omega_n)\} \{\hat{a}_{i,1}(\omega_n)\}$ .” to “...the same as  $\{\hat{a}_{i,2}(\omega_o)\} \{\hat{a}_{i,1}(\omega_n)\}$ .”  
Paragraph 3.b.ii, 2nd line. Change “...which exactly...” to “...which are exactly...”

Page 15

Paragraph 3.b.vii.(1). Change “...exactly the value” to “...exactly the same value”

ERRATA AD A 274 079

Page 19

Table 2, last cell. The Sellmeier equation should read:

$$n_i^2 = A_i + (B_i / [1 - (C_i/\lambda)^2]) - D_i\lambda^2$$

Page 30

Table 11. Change  $d_{\text{eff}}$  for KTP, 0.675  $\mu\text{m}$ -SHG, Type II from 2.603 to 2.989.

Page 34

Paragraph 7.a.iv.(2). Change the sentence "For the arsenates, both CTA and KTA experience about an 8% loss while the loss for RTA appears minimal at best." to "None of the arsenates experience significant transmission loss at 3.17  $\mu\text{m}$ ."

Page 35

Change paragraph 7.b.ii.(3) to read:

(3) 3.17/1.60/1.064  $\mu\text{m}$ , Type III. While KTP has the largest  $d_{\text{eff}}$ , its absorption loss makes it a poor candidate. The arsenate KTA has the least walkoff, a slightly smaller  $d_{\text{eff}}$  than KTP and negligible transmission loss. The only other isomorph candidate, RTA, has only a slightly smaller  $d_{\text{eff}}$  and slightly larger walkoff than KTA. The preferred isomorph is KTA.

Page 37

Changes to Table 12 are minor and involve small changes to a few  $d_{\text{eff}}$  values, all Type I walkoff angles, and some changes in the reference angle used to calculate the relative walkoff for the other two wavelengths. An updated Table 12 has been provided (note:  $\vec{k}$  added to updated table).

Appendix B,  
pages 47 - 51

Replace with the attached MathCad worksheet. The original worksheet incorrectly treats the isomorph RTA as a negative crystal (it is positive), and incorrectly calculates relative walkoff. Additionally, a few other simplifications were made. Descriptions of the changes are as follows:

Eqns B-3a and B-3b ensure that the crystal type is identified as  $\pm 1$ . Eqns B-6a and B-6b identify the correct angle  $\theta$  column of the data matrix. Eqn B-6c creates the appropriate phase match angle pair matrix for that phase match type. Eqns B-15a, B-15b and B-15c correctly identify the  $a_i$ ,  $a_j$ , and  $a_k$  unit vectors and eqn B-16 creates the column vector,  $a_k$ . Eqns B-19a through B-19c calculate the walkoff angle for the selected phase match type. Eqns B-19d and B-19e setup for eqn B-19g which calculates the relative walkoff angles. The smallest walkoff angle identifies the column which has the correct relative walkoff angles (e.g., if  $\rho_3$  is smaller than the other two angles, then the third column has the correct relative walkoff angle values).

Appendix D,  
pages 61 - 65

Tables D-1 through D-5 are replaced by the attached page of tables.



DALE L. FENIMORE, Captain, USAF  
Electro-Optics Projects Engineer  
Electro-Optics Sources Branch

**Attachments:**

1. Table 12, Update
2. Appendix B, Update
3. Appendix D, Update



Table D-1. Nonlinear Characteristics, KTP

$\lambda_1/\lambda_2/\lambda_3$	Type	$\vec{k} (\theta, \phi)$	$\rho_1/\rho_2/\rho_3$	$d_{eff}$
1.064/1.064/0.532	I	45.64, 36.93	47.63/47.63/*8.49	0.423
	II	90.00, 25.99	3.47/*0.0/4.87	3.268
1.35/1.35/0.675	I	37.24, 31.27	44.53/44.53/*8.16	0.366
	II	58.70, 0.00	*0.0/44.68/0.0	2.989
4.043/1.444/1.064	I	36.31, 31.61	38.07/43.92/*7.12	0.438
	II	44.33, 0.00	*0.0/48.86/0.0	2.387
3.176/1.60/1.064	I	34.81, 30.10	39.62/42.70/*7.32	0.398
	II	44.85, 0.00	*0.0/48.55/0.0	2.412
	III	77.36, 0.00	20.13/*0.0/0.0	3.496

Table D-2. Nonlinear Characteristics, RTP

$\lambda_1/\lambda_2/\lambda_3$	$\vec{k} (\theta, \phi)$	$\rho_1/\rho_2/\rho_3$	$d_{eff}$
1.064/1.064/0.532	I	52.08, 23.32	48.48/48.48/*13.62
	II	90.00, 41.70	11.55/*0.0/13.09
1.35/1.35/0.675	I	26.89, 53.47	27.15/27.15/*17.37
	II	65.95, 0.00	0.0/40.83/*0.0
4.043/1.444/1.064	I	27.81, 52.38	21.35/28.33/*16.87
	II	52.79, 0.00	*0.0/51.38/0.0
3.176/1.60/1.064	I	25.94, 49.60	20.98/24.62/*17.99
	II	53.16, 0.00	*0.0/50.74/0.0
	III	90.00, 45.35	*0.0/11.33/11.60

Table D-3. Nonlinear Characteristics, KTA

1.064/1.064/0.532	I	48.64, 39.89	45.52/45.52/*5.26	0.231
1.35/1.35/0.675	I	38.62, 34.09	43.13/43.13/*5.31	0.164
	II	61.67, 0.00	*0.0/39.43/0.0	2.781
4.043/1.444/1.064	I	33.31, 64.32	31.41/39.05/*3.96	0.406
	II	45.72, 0.00	0.0/45.68/*0.0	2.207
3.176/1.60/1.064	I	32.41, 53.98	34.73/38.27/*5.08	0.174
	II	46.01, 0.00	*0.0/45.10/0.0	2.220
	III	90.00, 16.40	*0.0/1.19/1.66	3.154

Table D-4. Nonlinear Characteristics, RTA

1.064/1.064/0.532	I	53.11, 41.37	38.92/38.99/*6.98	0.469
1.35/1.35/0.675	I	41.57, 36.72	38.72/38.72/*6.60	0.496
	II	70.40, 0.00	*0.0/27.10/0.0	3.357
4.043/1.444/1.064	I	40.48, 13.55	26.22/40.05/*2.89	1.465
	II	42.48, 0.00	0.0/40.95/*0.0	2.320
3.176/1.60/1.064	I	37.36, 25.56	31.09/37.54/*5.15	0.952
	II	44.43, 0.00	0.0/40.92/*0.0	2.413
	III	90.00, 58.63	*0.0/3.78/3.22	2.355

Table D-5. Nonlinear Characteristics, CTA

1.064/1.064/0.532	I	64.20, 41.82	24.45/24.58/*9.65	0.217
1.35/1.35/0.675	I	51.56, 27.57	31.63/31.63/*9.06	0.226
	II	90.00, 53.40	7.80/*0.0/7.60	2.492
4.043/1.444/1.064	I	34.16, 61.88	21.27/24.47/*8.88	0.135
	II	61.51, 0.00	0.0/30.83/*0.0	3.110
3.176/1.60/1.064	I	31.97, 59.41	20.98/22.79/*9.66	0.177
	II	62.60, 0.00	*0.0/29.85/0.0	3.145

## Notes:

- Wavelengths ( $\lambda_1, \lambda_2, \lambda_3$ ) given in  $\mu\text{m}$
- k-Vector given in degrees
- Walkoff ( $\rho$ ) given in milliradians. Starred angle is the reference angle from which the other two angles are measured
- $d_{eff}$  given in terms of pm/V

These tables replace those found on pages 61 - 65 of the final report.

# CALCULATE BIAxIAL/UNIAXIAL CRYSTAL NONLINEAR COEFFICIENT ( $d_{eff}$ ) and WALKOFF ( $\rho$ ) FOR POSITIVE/NEGATIVE CRYSTALS

## OBTAIN DATA FROM DATA FILES

Matrix := READPRN(pm\_data\_rta)      d\_ijk := READPRN(dijk\_rta)      n := READPRN(indicesd\_rta)      (B-1a, b, c)

## IDENTIFY ORIGIN FOR WORKSHEET MATRICES

ORIGIN := 0      (B-2)

d\_ijk for the crystal

$$d_{ijk} = \begin{pmatrix} 0.00 & 0.00 & 0.00 & 0.00 & 1.90 & 0.00 \\ 0.00 & 0.00 & 0.00 & 3.60 & 0.00 & 0.00 \\ 2.30 & 3.80 & 15.80 & 0.00 & 0.00 & 0.00 \end{pmatrix}$$

Indices of Refraction

$$n = \begin{pmatrix} 1.7576751 & 1.7905609 & 1.8026541 \\ 1.7756109 & 1.7982079 & 1.8092106 \\ 1.8278463 & 1.8655065 & 1.8809392 \end{pmatrix}$$

Select Positive or Negative Crystal Type with a POSITIVE or NEGATIVE Number.

NOTE: Unless properly selected, the calculated value for  $d_{eff}$  and walkoff angles may not be correct.

CT := 1      CT := if(CT=0, if(|CT| > 1, CT, |CT|<sup>-1</sup>), CT)      CT = 1      (B-3a, b)

PHASE MATCH angles data file LEGEND {Matrix}, (by column):  $\lambda_1, \lambda_2$ , &  $\lambda_3$ ;  $\phi$ ;  $\theta(I)$ ;  $\theta(II)$ ;  $\theta(III)$

SELECT AN ANGLE  $\phi$  FOR WHICH AN ANGLE  $\theta$  EXISTS (for Type I, II, or III Selected Below)

i := 0      PMID := 2      (B-4)

$\lambda := [(Matrix^{<0>})_i, (Matrix^{<1>})_i, (Matrix^{<2>})_i]$       (B-5a)

$\lambda_1 := \lambda_{0,0}$        $\lambda_2 := \lambda_{0,1}$        $\lambda_3 := \lambda_{0,2}$       (B-5b, c, d)

$\lambda_1 = 3.176$        $\lambda_2 = 1.6000$        $\lambda_3 = 1.0640$

C := (4 5 6)      c := if(PMID=3, C<sub>0,2</sub>, if(PMID=2, C<sub>0,1</sub>, C<sub>0,0</sub>))      (B-6a, b)

T := augment(Matrix^{<0>}, Matrix^{<3>})      (B-6c)

$A_i := (T^{<0>})_{i-deg}$        $\beta_i := (T^{<1>})_{i-deg}$       (B-7a, b)

$\theta := A_i$        $\phi := \beta_i$       (B-7c, d)

$\theta = 44.4295^\circ \text{deg}$        $\phi = 0.0000^\circ \text{deg}$

SELECT Phase Match Category for Desired Nonlinear Coefficient ( $d_{eff}$ )

1 - SHG/SFM (" $\lambda_3$ ")      2 - DFM-32/OPA-32 (" $\lambda_1$ ")  
3 - DFM-31/OPA-31 (" $\lambda_2$ ")      4 - OPO (" $\lambda_1$ ")

CATEGORY := 4      (B-8)

This region begins the calculation for the effective non-linear coefficient ( $d_{eff}$ ).  
These calculations are NOT limited to the principle-axis.

This is the solution for the OPTIC AXIS,  $\Omega$

$$\Omega := \begin{bmatrix} \arcsin \left[ \frac{n_{2,0} \left[ \frac{(n_{1,0})^2 - (n_{0,0})^2}{(n_{2,0})^2 - (n_{0,0})^2} \right]^{.5}}{n_{1,0}} \right] + 10^{-18} \\ \arcsin \left[ \frac{n_{2,1} \left[ \frac{(n_{1,1})^2 - (n_{0,1})^2}{(n_{2,1})^2 - (n_{0,1})^2} \right]^{.5}}{n_{1,1}} \right] + 10^{-18} \\ \arcsin \left[ \frac{n_{2,2} \left[ \frac{(n_{1,2})^2 - (n_{0,2})^2}{(n_{2,2})^2 - (n_{0,2})^2} \right]^{.5}}{n_{1,2}} \right] + 10^{-18} \end{bmatrix}$$

This angle,  $\Omega$ , is measured from the z-axis to the optic axis.

NOTE: the  $10^{-18}$  value is intended to prevent  $\tan 2\delta$  from experiencing a singularity.

$$\Omega = \begin{pmatrix} 31.107 \\ 19.167 \\ 17.333 \end{pmatrix} \cdot \text{deg}$$

(B-9)

This is used to calculate the polarization angle, " $\delta$ ". This angle is formed by the direction of the slow ray electric displacement unit vector,  $e_1$ , from the surface of the plane formed by the wavefront vector ( $k$ ) and the z-axis

$$\tan 2\delta := \begin{bmatrix} \frac{\cos(\theta) \cdot \sin(2\phi)}{\cot(\Omega_{0,0})^2 \cdot \sin(\theta)^2 - \cos(\theta)^2 \cdot \cos(\phi)^2 + \sin(\phi)^2} \\ \frac{\cos(\theta) \cdot \sin(2\phi)}{\cot(\Omega_{1,0})^2 \cdot \sin(\theta)^2 - \cos(\theta)^2 \cdot \cos(\phi)^2 + \sin(\phi)^2} \\ \frac{\cos(\theta) \cdot \sin(2\phi)}{\cot(\Omega_{2,0})^2 \cdot \sin(\theta)^2 - \cos(\theta)^2 \cdot \cos(\phi)^2 + \sin(\phi)^2} \end{bmatrix}$$

$$\tan 2\delta = \begin{pmatrix} 0.0000 \\ 0.0000 \\ 0.0000 \end{pmatrix}$$

(B-10a)

$$\delta_{adj} := \text{if}(\cos(\theta) \cdot \sin(2\phi) = 0, 0, \text{if}(\cos(\theta) \cdot \sin(2\phi) > 0, 0, \pi))$$

$$\delta_{adj} = 0.0000$$

$$\cos(\theta) \cdot \sin(2\phi) = 0.0000$$

(B-10b)

$$\delta := \begin{bmatrix} (\arcsin(\tan 2\delta_{0,0}) + \delta_{adj}) \cdot 0.5 \\ (\arcsin(\tan 2\delta_{1,0}) + \delta_{adj}) \cdot 0.5 \\ (\arcsin(\tan 2\delta_{2,0}) + \delta_{adj}) \cdot 0.5 \end{bmatrix}$$

$$\delta = \begin{pmatrix} 0.000 \\ 0.000 \\ 0.000 \end{pmatrix} \cdot \text{deg}$$

(B-10c)

The following are the solutions for the SLOW (b1) rays and the FAST (b2) rays. These solutions represent the UNIT VECTORS of the electric displacement vectors. Columns represent  $\lambda_1$ ,  $\lambda_2$ , &  $\lambda_3$ , respectively.

$$a := \cos(\theta) \cdot \cos(\phi) \cdot \cos(\delta_{0,0}) + \sin(\phi) \cdot \sin(\delta_{0,0})$$

$$b := \cos(\theta) \cdot \sin(\phi) \cdot \cos(\delta_{0,0}) - \cos(\phi) \cdot \sin(\delta_{0,0})$$

(B-11a,b)

$$c := \cos(\theta) \cdot \cos(\phi) \cdot \cos(\delta_{1,0}) + \sin(\phi) \cdot \sin(\delta_{1,0})$$

$$d := \cos(\theta) \cdot \sin(\phi) \cdot \cos(\delta_{1,0}) - \cos(\phi) \cdot \sin(\delta_{1,0})$$

(B-11c,d)

$$e := \cos(\theta) \cdot \cos(\phi) \cdot \cos(\delta_{2,0}) + \sin(\phi) \cdot \sin(\delta_{2,0})$$

$$f := \cos(\theta) \cdot \sin(\phi) \cdot \cos(\delta_{2,0}) - \cos(\phi) \cdot \sin(\delta_{2,0})$$

(B-11e,f)

$$aa := \cos(\theta) \cdot \cos(\phi) \cdot \sin(\delta_{0,0}) - \sin(\phi) \cdot \cos(\delta_{0,0})$$

$$bb := \cos(\theta) \cdot \sin(\phi) \cdot \sin(\delta_{0,0}) + \cos(\phi) \cdot \cos(\delta_{0,0})$$

(B-11g,h)

$$cc := \cos(\theta) \cdot \cos(\phi) \cdot \sin(\delta_{1,0}) - \sin(\phi) \cdot \cos(\delta_{1,0})$$

$$dd := \cos(\theta) \cdot \sin(\phi) \cdot \sin(\delta_{1,0}) + \cos(\phi) \cdot \cos(\delta_{1,0})$$

(B-11i,j)

$$ee := \cos(\theta) \cdot \cos(\phi) \cdot \sin(\delta_{2,0}) - \sin(\phi) \cdot \cos(\delta_{2,0})$$

$$ff := \cos(\theta) \cdot \sin(\phi) \cdot \sin(\delta_{2,0}) + \cos(\phi) \cdot \cos(\delta_{2,0})$$

(B-11k,l)

$$b_1 := \begin{pmatrix} a & c & e \\ b & d & f \\ \sin(\theta) \cdot \cos(\delta_{0,0}) & \sin(\theta) \cdot \cos(\delta_{1,0}) & \sin(\theta) \cdot \cos(\delta_{2,0}) \end{pmatrix}$$

$$b_2 := \begin{pmatrix} aa & cc & ee \\ bb & dd & ff \\ \sin(\theta) \cdot \sin(\delta_{0,0}) & \sin(\theta) \cdot \sin(\delta_{1,0}) & \sin(\theta) \cdot \sin(\delta_{2,0}) \end{pmatrix}$$

(B-11m,n)

**This section calculates the electric field's two polarization components,  $\lambda_1, \lambda_2$ , and  $\lambda_3$  (top to bottom), respectively.**

Column 1 is for the SLOW rays ( $e_1$ ); column 2 calculates the FAST rays ( $e_2$ ).

$$Pb := \begin{bmatrix} \left[ \frac{(b_{10,0})^2}{(n_{0,0})^4} + \frac{(b_{11,0})^2}{(n_{1,0})^4} + \frac{(b_{12,0})^2}{(n_{2,0})^4} \right]^{0.5} & \left[ \frac{(b_{20,0})^2}{(n_{0,0})^4} + \frac{(b_{21,0})^2}{(n_{1,0})^4} + \frac{(b_{22,0})^2}{(n_{2,0})^4} \right]^{0.5} \\ \left[ \frac{(b_{10,1})^2}{(n_{0,1})^4} + \frac{(b_{11,1})^2}{(n_{1,1})^4} + \frac{(b_{12,1})^2}{(n_{2,1})^4} \right]^{0.5} & \left[ \frac{(b_{20,1})^2}{(n_{0,1})^4} + \frac{(b_{21,1})^2}{(n_{1,1})^4} + \frac{(b_{22,1})^2}{(n_{2,1})^4} \right]^{0.5} \\ \left[ \frac{(b_{10,2})^2}{(n_{0,2})^4} + \frac{(b_{11,2})^2}{(n_{1,2})^4} + \frac{(b_{12,2})^2}{(n_{2,2})^4} \right]^{0.5} & \left[ \frac{(b_{20,2})^2}{(n_{0,2})^4} + \frac{(b_{21,2})^2}{(n_{1,2})^4} + \frac{(b_{22,2})^2}{(n_{2,2})^4} \right]^{0.5} \end{bmatrix} \quad (B-12)$$

**This section calculates the UNIT VECTORS for the polarization components for the electric fields.** The SLOW rays are calculated by "a1," the FAST rays by "a2." The rows represent the x, y, and z-axis components, respectively, the columns represent  $\lambda_1, \lambda_2$  &  $\lambda_3$  (left to right), respectively.

$$a1 := \begin{bmatrix} \frac{b_{10,0}}{Pb_{0,0} \cdot (n_{0,0})^2} & \frac{b_{10,1}}{Pb_{1,0} \cdot (n_{0,1})^2} & \frac{b_{10,2}}{Pb_{2,0} \cdot (n_{0,2})^2} \\ \frac{b_{11,0}}{Pb_{0,0} \cdot (n_{1,0})^2} & \frac{b_{11,1}}{Pb_{1,0} \cdot (n_{1,1})^2} & \frac{b_{11,2}}{Pb_{2,0} \cdot (n_{1,2})^2} \\ \frac{b_{12,0}}{Pb_{0,0} \cdot (n_{2,0})^2} & \frac{b_{12,1}}{Pb_{1,0} \cdot (n_{2,1})^2} & \frac{b_{12,2}}{Pb_{2,0} \cdot (n_{2,2})^2} \end{bmatrix} \quad a2 := \begin{bmatrix} \frac{b_{20,0}}{Pb_{0,1} \cdot (n_{0,0})^2} & \frac{b_{20,1}}{Pb_{1,1} \cdot (n_{0,1})^2} & \frac{b_{20,2}}{Pb_{2,1} \cdot (n_{0,2})^2} \\ \frac{b_{21,0}}{Pb_{0,1} \cdot (n_{1,0})^2} & \frac{b_{21,1}}{Pb_{1,1} \cdot (n_{1,1})^2} & \frac{b_{21,2}}{Pb_{2,1} \cdot (n_{1,2})^2} \\ \frac{b_{22,0}}{Pb_{0,1} \cdot (n_{2,0})^2} & \frac{b_{22,1}}{Pb_{1,1} \cdot (n_{2,1})^2} & \frac{b_{22,2}}{Pb_{2,1} \cdot (n_{2,2})^2} \end{bmatrix} \quad (B-13a, b)$$

**Categories:** CATEGORY = 4  
1 = SHG/SFM, 2 = OPO-32/DFM-32  
3 = OPO-31/DFM-31, 4 = OPO

**Crystal Type** (Positive or Negative  
Number indicates Type)  
CT = 1

**Phase Match Type**  
PMID = 2

Identify which column to use for the specific phase match category selected

$$C_i := \text{if}(\text{CATEGORY}=1, 2, \text{if}(\text{CATEGORY}=2, 0, \text{if}(\text{CATEGORY}=3, 1, 2))) \quad C_i = 2 \quad (a_i) \quad (B-14a)$$

$$C_j := \text{if}(\text{CATEGORY}=1, 0, \text{if}(\text{CATEGORY}=2, 1, \text{if}(\text{CATEGORY}=3, 0, 0))) \quad C_j = 0 \quad (a_j) \quad (B-14b)$$

$$C_k := \text{if}(\text{CATEGORY}=1, 1, \text{if}(\text{CATEGORY}=2, 2, \text{if}(\text{CATEGORY}=3, 2, 1))) \quad C_k = 1 \quad (a_k) \quad (B-14c)$$

### **Setup the $a_i, a_j$ , and $a_k$ vectors**

Type I, II, and III

$$a_i := \text{if}(CT \geq 0, a2^{<C_i>}, a1^{<C_i>}) \quad (B-15a)$$

$$a_j := \text{if}(CT \geq 0, \text{if}(PMID=2, a2^{<C_j>}, a1^{<C_j>}), \text{if}(PMID=2, a1^{<C_j>}, a2^{<C_j>})) \quad (B-15b)$$

$$a_k := \text{if}(CT \geq 0, \text{if}(PMID=3, a2^{<C_k>}, a1^{<C_k>}), \text{if}(PMID=3, a1^{<C_k>}, a2^{<C_k>})) \quad (B-15c)$$

### Setup the $a_{jk}$ column-vector

$$a_{jk} := \begin{bmatrix} a_{j0,0} a_{k0,0} \\ a_{j1,0} a_{k1,0} \\ a_{j2,0} a_{k2,0} \\ a_{j1,0} a_{k2,0} + a_{j2,0} a_{k1,0} \\ a_{j0,0} a_{k2,0} + a_{j2,0} a_{k0,0} \\ a_{j0,0} a_{k1,0} + a_{j1,0} a_{k0,0} \end{bmatrix} \quad (B-16)$$

### Effective Nonlinear Coefficient

$$d_{eff} := |a_i (d_{ijk} a_{jk})| \quad (B-17)$$

### WALKOFF Angle ( $\rho$ ) Calculations (column1: SLOW rays, column 2: FAST rays)

By row, starting at the top is the calculation for the  $\lambda_1$ ,  $\lambda_2$ , &  $\lambda_3$ , respectively

$$\rho := \begin{bmatrix} \text{acos} \left[ \frac{\left( \frac{b_{10,0}}{n_{0,0}} \right)^2 + \left( \frac{b_{11,0}}{n_{1,0}} \right)^2 + \left( \frac{b_{12,0}}{n_{2,0}} \right)^2}{Pb_{0,0}} \right] & \text{acos} \left[ \frac{\left( \frac{b_{20,0}}{n_{0,0}} \right)^2 + \left( \frac{b_{21,0}}{n_{1,0}} \right)^2 + \left( \frac{b_{22,0}}{n_{2,0}} \right)^2}{Pb_{0,1}} \right] \\ \text{acos} \left[ \frac{\left( \frac{b_{10,1}}{n_{0,1}} \right)^2 + \left( \frac{b_{11,1}}{n_{1,1}} \right)^2 + \left( \frac{b_{12,1}}{n_{2,1}} \right)^2}{Pb_{1,0}} \right] & \text{acos} \left[ \frac{\left( \frac{b_{20,1}}{n_{0,1}} \right)^2 + \left( \frac{b_{21,1}}{n_{1,1}} \right)^2 + \left( \frac{b_{22,1}}{n_{2,1}} \right)^2}{Pb_{1,1}} \right] \\ \text{acos} \left[ \frac{\left( \frac{b_{10,2}}{n_{0,2}} \right)^2 + \left( \frac{b_{11,2}}{n_{1,2}} \right)^2 + \left( \frac{b_{12,2}}{n_{2,2}} \right)^2}{Pb_{2,0}} \right] & \text{acos} \left[ \frac{\left( \frac{b_{20,2}}{n_{0,2}} \right)^2 + \left( \frac{b_{21,2}}{n_{1,2}} \right)^2 + \left( \frac{b_{22,2}}{n_{2,2}} \right)^2}{Pb_{2,1}} \right] \end{bmatrix} \quad (B-18)$$

### Select correct walkoff and relative walkoff angles according to phase match category

$$v := 180 \pi^{-1}$$

$$\rho_1 := \text{Re} \left( \text{if} (CT \geq 0, \text{if} (PMID = 2, \rho_{0,1}, \rho_{0,0}), \text{if} (PMID = 2, \rho_{0,0}, \rho_{0,1})) \cdot v \right) \quad (B-19a)$$

$$\rho_2 := \text{Re} \left( \text{if} (CT \geq 0, \text{if} (PMID = 3, \rho_{1,1}, \rho_{1,0}), \text{if} (PMID = 3, \rho_{1,0}, \rho_{1,1})) \cdot v \right) \quad (B-19b)$$

$$\rho_3 := \text{Re} \left( \text{if} (CT \geq 0, \rho_{2,1}, \rho_{2,0}) \cdot v \right) \quad (B-19c)$$

$$\rho_3 := \text{Re} \left( \text{if} (CT \geq 0, \rho_{2,1}, \rho_{2,0}) \cdot v \right) \quad (B-19d)$$

$$T := \begin{pmatrix} 1 & 2 & 2 \\ 2 & 1 & 2 \\ 2 & 2 & 1 \end{pmatrix} \quad t := \text{if} (PMID = 3, T^{<2>}, \text{if} (PMID = 2, T^{<1>}, T^{<0>})) \quad (B-19e, f)$$

$$rp := \begin{bmatrix} \rho_1 & \left( \begin{vmatrix} t_0 & t_0 \\ \rho_1 & -\rho_2 \end{vmatrix} \right)^{(t_0)^{-1}} & \left( \begin{vmatrix} t_1 & t_1 \\ \rho_1 & -\rho_3 \end{vmatrix} \right)^{(t_1)^{-1}} \\ \left( \begin{vmatrix} t_0 & t_0 \\ \rho_2 & -\rho_1 \end{vmatrix} \right)^{(t_0)^{-1}} & \rho_2 & \left( \begin{vmatrix} t_2 & t_2 \\ \rho_2 & -\rho_3 \end{vmatrix} \right)^{(t_2)^{-1}} \\ \left( \begin{vmatrix} t_1 & t_1 \\ \rho_3 & -\rho_1 \end{vmatrix} \right)^{(t_1)^{-1}} & \left( \begin{vmatrix} t_2 & t_2 \\ \rho_3 & -\rho_2 \end{vmatrix} \right)^{(t_2)^{-1}} & \rho_3 \end{bmatrix} \frac{\pi}{0.18} \quad (B-19g)$$

### Create the Matrix for Writing a Line of Data to the Data File

$$data := (\lambda_1 \lambda_2 \lambda_3 \theta_v \phi_v d_{eff} \rho_1 \rho_2 \rho_3) \quad (B-20a)$$

### Writes Data to the Data File Specified

$$\text{APPENDPRN}(dw\_info, rta) := data_{\text{row}} \quad (B-20b)$$

# **CONSOLIDATED INFORMATION**

Crystal: RTA

Electric Displacement Unit Vectors, b1 = slow ray, b2 = fast ray

$$b_1 = \begin{pmatrix} -0.7141 & -0.7141 & -0.7141 \\ 0.0000 & 0.0000 & 0.0000 \\ 0.7000 & 0.7000 & 0.7000 \end{pmatrix}$$

$$b_2 = \begin{pmatrix} 0.0000 & 0.0000 & 0.0000 \\ 1.0000 & 1.0000 & 1.0000 \\ 0.0000 & 0.0000 & 0.0000 \end{pmatrix}$$

Polarization Unit vectors, a1 = "slow" rays, a2 = "fast" rays

$$a_1 = \begin{pmatrix} -0.7409 & -0.7421 & -0.7432 \\ 0.0000 & 0.0000 & 0.0000 \\ 0.6716 & 0.6702 & 0.6691 \end{pmatrix}$$

$$a_2 = \begin{pmatrix} 0.0000 & 0.0000 & 0.0000 \\ 1.0000 & 1.0000 & 1.0000 \\ 0.0000 & 0.0000 & 0.0000 \end{pmatrix}$$

Polarization Unit vectors

a<sub>i</sub> = "Generated Wavelength", a<sub>j</sub> and a<sub>k</sub> = "Applied" Wavelengths

$$a_i = \begin{pmatrix} 0.0000 \\ 0.0000 \\ 0.0000 \end{pmatrix}$$

$$a_j = \begin{pmatrix} 0.0000 \\ 1.0000 \\ 0.0000 \end{pmatrix}$$

$$a_k = \begin{pmatrix} -0.7421 \\ 0.0000 \\ 0.6702 \end{pmatrix}$$

$$a_{jk} = \begin{pmatrix} 0.0000 \\ 0.0000 \\ 0.0000 \\ 0.6702 \\ 0.0000 \\ -0.7421 \end{pmatrix}$$

a<sub>jk</sub> Color vector ==>

Polarization Components for the Electric Fields (col = slow & fast respectively)

$$Pb = \begin{pmatrix} 0.3120 & 0.3172 \\ 0.3001 & 0.3093 \\ 0.2957 & 0.3055 \end{pmatrix}$$

Miscellaneous Information

$$\theta = 44.4295^\circ \text{deg} \quad \phi = 0.0000^\circ \text{deg}$$

$$\lambda_1 = 3.1761 \quad \lambda_2 = 1.6000$$

$$\lambda_3 = 1.0640$$

CATEGORY = 4

1- SHG/SFM, 2-OPA/DFM-32  
3-OPA/DFM-31, 4-OPO

d<sub>ijk</sub> Tensor

Indices of Refraction (λ by columns)

$$d_{ijk} = \begin{pmatrix} 0.00 & 0.00 & 0.00 & 0.00 & 1.90 & 0.00 \\ 0.00 & 0.00 & 0.00 & 3.60 & 0.00 & 0.00 \\ 2.30 & 3.80 & 15.80 & 0.00 & 0.00 & 0.00 \end{pmatrix}$$

$$n = \begin{pmatrix} 1.7577 & 1.7906 & 1.8027 \\ 1.7756 & 1.7982 & 1.8092 \\ 1.7778 & 1.8655 & 1.8809 \end{pmatrix}$$

Polarization Vector

d<sub>ajak</sub> := d<sub>ijk</sub> · a<sub>jk</sub>

Walkoff, column 1 = slow rays

column 2 = fast rays, λ by row(s)

in degrees and milliradians, resp.

$$d_{ajak} = \begin{pmatrix} 0.0000 \\ 2.4128 \\ 0.0000 \end{pmatrix}$$

$$\rho = \begin{pmatrix} 2.2385 & 1.2074 \cdot 10^{-6} \\ 2.3443 & 1.2074 \cdot 10^{-6} \\ 2.4302 & 0.0000 \end{pmatrix} \cdot \text{deg}$$

Nonlinear Coefficient (pm/V)

d<sub>eff</sub> = 2.4128

$$\rho \cdot 10^3 = \begin{pmatrix} 39.0683 & 2.1073 \cdot 10^{-5} \\ 40.9163 & 2.1073 \cdot 10^{-5} \\ 42.4158 & 0.0000 \end{pmatrix}$$

Phase Match Type:

Crystal Type (+/- number indicates type)

PMID = 2

CT = 1

Angle of OPTIC Axis from z-axis

$$\Omega = \begin{pmatrix} 31.1070 \\ 19.1667 \\ 17.3332 \end{pmatrix} \cdot \text{deg}$$

Polarization angle

$$\delta = \begin{pmatrix} 0.0000 \\ 0.0000 \\ 0.0000 \end{pmatrix} \cdot \text{deg}$$

Relative Walkoff angle in milliradians

Use associated walkoff column below for the smallest walkoff angle

(ρ<sub>1</sub>, ρ<sub>2</sub>, or ρ<sub>3</sub>) as indicated to the right.

ρ<sub>1</sub>      ρ<sub>2</sub>      ρ<sub>3</sub>

$$\rho = \begin{pmatrix} 0 & 40.9163 & 0 \\ 40.9163 & 40.9163 & 40.9163 \\ 0 & 40.9163 & 0 \end{pmatrix}$$

Worksheet Walkoff values (by selected phase match type) in degrees

$$\rho_1 = 0$$

$$\rho_2 = 2.344$$

$$\rho_3 = 0$$



DEPARTMENT OF THE AIR FORCE

WRIGHT LABORATORY (AFMC)  
WRIGHT-PATTERSON AIR FORCE BASE, OHIO

5-3-94

FROM: WL/DOA  
Wright-Patterson AFB OH 45433-6523

SUBJ: Notice of Changes in Technical Report(s) AD A274079/WL-TR-93-5029

TO: Defense Technical Information Center  
Attn: DTIC-OCC  
Cameron Station  
Alexandria VA 22304-6145

Please change subject report(s) as follows:

*Please make corrections or keep  
the attached with the above  
report.*

JUDY K. SZCZUR  
Chief, STINFO and Technical Editing Division  
Operations and Support Directorate